# A Study of Endosomal Factors Involved in Membrane Fusion Mediated by the Ebola Virus Glycoprotein

Laura Odongo
Nairobi, Kenya

B.S. Łódź Univeristy of Technology, 2014
M.S. Łódź University of Technology, 2015
M.S. University of Virginia, 2018

A Dissertation presented to the Graduate Faculty of the University of Virginia
in Candidacy for the Degree of Doctor of Philosophy

Interdisciplinary Biophysics Program
Department of Molecular Physiology and Biological Physics
University of Virginia
May 2023

# Abstract

Ebola virus (EBOV) causes hemorrhagic fever associated with fatality rates of up to 90%. Its entry process is complex and incompletely understood yet could provide clues for novel therapeutics. EBOV entry into cells is mediated by its glycoprotein (GP) comprised of two subunits, GP1, which is responsible for cell attachment, and GP2, which drives membrane fusion. Following attachment and internalization into host cells, EBOV is trafficked to late endosomes/lysosomes where its glycoprotein (GP1 subunit) is processed to a 19-kDa form by endosomal cathepsins B and L (CatB and L), allowing GP to bind to its intracellular receptor Niemann Pick C1 (NPC1). Evidence suggests that an additional factor following EBOV GP-NPC1 binding is required to trigger conformational changes in GP that drive fusion of the viral and endosomal membranes. The cellular factor(s) that act on GP to induce these conformational changes remain unknown, as low pH and NPC1 binding appear insufficient to trigger fusion. A cathepsin protease inhibitor, E-64d, as well as pH raising agents have been shown to block infection by pseudoparticles bearing 19-kDa GP1, suggesting further cathepsin action is needed to trigger fusion. The identification of the final fusion trigger, however, has been impeded, in part due to a lack of tools to assess the biochemical requirements for EBOV GP-mediated fusion within endosomes. To address this limitation, I developed a new *in vitro* system to study fusion in the endosomal milieu. In this system, late endosomes are isolated from cells and used to prepare supported planar endosomal membranes (SPEMs) and fusion of fluorescent (pseudo)virus particles is monitored by total internal reflection fluorescence microscopy (TIRFm) (Chapter 2). The system was validated by recapitulating pH-dependent fusion of influenza and Lassa viruses, the latter with endosomes both positive and negative for the Lassa virus intracellular receptor, Lamp1. Additionally, I explored the effect of the late endosomal lipid, bis(monoacylglycero)phosphate (BMP), on docking and lipid mixing of HIV particles pseudotyped with Lassa virus GP (Appendix A). Using SPEMs, I show in Chapter 2 that fusion mediated by 19-kDa EBOV GP depends on low pH and is enhanced by $Ca^{2+}$, as reported in other studies. I further demonstrate that SPEMs retain cathepsin activity

and that E-64d inhibits 19-kDa EBOV GP-mediated fusion at the hemi- and full fusion stages. Moreover, addition of cathepsins augments both hemi- and full fusion. Collectively the findings support the proposal that additional cathepsin activity is needed beyond generating 19 kDa GP1.

In Chapter 3, I contributed to exploring the role of cholesterol on EBOV fusion and entry. Cholesterol serves critical roles in enveloped virus fusion by modulating membrane properties, including intrinsic curvature. We found that EBOV GP interacts directly with cholesterol via several glycines in the membrane-proximal external region and transmembrane (MPER/TM) domains. We also demonstrated that cholesterol in the viral membrane promotes membrane fusion and cell entry. Further, compared to the wild-type counterpart, a mutation in the cholesterol binding site of the TM domain (G660L) resulted in a higher probability of stalling GP2 proteoliposome fusion at the hemifusion stage and lower cell entry of virus-like particles bearing this mutation.

In Chapter 4, the crystal structure of the luminal domain C of NPC1 (NPC1-C) in the space group $P2_1$ is described. The crystallization conditions were different from those of other published NPC1-C crystal structures and new purification protocols for glycosylated and non-glycosylated NPC1-C are described. The effect of glycosylation on the thermal stability of NPC1-C has also been explored (Appendix B).

# Acknowledgements

This has been one of my most difficult, rewarding, arduous, thrilling, punishing, intellectually stimulating, and did I mention, difficult experiences of my life! I have grown both as a scientist and person and, needless to say, I did not gain this character development in a vacuum. There are so many people I must extend my gratitude to for helping me with the incredible adventure that was grad school. Thank you to my advisors, The Grownups, as the students in the lab have referred to them: Drs. Lukas Tamm, Judith White, and Volker Kiessling. Lukas, thank you for allowing me to join your lab and pursue my interests both in and out of the lab as I tried to figure out what I want to be when I grow up. Judy, thank you for mentoring me, even in your retirement. I am grateful for your guidance, enviable organizational skills as well as your kindness and generosity. Volker, thank you for the invaluable help and advice you have given me over the years. Many thanks to Dr. David Castle who helped immensely in the beginning stages of my main thesis project. One of my fondest memories from my time in grad school is working with David and Judy at the bench one December morning as they helped me optimize a protocol.

I would like to extend my gratitude to my thesis committee for your helpful mentorship: Drs. Owen Pornillos, Jim Cassanova, and Zygmunt Derewenda. Special thanks to Dr. Barbie Ganser-Pornillos for providing additional support and guidance. I also had a special support team without whom I would not have made it this far: Drs. Tim Raines, Crystal Richardson, Jasmine Crenshaw, and Janet Cross. You all cared not only for my development as a scientist but as a person as well. Dr. Crenshaw, our biweekly meetings were instrumental in keeping me on track, academically and personally. Thank you so very much!

Next on my list of people to thank is Dr. Jinwoo Lee, a man with the patience of a saint as he helped me find my footing in the lab and build my confidence as a scientist. I am grateful to my other colleagues (past and present) and friends in the Tamm and White labs including Amanda Ward, Maya Cabot, Patrick Seelheim, Binyong Liang, Raghavendar Sanganna Gari, Alex Kreutzberger, Margaret Grant, Weronika Tomaka, Daria Sokovikova, Katie Kraichely, Connor Sandall, Beth Habtegebrael, Christine Hulseberg, Elizabeth Nelson, Kasia Szymańska-de Wijs, and Lucie Fénéant. They supported me and kept me sane over the years, even sporadically developing a mild obsession with Dracula (thanks, Katie)! The encouragement I received from my colleagues and the incredible friendships we developed kept me afloat. Thank you all for making the Tamm lab a wonderful place to work.

I could not have done any of this without friends who essentially became my chosen family, with my main cheerleaders being Revay Corbett, Alexys Riddick, Yi Hao, Akeem Wells, Chase Rohan, Angela Myklestad, Seth Engel, Saubhagya Jayarajan, Maria Konzolo, Louis Gulavic, Marcus Wolfe, Brittany Martínez, and Brandon Podyma. It is impossible to find the words to fully express how much you all mean to me. I truly appreciate each and every one of you! Once a month, I would have family dinner with Jacob Wolpe, Abigail Wolpe, and Xavier Horton. The good food and even better company made the dinners such a delight. I will miss these dinners.

“Last but not least, I wanna thank me.” I jest! I simply could not resist quoting Snoop Dogg here. Let’s try that again: Lastly, I’d like to express my appreciation for my family, especially my parents, Benedict and Iwona Odongo. I would not be who or where I am if it were not for them. Dziękuję Wam bardzo! To my brother, Miko; cousin, Mercy; and uncle, Hannington: asanteni! I love you all so very much!

This dissertation is dedicated to my parents, Benedict and Iwona Odongo.
Thank you for your support and encouragement.

# Table of Contents

# Chapter 1. Introduction

## 1.1 Overview of Virus Entry

A virus can be defined as "a package of genetic information protected by a protein shell for delivery into a host cell to be expressed and replicated." (Taylor, 2014). There is ongoing debate as to whether viruses are "living" organisms, but regardless viruses infiltrate all forms of life. There are an estimated $10^{31}$ viruses, a majority of which are bacteriophages (Cobián Güemes et al., 2016). Mammals and birds are estimated to host 1.67 million undiscovered viruses, and, of these, some 700,000 have the potential to infect humans (Carroll et al., 2018), but only about 200 viruses have been confirmed to infect humans (Woolhouse et al., 2012).

There are currently two major virus classification schemes: the International Committee on Taxonomy of Viruses (ICTV) system and the Baltimore classification system (Kuhn, 2021). Viruses are also grouped based on their size and shape, composition and structure of their genomes and mode of replication as well as the presence or absence of a lipid envelope (Gelderblom, 1996). Viruses with a lipid envelope will be the major focus of this dissertation.

Being obligate intracellular parasites, viruses must gain entry into host cells. Once inside, they take control of the cell for their needs: protein translation, genome replication, particle assembly, and, finally, exit from the host cell by budding, exocytosis, or cell lysis (Ryu, 2017). Viruses have evolved numerous mechanisms to enter cells. There are two main steps of virus entry: attachment to cell surface receptors and delivery of the viral genome into the cytoplasm. The main points of entry into the cell are directly at the plasma membrane or the limiting membrane of an intracellular organelle. Virus entry occurs by penetration (for non-enveloped viruses) or membrane fusion (for enveloped viruses) (Dimitrov, 2004).

### 1.1.1 Virus attachment

Infection is initiated by attachment of the virus to the cell surface, which involves two types of host cell surface proteins: attachment factors and virus receptors. Attachment factors recruit and capture viruses but do not necessarily trigger virus penetration into the cytoplasm. Attachment factors are generally non-specific and can be used by diverse viruses. Glycosaminoglycans, which are sulfated glycan side chains of glycoproteins typified by heparins and heparan sulfate, serve as attachment factors for various types of viruses (Dai et al., 2020; Jolly & Sattentau, 2013; Ryu, 2017). Glycosaminoglycans are ubiquitously expressed in most human cell types and have a global negative charge, allowing for electrostatic interaction with positively-charged viral surface proteins (Cagno et al., 2019). Heparan sulfate proteoglycans facilitate entry of several viruses including herpes simplex virus (Shukla et al., 1999), hepatitis B virus/hepatitis delta virus (Lamas Longarela et al., 2013; Leistner et al., 2008), Ebola virus (Tamhankar et al., 2018), dengue virus (Germi et al., 2002), human immunodeficiency virus type 1 (HIV-1) (Saphire et al., 2001), and echoviruses 5 and 6 (Goodfellow et al., 2001; Israelsson et al., 2010).

Virus receptors are host molecules that are essential for productive infection. Interaction with entry receptors is virus-specific and determines cell tropism (Ryu, 2017). Virus binding to their receptors leads to one of the following: (i) activation of specific signal pathways essential for viral entry, (ii) targeting the virus particle for endocytosis, (iii) conformational changes in the viral fusion protein that result in virus and host membrane fusion at the cell surface or within endosomes (Grove & Marsh, 2011). Viruses exploit various cell surface components ranging from glycoproteins to phospholipids (Ryu, 2017). A variety of the cellular surface proteins are utilized as entry receptors, including integrins, transferrin receptor, low-density lipoprotein receptor, nectins, and members of immunoglobulin superfamily, e.g., CD4 (Dai et al., 2020). Some viruses require coreceptors for efficient entry. For instance, the fusion protein of HIV initially interacts with CD4, which induces a conformational change in the HIV surface protein that exposes a binding site to its co-receptor, CCR5 or CXCR4 (Dimitrov, 2004).

Non-protein receptors may also serve as entry receptors. For example, sialic acid is a ubiquitously expressed carbohydrate moiety attached to glycoproteins and glycolipids on the cell surface and is used by influenza virus, reovirus adenovirus, and rotavirus for entry (Stencel-Baerenwald et al., 2014). Table 1.1 lists the attachments factors and receptors for some viruses.

**Table 1.1 Different types of host molecules utilized by representative viruses for each Baltimore class. Adapted from (Dai et al., 2020).**

| Baltimore subtype | Virus | Envelope | Attachment factor | Entry receptor | Reference |
|---|---|---|---|---|---|
| I: dsDNA | Herpes simplex virus | + | HS | Integrin, HVEM, Nectin1/2 | (Gianni et al., 2013; Karasneh & Shukla, 2011) |
| | Human papillomavirus | - | HS | Integrin, GFR, CD63, CD151 | (Raff et al., 2013; Shafti-Keramat et al., 2003) |
| II: +ssDNA | Canine parvovirus | - | SA | TfR | (Lee et al., 2019; Löfling et al., 2013) |
| | Porcine circovirus | - | HS, SA | TfR | (Misinzo et al., 2006; Nauwynck et al., 2012) |
| III: dsRNA | Rotavirus | - | SA, HBGA | Integrin, HSC70 | (Hu et al., 2012; Ruiz et al., 2009; Zárate et al., 2003) |
| | Bluetongue virus | - | HS, SA | Integrin, TfR, CD63 | (Forzan et al., 2007; Mecham & McHolland, 2010) |
| IV: +ssRNA | Bovine viral diarrhoea virus | + | HS | LDLR, CD64 | (Agnello et al., 1999; Maurer et al., 2004) |
| | Human rhinovirus | - | - | LDLR, ICAM1 | (Kolatkar et al., 1999) |
| V: -ssRNA | Measles virus | + | SA | Nectin4, CD150, CD64 | (Delpeut et al., 2014; Schneider-Schaulies et al., 2001; Talekar et al., 2013) |
| | Canine distemper virus | + | HS | Nectin4, CD150 | (Fujita et al., 2007; Pratakpiriya et al., 2012; von Messling et al., 2005) |
| VI: +ssRNA-RT | HIV | + | HS, lectins | CD4, CCR5/CXCR4 | (Monini et al., 2012; Saphire et al., 2001) |
| VII: dsDNA-RT | Hepatitis B virus | + | HS | NTCP, HSC70 | (Glebe & Bremer, 2013; Ryu et al., 2000; Zhang et al., 2011) |
| | Human T-lymphotropic virus-1 | + | HS | GLUT1 | (Ghez et al., 2006; Lambert et al., 2009) |

Abbreviations of some receptors are CD: cluster of differentiation; CCR5: C-C chemokine receptor type 5; CXCR4: CX-C chemokine receptor type 4; HBGA: histo-blood group antigen; GFR: growth factor receptor; GLUT1: glucose transporter 1; HS: heparan sulfate; HSC70: heat shock cognate 71-kDa protein; HVEM: herpesvirus entry mediator,

belonging to tumour necrosis factor receptor family and a regulator of immune responses); ICAM1: intercellular adhesion molecule 1; LDLR: low-density lipoprotein receptor; NTCP: sodium taurocholate co-transporting polypeptide; SA: sialic acid; TfR: transferrin receptor.

### 1.1.2 Virus penetration

Penetration into the cytoplasm follows attachment of the viral particle to the cell surface. Viruses penetrate either the plasma membrane or the limiting membrane of an intracellular organelle (Marsh & Helenius, 2006). Viruses that fuse at the cell surface include herpes simplex virus, Sendai virus, and most retroviruses, including HIV (Marsh & Helenius, 2006). For viruses that are internalized, virus binding to receptors activates receptor-mediated signaling-induced endocytosis (Boulant et al., 2015). Internalization occurs via various routes. Influenza A virus (Rust et al., 2004) and vesicular stomatitis virus (Cureton et al., 2009) enter cells by clathrin-mediated endocytosis while Hepatitis B virus uses a caveolin-mediated endocytosis pathway (Macovei et al., 2010). Some viruses are internalized by a cholesterol-dependent endocytic pathway that is independent of clathrin and caveolin, such lymphocytic choriomeningitis (LCMV) (Rojek et al., 2008) and simian virus 40 (Damm et al., 2005). Other viruses, e.g., vaccinia virus (Mercer & Helenius, 2008) and coxsackievirus B (Coyne et al., 2007), induce their internalization by macropinocytosis. Finally, mimivirus infects cells through phagocytosis (Ghigo et al., 2008). Of note, some viruses can use more than one mode of internalization depending on the cell type.

Upon reaching the site of penetration, viral proteins facilitate transport into the cytoplasm. Viral fusion proteins drive fusion of the viral and host membrane to create a pore through which the genomic cargo is transferred into the cytoplasm (Plemper, 2011). Membrane fusion is a thermodynamically favorable process but has a high kinetic barrier. Close apposition of the two membranes must overcome repulsive forces including the hydration barrier created by a layer of water associated with the head groups of polar lipids (Kielian, 2014). Membrane fusion is sensitive to lipid composition since lipids have intrinsic preferred curvatures, which may promote or inhibit fusion (Chernomordik & Kozlov, 2003). The energy to overcome these kinetic barriers is

provided by viral fusion proteins. Viral fusion proteins exist in a metastable state in the virus envelope. In this state, the protein structure is kinetically trapped in a local free energy minimum, separated from the global free energy minimum conformation by a high energy barrier (Ghosh & Ranjan, 2020). It is thought that destabilizing agents, e.g., low pH and/or cellular receptor(s), trigger conformational changes from the metastable state to reach the lowest energy conformation (Carr et al., 1997). The conformational changes viral fusion proteins undergo upon triggering releases significant conformational energy required to drive membrane fusion (Chernomordik & Kozlov, 2003).

When the active viral membrane fusion protein receives the “fusion trigger” signal, it inserts into the target membrane via a hydrophobic fusion peptide (or loop) (Figure 1.1, iii) (White & Whittaker, 2016). This conformation is termed the “prehairpin intermediate” or “extended intermediate.” (Bullough et al., 1994; White & Whittaker, 2016). The viral protein folds onto itself (Figure 1.1 iv), forming a hairpin or six-helix bundle (Figure 1.1 v) (Malashkevich et al., 1999; Weissenhorn et al., 1998). Formation of the six-helix bundle overcomes the hydration repulsion, bringing the apposing membranes closer together (Harrison, 2008). Further conformational changes bring the fusion loop and transmembrane domains together to promote fusion pore formation (Figure 1.1 vi) (Kemble et al., 1993; Lai & Freed, 2015; Lee et al., 2017; Tamm et al., 2003).

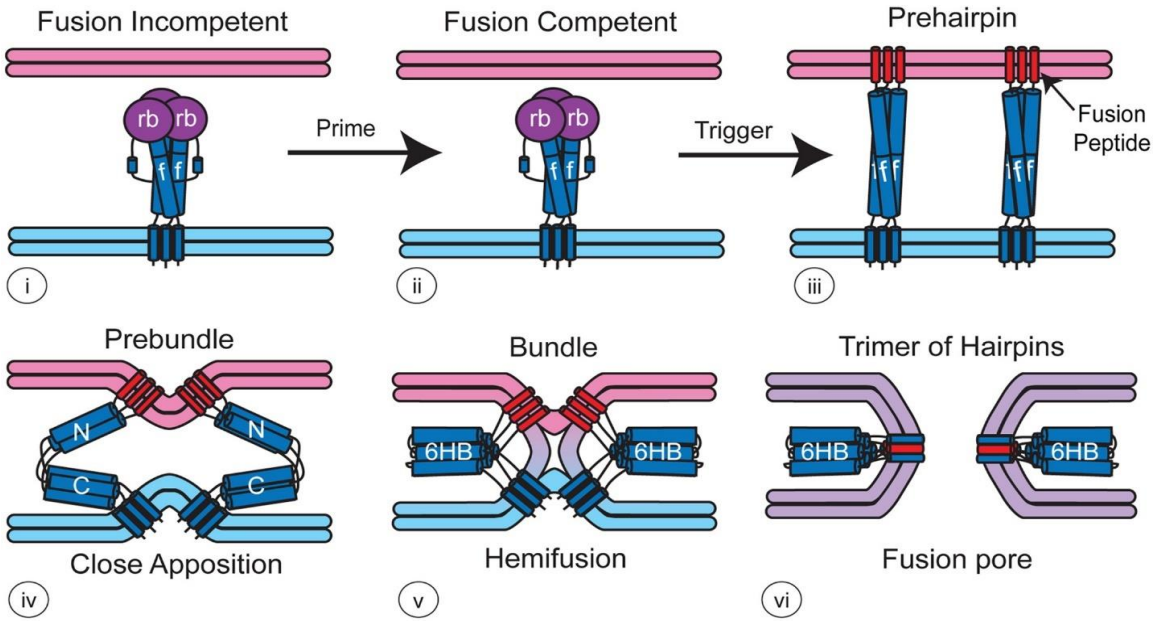


**Figure 1.1. Model of membrane fusion driven by viral fusion proteins**. The model shown is for a class I fusion protein, but related models apply to class II and III fusion proteins. A viral fusion protein is rendered fusion-competent in a priming step, which typically involves proteolytic cleavage (i). The fusion-competent protein (ii) is triggered to undergo conformational changes that result in a prehairpin where the fusion peptide is projected into the target membrane (iii). The prehairpin folds back onto itself, drawing the two membranes in close apposition (iv) until it forms a six-helix bundle resulting in membrane hemifusion (v). Association of the fusion peptide and transmembrane domains promote fusion pore opening. Adapted from (White & Whittaker, 2016).

Viral fusion proteins can be classified into three categories based on their structural and mechanistic characteristics. Class I fusion proteins (e.g., hemagglutinin of influenza virus) are synthesized as fusion-inactive precursors that require proteolytic activation to gain fusion competence. They are all homotrimers and largely α-helical. Class II fusion proteins, such as the E protein of dengue virus, are synthesized as polyprotein precursors that are proteolytically processed during biosynthesis to form dimers. During fusion, these proteins undergo conformational rearrangements that convert the dimer into a stable hairpin trimer comprising β-sheet structures. Lastly, class III fusion proteins do not require proteolytic processing, e.g., G protein of vesicular stomatitis virus. They display features of both class I and II fusion proteins: they have a

central α-helical coiled coil (similar to class I fusion proteins) with their fusion loops located at the tip of an elongated β-sheet (akin to class II fusion proteins) (Más & Melero, 2013).

There are four recognized ways by which viral fusion proteins are triggered: (i) binding to a receptor(s) (e.g., HIV Env, paramyxovirus F protein), (ii) exposure to low pH (e.g., influenza HA, VSV G protein) (iii) binding to a receptor following exposure to low pH (e.g., ASLV Env), and (iv) binding to a receptor following proteolytic cleavage (e.g., MERS S protein) (Figure 1.2) (White & Whittaker, 2016). There is growing evidence that there is a fifth triggering mechanism that involves binding to receptor, low pH, and proteolytic cleavage of the viral fusion proteins of Ebola virus and severe acute respiratory syndrome coronavirus 2 (SARS-CoV2) (discussed in Chapter 2).

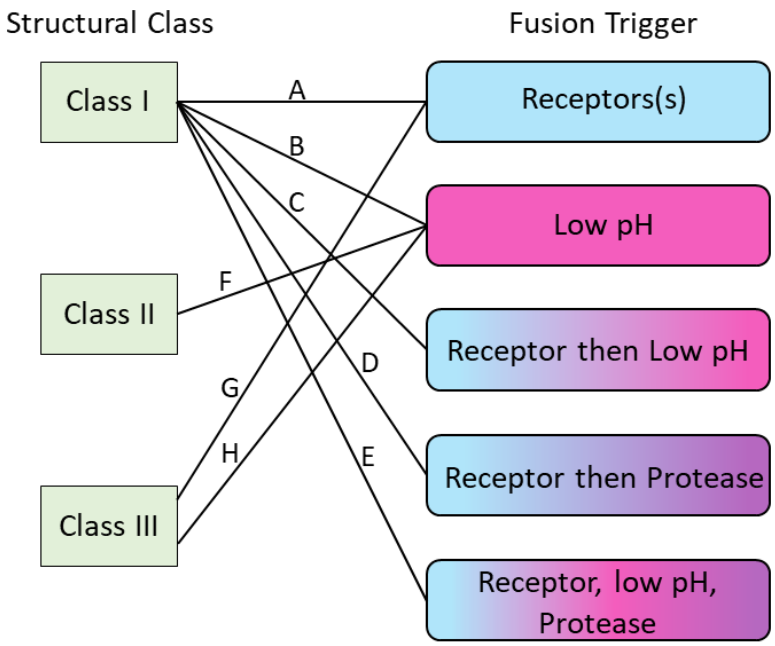


**Figure 1.2. Diversity of viral fusion proteins.** Viral fusion proteins are classified based on their structure (left) and mode of fusion triggering (right). Representative fusion proteins of different classes that employ different fusion triggers are: (A) influenza HA, (B) paramyxovirus F and most retroviral Env proteins, (C) α-retroviral Env proteins, (D) SARS-CoV 1 Spike protein, (E) Ebola virus GP and SARS-SoV 2 Spike protein, (F) the E and E1 protein, respectively, of TBEV and SFV, (G) VSV G, and (H) HSV gB. Modified from (White & Whittaker, 2016).

## 1.2 Overview of Ebola virus

Ebola virus is the best-known member of the *Filoviridae* family, which belong to the order *Mononegavirales*. Members of this family are variously shaped, but often, filamentous, and comprise 15-19 kb RNA genomes that are linear, negative-sense and non-segmented (Kuhn et al., 2019). Currently, there are six recognized genera of the family, *Cuevavirus, Dianlovirus, Ebolavirus, Marburgvirus, Striavirus,* and *Thamnovirus*, and eleven species (Figure 1.3). *Ebolavirus* and *Marburgvirus* genera contain human pathogens, which cause a severe hemorrhagic fever referred to as Ebola virus disease (EVD) and Marburg virus disease, respectively (Kuhn et al., 2019). The *Ebolavirus* genus includes six species: Ebola virus (EBOV), Sudan virus (SUDV), Bundibugyo virus (BUBV), Taï Forest virus (formerly Côte d'Ivoire ebolavirus) (TAFV), Reston virus (RESTV) and, the newest member, Bombali virus. EBOV, SUDV and BDBV are highly lethal human pathogens (Kuhn et al., 2019) and, although RESTV is not known to cause disease in humans, asymptomatic infections have been reported (Cantoni et al., 2016). TAFV has been reported to be the cause of a single case of severe but non-lethal human disease (Le Guenno et al., 1995), and Bombali virus was discovered in insectivorous bats of two species in Sierra Leone (Goldstein et al., 2018). The *Marburgvirus* genus contains a single species with two related viruses, Marburg virus and Ravn virus, both of which cause severe disease in humans (Kuhn et al., 2019).

The four other genera are not known to cause hemorrhagic fever in humans. *Cuevavirus* genus, contains a single species, Lloviu virus, which was discovered in dead insectivorous bats in Spain (Negredo et al., 2011). There is also only one species in the *Dianlovirus* genus, Měnglà virus, which was identified in fruit bats in China (Yang et al., 2019). The remaining two genera have piscine hosts, with Huángjiāo virus (*Thamnovirus* genus) and Xīlǎng virus (*Striavirus* genus) being discovered in hairy frogfish (*Antennarius striatus*) and greenfin horse-faced filefish (*Thamnaconus septentrionalis*), respectively, captured in the East China Sea and South China Sea (Shi et al., 2018).

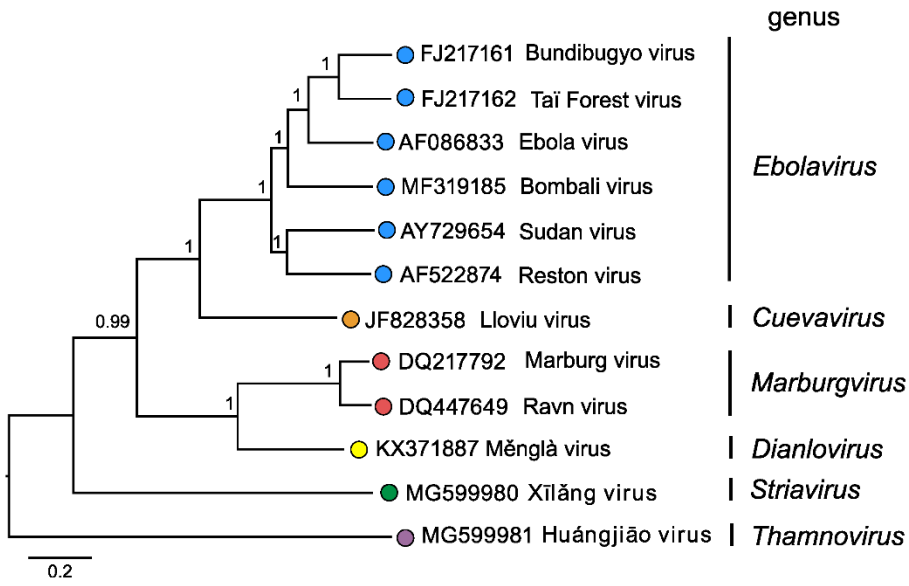


**Figure 1.3** Phylogenetic relationships of filoviruses. Maximum-likelihood tree demonstrating the six genera of the family inferred from the coding-complete or complete filovirus genome sequences. Analysis was performed by Nicholas Di Paola, USAMRIID, Fort Detrick, MD, USA. Adapted from (Kuhn et al., 2019).

### 1.2.1 History of Filovirus outbreaks

The first reported filovirus outbreak was in Marburg and Frankfurt, Germany, and Belgrade, Yugoslavia (now Serbia) in 1967. Laboratory personnel became infected when performing experiments on grivet monkeys imported from Uganda, which were infected with MARV (Slenczka, 2017). During the outbreak, several cases of nosocomial infections were observed as well as one case of sexual transmission, where a woman contracted the virus from her husband who had been infected three months earlier (Slenczka, 2017). To date, there have been a total of fifteen known MARV outbreaks (CDC).

Ebola viruses first emerged in 1976 in two concurrent outbreaks in Yambuku, Bumba, Abumombazi and Kinshasa in Zaire (now Democratic Republic of Congo) and Nzara, Maridi, Tembura and Juba in southern Sudan (now South Sudan) ("Ebola haemorrhagic fever in Sudan, 1976. Report of a WHO/International Study Team," 1978;

"Ebola haemorrhagic fever in Zaire, 1976," 1978). It was initially thought that these infections were caused by Marburg virus, but it was later determined that they were caused by a similar but different virus. The virus isolates came to be known as Ebola virus (formerly Zaire ebolavirus) and Sudan virus.

Since 1976, there have been numerous outbreaks in various countries (Languon & Quaye, 2019). The largest outbreak to date was the 2013-2016 West African outbreak, with over 28,600 cases and 11,325 deaths (WHO). Genomic analyses suggest that the initial case was a zoonotic transmission event followed by human-to-human transmission (Gire et al., 2014). The index case was a 2-year-old boy in a village near Guéckédou, Guinea (Baize et al., 2014; Marí Saéz et al., 2015); after which the virus rapidly spread to other parts of Guinea, Sierra Leone, Liberia, Nigeria, Mali, Spain, and USA (WHO). There have since been other outbreaks in DRC (2017, 2018, 2021 and 2022), Guinea (2021) and Uganda (2022) (CDC). The rise in Ebola virus disease outbreaks has been associated with increased human contact with wildlife due to deforestation, hunting, and mining (Rugarabamu et al., 2020).

### 1.2.2 Filovirus reservoirs

Index cases that initiate filovirus outbreaks are linked to spillover events occurring when humans come into contact with the reservoir (Amman et al., 2017). The initial infections are followed by human-to-human transmission. Bats have been implicated in numerous spillover events associated with severe disease (Wang & Anderson, 2019). Evidence collected to date points to cave-dwelling fruit bats, Egyptian rousette bats (*Rousettus aegypticus*), as the reservoir for MARV and RAVN (Amman et al., 2012; Towner et al., 2007). Additionally, the nature of filovirus infection appears to be seasonal. An ecologic investigation was performed on Egyptian rousette bats in Kitaka gold mine and Python cave in Uganda, where spillover events occurred in miners and tourists. The prevalence of active Marburgvirus infection spiked in older juvenile bats (~6 months) and this coincided with spillover events to humans (Amman et al.,

2012). Other filoviruses have also been detected in bats. Lloviu viral RNA was detected in insectivorous bats (*Miniopterus schreibersii)* in Cueva del Lloviu, Spain (Negredo et al., 2011) and Bükk mountain in northeast Hungary (Kemenesi et al., 2018). RESTV RNA was also identified in *M. schreubersii* bats in the Phillipines (Jayme et al., 2015). Bombali virus was first detected in free tailed bats of two species, Angolan free-tailed bat (*Mops condylurus*) and little free-tailed bat (*Chaerephon pumilus*), in Bombali district in Sierra Leone (Goldstein et al., 2018). Bombali virus has since been detected in *M. condylurus* bats in Kenya, Guinea and Mozambique (Forbes et al., 2019; Karan et al., 2019; Lebarbenchon et al., 2022). Měnglà virus was detected in *Rousettus* bats in Měnglà County, Yunnan Province, China (Yang et al., 2019). Finally, immunoglobulin G antibodies specific to SUDV, TAFV, BDBV, RESTV and Lloviu virus were detected in Egyptian fruit bats in Zambia (Changula et al., 2018).

While Měnglà virus, Lloviu virus and Bombali virus have been detected in bats, the role of bats in the EBOV transmission cycle is still debated, since no complete EBOV genome has been sequenced from any bat sample (Wang & Anderson, 2019). Several pieces of evidence point to bats as the reservoir for EBOV. Two EBOV outbreaks have been linked to an index case associated with bats (Leroy et al., 2009; Marí Saéz et al., 2015). Moreover, detection of RESTV in bats (Jayme et al., 2015) further supports bats as reservoirs for ebolaviruses.

### 1.2.3 Pathogenesis

A combination of animal studies, *in vitro* research and clinical data from human beings has provided a general understanding of Ebola virus disease (EVD) pathogenesis. EBOV appears to enter the host through mucosal surfaces, breaks and abrasions in the skin (Feldmann & Geisbert, 2011b). Macrophages and dendritic cells (DC) are the first cells to be infected, allowing for EBOV to spread from the site of infection to regional lymph nodes, liver, and spleen (Geisbert et al., 2003). EBOV-infected macrophages and DCs migrate out of the spleen and lymph nodes to other tissues, thereby disseminating

the infection. EBOV can infect many cell types, in addition to DCs and macrophages, including Kupffer cells, fibroblasts, hepatocytes, endothelial and epithelial cells as well as adrenal gland tissues (Geisbert et al., 2003).

EBOV has evolved to counteract the host immune system. EBOV infection is associated with inadequate immune response and decreased production of coagulation factors (Feldmann & Geisbert, 2011b). The type I interferon response, an important host defense, is suppressed by viral proteins, VP24 and VP35 (described in a later section of this chapter) (Kühl & Pöhlmann, 2012). VP24 and VP35 also cause abnormal secretion of cytokines and chemokines and thus lead to a lack of proper DC maturation (Lubaki et al., 2013). By impairing DC maturation, EBOV impedes activation of lymphocytes including natural killer, T and B cells (Furuyama & Marzi, 2019). Uncontrolled EBOV replication induces hypersecretion of cytokines, chemokines and growth factors, creating a so-called "cytokine storm." This dysregulated response results in increased vascular permeability, end-stage organ failure, sepsis syndrome, and death (Furuyama & Marzi, 2019).

The dysregulation of the T cell response appears to be a key component in EVD pathophysiology. Indeed, surviving EVD patients were found to present an early and robust antibody response against EBOV (McElroy et al., 2015; Reynard et al., 2019). While T cell activation was observed in both fatal and non-fatal cases, Ruibal *et al.* hypothesize that the increased expression of T cell inhibitory molecules ultimately triggers expression of pro-inflammatory cytokines in fatal cases (Ruibal et al., 2016). It is also worth noting that a study of survivors of EVD from the 2013-2016 West African outbreak indicated that these individuals displayed robust T cell responses to various EBOV epitopes two years after viral clearance (Wiedemann et al., 2020). Another observation seen after the acute phase of EVD, is an increase in EBOV-specific neutralizing antibodies (Luczkowiak et al., 2016). The neutralizing antibodies may not play a large role in recovery from acute EVD; however, some EVD survivors' serum contains antibodies that can still neutralize live virus 40 years post-initial infection (Rimoin et al., 2018).

As the disease progresses, there is accumulation of nitrogen oxide in the blood, which is associated with cardiac stress and heart failure and contributes to virus-induced shock (Sanchez et al., 2004). Another factor, which was recently identified as a contributor to EVD pathogenesis, is electrolyte imbalance. Analysis of data from patients revealed hypokalemia, hypocalcemia, hypomagnesemia, and hyponatremia (Uyeki et al., 2016). Clinical care that targets electrolyte abnormalities have been associated with reduced case fatality rates (Muñoz-Fontela & McElroy, 2017).

Other factors that may play a role in EVD pathogenesis, but require further study, are co-infection with malaria, which has been associated with increased EVD-related mortality (Vernet et al., 2017). Additionally, comorbidities like malnutrition may contribute to higher case fatality rates (Muñoz-Fontela & McElroy, 2017).

### 1.2.4 Clinical Manifestation

**Acute EVD:** Symptoms begin 5-7 days post exposure, with the incubation period varying from 1 to 21 days. The duration of the incubation period depends on the route of infection, with shorter periods for percutaneous exposure and longer periods for animal-to-human or human-to-human transmission (Velásquez et al., 2015). Rare cases of asymptomatic or pauci-symptomatic infection have been reported (Timothy et al., 2019). Following disease onset, patients present with a non-specific febrile illness with symptoms including arthralgia, anorexia, malaise, headache, myalgia, and rash. As the disease progresses, severe gastrointestinal symptoms develop including, nausea, vomiting, and high-volume diarrhea (Jacob et al., 2020).

The onset of detectable viremia, persistent fever, and increased gastrointestinal fluid loss occurs 6-10 days from disease onset. The terminal phase of the disease (7-12 days following disease onset) is characterized by tissue hypoperfusion and vascular leakage as well as dysregulated inflammation, which leads to multiple organ dysfunction syndrome (Jacob et al., 2020). A subset of patients develop encephalopathy and neurological symptoms (de Greslan et al., 2016). Patients who do not improve by the

first week will die as a result of hypovolemic shock or multiorgan failure, starting with acute kidney injury (Casillas et al., 2003).

**Post-Ebola Syndrome (PES):** Patients who survive EVD experience severe sequelae that persist during convalescence, a condition referred to as post-Ebola syndrome (PES) (Scott et al., 2016). The symptoms include musculoskeletal pain, rash, dry flaky skin, vision loss, hearing loss, impotence, bleeding, menstrual cessation, and general weakness (Scott et al., 2016). Neuropsychiatric sequelae including long-term anxiety, depression and post-traumatic stress have also been reported (Büttiker et al., 2022). The virus is cleared from most of the body following acute illness. However, virus clearance is delayed in immune-privileged sites in the body including semen, the eye, the central nervous system, and the fetus, placenta, amniotic sac/fluid, and mammary gland in women infected during pregnancy (Vetter et al., 2016). Viral RNA has also been identified in other body fluids including vaginal secretions, urine, sweat, and saliva for weeks and even months after disease onset (Vetter et al., 2016). While it appears that complete viral clearance can take months, reports of recrudescence are rare.

### 1.2.5 Therapeutic Strategies

The World Health Organization (WHO) recommends supportive care (rehydration with oral or intravenous fluids) in addition to administration of Inmazeb or Ebanga (WHO, 2021), which are monoclonal antibodies evaluated for EVD treatment in the Pamoja Tulinde Maisha (PALM; Kiswahili for “Together We Save Lives”) trial (Mulangu et al., 2019). Inmazeb (also known as REGN-EB3) was the first FDA-approved treatment for EVD caused by EBOV of the *Zaire ebolavirus* species (FDA, 2020a). Ebanga (also known as ansuvimab-zykl or mAb114) was approved soon after Inmazeb (FDA, 2020b). Inmazeb is a cocktail of three human monoclonal antibodies and Ebanga is comprised of a single monoclonal antibody (Tshiani Mbaya et al., 2021). Nucleoside analogue drugs, including favipiravir and remdesivir, as well as small interfering RNA (siRNA), TKM-130803, were designed and tested for treatment of EVD (Mulangu et al.,

2019; Scott et al., 2020; Sissoko et al., 2016). These small molecule inhibitors did not improve survival in clinical trials.

There are currently three approved vaccines against Ebola virus: Ervebo (FDA-approved) (FDA, 2019), Zabdeno/Mvabea (approved for medical use in the EU) (EMA, 2020a, 2020b), and Ad5-EBOV vaccine (approved for emergency use by the China Food and Drug Administration) (Y. Li et al., 2018). It is important to note that the aforementioned treatments and vaccines are targeted at *Zaire ebolavirus*. With Sudan virus being the causative agent for several outbreaks, there is a need for vaccine and treatment options against this virus. In fact, during the preparation of this dissertation (November 2022), WHO announced plans to begin a clinical trial for three vaccine candidates against Sudan virus, the virus responsible for the 2022 outbreak in Uganda (WHO, 2022b).

## 1.3 Overview of EBOV Replication Cycle

### 1.3.1 Structure of EBOV particles

Filoviruses are usually filamentous in shape, varying in length (average of 1 - 2.6 µm) with a diameter of 96-98 nm. Filoviral genomes are linear, non-segmented, negative-sense RNA molecules, containing 15-19 kb (Kuhn et al., 2019). Most filoviruses encode seven major structural proteins: nucleoprotein (NP), VP35, VP40, glycoprotein (GP), viral protein 40 (VP40), VP24 and large protein (L) (Sanchez et al., 1993). It is noteworthy that the newly discovered fish filoviruses lack some protein homologs. Xīlǎng virus lacks a clear VP24 homolog and Huángjiāo virus lacks VP24, VP30, VP35, and VP40 homologs. These differences would suggest that genome replication and transcription are different than for the other filoviruses (Hume & Mühlberger, 2019).

The EBOV particle is wrapped in a host-derived-membrane covered with GP, which is the only surface protein (Figure 1.4). The inner leaflet of the membrane is lined with VP40, which gives the virus its filamentous shape. The inner core structure, referred to as the nucleocapsid, comprises the viral RNA genome and five associated viral proteins: NP (encapsidates the viral genome), VP30 (a polymerase cofactor), VP35 (another polymerase cofactor), VP24 (nucleocapsid maturation factor) and L (RNA-dependent RNA polymerase) (Hume & Mühlberger, 2019).

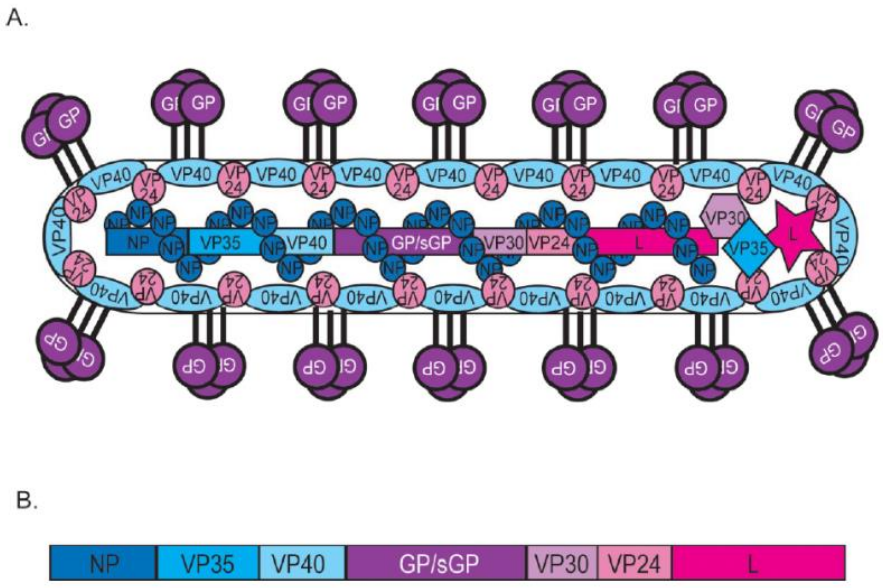


**Figure 1.4. Structure and genome organization of Ebola virus. A.** Morphology of an EBOV particle. The nucleocapsid is composed of the RNA genome (represented by the colored rectangles), nucleoprotein (NP), RNA-dependent RNA polymerase (L) as well as viral proteins 24, 30 and 35. The matrix protein, VP40, interacts with the inner leaflet of the host-derived viral membrane. The surface of the virion is decorated with glycoproteins (GP). **B.** Ebola virus genome organization. Figure created by Kathryn Schornberg. Used with permission from her thesis (Figure 1.1).

## 1.3.2 EBOV proteins and their functions

**Nucleoprotein (NP).** NP comprises 739 amino acids, with a hydrophobic N-terminal half and a hydrophilic C-terminal half (Sanchez et al., 1989). NP oligomerizes into long, linear filaments, encapsidating the viral RNA genome. Additionally, NP interacts with other

EBOV proteins, VP35, VP24 and L, to form the nucleocapsid (Takamatsu et al., 2018; Wan et al., 2017). Post-translational modifications of NP, glycosylation, including sialylation, are thought to be required for viral assembly (Huang et al., 2002; Watanabe et al., 2006).

**VP35:** The protein VP35 serves as a cofactor for RNA polymerase and is analogous to viral phosphoproteins of other mononegaviruses. VP35, made up of 340 amino acids, also interacts with the viral RNA polymerase as well as NP, conferring specificity for filoviral genomic RNA (Kirchdoerfer et al., 2017). Phosphorylation of VP35 is critical for its role in transcription and replication (Zhu et al., 2020). Further, VP35 also blunts the innate immune response by suppression of the type I interferon response and RNA interference (Basler et al., 2000; Haasnoot et al., 2007).

**VP40:** The matrix protein, VP40, is the most abundant protein in virions. VP40 comprises 326 amino acids and is important for transcription regulation, viral assembly and budding at the plasma membrane. Expression of VP40 alone is sufficient for the formation of filamentous virus-like particles. Additionally, VP40 interacts with NP and VP35, chaperoning the nucleocapsid to viral budding sites at the plasma membrane (Kirchdoerfer et al., 2017). VP40 also interacts with phosphatidylserine (PS) and phosphatidylinositol 4,5-bisphosphate ($PI(4,5)P_2$), interactions that stabilize and/or induce extensive VP40 oligomerization required for virion assembly (Adu-Gyamfi et al., 2015; Johnson et al., 2016). VP40 can perform all these functions likely due to the ability of VP40 to adopt three distinct oligomeric states, dimer, hexamer, and octamer (Bornholdt et al., 2013; Hoenen et al., 2010). The VP40 matrix in the virion disassembles during viral entry. Low pH, as found in endosomes, weakens the VP40-lipid interactions, reducing the energy barrier for membrane fusion (Winter et al., 2022)

**VP30:** The protein VP30 (288 amino acids long) is unique among filoviruses, having no corresponding protein in other mononegaviruses. VP30 is a transcription activator, facilitating the switch from replication to transcription (Bach et al., 2020). VP30 also binds to zinc and RNA (John et al., 2007) and interacts with NP and VP35 (Biedenkopf et

al., 2013; Hartlieb et al., 2007). The NP-VP30 and VP30-VP35 interactions are influenced by the reversible phosphorylation of VP30, which in turn may explain VP30's ability to modulate the polymerase complex between transcriptase and replicase (Biedenkopf et al., 2013; Takamatsu et al., 2022).

**VP24:** The VP24 protein is a minor matrix protein, composed of 251 amino acids. VP24 is involved in inhibition of replication and transcription, nucleocapsid formation and genome packaging (Kirchdoerfer et al., 2017; Takamatsu et al., 2018). VP24 interacts with NP and VP35, with the interaction between NP and VP24 found to be essential for nucleocapsid formation and packaging into the virion (Banadyga et al., 2017). Like VP35, VP24 also blocks type I interferon signaling. It does so by preventing nuclear import of the host transcription factor, STAT1, by competitively binding to the host nuclear transporter, karyopherin alpha (Schwarz et al., 2017). Karyopherin-bound VP24 undergoes nucleocytoplasmic trafficking to return to the cytoplasm, presumably to perform its other tasks besides immune evasion (Harrison et al., 2021).

**Large protein (L):** The RNA-dependent RNA polymerase, L, is the largest protein produced by EBOV; it contains 2212 amino acids. The L protein has six catalytic motifs, which impart L with the capacity to perform all enzymatic activities required for RNA synthesis, including RNA-dependent RNA-polymerization, capping and methyltransferase activities (Poch et al., 1990; Yuan et al., 2022).

**Glycoprotein (GP):** The EBOV *GP* gene encodes four proteins: GP, secreted GP (sGP), small secreted GP (ssGP), and Δ-peptide (Figure 1.5) (Mehedi et al., 2011; Sanchez et al., 1996; Volchkov et al., 1995; Volchkova et al., 1999), which is achieved by transcriptional editing (Feldmann et al., 2001) performed by the L protein. The primary gene product is sGP, the product of unedited GP mRNA. Transmembrane GP, the form that sits on the virion surface, is translated from edited mRNA resulting from the addition of a single adenosine nucleotide to the editing site. The deletion of one or insertion of two adenosine nucleotides allows for a switch to a third open reading frame, generating ssGP (Feldmann et al., 2001). This RNA editing mechanism is both a mechanism for host

evasion as well as a means to modulate GP expression levels for optimal virus production and infectivity (Mohan et al., 2015).

sGP is produced as pre-GP and transported to the Golgi apparatus where it is glycosylated and converted by proteolysis to mature sGP and Δ-peptide (Feldmann et al., 2001). sGP forms disulphide-linked homodimers, which act as a decoy antigen resulting in antigenic subversion (Mohan et al., 2012). Δ-peptide has viroporin activity, giving it enterotoxic activity (He et al., 2017; Melnik et al., 2022). ssGP is secreted in monomeric form and its role in EVD pathogenesis remains unclear.

Full-length GP comprises 676 amino acids and is produced as pre-$GP_0$. Pre-$GP_0$ undergoes a series of processing events in the endoplasmic reticulum, including signal peptide removal, N-glycosylation, and oligomerization. This is followed by acylation, O-glycosylation and maturation of the N-glycans in the Golgi apparatus. Finally, pre-GP is cleaved by the protease, furin, to GP1 and GP2 (reviewed in (Feldmann et al., 2001)). GP1 and GP2 form a heterodimer linked by a C53-C609 disulfide bond and non-covalent interactions (Bale et al., 2012; Jeffers et al., 2002; Lee & Saphire, 2009). On the surface of EBOV particles, the GP1-GP2 heterodimer forms a trimer, GP. GP1 is responsible for cell surface attachment and receptor-binding, and bears most of the glycosylation in the glycan cap and mucin-like domain. GP2 drives fusion of the viral and host membranes. It is worth noting that high levels of GP expression result in rounding and detachment of cells and downregulates cell surface protein expression (Francica et al., 2009; Simmons et al., 2002; Yang et al., 2000). EBOV modulates the amount of GP being produced by employing transcriptional editing of the *GP* gene (Feldmann et al., 2001) and hijacking the proteostasis mechanism of the cell, triggering GP misfolding and degradation when GP levels become high (J. Zhang et al., 2022).

There is an additional soluble form of GP, shed GP, which is generated by cleavage of membrane-bound trimeric GP by the cellular zinc-dependent metalloprotease TACE. Shed GP acts as a decoy antigen by blocking neutralizing antibodies (Dolnik et al., 2004). Shed GP also contributes to the dysregulated

inflammatory response in EVD by inducing non-infected dendritic cells and macrophages to release pro- and anti-inflammatory cytokines and affect vascular permeability (Escudero-Pérez et al., 2014; Scherm et al., 2022).

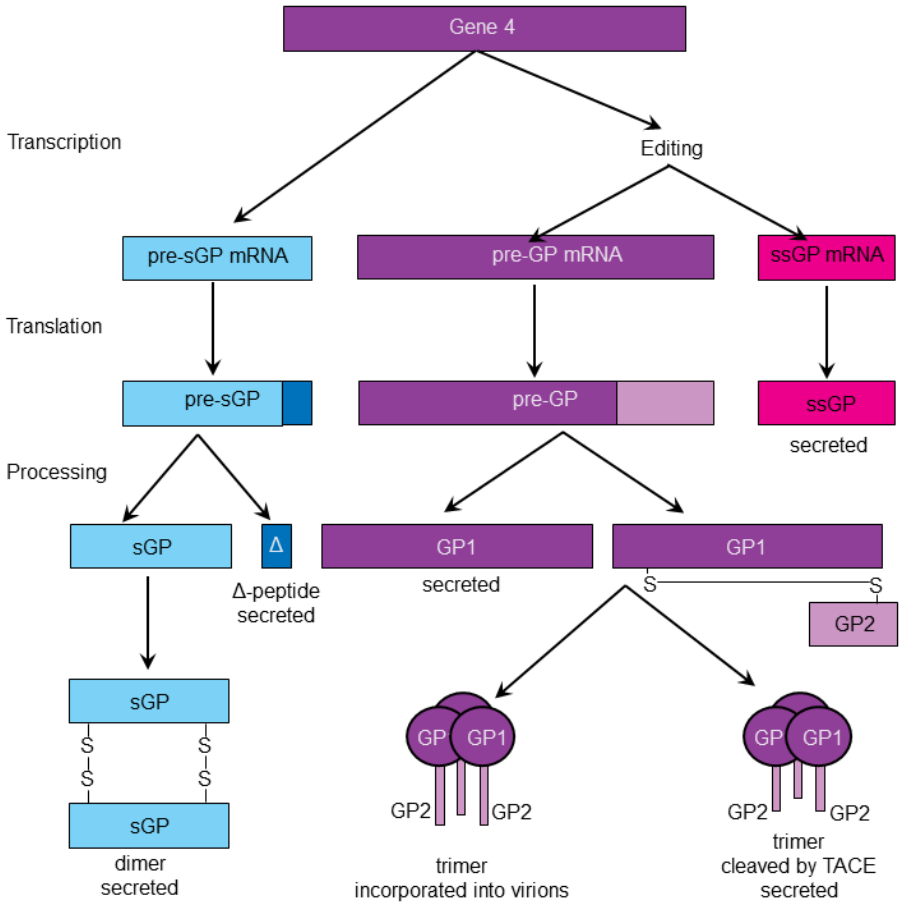


**Figure 1.5. Forms of Ebola virus glycoproteins.** Gene 4 encodes three forms of GP through a co-transcriptional editing mechanism. Soluble GP (sGP), the main transcription product, is synthesized as pre-sGP. Subsequent cleavage with furin produces sGP and Δ-peptide, both of which are secreted from cells. Alternative transcriptional editing results in the production of ssGP. A third transcriptional editing events results in the production of full-length GP, which is cleaved by furin to form two subunits, GP1 and GP2. GP1 and GP2 remain associated by a disulfide bond, forming a heterodimer, which trimerizes prior to incorporation into the cell surface in preparation for viral budding. Cleavage of GP at the cell surface by the zinc metalloprotease TACE generates shed GP. Figure created by Kathryn Schornberg. Used with permission from her thesis (Figure 1.3).

### 1.3.3. Replication cycle

The EBOV replication cycle (Figure 1.6) is typical for a negative-sense RNA virus. The cycle begins with EBOV attachment to various host factors, including lectins (DC-SIGN, L-SIGN), TYRO3 receptor family members and the PS-binding receptor, TIM1 (Hoenen et al., 2019), none of which are strictly necessary for attachment. The virus is then internalized into the host cells by macropinocytosis and transported into endosomes (Aleksandrowicz et al., 2011; Nanbo et al., 2010). In the endosome system, GP is cleaved by host cathepsins producing the fusion-competent $GP_{cl}$, which interacts with the EBOV endosomal receptor NPC1, after which fusion of viral and endolysosomal membranes occurs (Carette et al., 2011; Côté et al., 2011; E. H. Miller et al., 2012; Ng et al., 2014). The final fusion trigger for membrane fusion has not yet been identified, as discussed further in Chapter 2. Upon fusion, the ribonucleoprotein (RNP) complex is released into the cytoplasm. The RNP complex comprises the RNA genome, NP, VP30, VP35 and L. While the details of the uncoating process are poorly understood, it has been proposed that VP24 dissociation from the RNP complex relaxes the rigid nucleocapsid packing making it transcription- and replication-competent (Banadyga et al., 2017; Watt et al., 2014). Primary transcription occurs in the cytoplasm and is facilitated by the RNP complex proteins brought into the cell. The viral mRNAs are translated into proteins by host ribosomes. The newly synthesized proteins form inclusion bodies in which further secondary transcription and genome replication occurs, producing more viral genomic RNA from the complementary positive sense RNA. Genome transcription is mediated by all of the proteins in the RNP (Hoenen et al., 2019). The balance between replication and transcription is modulated by the phosphorylation status of VP30, supporting transcription in its non- or weakly phosphorylated state (Biedenkopf et al., 2016). VP24 binds to the newly formed RNP complexes, condensing them for efficient genome packaging (Banadyga et al., 2017; Watt et al., 2014). The nucleocapsids are then transported to the plasma membrane in an actin-dependent manner (Schudt et al., 2015). VP40 is also transported to the cell surface. Meanwhile, GP is post-translationally modified in the endoplasmic reticulum

and Golgi apparatus, producing O- and N-glycosylated GP (Hoenen et al., 2019). GP is transported to VP40 sites near the plasma membrane. VP40 directs virion assembly and egress through its interactions with several host factors including the endosomal sorting complex required for transport (ESCRT) machinery (Gordon et al., 2019). Additionally, VP40 induces PS clustering, which in turn facilitates optimal VP40 oligomerization (Husby et al., 2022). Lastly, GP interacts with host scramblases, resulting in their incorporation into budding virions where they mediate exposure of PS on the outer leaflet of the virion membrane (Nanbo et al., 2018). Exposure of PS is critical to the infectivity of EBOV progeny (Tang et al., 2022).

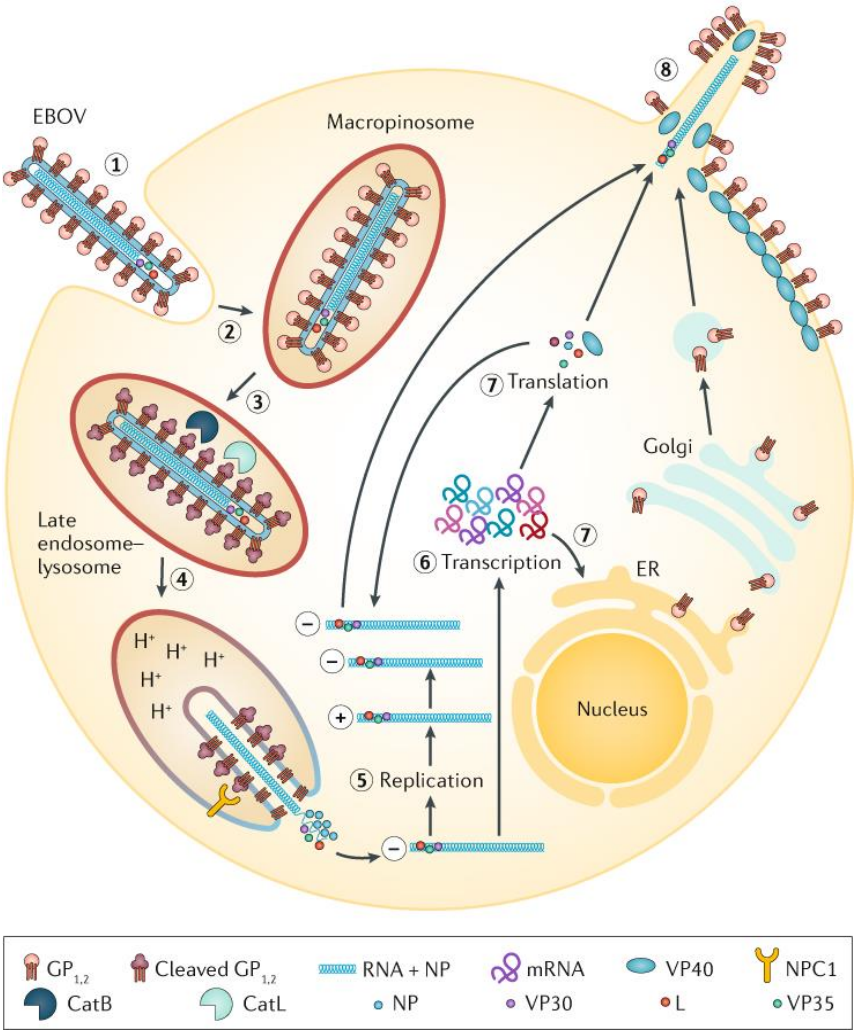


**Figure 1.6. Ebola virus replication cycle.** Ebola virus has a 19-kb single-stranded negative-sense RNA genome that encodes seven structural proteins: nucleoprotein (NP), polymerase cofactor (VP35), matrix protein (VP40), glycoprotein (GP), transcriptional activator (VP30), nucleocapsid-associated protein (VP24) and large protein (L). Adapted from Jacob et al., 2020 and Kuhn et al., 2019. B. Ebola virus (EBOV) binds to attachment factors and receptors on the cell surface through the viral spike protein, glycoprotein (GP) (1). The virus is then internalized via macropinocytosis (2) and trafficked to an endosomal compartment. Cysteine proteases cathepsin B (CatB) and cathepsin (CatL) in endosomes digest GP1 to a 19-kDa form (3), exposing the receptor-binding domain of GP1. The exact type of endosome wherein GP is cleaved has not yet been established. Primed GP1 interacts with the EBOV receptor NPC1, after which GP2-mediated fusion of the viral and endosomal membranes is triggered (4). After fusion, the viral nucleocapsid is released into the cytoplasm, where the genome is replicated (5) and transcribed (6) with the aid of the viral proteins VP35, VP30 and L, and viral mRNAs are then translated (7). mRNAs encoding GP are brought to the endoplasmic reticulum (ER), where GP is

synthesized, modified with *N*-linked sugars and trimerized. GP is further modified in the Golgi and delivered to the plasma membrane in secretory vesicles. The other viral proteins (VP24, VP35, VP30, VP40 and L) and the ribonucleoprotein complex (RNA with nucleoprotein) are transported to the plasma membrane where virion budding occurs (8). Adapted from (Jacob et al., 2020).

## 1.4 EBOV entry

EBOV entry into host cells comprises a series of carefully choreographed events that can be divided into five steps: (i) attachment to the host cell surface, (ii) internalization, usually by macropinocytosis, and trafficking through the endocytic pathway to endolysosomes, (iii) priming of GP by host cysteine proteases, followed by (iv) binding to host receptor, NPC1, and (v) fusion of viral and endosomal membranes culminating with the delivery of the nucleocapsid into the cytoplasm.

### 1.4.1 Attachment to the cell surface

EBOV initially attaches to the cell surface through nonspecific interactions with various plasma membrane proteins. EBOV can bind to at least two types of host cell surface receptors: carbohydrate-binding receptors and phosphatidylserine (PS) receptors. EBOV host factor usage is highly promiscuous, with none of the cell attachment factors identified thus far being explicitly essential for filoviral infection across cell types. Indeed, overexpression of any of several EBOV attachment-promoting factors rendered an unsusceptible cell line susceptible to infection with EBOV (Zapatero-Belinchón et al., 2019).

The N- and O-linked glycans on EBOV GP bind to two groups of carbohydrate-binding receptors, which are C-type lectins and glycosaminoglycans. Five structurally related C-type lectin receptors have been shown to interact with EBOV GP and enhance infection: dendritic cell-specific ICAM-3-grabbing non-integrin (DC-SIGN) (Alvarez et al., 2002; Baribaud et al., 2002; Lasala et al., 2003; Lin et al., 2003; Marzi et al., 2007; Peng

et al., 2022); liver/lymph node-specific ICAM-3 grabbing non-integrin (L-SIGN) (Alvarez et al., 2002; Marzi et al., 2007); lymph node sinusoidal endothelial cell C-type lectin (LSECTin) (Gramberg et al., 2005; Powlesland et al., 2008); asialoglycoprotein receptor 1 (ASGPRI) (Lin et al., 2003); and human macrophage galactose- and acetylgalactosamine-specific C-type lectin (hMGL) (Takada et al., 2004). Recently, EBOV entry into dendritic cells was shown to require the I-type lectin, Siglec-1 (sialic acid-binding Ig-like lectin 1), which recognizes sialylated gangliosides on the EBOV membrane (Perez-Zsolt et al., 2019).

EBOV GP has recently been reported to bind to glycosaminoglycans (O'Hearn et al., 2015; Salvador et al., 2013; Tamhankar et al., 2018). Glycosaminoglycans are linear, anionic heteropolysaccharides, usually attached to a core protein and are exemplified by heparin and heparan sulfate (Kamhi et al., 2013). The degree of sulfation and the structure of the carbohydrate backbone affects the EBOV GP-glycosaminoglycan interaction (Salvador et al., 2013). Moreover, knockdown of exostosin 1, a glycosyltransferase involved in the biosynthesis of heparan sulfate, impaired GP-mediated entry (O'Hearn et al., 2015).

EBOV can also exploit the host apoptotic clearance machinery through PS-dependent binding to attach to host cells. Of the known PS-binding receptors, the TAM (Tyro3, Axl and Mer) family of receptor tyrosine kinases (Dahlmann et al., 2015; Shimojima et al., 2006) and T-cell immunoglobulin and mucin domain 1 receptors TIM-1 and TIM-4 (Dahlmann et al., 2015; Jemielity et al., 2013; Kondratowicz et al., 2011; Moller-Tank et al., 2013; Rhein et al., 2016) have been implicated in filovirus entry. A hallmark of apoptosis is exposure of PS on the external leaflet of the plasma membrane. Outside of EBOV infection, the PS receptors are involved in clearance of PS-enriched apoptotic cells. EBOV masquerades as apoptotic debris in a mechanism referred to as apoptotic mimicry. This route of entry is advantageous as EBOV can gain entry into cells while also dampening the host immune response (Amara & Mercer, 2015). Additionally, phosphatidylethanolamine (PE), another phospholipid that is exposed during apoptosis in certain cell types, is also a ligand for TIM-1 and can facilitate EBOV entry (Richard et

al., 2015). While TIM receptors directly interact with PS (Freeman et al., 2010), TAM-family receptors bind PS indirectly via growth arrest specific gene 6 (Gas6) or protein S (Morizono et al., 2011).

EBOV associates with cholesterol- and sphingomyelin-rich microdomains (previously called lipid rafts) at the cell surface (Bavari et al., 2002; Jin et al., 2020). Further, acid sphingomyelinase, which cleaves sphingomyelin to phosphocholine and ceramide, is important for EBOV entry (M. E. Miller et al., 2012). Accumulation of ceramide in cellular membranes results in the formation of ceramide-enriched membrane platforms that have altered biophysical properties. These platforms trap and, hence, cluster receptor molecules. Receptor clustering may result in the increased association with intracellular signaling molecules, thereby facilitating signal transduction that would initiate macropinocytosis (Zhang et al., 2009).

### 1.4.2 Internalization and trafficking through endocytic pathway

Following attachment to the cell surface, EBOV is internalized mainly through macropinocytosis (Nanbo et al., 2010). There is evidence that in some cases EBOV is taken up via clathrin- (Aleksandrowicz et al., 2011; Bhattacharyya et al., 2010) and caveolae-mediated endocytosis (Empig & Goldsmith, 2002; Sanchez, 2007). Macropinocytosis is an actin-dependent process initiated with plasma membrane ruffling, which leads to formation of protrusions that fall back onto the plasma membrane generating large, irregular-shaped vacuoles called macropinosomes (Mercer & Helenius, 2009). EBOV internalization is dependent on actin function; inhibition of actin polymerization reduces EBOV entry and infection (Nanbo et al., 2010; Saeed et al., 2010). Macropinocytosis depends on several host factors, including cellular kinases, phospholipases, Rho GTPases, and $Na^+/H^+$ exchangers, all of which have been implicated in EBOV entry (Davey et al., 2017). The initial stimulus for macropinocytosis is the activation of receptor tyrosine kinases (RTK). Indeed, EBOV activates RTKs via interaction with TAM molecules (Hunt et al., 2011; Kuroda et al., 2020), which in turn

leads to the activation of the PI3K/Akt (Aleksandrowicz et al., 2011; Nanbo et al., 2010; Saeed et al., 2008; Stewart et al., 2021) and phospholipase C pathways (Hunt et al., 2011) as well as $Na^+/H^+$-exchanger activity (Aleksandrowicz et al., 2011). Of note, while interaction with TAM molecules occurs via PS in the viral membrane, EBOV GP is necessary for macopinocytotic uptake (Mulherkar et al., 2011; Nanbo et al., 2010). Subsequent actin remodeling, which is required for membrane ruffling and dependent on Rho GTPases including RhoB, Cdc42 and Rac1, as well as Arp2 complexes, is essential for EBOV entry (Nanbo et al., 2010; Quinn et al., 2009; Saeed et al., 2010). Finally, the macropinosome is formed by a single membrane fission event. The closure of macopinosomes is modulated by carboxy-terminal-binding protein-1/brefeldin A-ADP ribosylated substrate (CtBP/BARS), which is activated by the kinase, Pak1 (Mercer & Helenius, 2009). Disruption of Pak1 and CtBP/BARS function in cells reduced EBOV uptake and infection (Nanbo et al., 2010).

Once they detach from the plasma membrane, the macropinosomes move deeper into the cytoplasm. They undergo acidification and mature similarly to endosomes, with the same early and late endosome markers, Rab5 and Rab7, respectively (Mercer & Helenius, 2009). Rab5 and Rab7 are small GTPases that regulate vesicular transition from early to late endosomes and from late endosomes to lysosomes, respectively (Davey et al., 2017). Indeed, EBOV entry and infection is dependent on Rab5 and Rab7 function (Nanbo et al., 2010).

Other cellular host factors involved in maturation and fusion of late endocytic compartments have been implicated in EBOV entry. The homotypic fusion and protein sorting (HOPS) complex as well as its regulator, UV radiation resistance-associated gene (UVRAG), are required for efficient viral entry (Bo et al., 2020; Carette et al., 2011). PIKfyve-ArPIKfyve-Sac3 complex, which is primarily localized at endosomal membranes, is also critical for EBOV entry (Carette et al., 2011; Kang et al., 2020; Nelson et al., 2017; Qiu et al., 2018). PIKfyve (phophoinositide kinase, FYVE-type zinc finger containing) kinase activity is thought to be activated by initial EBOV activation of PI3k/Akt pathway via RTK interaction (Stewart et al., 2021). PIKfyve facilitates the production of

phosphatidylinositol (3,5) bisphosphate ($PI(3,5)P_2$), which plays a role in endosome ion homeostasis by regulating ion channels, e.g., , two-pore channels (TPC) (Dong et al., 2010). TPCs are calcium channels that are important for EBOV entry (Du et al., 2022; Sakurai et al., 2015; Simmons et al., 2016; Spence et al., 2016). The role of calcium in EBOV entry goes beyond efficient endosome maturation. Calcium interacts with EBOV GP2 inducing conformational changes that enhance membrane fusion (Das et al., 2020; Nathan et al., 2020).

### 1.4.3 Proteolytic processing of GP

EBOV GP, like other class I viral proteins, undergoes a priming event to render it responsive to its fusion trigger (White & Whittaker, 2016). GP is initially cleaved by furin, a ubiquitous subtilisin-like endoprotease, during GP biosynthesis, yielding GP1 and GP2, which remain covalently bound via a disulfide bridge (Volchkov et al., 1998; Wool-Lewis & Bates, 1999). Furin processing of GP is, however, not essential for EBOV infection as priming can occur on incoming particles with GP lacking a furin cleavage site (Wool-Lewis & Bates, 1999). In either case, GP1 is further cleaved by cathepsins B and L (CatB and CatL) (Chandran et al., 2005; Kaletsky et al., 2007; Schornberg et al., 2006), endosomal proteases that are optimally active at low pH (Turk et al., 2012). Both CatB and CatL are endopeptidases, with CatB also possessing carboxydipeptidase activity (Turk et al., 2012). Cathepsin cleavage removes the heavily glycosylated glycan cap and mucin-like domain of GP1, generating fusion-competent $GP_{cl}$, which comprises 19-kDa GP1 and GP2 (Figure 1.7) (Bale et al., 2011; Chandran et al., 2005; Dube et al., 2009; Hood et al., 2010; Schornberg et al., 2006). The extensive proteolytic processing of GP serves two roles: exposing the receptor-binding domain, allowing $GP_{cl}$ to interact with NPC1 (Bale et al., 2011; Bornholdt et al., 2016; E. H. Miller et al., 2012; Wang et al., 2016) and potentiating fusion-relevant GP for subsequent conformational changes (Brecher et al., 2012). This is likely due to the proteolytic removal of the β13-β14 loop, which overlies the fusion loop in GP2 to prevent premature release of the fusion loop (Lee et al., 2008; Wang et al., 2016). While priming of GP is required for EBOV entry, it is

insufficient to induce large-scale conformational changes in the pre-fusion state of GP (Bale et al., 2011). Although cathepsin cleavage of GP renders it fusion-competent, entry of $GP_{cl}$-bearing viruses is still sensitive to a broad-spectrum cysteine protease inhibitor, E-64d, as well as agents that raise endosomal pH, suggesting a need for additional cathepsin-dependent cleavage downstream of the initial cleavage event (Mingo et al., 2015; Spence et al., 2016). Hence, endoproteolytic cleavage of GP1 in the β13-β14 loop (residues 190-213) may be mediated by CatB or CatL, followed by CatB-mediated carboxydipeptidase cleavage of additional residues to generate 19-kDa GP1. An ill-defined additional cysteine protease cleavage may also be needed (further discussed in Chapter 2).

Cleavage of GP is necessary for entry of all filoviruses, but dependence of filoviruses on individual proteases differs (Misasi et al., 2012; Ng et al., 2014). EBOV entry into Vero cells and human dendritic cells is dependent on CatB, but not CatL (Chandran et al., 2005; Martinez et al., 2010; Schornberg et al., 2006). TAFV entry is also strongly CatB-dependent, while SUDV, RESTV, LLOV and MARV GP-mediated entry has a reduced requirement for CatB activity (Marzi et al., 2012; Misasi et al., 2012; Ng et al., 2014; Wong et al., 2010). The molecular basis for these differences in cathepsin preference remain to be determined.

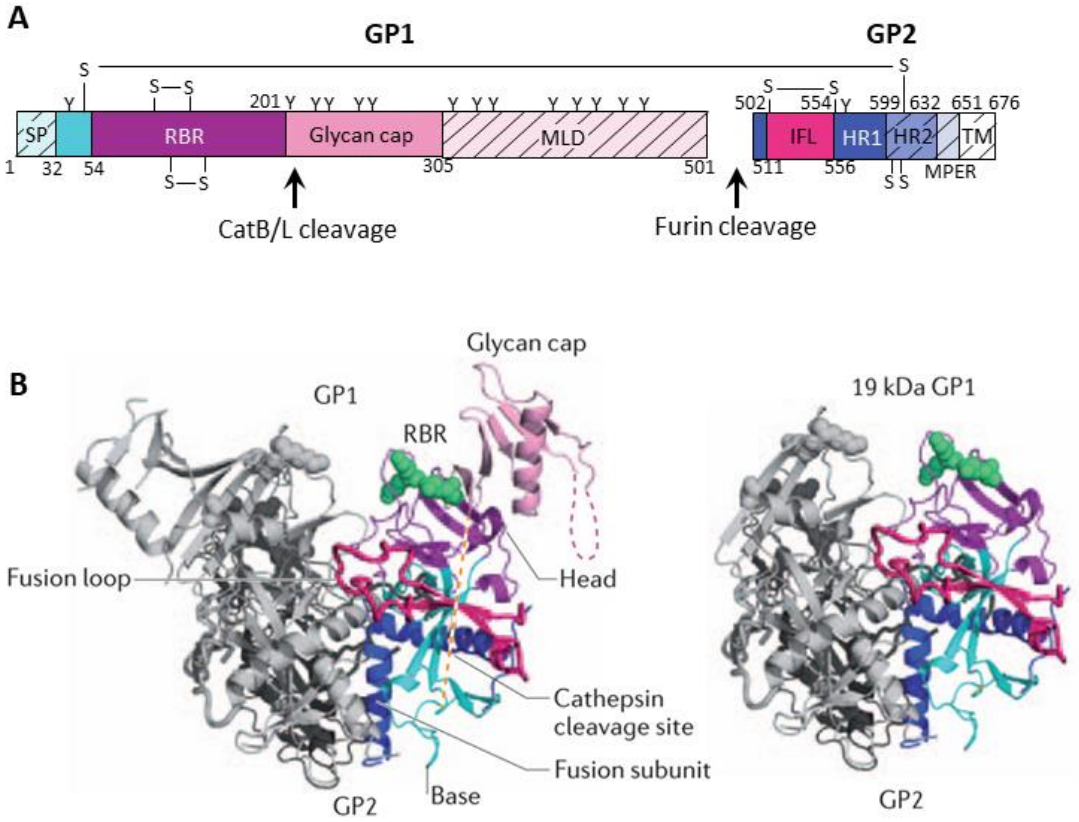


**Figure 1.7. Structure of EBOV GP. A.** Domain schematic of EBOV GP. SP - signal peptide, RBR - receptor-binding region, MLD - mucin-like domain, IFL - internal fusion loop, HR1 - heptad repeat 1, HR2 - heptad repeat 2, MPER - membrane-proximal external region, TM - transmembrane domain. The Y symbols indicate the predicted N-linked glycosylation sites. The hatched regions designate regions that are not in the crystal structure. **B.** Structures of the ectodomain of EBOV GP pre-fusion trimer without the mucin-like domain (PDB: 3CSY) and a model of proteolytically primed GP, $GP_{cl}$. The $GP_{cl}$ model assumes no conformational changes occur from cathepsin cleavage. One monomer of the trimer is shown in color, and the other two are grey. The green spheres represent Lys114, Lys115 and Lys140 in the RBR; mutations of these residues impair binding of $GP_{cl}$ to NPC1. Figure 1.7B from (White & Schornberg, 2012).

### 1.4.4 Interaction of GP with intracellular host receptor, NPC1

Exposure of the receptor-binding domain of GP following cathepsin cleavage of the glycan cap and mucin-like domain allows the virus to bind to its endosomal receptor,

Niemann-Pick type C protein 1 (NPC1) (Jan E. Carette et al., 2011; Côté et al., 2011). NPC1 is a large 13-pass transmembrane protein that is localized to the limiting membrane of endolysosomes. Besides the transmembrane regions, NPC1 has three large luminal domains, A, C, and I (Davies & Ioannou, 2000). NPC1 is involved in cholesterol homeostasis in the cell by facilitating cholesterol export from lysosomes (Kwon et al., 2009). Of note, NPC1 is required for entry of most filoviruses (Jan E. Carette et al., 2011; Côté et al., 2011; Goldstein et al., 2018; Ng et al., 2014; Yang et al., 2019). It is not yet known if the recently identified piscine filoviruses, Huángjiāo virus and Xīlǎng virus, also require NPC1 for entry.

Proteolytically primed EBOV $GP_{cl}$, but not uncleaved GP, binds directly with domain C of NPC1 (NPC1-C) (Krishnan et al., 2012; E. H. Miller et al., 2012). While NPC1-C is minimally sufficient for GP binding, EBOV infection is more efficient with full-length NPC1, implying direct or indirect contributions from the other parts of the protein (E. H. Miller et al., 2012). Moreover, NPC1 mutational studies showed that NPC1's cholesterol trafficking function can be decoupled from its role as a filoviral entry factor (Côté et al., 2011; Herbert et al., 2015). Structures of the $GP_{cl}$:NPC1-C and $GP_{cl}$:NPC1 complex allowed for further elucidation of the nature of the interaction (Gong et al., 2016; Han Wang et al., 2016). These structures revealed that two loops in NPC1-C engage with a hydrophobic cavity in the head of $GP_{cl}$. Interestingly, these loops are also required for binding to NPC2, a soluble lysosomal protein involved in cholesterol homeostasis (Li et al., 2016), suggesting that the $GP_{cl}$:NPC1-C interaction evolved as a form of molecular mimicry (Davey et al., 2017). The basis for requirement of $GP_{cl}$:NPC1 binding is still unclear but a number of non-mutually exclusive hypotheses have been proposed (Miller & Chandran, 2012; Han Wang et al., 2016; White & Whittaker, 2016). NPC1-binding may play a role in directing EBOV to the limiting membrane of the endolysosome (and away from the small vesicles within endoslysosomes). NPC1 may also induce conformational changes that are critical for membrane fusion initiation.

NPC1 has been shown to contribute to EBOV host tropism and species-specific susceptibility. The presence of phenylalanine at position 502 (instead of aspartate) in

cells from African straw-colored fruit bats (*Eidolon helvum*) renders the cells refractory to EBOV infection (Ng et al., 2015). Further, cells from a snake, Russell's viper (*Daboia ressullii*), are resistant to EBOV entry and infection due to the presence of a tyrosine residue (instead of phenylalanine) at position 503 in NPC1-C (Ndungo et al., 2016). Indeed, investigation of the evolution of *NPC1* in bats revealed that some residues involved in the $GP_{cl}$:NPC1-C interaction are under positive selection in mammals (Ng et al., 2015; Pontremoli et al., 2016). These findings suggest that filovirus-dependent positive selection of *NPC1* in mammals drove the evolution of NPC1-C.

### 1.4.5 EBOV-host membrane fusion

NPC1-bound GP is proposed to undergo a series of conformational rearrangements that culminate with the fusion of the viral and host endolysosomal membranes, delivering the nucleocapsid to the cytoplasm (White & Whittaker, 2016). As discussed above, the fusion cascade is primed by relaxation of the structural constraints on the fusion loop in GP2, which is achieved by the CatB/L removal of the mucin-like and glycan cap domains. Primed GP binds to NPC1 inducing conformational changes that likely make the release of the fusion loop more facile (Wang et al., 2016). Low endosomal pH is required not only for optimal proteolytic priming of GP but also plays a direct role in $GP_{cl}$-mediated fusion. The low pH induces a conformational change in the fusion loop, which in turn enhances membrane insertion and triggers the fusion activity of the fusion loop (Gregory et al., 2011; Gregory et al., 2014; Lee et al., 2016). Additionally, low pH stabilizes the post-fusion conformation of EBOV GP2 (Harrison et al., 2013). $Ca^{2+}$ is also critical for EBOV entry. Blocking calcium transport channels, two-pore channels, inhibits EBOV infection (Sakurai et al., 2015). These channels likely create a high local concentration of $Ca^{2+}$ near the limiting membrane, promoting EBOV GP-mediated fusion. $Ca^{2+}$ induces additional conformational changes in the fusion loop that enhance membrane fusion (Das et al., 2020; Nathan et al., 2020). $Ca^{2+}$ interacts with negatively charged residues in GP2, D522 and E540 (Nathan et al., 2020), thereby neutralizing them, which in turn may trigger the release of the fusion loop from the

hydrophobic cleft in which it resides (Das et al., 2020). Using a virus-liposome lipid mixing assay and single-molecule Förster resonance energy transfer (smFRET)-imaging, Munro and coworkers show that low pH, $Ca^{2+}$, and NPC1-C synergistically induce fusion-relevant conformational changes in GP2 (Das et al., 2020).

The final fusion trigger for EBOV remains incompletely defined. Thus far, attempts to reconstitute EBOV $GP_{cl}$-catalyzed full fusion to cells have been unsuccessful (Fénéant et al., 2019; E. H. Miller et al., 2012). EBOV entry is remains sensitive to the broad cysteine protease inhibitor, E-64d (E. H. Miller et al., 2012; Schornberg et al., 2006), suggesting that additional proteolytic cleavage of NPC1-bound $GP_{cl}$ or an endosomal protein is required for a full membrane fusion reaction. Moreover, *in vitro* treatment with mildly reducing agents induced $GP_{cl}$, but not unprimed GP, to bind to liposomes, indicating that reduction of the GP1-GP2 intersubunit disulfide bond by an undetermined mechanism may be involved in fusion (Brecher et al., 2012).

## 1.5 Methods for studying virus entry

EBOV requires high biosafety level 4 (BSL-4) confinement, making it difficult to study the authentic virus. An alternative approach to studying dangerous pathogens like EBOV is the use of pseudotyped viruses, which can be safely handled under BSL-2 laboratory conditions. The term “pseudotype” was first used to describe the genetically defective Rous sarcoma virus bearing the surface envelope protein of avian leukosis helper virus (Rubin, 1965). A pseudotyped virus, or pseudovirus, refers to a viral particle comprising a virus core/backbone surrounded by a cell-derived membrane with envelope proteins from a different virus (Q. Li et al., 2018). The genome of the parent virus is modified to prevent generation of infectious progeny viruses. There are three common pseudovirus packaging systems that have been used to study EBOV entry: lentiviral (HIV), retroviral (murine leukemia virus, MLV), and vesicular stomatitis virus (VSV) packaging systems (reviewed in (Q. Li et al., 2018)).

Commonly used bulk assays for studying virus fusion and entry, including virus-liposome fusion, cell-cell fusion, infectivity, and virus-liposome co-flotation assays, provide valuable information on the membrane fusion and entry process. However, the timescales are measured in tens of seconds or minutes and the data are limited to the average of an ensemble. Single virus tracking microscopy techniques in cells and with membrane surrogates can offer more details on the intermediate steps of virus entry. These techniques are typically based on fluorescence imaging, with the most commonly employed microscope configurations being epifluorescence, confocal, and total internal reflection fluorescence (TIRF) microscopy (Nathan & Daniel, 2019). In order to visualize them, virions are labeled (at their membranes and/or in their interiors) with organic dyes, quantum dots, or fluorescent proteins (S.-L. Liu et al., 2020). Membrane hemi and full fusion can be monitored with the use of lipophilic dyes, e.g., long chain carbocyanine dyes such as DiD, DiI and DiO. Fusion pore formation is typically identified by monitoring the release of a fluorescent label out of the interior of the virus (Floyd et al., 2008).

TIRF microscopy is useful for the study of virus binding, hemifusion, initial fusion pore formation, and completion of fusion with biomimetic membranes in the form of supported lipid bilayers (SLBs). The composition of these bilayers can vary since they can be prepared using liposomes, proteoliposomes or cell plasma membrane blebs (Nathan & Daniel, 2019). For the more complex SLBs with membrane proteins, a polymer cushion may be included to maintain mobility (Wagner & Tamm, 2000). SLBs provide a versatile platform to probe various aspects of virus entry. For instance, kinetic analysis of influenza HA-driven fusion revealed that three HA molecules are required to mediate hemifusion (Floyd et al., 2008). West Nile Virus requires at least two adjacent trimers to catalyze hemifusion (Chao et al., 2014), while vesicular stomatitis virus requires a cluster of four trimers (Kim et al., 2017). In another application of planar supported lipid bilayers, SLBs prepared from plasma membrane blebs have been used to examine the effect of restriction factors, Serinc, on HIV fusion (Ward et al., 2020) and to ascertain the

membrane phase preferences of HIV receptors and thereby the HIV entry site at the plasma membrane (Yang et al., 2017).

Studying fusion of endosome-entering viruses in intact cells can be challenging, since it is difficult to control fusion within living cells. An open, cell-free system with endosomal membranes in which fusion can be measured in a controllable manner would be beneficial. To this end, Kasson and coworkers (Haldar et al., 2020) developed a strategy to measure single-virus fusion in endosomes. They isolated influenza virus-containing endosomes from BHK-21 cells, immobilized them and controllably triggered fusion. Their findings indicate that endosome membrane deformability, and not curvature, affects fusion kinetics.

## 1.6 Research Goals and Significance

As alluded to above, many aspects of the late stages of EBOV entry into cells are currently not known and debated in the field. Therefore, the primary aim of my thesis research was to develop methods to provide further insight into the molecular processes that govern the late stages of EBOV entry. To this end, we developed an *in vitro* fluorescence assay, comprising planar supported membranes derived from NPC1-bearing endosomes as target membranes (Chapter 2). We call these membranes SPEMs, standing for supported planar endosomal membranes. The assay was validated by recapitulating the known pH dependencies of other pH-dependent, enveloped viruses: influenza and Lassa. We were then able to reconstitute EBOV GP-mediated fusion with SPEMs and pseudoviruses bearing Ebola GP. We subsequently used the system to examine the effect of adding cathepsins to the system. Surprisingly, the fusion efficiency of EBOV GP-bearing pseudoviruses exposed to low pH and $Ca^{2+}$ was high without the addition of cathepsins. Reasoning that the SPEMs may retain cathepsins we next included the cysteine cathepsin inhibitor, E-64d, in the assay, and in agreement with previous findings, there was reduced fusion efficiency, suggesting the SPEMs retain cathepsin activity. Collectively the findings discussed in Chapter 2 provide evidence that

cathepsin action is required not only for the initial proteolytic activation of GP to $GP_{cl}$ but also for a further activation step after the binding of viral particles to the endosomes for optimal EBOV GP-mediated full fusion. The broader significance of this work is that this system could also be used for the study of other enveloped, and perhaps even non-enveloped, viruses that enter through endosomes.

There is growing evidence that membrane properties of both viral and target membranes play a role in virus entry. In Chapter 3, we examine the role of cholesterol in EBOV entry as well as probe for any direct interaction between EBOV GP and cholesterol. We found that cholesterol enhances membrane fusion, and that GP does interact with cholesterol via its MPER/TM domains.

In an effort to examine the basis for increased infectivity of the A82V EBOV GP variant in the 2014-2016 Ebola Outbreak in West Africa (Diehl et al., 2016; Urbanowicz et al., 2016; Wang et al., 2017), we sought obtain the crystal structure of primed A82V EBOV GP in complex with NPC1-C (Chapter 4). The proteins did not co-crystallize; rather NPC1-C crystallized alone. We thus obtained a new crystal structure of NPC1-C, contributing to an existing body of work on NPC1-C.

# Chapter 2. An in vitro system for studying virus fusion with endosomal membranes and a possible new role for cathepsin B in Ebola virus glycoprotein activation

Laura Odongo, Betelihem Habtegebrael, Volker Kiessling, Judith M. White, Lukas K. Tamm

*Manuscript in preparation*

My contribution to this work includes preparation and characterization of endosomes and subsequent supported planar endosomal membranes, the preparation of recombinant influenza virus and Lassa and Ebola pseudoviruses, all fusion and infectivity experiments with these viruses, as well as the data analysis of all single-particle fusion experiments.

## 2.1 Abstract

Ebola virus (EBOV) causes a hemorrhagic fever associated with fatality rates up to 90%. The EBOV entry process is complex and incompletely understood. Following attachment to host cells, EBOV is trafficked to late endosomes/lysosomes where its glycoprotein (GP) is processed to a 19-kDa form, allowing the glycoprotein to bind to its intracellular receptor Niemann-Pick C1. We previously showed that the cathepsin protease inhibitor, E64d, blocks infection by pseudovirus particles bearing 19-kDa GP, suggesting that further cathepsin action is needed to trigger fusion. This, however, has not been demonstrated directly. Since 19-kDa Ebola GP fusion occurs in late endosomes, we devised a system in which enriched late endosomes are used to prepare supported planar endosomal membranes (SPEMs) and fusion of fluorescent (pseudo)virus particles

is monitored by TIRF microscopy. We validated the system by demonstrating the pH dependencies of influenza virus HA- and Lassa virus GP-mediated fusion. Using SPEMs, we next showed that fusion mediated by 19-kDa Ebola GP is dependent on low pH and enhanced by $Ca^{2+}$, consistent with other studies. We further showed that addition of cathepsins (somewhat more prominently with cathepsin B than L) augments both hemi- and full fusion. Subsequently we found that SPEMs appear to retain cathepsin activity, and that E-64d inhibits full fusion mediated by 19-kDa GP. Hence, we provide both gain- and loss-of-function evidence that further cathepsin action enhances the fusion activity of pre-primed 19-kDa Ebola GP. Thus, we have provided new evidence for how Ebola GP mediates fusion with endosomes, and we have developed a novel approach employing SPEMs that can now be used for studies of any virus that fuses in endosomes.

## 2.2 Introduction

Ebola virus (EBOV), a negative-sense, single-stranded RNA virus belonging to the Ebolavirus genus within the *Filoviridae* family, causes a hemorrhagic fever associated with fatality rates of up to 90% (de La Vega et al., 2015). EBOV infections continue to be a major threat to human health, particularly in parts of Central and West Africa. There are currently three approved vaccines against EBOV: Ervebo (FDA-approved) (FDA, 2019), Zabdeno/Mvabea (approved for medical use in the EU) (EMA, 2020a, 2020b), and Ad5-EBOV vaccine (approved by the China Food and Drug Administration for emergency use) (Y. Li et al., 2018), but no vaccine is approved for other filoviruses, including *Sudan ebolavirus*, which is currently causing an outbreak in Uganda (WHO, 2022a). During the 2018-2020 EBOV Outbreak in the Democratic Republic of Congo, four investigational agents were evaluated in the Pamoja Tulinde Maisha (PALM [“Together We Save Lives” in Kiswahili]) study. Two products demonstrated efficacy against EBOV: Ebanga (also known as mAb114), which is a single monoclonal antibody, and Inmazeb (also known as REGN-EB), which comprises a cocktail of three monoclonal antibodies (Tshiani Mbaya et al., 2021). The U.S. FDA approved both medications for Ebola Virus Disease therapy (FDA, 2020a, 2020b). EBOV has been reported to persist in immune-privileged sites

(Jacob et al., 2020; Schindell et al., 2018), thus a promising treatment strategy would be to combine mAbs with small molecules to completely clear the virus (Tshiani Mbaya et al., 2021). It is also worth noting that the currently available vaccines and treatments are injectables and there remains a need for easily administered (e.g., oral) anti-filoviral drugs. Gaining a better understanding of the virus is essential to guide the development of additional antiviral therapies against EBOV and other filoviruses. One promising route to antiviral therapies, which has proved successful to combat other viral infections, would be to develop novel entry inhibitors. To do so, there is a need to better understand the mechanism of EBOV cell entry.

EBOV entry into host cells is mediated by the viral glycoprotein (GP), which resides on the virion surface. GP is a class I fusion protein comprising two subunits: a receptor-binding subunit (GP1) and a fusion subunit (GP2) (White & Whittaker, 2016). Following attachment to the cell surface, the virus particles undergo internalization by macropinocytosis and are trafficked to late endosomes/lysosomes (Nanbo et al., 2010; White & Whittaker, 2016). In this compartment, GP1 is cleaved by the low-pH activated endosomal cysteine proteases cathepsin B and cathepsin L, removing the heavily glycosylated mucin-like domain and glycan cap to generate a cleaved form of GP1 (approx. 19 kDa) (Dube et al., 2009; Saeed et al., 2010; Schornberg et al., 2006). The cleavage of GP1 exposes the receptor-binding site for the EBOV endosomal receptor, Niemann-Pick C1 (NPC1) (Carette et al., 2011; Côté et al., 2011; E. H. Miller et al., 2012). After binding to NPC1, GP2 goes on to facilitate fusion of the viral and endosomal membranes by means of a poorly understood mechanism, which appears to be more complex than that of many other enveloped viruses fusing at low pH.

Low pH and GP1 interaction with NPC1 are both necessary but apparently not sufficient to induce complete EBOV membrane fusion (Bale et al., 2011; Brecher et al., 2012; Fénéant et al., 2019; E. H. Miller et al., 2012). Recent work by Munro and coworkers (Durham et al., 2020) suggests that upon binding to NPC1, GP1 undergoes conformational changes that enable GP2 to mediate the lipid mixing stage of fusion, a process also requiring low pH and enhanced by $Ca^{2+}$. $Ca^{2+}$ has also been shown to have

direct effects on the fusion loop found within GP2 (Gregory et al., 2011; Nathan et al., 2020). However, the infectivity of EBOV particles containing cleaved GP1 remains sensitive to a general cysteine protease inhibitor (E-64d), as well as agents that raise endosomal pH (Mingo et al., 2015; Spence et al., 2016). This suggests that an additional step is required for full and efficient fusion leading to a fusion pore that can transmit the viral RNA into the cytoplasm to initiate replication. This additional step has not yet been identified and it remains unclear (i) if $Ca^{2+}$, in addition to low pH and the GP1-NPC1 interaction, can drive full fusion, (ii) if yet an additional trigger is needed for full fusion, and (iii) if the final fusion trigger can only be found in late endosomes/lysosomes. Identification of a final trigger for full EBOV fusion has proven difficult in large part because full fusion, recorded as infection, has only been monitored in intact cells. The ability to measure the EBOV GP-mediated full fusion reaction (i.e., fusion of both leaflets of the bilayers) in an open cell-free system with accessible endosomal membranes would be beneficial because different factors could be added or omitted and thus their effects could be individually investigated at the experimenter's will. To date, such a system has not been developed.

To overcome this technical hurdle, we developed a novel target membrane system with which to study fusion of virus particles with NPC1-containing late endosomes displayed on a supported planar membrane, which we term a supported planar endosomal membrane (SPEM). We then used SPEMs in an *in vitro* fusion assay that uses total internal reflection fluorescence (TIRF) microscopy to visualize binding and fusion (both hemifusion and full fusion) between (pseudo)viruses bearing a viral GP and SPEMs. We first validated the system with an influenza virus (fowl plague virus) and with pseudoviruses containing GP from the arenavirus Lassa Fever virus. After establishing and validating this new *in vitro* fusion assay with viruses with well understood fusion behavior, we proceeded to show that fusion mediated by 19-kDa EBOV GP is dependent on low pH and enhanced by $Ca^{2+}$, consistent with other studies (Das et al., 2020; Nathan et al., 2020). We also found that SPEMs appear to retain cathepsin activity, that E-64d inhibits EBOV GP-mediated fusion, and that the addition of cathepsin B enhances fusion.

## 2.3 Results

### Supported planar endosomal membranes (SPEMs) as fusion targets for endosome-entering viruses

We developed a new assay employing endosomal membranes on a supported lipid bilayer (SPEMs) as target membranes for measuring hemifusion and full fusion of viral particles that fuse in endosomes. This open *in vitro* format affords facile access to examine the roles of candidate fusion triggering factors that normally function within endosomes. To prepare SPEMs (see Methods for details), we homogenized HEK 293T cells, removed nuclei by centrifugation and fractionated the resultant post-nuclear supernatant. The workflow to obtain an endosome enriched fraction is shown in Supplemental Figure 2.S1. Analysis on a continuous OptiPrep gradient indicated that late endosomes are enriched in the range 7%-14% OptiPrep (Fractions 3-7 in Supplemental Figure 2.S2). We therefore separated the post-nuclear supernatant on an OptiPrep 7%/14%/25% step gradient and, consistently, found that the 7%/14% interface is enriched for the late endosome markers NPC1 and Lamp1 (fraction FR1 in Figure 2.1A). This fraction also contains some early endosome, plasma membrane and ER markers, which is consistent with previously published endosome enrichment schemes (de Araùjo et al., 2008). The visible band at the 7%/14% Optiprep interface was collected, dialyzed against HMA pH 7.4 buffer, and used to prepare SPEMs.

To prepare SPEMs, a polymer-supported lipid monolayer was transferred to a quartz slide (Kalb et al., 1992), and an aliquot of the endosome enriched sample was added to the monolayer to prepare the second leaflet of the supported membrane (Figure 2.1B). This approach is similar to our previous approaches to display plasma membranes as target membranes for HIV fusion (Ward et al., 2020; Yang et al., 2017) and reconstituted membranes to study SNARE-mediated exocytosis (A. J. B. Kreutzberger et al., 2017). Immunofluorescence analysis indicated that SPEMs contain both NPC1 and Lamp1 with many of their ectodomains facing outward, but also some in inward facing orientations (Supplemental Figure S3). Fluorescence recovery after photobleaching indicates that the SPEMs exhibit long-range lateral lipid mobility with a

diffusion coefficient of 1.65 ± 0.1 x $10^{-9}$ $cm^2/s$ consistent with lipid diffusion in a fluid lipid bilayer (Figure 2.1C). The observation of lateral diffusion over many microns also means that the SPEMs consisted of lipid bilayers that extend over large areas on the planar support. Since a significant fraction of the late endosomal membrane proteins NPC1 and Lamp1 are both displayed in an outward facing orientation in the SPEMs, they are accessible for interaction with viruses approaching the SPEM surface.

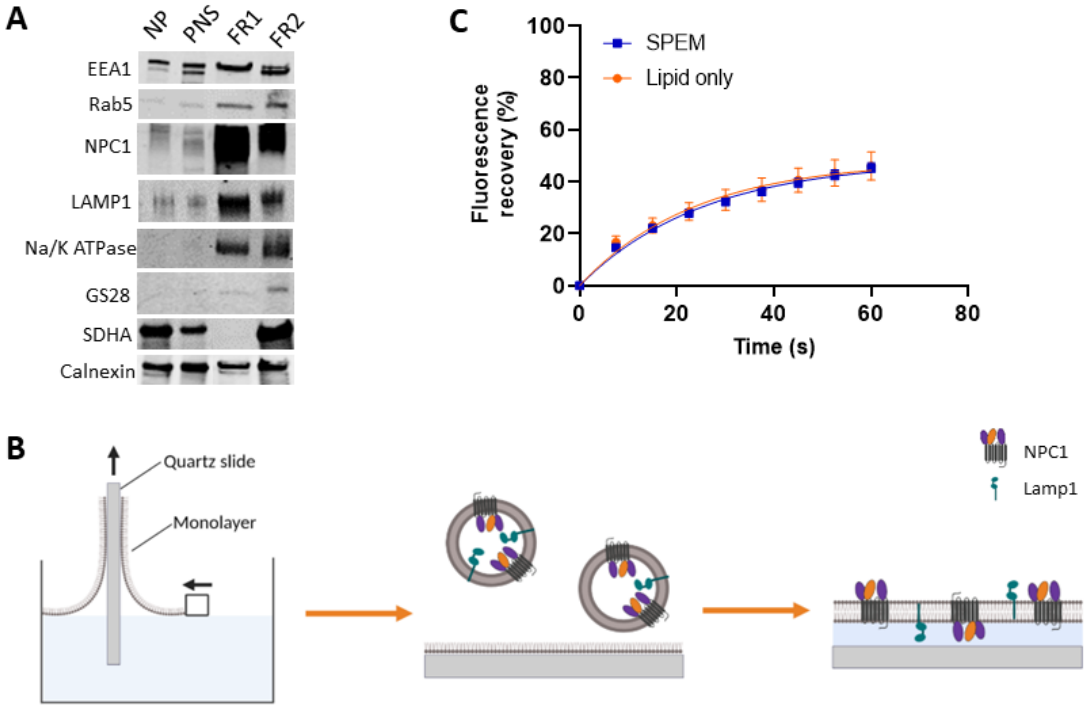


**Figure 2.1. Preparation of supported planar endosomal membranes (SPEMs). A.** Immunoblots of gradient fractions probed for different organelle markers: early endosomes (EEA1 and Rab5), late endosomes, endolysosomes (NPC1 and Lamp1), plasma membrane (Na/K ATPase), Golgi apparatus (GS28), mitochondria (SDHA – succinate dehydrogenase complex subunit A), and ER (calnexin). NP - nuclear pellet; PNS - post-nuclear supernatant; FR - fraction; FR1 - 7%-14% optiprep interface; FR2 - 14%-25% optiprep interface. **B.** Cartoon showing preparation of SPEMs. A lipid monolayer was transferred onto a clean quartz slide by immersing and pulling it through a monolayer of a lipid mix of brain phosphatidylcholine (PC), cholesterol and DPS in the ratio 77:20:3. Next, the lipid monolayer covered slide was assembled into a watertight flow cell and endolysosomes from FR1 were injected into the flow cell. The endolysosomes spontaneously spread on the supported monolayer to form SPEMs. **C.**

Fluorescence recovery after photobleaching (FRAP) experiment on SPEMs. Carboxy-fluorescein-PE was included in the monolayer prior to preparation of the bilayer. Quantification of fluorescence recovery after photobleaching in SPEMs as well as a lipid-only bilayer of brain PC and cholesterol (4:1). At least ten regions on four independently prepared lipid-only bilayers and SPEMs were sampled to determine the average values reported.

As a first proof of concept, we assessed the ability of fowl plague virus (FPV), an influenza virus, to fuse with SPEMs. To do this, we incorporated the membrane dye DiD into the FPV membrane during virus production, added the particles to SPEMs, and monitored fusion events by TIRF microscopy for at least 2.5 minutes (Figure 2.2A). Three types of events were observed: docking (binding) to the SPEM, hemifusion and full fusion (Figure 2.2B). Docking was characterized by the sudden appearance of punctate fluorescence, hemifusion by a decrease in fluorescence intensity to about half the initial intensity, and full fusion by the decrease in fluorescence intensity to background fluorescence. The distinction between hemi- and full fusion is possible in this case because both leaflets of the particle envelope were labeled with DiD using the protocol of label incorporation during virus production (Yang et al., 2017). FPV fusion events were monitored for at least 2.5 minutes. As expected for influenza virus (White et al., 1981), fusion to SPEMs was highly pH dependent: an approximately 6-8 times higher fusion probability was observed at pH 5.5 when compared to pH 6.5 or 7.4 (Figure 2.2C).

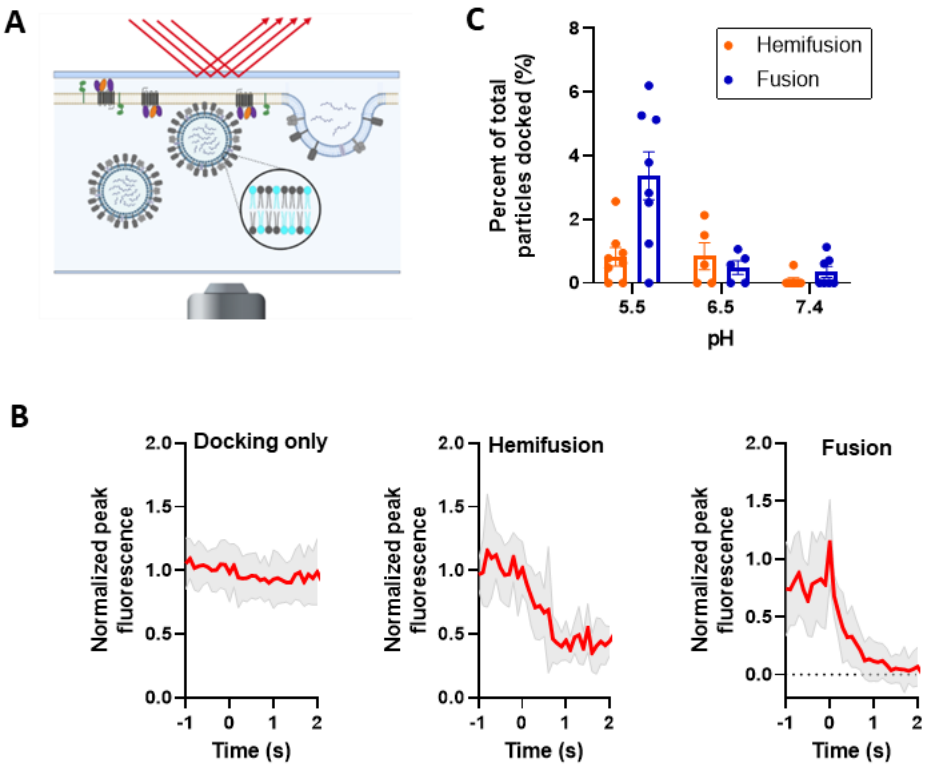


**Figure 2.2. Influenza virus (FPV) fusion to SPEMs. A.** Cartoon depicting DiD-labeled fowl plague virus (FPV) fusion to SPEMs. FPV was labeled with DiD during viral production, hence the membrane label (cyan) is present in both leaflets. **B.** Intensity traces of particles undergoing docking only (23 traces from pH 7.4 condition), hemifusion (seven intensity traces from pH 5.5 condition) and full fusion (21 intensity traces from pH 5.5 condition) were aligned and averaged (red traces). The shaded area represents standard deviation. **C.** pH dependence of hemifusion (orange) and full fusion (blue) of DiD-labeled FPV to SPEM. Movies were recorded at a frame rate of 100 ms for a minimum of 2000 frames. The total number of docked particles was quantitated for each condition. Each data point represents events observed on one separately prepared SPEM. Error bars indicate standard error.

We next tested SPEMs as targets for fusion of pseudoviruses. For this, we labeled the membranes of HIV pseudovirus particles bearing the Lassa virus (LASV) glycoprotein (GP) with a fluorescent lipid, Atto-488-DMPE. As these particles were labeled post pseudovirus production, the lipid dye is only found in the outer leaflet of their membrane envelopes (Ward et al., 2020). Thus, we only observed lipid mixing between

the viral outer leaflet with the SPEMs in these experiments (Figure 2.3A). Fluorescence decay time constants were determined for each event observed in the single particle recordings to differentiate between lipid mixing and undocking events (Supplemental Figure 2.S4). We assessed the ability of the LASV GP pseudotyped particles to fuse with SPEMs at different values of pH. LASV GP pseudovirus fusion events were monitored for 2.5 minutes. As expected, fusion efficiency increased when the pH was lowered from 7.4 to below 6.0 and sharply increased at pH 5.5 with SPEMs derived from wild-type cells (Figure 2.3C; black data points). The fusion probability decreased again when the pH was further lowered. Since Lamp1 is the endosomal receptor for LASV (Jae et al., 2014), we examined fusion to SPEMs prepared from cells in which Lamp1 had been knocked out using CRISPR/Cas9 gene editing (Figure 2.3B) (Hulseberg et al., 2018). We previously showed that plasma membrane displayed Lamp1 upwardly shifts the pH-dependence of pseudovirus-to-cell and cell-to-cell fusion (Hulseberg et al., 2018). As seen in Figure 2.3C, a similar result was observed for fusion to SPEMs: at pH 5.5, more fusion is seen to SPEMs from WT cells than to SPEMs derived from Lamp1-negative cells; with Lamp1-negative SPEMs, the pH profile did not show a peak at pH 5.5, but gradually further increased at lower values of pH. We also assessed binding of LASV GP pseudovirus to SPEMs with or without Lamp1 and observed increased binding to both sets of SPEMs with reduction in pH, indicating that Lamp1 primarily affects the ability of the LASV particles to fuse, but does not dramatically change the binding of these particles to endosomal membranes (Supplemental Figure 2.S5), which likely contain additional attachment factors for LASV GP.

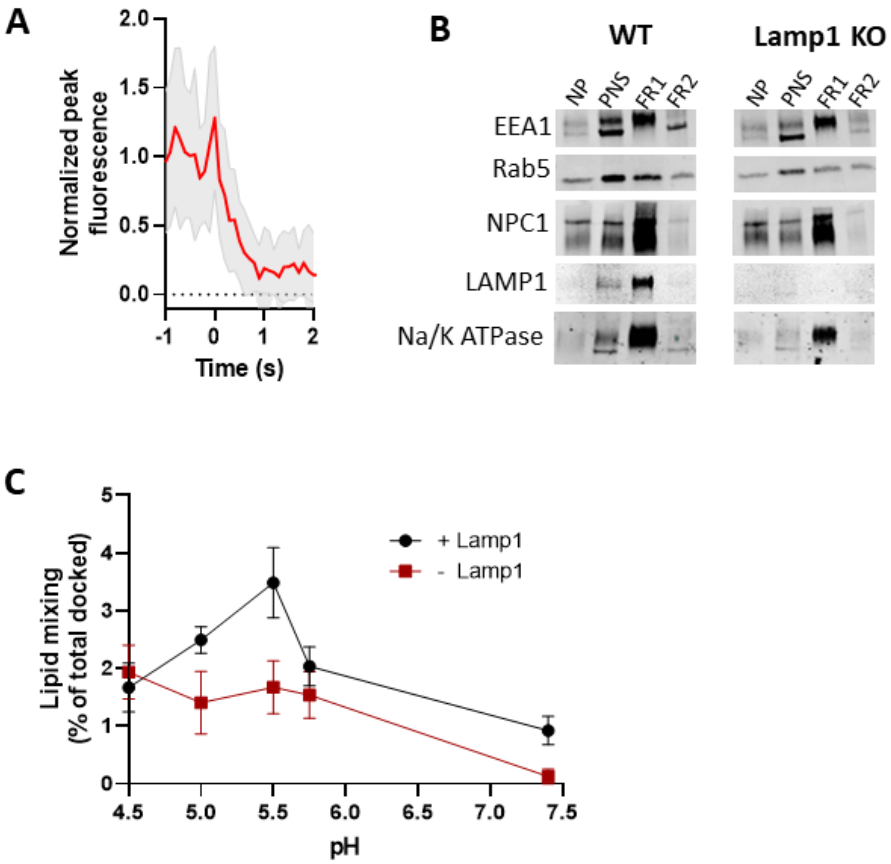


**Figure 2.3. Lassa virus GP pseudovirus fusion to SPEMs. A.** 20 intensity traces of fusion of HIV pseudovirions bearing Lassa GP, labeled with Atto488-DMPE in the outer membrane leaflet, were aligned and averaged. (Particles in this average curve were taken from the pH 5.5, no Lamp 1 condition.) The virus particles were introduced into the flow cell at the indicated pH. Movies were recorded at a frame rate of 100 ms for a minimum of 1500 frames. **B.** Immunoblots of gradient fractions from HEK293T WT and Lamp1 KO cells probed for different organelle markers as denoted in the legend to Figure 2.1. **C.** Fraction of particles bearing Lassa GP that underwent lipid mixing with SPEMs with or without Lamp1 at the indicated pHs. Error bars indicate standard error.

**Ebola Virus Glycoprotein-Mediated Membrane Fusion with SPEMs**

We prepared HIV pseudoviruses with EBOV GP lacking its mucin-like domain (GPΔ). The pseudovirus membrane was labeled with 1 µM DiD during viral production (Materials and Methods) so as to label both leaflets of the pseudovirus envelope. The glycan cap was proteolytically removed with thermolysin (Schornberg et al., 2006) to

generate the 19 kDa form of GP ($GP_{cl}$). The infectivity of the pseudoviruses was largely maintained in the presence of DiD in the membrane (Figure 2.S6). This labeling strategy allowed us to distinguish hemi- and full fusion events (Figure 2.4A).

We first explored the dependence of GPΔ-mediated fusion on cleavage to 19 kDa, pH and $Ca^{2+}$. Fusion was scored after 2.5 minutes. Minimal fusion was observed with GPΔ under any condition tested. With $GP_{cl}$, minimal fusion was observed at pH 7.4, but significant fusion was observed at pH 5.5, which was further enhanced by the addition of $Ca^{2+}$ (0.5 mM $CaCl_2$) (Das et al., 2020) (Figure 2.4B). Addition of $Mg^{2+}$ (0.5 mM $MgCl_2$) resulted in a similar extent of $GP_{cl}$-mediated fusion compared to the EDTA condition. The roles of low pH and $Ca^{2+}$ are in agreement with those of Munro and co-workers (Das et al., 2020) but here the results extend to full fusion.

Since we and others previously observed that infection mediated by pseudovirions bearing EBOV $GP_{cl}$ is inhibited by the general cysteine protease inhibitor E-64d (Schornberg et al., 2006; Spence et al., 2016), we reasoned that addition of cathepsin might enhance fusion and so we examined the effect of adding cathepsins to the system. We prebound EBOV $GP_{cl}$ pseudoviruses to SPEMs at neutral pH, introduced activated cathepsin B or L (CatB or CatL) to the flow chambers at pH 5.5, and then acquired 2.5-min long movies every 5 minutes for a total time period of 30 minutes (Supplemental Figure 2.S7). Addition of CatB mildly augmented the extent of full fusion over time (Figure 2.4C), whereas the extent of fusion with CatL appeared more similar to that seen with no added cathepsin (Figure 2.4D).

Having observed considerable full fusion after simply lowering the pH of SPEM-prebound pseudovirus particles, which was only marginally enhanced by the addition of catB, we sought to explore whether the SPEMs harbor any cathepsin activity; we did this by including the cysteine protease inhibitor, E-64d, in the fusion assay. SPEMs were incubated with 100 μM E-64d followed by the introduction and binding of EBOV pseudoviral particles to the SPEMs at neutral pH. Low pH medium supplemented with 100 μM E-64d was then introduced into the flow chamber and 2.5-min long movies

were collected as above (Supplemental Figure 2.S8). The inhibitor caused a marked decrease in EBOV $GP_{cl}$-mediated full fusion (Figure 2.4E), suggesting that the SPEMs retain cathepsin activity. However, hemifusion efficiency remained unaffected by the E-64d treatment (Figure 2.4F). Immunofluorescence analysis indicates that there is cathepsin B associated with the SPEMs (Supplemental Figure 2.S9). Collectively these data suggest that SPEMs retain cathepsin activity that enhances the fusion activity of EBOV $GP_{cl}$ pseudovirions at low pH. Ongoing experiments are testing this idea.

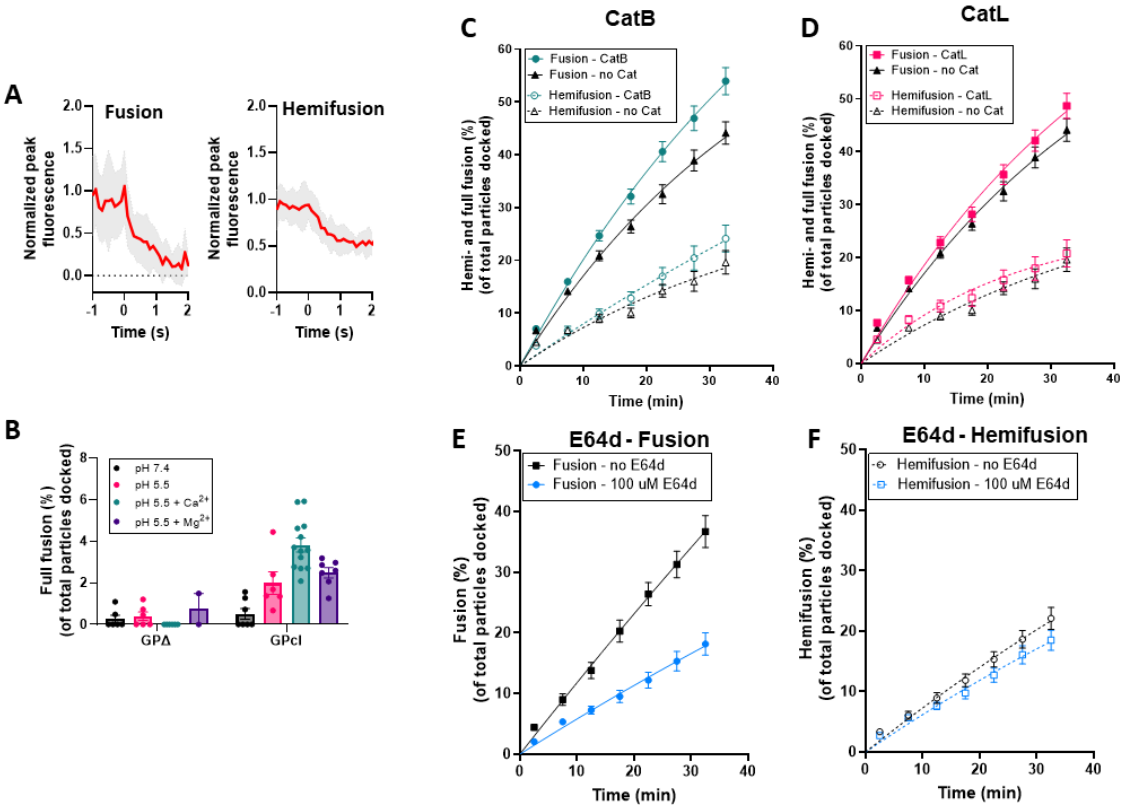


**Figure 2.4. Ebola virus GP pseudovirus fusion to SPEMs. A.** Intensity traces of DiD-labeled EBOV $GP_{cl}$ pseudovirions undergoing hemifusion (23 intensity traces from pH 5.5, no $Ca^{2+}$ condition) and full fusion (21 intensity traces from pH 5.5, no $Ca^{2+}$ condition). Ebola pseudoviruses were labeled with 1 mM DiD during viral production so as to label both membrane leaflets. Traces were aligned and averaged (red traces). The shaded area represents standard deviation. **B.** DiD-labeled HIV particles pseudotyped with Ebola GPΔ treated with thermolysin to generate 19-kDa GP ($GP_{cl}$) or untreated (GPΔ) fusing with SPEMs at pH 7.4 and pH 5.5 in the presence and absence of $Ca^{2+}$ or $Mg^{2+}$ (0.5 mM $CaCl_2$ or $MgCl_2$). Each data point represents events observed on one SPEM. **C.** Cumulative distribution function for full fusion and stalled hemifusion of EBOV

$GP_{cl}$ pseudovirus with SPEMs in the presence or absence of cathepsin B (0.4 ug/mL). Movies were recorded when cathepsin B in low pH buffer was being pumped into the flow cell chamber (0') as well as 5, 10, 15, 20, 25 and 30 minutes after. Residual $Ca^{2+}$ was present from thermolysin treatment done to obtain cleaved GP. Error bars indicate standard error. **D.** Cumulative distribution function for full fusion and stalled hemifusion of EBOV $GP_{cl}$ pseudovirus with SPEMs in the presence or absence of cathepsin L (0.4 ug/mL). Movies were recorded when cathepsin L in low pH buffer was being pumped into the flow cell chamber (0') as well as 5, 10, 15, 20, 25 and 30 minutes after. Error bars indicate standard error. **E-F.** Cumulative distribution function for full fusion **(E)** and stalled hemifusion **(F)** of EBOV $GP_{cl}$ pseudovirus with SPEMs in the presence or absence of 100 µM E-64d. Movies were recorded when low pH buffer with or without E-64d was injected into the flow cell chamber (0') as well as 5, 10, 15, 20, 25 and 30 minutes after. Error bars indicate standard error.

## 2.4 Discussion

In this study, we developed supported planar endosomal membranes (SPEMs) from endosomes derived from HEK293T cells as a platform for studying enveloped viruses that enter the cell through fusion with the endosomal membrane. We validated the system by demonstrating the low pH dependence of influenza virus (FPV) fusion and the enhancement of low pH-dependent fusion of LASV GP pseudovirions by the presence of its intracellular receptor, Lamp1. For EBOV GP, we confirmed the need for its cleavage to the 19 kDa form and for low pH for fusion as well as the enhancing effect of $Ca^{2+}$ (Das et al., 2020; Nathan et al., 2020), extending these observations to requirements for full fusion. Finally, we provided evidence that the final trigger for optimal EBOV $GP_{cl}$-mediated fusion is, indeed, as originally hypothesized (Schornberg et al., 2006), further cathepsin cleavage.

SPEMs have many potential applications. In addition to value in assessing general requirements for hemi- and full fusion (e.g., pH and $Ca^{2+}$), SPEMs can also be used to examine the roles of endosomal viral receptors. We observed a difference in the fusion profile of LASV GP-mediated fusion across a pH range from 4.5 to 7.4 in the presence and absence of LASV receptor, Lamp1 (Figure 2.3). EBOV and LASV were the

first viruses shown to utilize intracellular receptors, NPC1 and Lamp1, respectively (Carette et al., 2011; Côté et al., 2011; Jae et al., 2014). Since those reports, other viruses have been shown to employ endosomal receptors: LCMV interacts with CD164 (Bakkers et al., 2022), and simian hemorrhagic fever virus and Lujo virus interact with CD63 (Raaben et al., 2017; Warren et al., 2022). It will be interesting to determine if these other endosomal receptors are absolutely required or shift the pH dependence of fusion, as we and others have seen for LASV (Bulow et al., 2020; Hulseberg et al., 2018; Y. Zhang et al., 2022). SPEMs may also have utility in studying the mechanisms of bilayer breaching by non-enveloped viruses.

EBOV entry into cells is complex. Studies over the past two decades have delineated major requirements including cleavage of EBOV GP to the 19-kDa form by the endosomal cysteine proteases CatB and CatL (Chandran et al., 2005; Marzi et al., 2012; Schornberg et al., 2006), binding to its endosomal receptor, NPC1 (Carette et al., 2011; Côté et al., 2011), with low pH and $Ca^{2+}$ inducing conformational changes in the GP2 subunit (Das et al., 2020; Gregory et al., 2014; Nathan et al., 2020). Conformational changes observed in the crystal structure of NPC1-bound $GP_{cl}$ suggest that binding to NPC1 makes the release of the fusion loop more facile (Wang et al., 2016). Our early work indicated that in intact cells, low pH-dependent infection by pseudoviruses bearing 19-kDa GP requires a further E-64d-sensitive step (Mingo et al., 2015). Attempts, however, to reconstitute EBOV $GP_{cl}$-catalyzed fusion at the plasma membrane in forced fusion experiments in response to low pH (Fénéant et al., 2019; E. H. Miller et al., 2012), or even low pH plus NPC1, $Ca^{2+}$, $K^{+}$, bis(monoacylglycerol)phosphate (BMP), reducing agent, elevated temperature or cathepsins B and L (Fénéant et al., 2019), have been unsuccessful (Fénéant et al., 2019; E. H. Miller et al., 2012). Our prior inability to induce fusion at the plasma membrane with 19 kDa GP pseudoviruses even in the presence of added cathepsins, may reflect a recent finding of Melikyan and coworkers (Y. Zhang et al., 2022). These investigators showed differences in LASV GP-mediated fusion pore formation with endosomal vs. plasma membranes. This further supports the benefit of using near-native endosomal membranes, as exemplified by the SPEM system we have

developed here, for *in vitro* studies of the fusion activity of viruses entering cells through endosomes. Of note, work done by Kasson and coworkers (Haldar et al., 2020) also incorporates the use of endosomes extracted from cells to study viral entry. They isolated influenza virus-containing endosomes from BHK-21 cells, immobilized them and controllably triggered fusion. Their findings suggest that endosome membrane deformability, and not curvature, affects fusion kinetics.

Ebola GP is cleaved to GP1 and GP2 during biosynthesis by furin (Volchkov et al., 1998) and additionally cleaved during viral entry by cathepsins B and L to a 19-kDa form (Chandran et al., 2005; Marzi et al., 2012; Schornberg et al., 2006). The infectivity of EBOV bearing 19-kDa GP is sensitive to a cysteine protease inhibitor (E-64d) and agents that raise endosomal pH (Mingo et al., 2015; Spence et al., 2016). This suggests an additional low pH-dependent proteolytic step is required for efficient fusion. We provide evidence that cathepsins not only prime Ebola GP to its 19 kDa form, but also exert an additional role post-NPC1 binding. Experiments are in progress in our laboratory to use a reversible cathepsin inhibitor to further test that cathepsin action does indeed provide a final fusion-enhancing effect. Interestingly, CatB appears more effective in this late activation step than CatL (Figure 2.4). Several studies have shown EBOV infection to be sensitive to CatB, but not CatL, in Vero E6 cells (Marzi et al., 2012) and dendritic cells (Martinez et al., 2010), which may explain why we see an increase in fusion when CatB is added. Because we saw only a modest increase in fusion with the addition of CatB (Figure 2.4C and D), as well as higher fusion efficiency than expected without additional cathepsin, we evaluated fusion in the presence and absence of E-64d. There was a marked decrease in full fusion efficiency (Figure 2.4E and F), while hemifusion remained the same. These finding are consistent with findings presented by Spence *et al.* (Spence et al., 2016), who observed EBOV $GP_{cl}$-mediated lipid mixing (specifically hemifusion) in cells treated with E-64d, but no infection in the presence of E-64d, as originally seen by Schornberg *et al.* (Schornberg et al., 2006). This suggests one of two things: (i) cathepsin further cleaves NPC1-bound GP1, releasing its hold on GP2, allowing GP2 to insert itself into the host membrane, thereby initiating the fusion

cascade, or (ii) cathepsin acts on a host cell factor present in the endosomal membrane that is required for optimal fusion. Additionally, fusion in the presence of E-64d is not completely inhibited. This suggests that other proteases may contribute to fusion, for example aspartic endoprotease, cathepsin D. Future experiments are needed to test these possibilities.

Our findings also indicate the presence of membrane-associated cathepsins in SPEMs (Figure 2.4E and Supplemental Figure 2.S9). While most cathepsins in endosomes and lysosomes are in soluble form in the lumen of these organelles, there is evidence that a small population of cathepsins are membrane-bound. Cathepsins are synthesized in the endoplasmic reticulum. The propeptide form of cathepsin is transported through the Golgi stacks where it binds to mannose-6-phosphate (M6P) receptors. The M6P-bound procathepsins are then trafficked to endo/lysosomes, where the low pH typically results in the dissociation of the enzyme-receptor complex (reviewed in (Yadati et al., 2020)). However, not all of the cathepsins may be discharged from M6P receptors. Also, some cathepsins are sorted to endosomes independent of M6P receptors and those cathepsins may remain bound to alternate receptors. M6P receptor-independent membrane-association has been reported in endosomes for cathepsins B and D in hepatic cells (Authier et al., 1995) and cathepsin D in macrophages (Diment et al., 1988). Finally, the low-density lipoprotein (LDL) receptor and Lrp1 (LDL receptor-related protein 1) transport cathepsins B and D to lysosomes in mouse embryonic fibroblasts (Markmann et al., 2015).

Triggering of membrane fusion by initial binding to receptor followed by proteolytic action has been reported for other viruses, notably coronaviruses, including severe acute respiratory syndrome coronavirus 1 (SARS-CoV-1) and 2 (SARS-CoV-2) as well as Middle East respiratory syndrome coronavirus (MERS-CoV). Coronaviruses require proteolytic activation of their spike proteins by cell surface or endosomal proteases for successful infection (Belouzard et al., 2009; Hoffmann, Kleine-Weber, Schroeder, et al., 2020; Millet & Whittaker, 2014). Furin cleavage primes the spike protein of SARS-CoV-2, during viral biosynthesis, to its subunits S1 and S2. The

transmembrane serine protease 2 (TMPRSS2), which resides in the plasma membrane, or cathepsin L (in endosomes) cleaves the spike protein at a specific locus (the S2' site), triggering fusion during viral entry (Bestle et al., 2020; Hoffmann, Kleine-Weber, & Pöhlmann, 2020; Hoffmann, Kleine-Weber, Schroeder, et al., 2020; T. Liu et al., 2020; Shang et al., 2020). Hence there are parallels between filoviral and certain coronaviral fusion in requiring both receptors and pre- and post-receptor binding protease steps. Additionally, mildly low pH (Kreutzberger et al., 2022) and calcium (Singh et al., 2022) have been shown to be required for efficient SARS-CoV-2 infection, which would indicate additional parallels.

In summary, the *in vitro* SPEM system we have developed provides a powerful tool with which to study the mechanism of fusion of endosome-entering viruses. SPEMs also provide an excellent platform to study the role of other viral proteins in fusion, for example the Ebola matrix protein VP40 (Winter et al., 2022), as well as the effect of viral glycoprotein mutations (e.g., A82V substitution in EBOV GP (Diehl et al., 2016)) on fusion. Although not tested in this study, this method may also be used to explore the mechanism by which non-enveloped viruses penetrate endosomes.

**Acknowledgements:** We thank Dr. David Castle for training and assistance with the endosome enrichment protocol. We also thank Dr. Amanda Ward for assistance with the preparation of recombinant influenza virus. Cartoons were created with BioRender.com. This work was supported by grant R01 AI30557 from the National Institutes of Health.

## 2.5 Materials and Methods

### Cells, plasmids, and reagents

HEK293T/17 cells (ATCC), Lamp1 KO HEK293T/17 cells (clone 2F6, described by Hulseberg et al. (Hulseberg et al., 2018)) and MDCK II cells (originally from Dr. Ari Helenius) were maintained in high glucose Dulbecco's Minimum Essential Media

(DMEM) (Gibco), supplemented with 10% fetal bovine serum (FBS) (Atlanta Biologicals), 2 mM L-glutamine (Gibco), 1 mM sodium pyruvate (Gibco) and 1% antibiotic-antimycotic (Gibco). HeLa-derived TZM-bl cells (NIH AIDS Reagent Program) were maintained in high glucose DMEM (Gibco), supplemented with 10% FBS (Atlanta Biologicals) and 1% antibiotic-antimycotic (Gibco). All cells were maintained at 37°C and 5% $CO_2$.

Plasmids for pseudovirus production, pFSW-Tat and psPAX2, were gifts from Dr. Jeremy Luban (University of Massachusetts Medical School). pHIV-Rev was a gift from Dr. Wen Yuan (University of Virginia). The surface protein plasmids: EBOV $GP_{\Delta\text{-mucin}}$ (VRC6002) of the Kikwit strain of EBOV GP and Lassa virus GP (LASV Josiah strain in pCMV) were originally from Dr. Gary Nabel and Dr. Gregory Melikyan (Emory University), respectively.

Antibodies against the NPC1 C-terminal tail (ab134113), Lamp1 C-terminal tail (ab24170) and EEA1 (ab2900) were from Abcam. The antibody for Lamp1 with the epitope in luminal region (H4A3) was from Developmental Studies Hybridoma Bank. The anti-NPC1 C-loop antibody (sc-271335) was from Santa Cruz Biotechnology. The succinate ubiquinone oxidoreductase antibody (2E3GC12FB2AE2) and sodium-potassium ATPase antibody (MA1-16731) were from ThermoFisher Scientific. The antibody against the Golgi SNARE protein, GS28, was a gift from Dr. David Castle at the University of Virginia. The anti-Rab5 antibody was a gift from Dr. Reinhard Jahn at the Max Planck Institute for Biophysical Chemistry. The calnexin antibody (ADI-SPA-860-D) was from Enzo Life Sciences. The monoclonal mouse-α-GP1 H3C8 antibody was a kind gift from Carolyn Wilson at the Food and Drug Administration.

**Fowl Plague Virus (FPV) preparation and membrane labeling**

Recombinant Influenza A/FPV/Rostock/1934(H7N1) attenuated with a monobasic cleavage site was created with a 12-plasmid system (Neumann et al., 1999) and grown as previously described (Hu et al., 2019). Briefly, 293T cells in infection medium (DMEM supplemented with 0.2% w/v Bovine Serum Albumin, 0.1% Fetal Calf Serum, 2 mM

glutamine, 1% Antibiotic/Antimycotic) were transfected with Lipofectamine 2000 and 1 g of each of 8 plasmids encoding each segment of the FPV genome and 4 plasmids expressing the components of the FPV ribonucleoprotein complex. Four hours after transfection, the media was changed to infection medium containing 1 µg/mL TPCK-Trypsin. Two days after transfection, the supernatant was harvested and cleared by pelleting 5000xg for 10 min. The cleared supernatant was added to 90% confluent MDCK II cells in infection media and allowed to enter for 1 hour at 37°C after which the media was replaced with infection media containing 1 µg/mL TPCK-Trypsin. Two days after infection, cytopathic effect was observed and the supernatant was harvested, cleared by centrifugation as above, aliquoted and frozen at -80°C. To avoid mutations from passage in culture, each subsequent preparation of FPV was performed by infecting MDCK II cells as described above with one of the original aliquots.

To prepare membrane-labeled virus, MDCK II cells grown to 80% density in T175 flasks were washed with 5 mL warmed phosphate-buffered saline (PBS). 7 mL of infection media (DMEM supplemented with 1 g BSA, 10% SCS, 1% antibiotic-antimycotic, 1% L-glutamine) mixed with one aliquot of previously prepared FPV was added and incubated for 1 hour at 37°C. The media was then aspirated and replaced with 15 ml infection media containing 0.625 µM DiD (1,1'--dioctadecyl-3,3,3',3'-tetramethylindodicarbocyanine, 4-chlorobenzenesulfonate salt) (ThermoFisher Scientific) and 1 µL of 2 µg/mL TPCK-Trypsin per 1 mL of infection media. After 48 hours, the culture supernatant was collected and cleared by centrifuging at 5,000xg for 15 min at 4°C. The virus was pelleted through a 25% sucrose-HMT cushion and resuspended in HMT buffer without sucrose, aliquoted and stored at -80°C until use.

**HIV pseudovirus production**

Virions pseudotyped with Ebola virus $GP_{\Delta mucin}$ (abbreviated as EBOV GPΔ) and Lassa virus (LASV) GP were produced in HEK293T/17 cells using Lipofectamine 2000 (Invitrogen). Cells grown to 60-80% confluency were transfected with 4.65 µg psPAX2 (Gag-Pol helper vector), 6.25 µg pFSW-Tat, 1 µg pHIV-Rev, and 1.5 µg of EBOV GP or

LASV GP. 4 to 6 hours post-transfection, the media was replaced with phenol red free DMEM supplemented with 10% FBS, 2 mM L-glutamine and 1 mM sodium pyruvate. Pseudovirus-containing media was collected 48 h post-transfection and clarified by low-speed centrifugation. HIV pseudoviruses were pelleted through a 25% sucrose-HMT (20 mM HEPES, 20 mM MES, 130 mM NaCl, 1 mM EDTA, pH 7.4) cushion and resuspended in HMT buffer without sucrose. The pseudovirus preparation was aliquoted and stored at -80°C. The concentration of HIV p24 was measured by ELISA (Wehrly & Chesebro, 1997).

Infection of TZM-bl cells by HIV pseudoviruses was performed as described by Sarzotti-Kelsoe et al. (Sarzotti-Kelsoe et al., 2014). Firefly luciferase activity was measured 2 days post-infection with BriteLite reagent (PerkinElmer Life Sciences) in a plate reader (GloMax Explorer, Promega). HIV pseudovirus preparations were diluted in Opti-MEM (Gibco) to the same concentration of p24.

**HIV pseudovirus membrane labeling**

The outer leaflet of pseudovirus membranes was labeled with the fluorescent membrane label, Atto488- dimyristoylphosphatidylethanolamine (DMPE) (MilliporeSigma) essentially as described (Ward et al., 2020). Briefly, Atto488-DMPE was dried on the bottom of a glass test tube to remove chloroform/methanol solvent and resuspended in buffer HB (20 mM HEPES, 150 mM NaCl, pH 7.4) to a concentration of 1.8 μg/mL. Using the p24 concentration of HIV pseudovirus, the virus was mixed with the dye suspension in a mass ratio of 4.4:1. The mixture was incubated at room temperature in the dark for 3 hours under slow rotation. To remove free Atto488-DMPE, the mixture was diluted to 1 mL in HB buffer and HIV pseudoviruses were pelleted by spinning at 21,000xg for 1 hour at 4°C. Atto488-DMPE labeled HIV pseudoviruses were stored in the dark at 4°C and used within 24 hours.

DiD labeling of HIV pseudoviruses was done as described in the FPV preparation and membrane labeling section above, which labels both leaflets of the viral envelope.

**Cleavage of EBOV GPΔ to produce 19kDa EBOV GP**

HIV pseudoviruses bearing EBOV-GPΔ were cleaved to the 19K form of GP with 0.5 mg/ml freshly prepared thermolysin (MilliporeSigma) in the presence of $CaCl_2$. Samples were incubated for 60 min at 37°C and the reaction terminated by adding 500 µM phosphoramidon (MilliporeSigma). Fresh thermolysin powder was obtained when GPΔ cleavage to19 kDa waned, as assessed by Western blotting.

**Late endosome enrichment protocol**

Late endosome enriched samples were prepared from HEK293T cells. Cells (five to ten 10-cm plates) were grown to about 90% confluency, then scraped into phosphate-buffered saline (PBS), and pelleted by centrifugation for 10 min at 1,000xg at 4°C. The cell pellet was washed in 3 ml homogenization buffer (10 mM HEPES, 3 mM imidazole, 250 mM sucrose, pH 7.4). Following the wash, the cell pellet was resuspended in 3 ml homogenization buffer supplemented with 1X protease inhibitor cocktail (ThermoFisher Scientific) and passed through a ball-bearing homogenizer with a 0.6368 cm bore and 0.6335-cm diameter ball (gift of Dr. David Castle). The homogenate was centrifuged for 15 min at 4,000xg at 4°C to pellet the nuclei. 60% Optiprep (iodixanol) (MilliporeSigma) was mixed with buffer (30 mM MOPS, 270 mM sucrose, 6 mM EDTA, pH 7.2) to obtain 7% and 14% Optiprep solutions for discontinuous gradients. The post-nuclear supernatant (PNS) was collected and mixed with an equal volume of 50% OptiPrep solution to obtain a final concentration of 25% Optiprep. This mixture was then transferred to a Beckmann SW 40 tube and overlayed carefully with 4 ml of 14% OptiPrep solution and 4 ml of 7% OptiPrep solution. This gradient was spun for 1.5 hours at 35,000 rpm at 4°C. A white band at the interface between 7% OptiPrep and 14% Optiprep was collected. This fraction, which was enriched in early and late endosomes, was dialysed in a cassette with 10,000-kDa molecular weight cutoff (ThermoFisher Scientific) against 4 liters HMA buffer (10 mM HEPES, 10 mM MES, 10 mM sodium acetate, 100 mM sodium chloride, pH 7.4). The protein concentration of the dialyzed preparation of endosomes was determined using a BCA protein assay kit (Thermo Scientific). The preparation of enriched endosomes was stored at 4$^{o}$C and used within

72 hours. We also tested whether endosome preparations could be frozen and stored at -80°C for use at a later time but determined that SPEMs prepared from frozen and thawed endosome preparations were malformed (no smooth appearance) compared to SPEMs from freshly prepared endosomes and no longer supported fusion of LASV pseudovirions although docking of these viruses was unchanged. However, SPEMs may be prepared from endosomes stored at 4°C for up to 2 weeks with only a small loss (~25%) of fusion permissiveness (Supplemental Figure 2.S10).

**Preparation of supported planar endosomal membrane**

Supported planar endosome membranes (SPEMs) were prepared using the Langmuir-Blodgett/vesicle fusion technique (Kalb et al., 1992; Wagner & Tamm, 2000). Quartz slides were cleaned by immersing in Piranha solution (3:1 mixture of 95% sulfuric acid and 30% hydrogen peroxide) for at least 15 min and thoroughly rinsing in deionized water. The first leaflet of the SPEM was prepared by Langmuir-Blodgett transfer directly onto the quartz slide. A lipid mixture of 4:1 brain phosphatidylcholine and cholesterol (Avanti Polar Lipids) with 3 mol% of DPS (1,2-dimyristoyl-*sn*-gycero-3-phosphatidylethanolamine-PEG3400-triethoxysilane (Wagner & Tamm, 2000)) in a chloroform solution was applied onto a water surface in a Nima 611 Langmuir-Blodgett trough to reach an initial surface pressure of ~10-15 mN/m. The solvent was allowed to evaporate for 10 to 15 min after which the monolayer was compressed at a rate of 10 $cm^2$/min to reach a surface pressure of 32 mN/m. After equilibration for 5 to 10 min, a clean quartz slide was dipped into the trough at a speed of 68 mm/min and slowly withdrawn at 5 mm/min while maintaining constant surface pressure at 32 mN/m. The quartz slides with the monolayer were dried in a desiccator overnight. To form the outer leaflet of the SPEM, a quartz slide was assembled in a custom-built microscopy flow cell and a suspension containing endosomes diluted to 0.5 mg/mL (as determined by BCA) in HMA buffer was injected into the flow cell and incubated for 1-1.5 hours at room temperature. Excess, unfused endosomes were removed by washing with ten volumes of HMA buffer.

**Total internal reflection fluorescence microscopy**

To study binding and/or fusion to SPEMs, fluorescently labeled pseudoviruses were diluted in HMA buffer to obtain roughly 100-200 particles per field of view. The pseudoviruses were injected into the flow cell and the fluorescence was monitored over time using prism-based TIRF microscopy. For pseudoviruses with the membrane label atto488-DMPE, the sample was excited with a 488 nm laser (OBIS 488 nm LX, Coherent) and the emission light was filtered through a dichroic mirror (DC505, Semrock) and a band-pass filter (BP535/40, Chroma). For DiD-labelled FPV and pseudovirus, the sample was excited with a 640 nm laser (OBIS 640 nm LX, Coherent) and the emission light was filtered through a dichroic mirror (DC660, Semrock) and a long-pass filter (LP665, Semrock). Videos were recorded by an EMCCD (DV887ESC-BV, Andor Technology) in frame transfer mode with an exposure time of 0.1 s. Laser intensity, shutter, and camera were controlled by a custom program written in LabView (National Instruments).

For experiments with cathepsins B and L, recombinant human cathepsin B, CatB (R&D Systems), was activated by incubating in HMA buffer pH 5.0 at room temperature for 15 min. Recombinant human cathepsin L, CatL (R&D Systems), was activated by diluting it in HMA buffer pH 5.5 and incubating on ice for 15 minutes. Ebola pseudoviruses were prebound to SPEMs at neutral pH and incubated for 5-7 minutes. Unbound virus was washed away with ten volumes of HMA buffer pH 7.4. The cathepsins were further diluted in HMA buffer pH 5.5 to 0.4 μg/mL and introduced into the flow cells. 2.5-minute videos were collected immediately following cathepsin/low pH addition to the flow cell (this was marked as time 0) and 5, 10, 15, 20, 25 and 30 min after from different field of views. Cumulative distribution functions of fusion efficiencies were derived from the data collected at the aforementioned time points and by extrapolating the observed fusion rate in 2.5 min to 5 min intervals.

For experiments with the cysteine protease inhibitor, E-64d (Sigma), a stock solution of E-64d was prepared by dissolving it in water. The SPEMs were incubated 100 μM E-64d in HMA buffer at pH 7.4 for 10 min. Ebola pseudoviruses were flowed in in HMA buffer

pH 7.4 with 100 µM E-64d and incubated for 5-7 min. Unbound virus was washed away with ten volumes of HMA buffer pH 7.4 with 50 µM E-64d. HMA buffer pH 5.5 with 100 uM E-64d was introduced into the flow cells and 2.5 min videos were collected immediately following the addition of E-64d/low pH (time 0) and 5, 10, 15, 20, 25 and 30 min after. Cumulative distribution functions were derived from the data collected as described above.

Intensities of single particles from regions of interest of 5 pixels $\times$ 5 pixels over time were extracted with a custom-built LabView program and classified as representing docking without fusion or docking with fusion based on the following criteria: a rapid increase in intensity followed by multiple frames of similar intensity without translation of the particle more than 4 pixels was classified as binding. If the intensity of the particle remained the same for the duration of the acquisition or slowly bleached over 15 seconds or more, this was considered docking without fusion. If the intensity of a docked particle decayed to background, which is characteristic for 2D diffusion of fluorophores away from the site of fusion, the event was classified as binding with fusion. To distinguish fusion events from undocking events, a minimal decay time cutoff of 0.3 s was used to classify a single event as fusion.

**Antibody staining of SPEMs**

SPEMs were prepared as described above. After excess, unfused endosomes were washed out of the flow cell, blocking buffer (15% FBS in PBS) was flowed in and incubated with the SPEM for 1 hour at room temperature. The primary antibody was diluted in blocking buffer at the indicated dilutions and incubated with the SPEM for 1 hour. Unbound primary antibody was washed with ten volumes of PBS. Secondary antibody conjugated to Alexa fluor 488 or 555 was diluted in blocking buffer and incubated with the SPEM for another hour at room temperature. Excess unbound secondary antibody was washed with twenty volumes PBS. The SPEM was then imaged on a TIRF microscope.

**Fluorescence recovery after photobleaching**

The lateral diffusion of lipids and integrity of the SPEMs was studied using fluorescence recovery after photobleaching (FRAP). 1 mol% of carboxyfluorescein-PE (CF-PE, Avanti Polar Lipids) was included in the monolayer prior to the preparation of the SPEM. Bilayers were bleached in a pattern of parallel stripes by a strong laser pulse (Smith & McConnell, 1978) and the mean intensities obtained from images before and after the bleach pulse were fit by the model:

$$F(t) = F_\infty + (F_0 - F_\infty)e^{(-Da^2t)}$$

where $F_0$ and $F_\infty$ are the initial and final fluorescence intensities after bleaching, respectively, a = 2π/p, p is the stripe period (12.7 μm), and D is the lateral diffusion coefficient. The mobile fraction (m.f.), which is a percentage of observed fluorescence recovery within the time frame of a FRAP experiment (60 s), is given by

$$m.f. = \frac{F_\infty - F_0}{F_{pre} - F_0} \times 200$$

where $F_{pre}$ is the fluorescence intensity before photobleaching. At least ten regions on four independently prepared SPEMs and bilayers were sampled to determine the reported average values.

## 2.6 Supplemental Figures

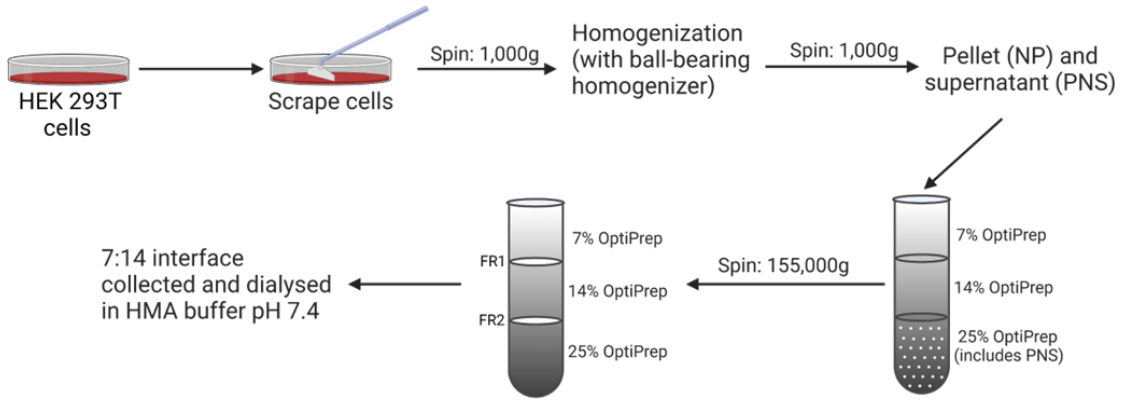


**Figure 2.S1. Endosome enrichment protocol.** Schematic diagram of subcellular fractionation using discontinuous Optiprep density gradient centrifugation. NP - nuclear pellet, NS - post-nuclear supernatant, FR1 - Fraction 1: 7%-14% optiprep interface, FR2 - Fraction 2: 14%-25% optiprep interface.

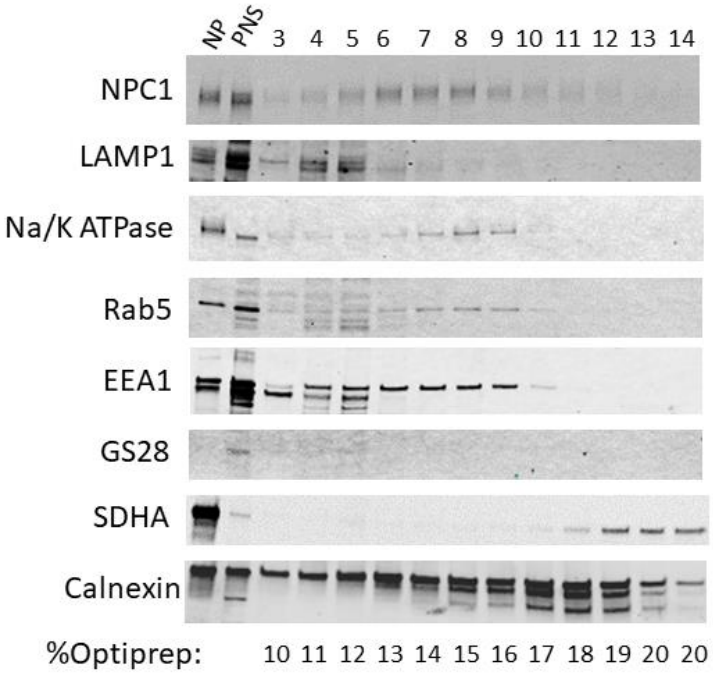


**Figure 2.S2.** Western blots of continuous gradient fractions probed for different organelle markers: late endosomes and lysosomes (NPC1 and Lamp1), early endosomes (EEA1 and Rab5), Golgi apparatus (GS28), mitochondria (SDHA – succinate

dehydrogenase complex subunit A), ER (calnexin) and plasma membrane (Na/K ATPase). The organelles were separated on a continuous 5% to 20% Optiprep gradient. Equal volume fractions were collected from the top (fraction 3) to the bottom (fraction 14); the first two fractions were not analyzed. Analysis of these fractions for organelle markers indicated that an enriched endosome fraction would band at a 7%/14% interface on a discontinuous OptiPrep step gradient. The values below the blots are the Optiprep concentrations derived from the refractive indices of the respective fractions measured at room temperature. NP - nuclear pellet; PNS - post-nuclear supernatant.

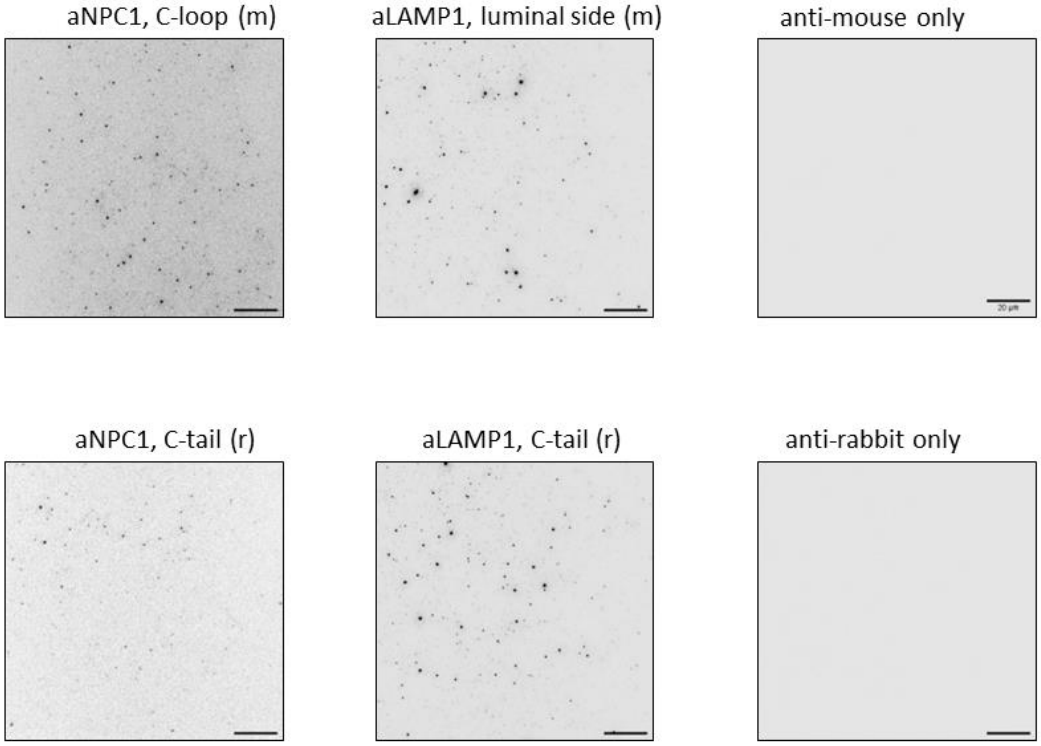


**Figure 2.S3. Assessment of sidedness of supported planar endosomal membranes (SPEMs).** Antibody staining of SPEMs showing orientation of endosomal membrane proteins. r - rabbit antibody, m - mouse antibody. The controls contain no primary antibody and only a donkey anti-mouse or donkey anti-rabbit antibody conjugated to alexa fluor 555. All primary antibodies were used at a 1:100 dilution in blocking buffer (15% FBS in PBS). The signal-to-noise ratio was adjusted to make the signal more apparent, with the secondary antibody only controls being scaled similarly to the Lamp1 images. The images are shown in reverse contrast. Scale bar: 20 µm.

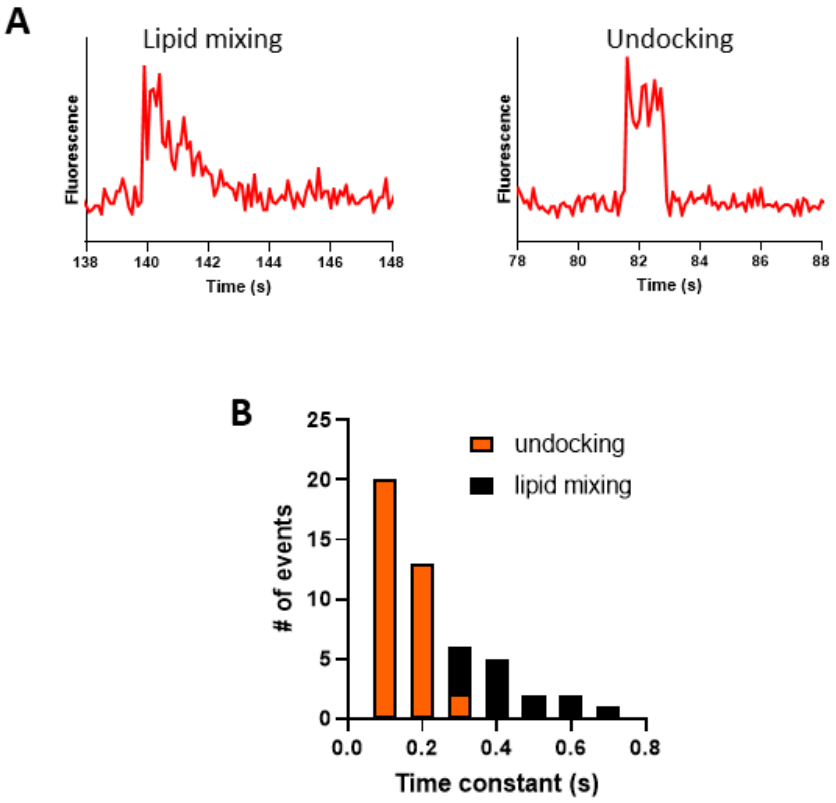


**Figure 2.S4. Decay time constants for lipid mixing and undocking events. A.** Fluorescence intensities of two different particles over time, with one undergoing lipid mixing (left) and the other undocking from the SPEM (right). **B.** Time constants of less than 0.3 s were denoted as undocking and those above 0.3 s were denoted as lipid mixing events. The lipid mixing and undocking events were taken from events observed in the SPEM with no Lamp1, pH 4.5 condition.

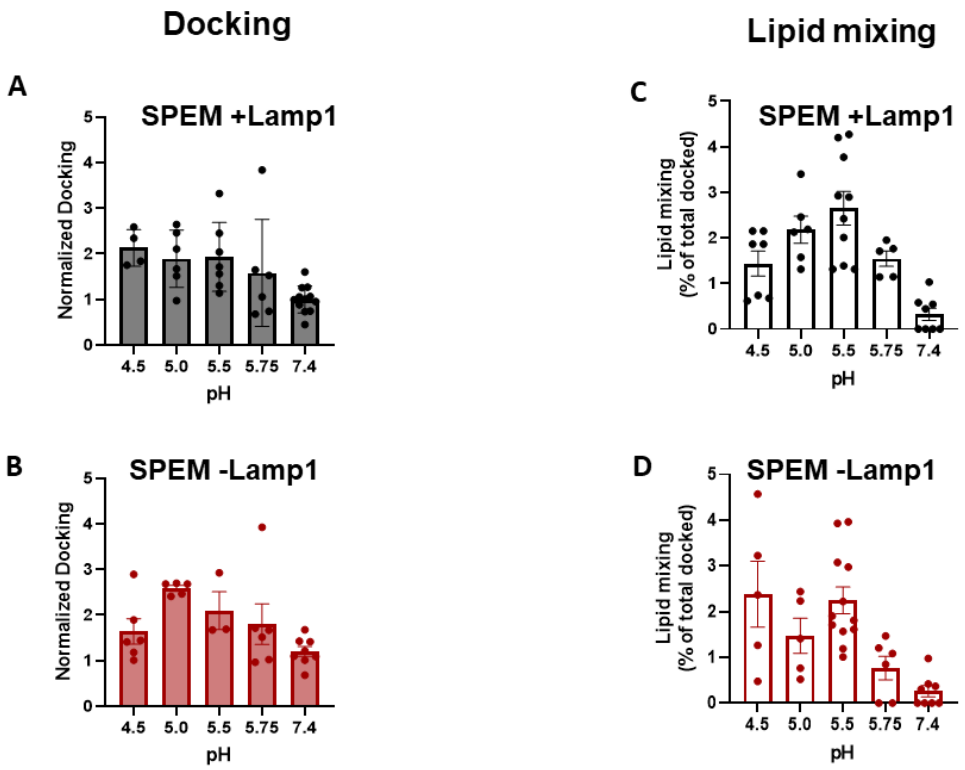


**Figure 2.S5. Docking and lipid mixing of Lassa GP pseudoviruses to SPEMs.** HIV pseudoviruses bearing Lassa GP and labeled with Atto488-DMPE (outer leaflet only) were flowed into the flow chambers with SPEMs and attached to and allowed to undergo lipid mixing with the SPEMs at the indicated pHs. **A and B.** Lassa pseudovirus associated with SPEMs with and without Lamp1 at the indicated pH. Docking for both SPEMs with and without Lamp1 was normalized to docking observed in the SPEM sample with Lamp1 at pH 7.4. **C and D.** Lipid mixing of Lassa GP pseudoviruses with SPEMs with and without Lamp1 at the indicated pH. Each data point represents events observed on one separately prepared SPEM. These data were averaged and plotted in Figure 3.3C. Error bars indicate standard error.

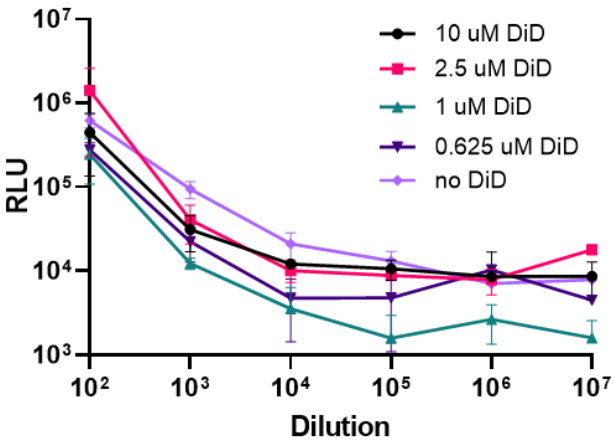


**Figure 2.S6. Infectivity of Ebola GP pseudoviruses labeled with different concentrations of DiD during viral production.** TZM-bl cells were incubated with serial dilutions of HIV particles pseudotyped with Ebola GP that had been labelled with 10, 2.5, 1, 0.625 □M or no DiD (mock) in triplicate in 96-well culture plates. The luciferase activity was measured 48 hours after incubation and is expressed as RLU after subtraction of background luminesce from control wells. Triplicate wells, in a 96 well plate, were analyzed for each sample at each dilution. The infectivity was measured for two independent pseudovirus preps. The error bars indicate standard error.

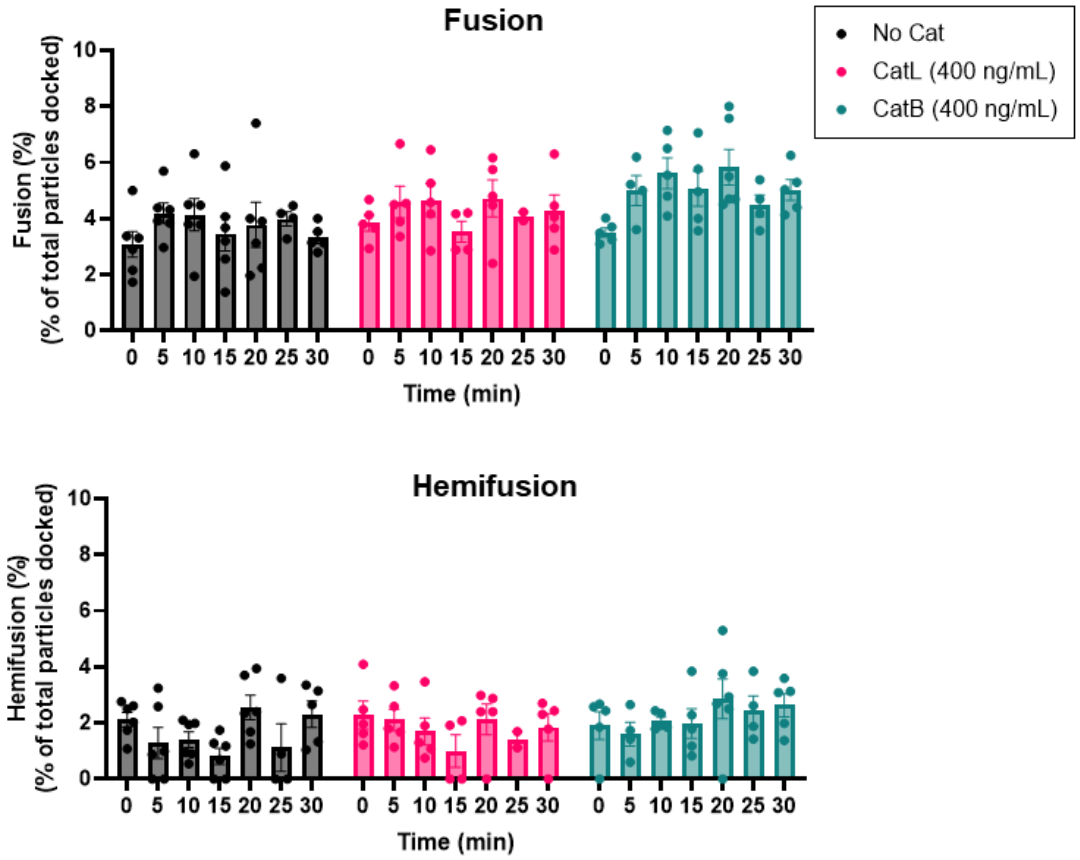


**Figure 2.S7. Fusion of Ebola pseudovirus with SPEMs in the presence or absence of cathepsin B or L at the indicated concentrations.** Movies were recorded immediately after cathepsin B/L (or no cathepsin) in low pH buffer was flowed into the flow cell chamber (0') as well as 5, 10, 15, 20, 25, and 30 minutes after. Residual $Ca^{2+}$ was present from thermolysin treatment done to obtain cleaved GP. Each data point represents events observed on one separately prepared SPEM. Error bars indicate standard error.

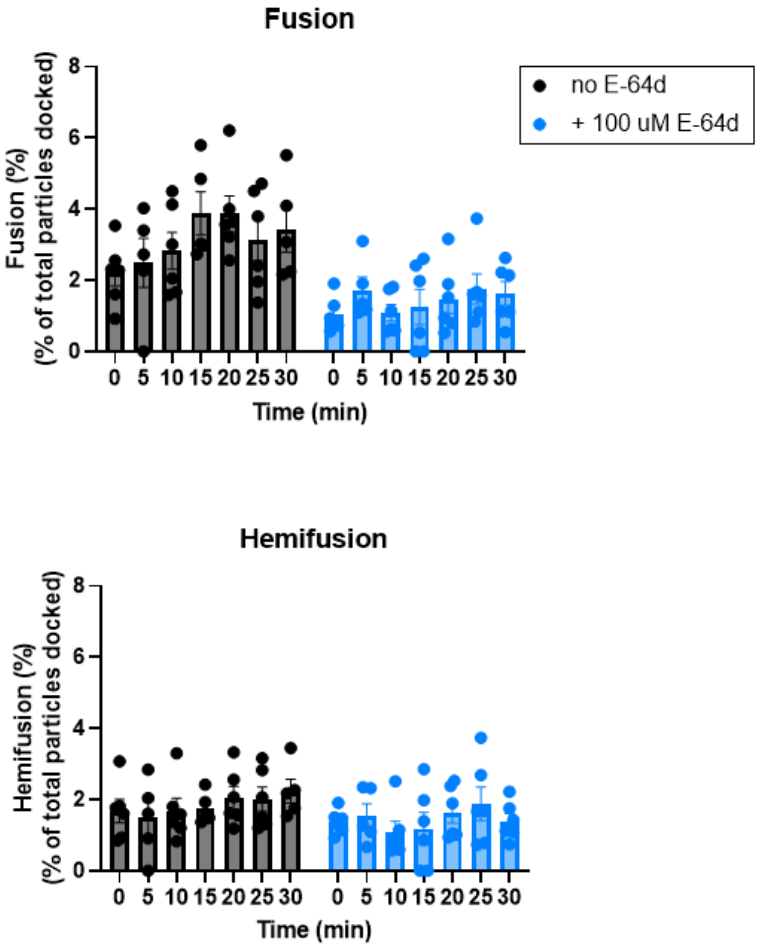


**Figure 2.S8. Fusion of Ebola pseudovirus with SPEMs in the presence or absence cysteine protease inhibitor, E-64d.** Movies were recorded immediately after E-64d in low pH buffer or only low pH buffer was flowed into the flow cell chamber (0') as well as 5, 10, 15, 20, 25, and 30 minutes after. Residual $Ca^{2+}$ was present from thermolysin treatment done to obtain cleaved GP. Each data point represents events observed on one separately prepared SPEM. Error bars indicate standard error.

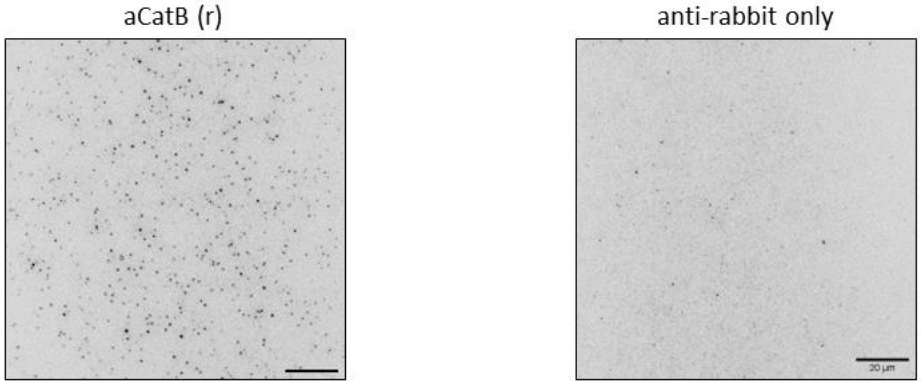


**Figure 2.S9. Assessment of presence of cathepsin B.** Antibody staining of SPEMs showing the presence of cathepsin B. r – rabbit antibody. The controls contain no primary antibody and only a donkey anti-rabbit antibody conjugated to alexa fluor 488.The cathepsin B antibody was used at a 1:2000 dilution in blocking buffer (15% FBS in PBS). The signal-to-noise ratio was adjusted to make the signal more apparent, with the secondary antibody only control being scaled similarly to the CatB image. The images are shown in reverse contrast. Scale bar: 20 µm.

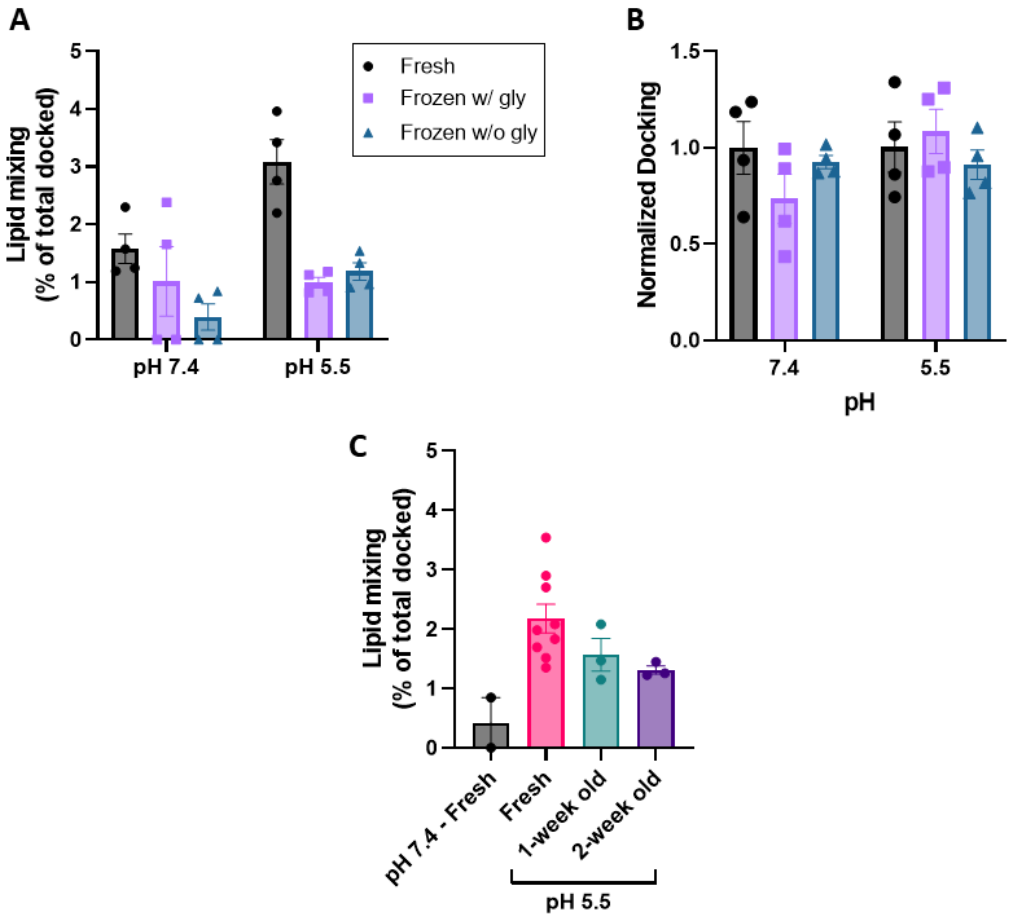


**Figure 10. Assessment of LASV GP-mediated fusion to SPEMs prepared from endosomes stored under different conditions.** HIV pseudoviruses bearing Lassa GP and labeled with Atto488-DMPE (outer leaflet only) were flowed into the flow chambers with SPEMs and attached to and allowed to undergo lipid mixing with the SPEMs at pH 7.4 and 5.5. **A.** Lipid mixing of Lassa pseudovirus with SPEMs prepared from freshly extracted endosomes, endosomes supplemented with 10% glycerol stored at -80°C (w/ gly) and endosomes without glycerol stored at -80°C (w/o gly). **B.** Docking of Lassa pseudovirus to SPEMs prepared from freshly extracted endosomes, endosomes supplemented with 10% glycerol stored at -80°C (w/ gly) and endosomes without glycerol stored at -80°C (w/o gly). **C.** Lipid mixing of Lassa pseudovirus with SPEMs prepared from freshly extracted endosomes, and endosomes stored at 4°C for one or two weeks.

# Chapter 3. Ebola virus glycoprotein interacts with cholesterol to enhance membrane fusion and cell entry

Jinwoo Lee, Alex J. B. Kreutzberger, Laura Odongo, Elizabeth A. Nelson, David A. Nyenhuis, Volker Kiessling, Binyong Liang, David S. Cafiso, Judith M. White, Lukas K. Tamm

Nature Structural & Molecular Biology. 2021. 28, 181–189.
doi: 10.1038/s41594-020-00548-4

My contribution to this work features in Figure 3.5C and D, and Supplemental Figures 3.S1 and 3.S6. I performed the single-particle fusion experiments with GP2 proteoliposomes (Figure 3.5C and D) and examined the oligomeric states of MPER/TM in micelles and bicelles (Figure 3.S1) and full-length GP2 in proteoliposomes (Figure 3.S6).

## 3.1 Abstract

Cholesterol serves critical roles in enveloped virus fusion by modulating membrane properties. The glycoprotein (GP) of Ebola virus (EBOV) promotes fusion in the endosome, a process that requires the endosomal cholesterol transporter NPC1. However, the role of cholesterol in EBOV fusion is unclear. Here we show that cholesterol in GP-containing membranes enhances fusion and that the membrane-proximal external region and transmembrane domain (MPER/TM) of GP interacts with cholesterol via several glycines in GP2 TM, notably G660. Compared to wild-type counterparts, a G660L mutation caused a more open angle between MPER and TM in a MPER/TM construct, higher probability of stalling at hemifusion for GP2

proteoliposomes, and lower cell entry of virus-like particles (VLPs). VLPs with depleted cholesterol show reduced cell entry and VLPs produced under cholesterol-lowering statin conditions show less entry than respective controls. We propose that cholesterol-TM interactions affect structural features of GP2 thereby facilitating fusion and cell entry.

## 3.2 Introduction

Ebola virus (EBOV) is a life-threatening pathogen known to cause hemorrhagic fevers (Feldmann & Geisbert, 2011a; Hoenen et al., 2006). The 2013–2016 epidemic in West Africa caused more than 10,000 casualties, and left survivors suffering with post EBOV disease (EVD) syndromes, such as increased intraocular pressure (Carod-Artal, 2015a, 2015b). It is unknown whether the virus was cleared from survivors, or if it persisted in specific tissues (Burki, 2016; Scott et al., 2016). While several treatment options are being explored against this deadly pathogen (Maxmen, 2019), a vaccine (Ervebo by Merck; https://www.fda.gov/news-events/press-announcements/first-fda-approved-vaccine-prevention-ebola-virus-disease-marking-critical-milestone-public-health) and a therapeutic cocktail of three monoclonal antibodies (Inmazeb by Regeneron; https://www.fda.gov/news-events/press-announcements/fda-approves-first-treatment-ebola-virus) have been recently approved .

The EBOV glycoprotein (GP) is the sole protein expressed in the viral membrane and is consequently the major target for neutralizing antibodies (Ito et al., 2001; Maruyama et al., 1999). GP, consisting of GP1 and GP2 subunits, is responsible for binding to cell surface attachment factors and mediating cellular entry through endosomes (Carette et al., 2011; Kondratowicz et al., 2011; Sakurai et al., 2015). Conformational changes in GP are thought to provide energy to overcome the barrier to membrane fusion (Harrison, 2008; Malashkevich et al., 1999; Weissenhorn et al., 1998; White et al., 2008). To do this GP binds to its endosomal receptor, Niemann-Pick C1 (NPC1), which in conjunction with low pH and perhaps other factors (Carette et al., 2011; Côté et al., 2011; Das et al., 2020; Fénéant et al., 2019), but independent of its

cholesterol transporting activity (Côté et al., 2011), triggers conformational changes that unclamp the hold that GP1 bears on GP2 and releases the fusion loop (FL) in GP2, so that it can embed in the target membrane. Subsequent folding of GP into a hairpin structure causes the viral and endosomal membranes to merge (Bortz et al., 2020; Das et al., 2020; Gregory et al., 2014; Harrison et al., 2011; Wang et al., 2016; White & Whittaker, 2016) (Figure 3.1A).

The FL of EBOV GP engages host endosomal membranes that contain NPC1, a cholesterol transporter. And, the transmembrane domain of GP is anchored in the viral membrane, which has a lipid composition reflecting that of the plasma membrane of producer cells and hence, a high concentration of cholesterol (Adu-Gyamfi et al., 2015; Carette et al., 2011; Côté et al., 2011). Lipid compositions of fusing membranes, including the amount of cholesterol, can strongly influence the energy barrier and thereby the efficiency of fusion (Churchward et al., 2005; Kreutzberger et al., 2015; Lee et al., 2013; Siegel, 2008; S.-T. Yang et al., 2016), and cholesterol has been shown to be important for the entry of several viruses (Biswas et al., 2008; Chlanda et al., 2016; Domanska et al., 2015; Wudiri et al., 2017; Yang et al., 2015; Yang et al., 2017; S. T. Yang et al., 2016). For examples, for HIV and influenza cholesterol in both viral and target membranes is critical for efficient fusion (Chlanda et al., 2016; Domanska et al., 2015; Sun & Whittaker, 2003; Yang et al., 2017; S.-T. Yang et al., 2016; S. T. Yang et al., 2016). However, a mechanistic understanding of any direct interaction of cholesterol with a viral GP is still lacking, and how cholesterol affects the participating membranes and the energy barrier for EBOV fusion have not been explored.

Despite this limited knowledge about potential cholesterol effects on EBOV fusion, there has been considerable debate about employing statins, cholesterol lowering drugs, to combat EBOV. Since EBOV disease is associated with endothelial barrier loss, Fedson et al. suggested benefits of using statins to suppress morbidity and mortality, due to their ability to improve endothelial integrity (in addition to lowering cholesterol levels) (Fedson et al., 2015). In addition, the statin simvastatin emerged in a screen of FDA-approved drugs for activity against EBOV in cell-based assays.

Shrivastava-Ranjan et al. subsequently found that statins block EBOV infection of cells *in vitro*, but the effects were not in the initial round of virus entry (Johansen et al., 2015). Instead, relatively high concentrations (20 and 50 μM) of lovastatin led to the production of EBOV particles defective for infecting a next set of cells (Shrivastava-Ranjan et al., 2018).

To address the question if cholesterol in the viral or target membrane directly affects membrane fusion and thereby viral entry and if it interacts directly with any portion of EBOV GP, we investigated cholesterol's role in these processes by setting up reconstituted single particle fusion and cell entry assays. The functional studies were complemented with biophysical assays for cholesterol binding to EBOV GP and measurements of tertiary structural changes in EBOV GP in response to cholesterol binding. Our results show that cholesterol physically interacts with the transmembrane domain of EBOV GP; that cholesterol in the viral membrane promotes membrane fusion and cell entry; and that producing viral-like particles in the presence of a few μM of the statin lovastatin results in particles that are severely compromised in their ability to enter cells.

## 3.3 Results

### Cholesterol in viral membrane enhances EBOV membrane fusion

Fusion of the EBOV membrane envelope with an endosomal membrane is essential for release of the viral genetic material into the cell cytoplasm to initiate an infection. As the only protein exposed on the external side of the viral membrane, the EBOV glycoprotein (GP) is solely responsible for receptor binding and membrane fusion. By analogy with other class I fusion proteins, the driving force for fusion is thought to be provided by conformational changes in the GP2 subunit that ultimately generate a six-helical bundle (White et al., 2008) (Figure 3.1A and B). In other systems lipid compositions of the participating membranes, including their cholesterol content, have been found to play pivotal roles in membrane fusion (Biswas et al., 2008; Chlanda et al., 2016; Churchward et al., 2005; Domanska et al., 2010; Kiessling et al., 2018; Alex J. B.

Kreutzberger et al., 2017; Kreutzberger et al., 2015; Lee et al., 2013; Liu & Boxer, 2020; Wudiri et al., 2017; S.-T. Yang et al., 2016). We therefore explored the role of cholesterol in viral surrogate and target membranes, for EBOV GP-mediated membrane fusion.

The effect of cholesterol on GP2-mediated EBOV fusion was first investigated by reconstituting full length GP2 into proteoliposomes (Lee et al., 2017) and assessing lipid mixing using a bulk fusion assay. Note that the endosomal receptor for EBOV, NPC1 (Carette et al., 2011; Côté et al., 2011), is not required in this 'minimal EBOV fusion system', as there is no need to release the GP1 clamp to expose GP2; GP2 proteoliposome fusion to liposomes is triggered solely by exposure to low pH (also see below). Förster resonance energy transfer (FRET) between Rhodamine (Rh) and nitrobenzoxadiazole (NBD) labeled lipids in target liposomes provided a measure of GP2-mediated lipid mixing, which was induced by lowering the pH to 5.5. Increasing cholesterol in the GP2 (viral analog) membrane enhanced fusion; increasing cholesterol in the target membrane caused a smaller enhancing effect (Figure 3.1C). Next, we tested the importance of cholesterol in the virus membrane, in the context of the full GP1/GP2 trimer, using a virus-like particle (VLP) cell entry assay. Depletion of VLP cholesterol with methyl-β-cyclodextran (MβCD) reduced entry efficiency by ~10-fold while cholesterol replenishment reversed this effect by ~50% (Figure 3.1D).

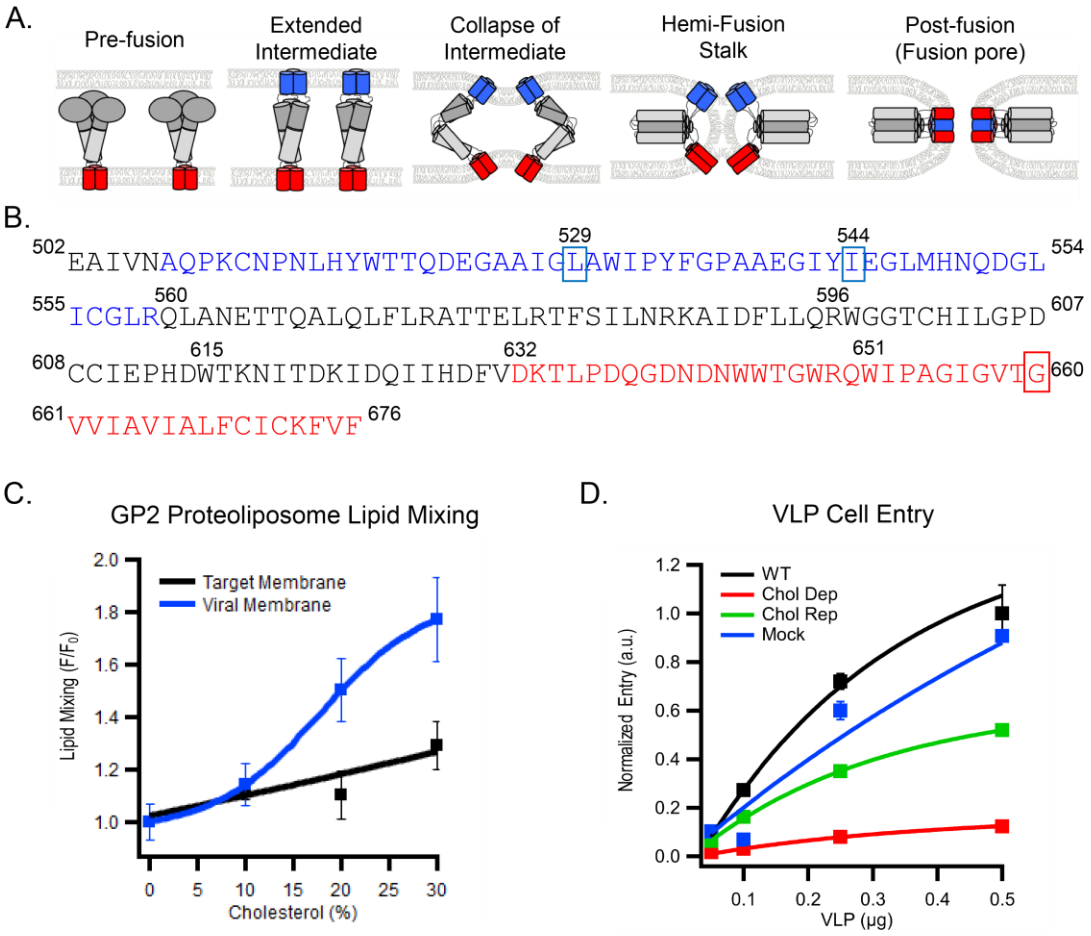


**Figure 3.1. Effect of cholesterol on EBOV membrane fusion. A.** Schematic of EBOV GP-mediated fusion highlighting the two membrane interacting domains. The fusion loop (FL) (blue) initiates fusion by interacting with the host cell membrane eventually pulling it towards the MPER/TM (red) embedded in the viral membrane. **B.** The EBOV GP2 sequence is shown using the same color scheme. Heptad repeats 1 and 2 that ultimately form the six-helix bundle extend from residues 560-595 and 615-631, respectively. Residues mutated in constructs used in this study are indicated with boxes. **C.** The relative extent of lipid mixing of GP2 proteoliposomes with target protein-free liposomes as observed by dequenching of FRET-paired lipid probes in the target liposome membrane. The fluorescent lipids NBD-DOPE and Rh-DOPE were included, each at 1.5 mol% in the liposome membrane to allow lipid mixing to be determined by dequenching of NBD fluorescence. The cholesterol content was varied in either the target or GP2 containing membrane while the cholesterol content in the other membrane was kept constant at 20% cholesterol. Data are mean and s.d. of triplicate measurements of the same reconstituted sample. **D.** Increasing amounts of VLPs, treated as indicated to modulate cholesterol content, were added to HEK293T cells and entry was monitored. Data are mean and s.d. of entry values from triplicate experiments

of the indicated input from the same VLP preparation. Based on cholesterol to protein ratios (see online Methods), the cholesterol content of the VLPs, relative to untreated VLPs, were: cholesterol-depleted VLPs, 1 %; cholesterol-repleted VLPs, 94 %; mock-treated VLPs, 79 %. Data for panels C and D are available as Source Data.

**Cholesterol interacts with the EBOV MPER/TM**

NMR spectroscopy was used to probe potential interactions between the membrane proximal extracellular region and transmembrane domain (MPER/TM) of GP2 and cholesterol. To do this an EBOV MPER/TM construct was prepared and incorporated into DMPC/DHPC (1:2 mol/mol, q=0.5) bicelles. Native gel electrophoresis showed that this construct behaves as a monomer in dodecyl-phosphocholine (DPC) micelles, but forms a higher oligomer, presumably a trimer, in DMPC/DHPC bicelles (Supplemental Figure 3.S1). $^{1}$H-$^{15}$N TROSY-HSQC spectra of EBOV MPER/TM in bicelles were then acquired at pH 5.5, in the absence or presence of varying concentrations of up to 20 mol% cholesterol (relative to DMPC) in the bicelles (Figure 3.2A). Three glycines (G655, G657, G660) and two nearby residues (I652, T659) in the TM domain showed chemical shifts upon adding cholesterol, with G660 (red box in Figure 3.1B) showing the most prominent change. This glycine is in a GXXXA motif that was previously suggested to bind cholesterol (Hacke et al., 2015). In order to test the hypothesis that G660 is required for the interaction of cholesterol with the EBOV MPER/TM, we mutated this glycine to leucine, (GXXXA to LXXXA), and performed the same solution NMR experiments. No chemical shift deviations were seen for G660L MPER/TM in the presence of cholesterol (Figure 3.2B). Figure 3.2C displays the chemical shift perturbations of WT and G660L induced by cholesterol along the sequence of EBOV MPER/TM.

To examine whether there is a direct interaction of cholesterol with EBOV MPER/TM, we employed the spin-labeled cholesterol analog 3β-doxyl-5α-cholestane and measured the attenuation of the amide proton signals along the sequence in comparison with the effects of cholesterol (Figure 3.2D and Supplemental Figure 3.S2).

Backbone amide proton resonances were dramatically reduced by the nitroxide paramagnetic spin probe of doxyl-cholestane in the region from W651 to A664, which comprises the headgroup contacting region of the EBOV MPER/TM structure including the GXXXA motif (residues 660–664) at the beginning of the TM domain. The amide proton signals of the remainder of the TM domain were also attenuated but to a lesser extent. These data further support the notion that cholesterol is in close contact with the TM domain of EBOV MPER/TM.

Secondary structure analyses using chemical shift indices of Cα atoms showed the same basic helix-break-helix structure for the G660L MPER/TM that had been previously described for the WT MPER/TM (Lee et al., 2017) (Supplemental Figure S.3A). Local backbone motions measured by heteronuclear NOEs, and by spin-lattice and spin-spin relaxation showed similar values and trends for G660L and WT (Supplemental Figure 3.S3B–D).

The absence of apparent differences in the secondary structure and backbone dynamics of the G660L compared to the WT MPER/TM does not exclude a potential change in tertiary structure. To test this hypothesis, we performed double electron electron resonance (DEER) experiments to measure distances and thus the angle between the two main segments of the EBOV MPER/TM structure. The MPER/TM construct was double labeled with *S*-(1-oxyl-2,2,5,5-tetramethyl-2,5-dihydro-1H-pyrrol-3-yl) methyl methanesulfonothioate (MTSL) at residues 643 and 670 and incorporated into DMPC/DHPC bicelles. The distance between the two probes in the mutant (G660L) MPER/TM was increased compared to the WT (Figure 3.3A) indicating that the angle between the MPER and TM domains is wider in G660L than that same angle previously determined by DEER in the WT MPER/TM structure (Lee et al., 2017) (Figure 3.3B and C). Observing DEER signals of MPER/TM reconstituted into POPC liposomes revealed similar trends (Supplemental Figure 3.S4).

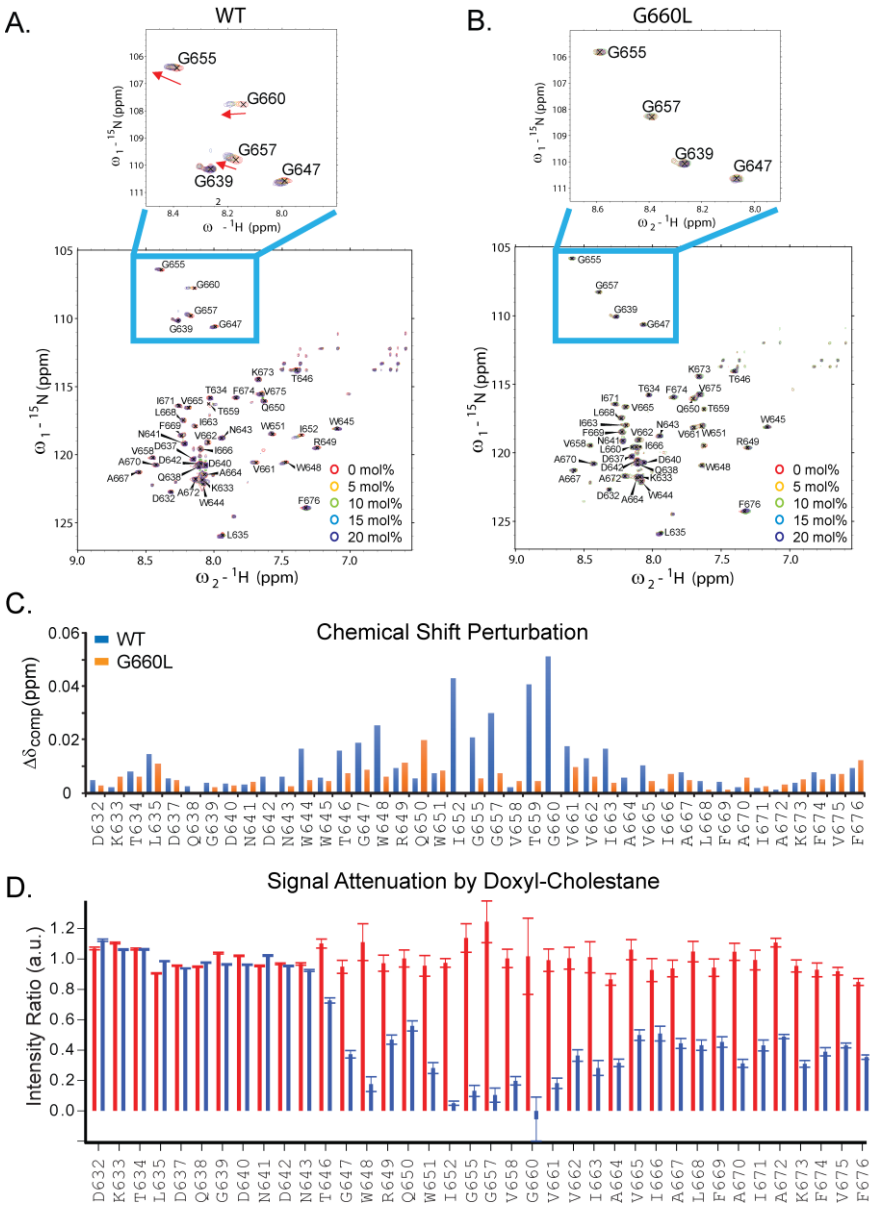


**Figure 3.2. Cholesterol interaction with the EBOV MPER/TM in DMPC/DHPC bicelles.** NMR spectra of WT (**A**) and G660L (**B**) EBOV MPER/TM in q=0.5 DMPC/DHPC bicelles were acquired in 0, 5, 10, 15, and 20 mol% cholesterol relative to DMPC. Red arrows denote peaks with the greatest changes. **C.** Chemical shift perturbations ($\Delta\delta comp = [\Delta\delta HN^2 + (\Delta\delta N/6.5)^2]^{0.5}$) in response to addition of 20 mol% cholesterol. WT (blue); G660L (green). **D.** Amide proton intensity changes with 5 mol% (relative to DMPC) cholesterol or 5 mol% 3β-doxyl-5α-cholestane added to EBOV MPER/TM in DMPC/DHPC bicelles. Red, intensity ratios between cholesterol and cholesterol-free bicelles. Blue, intensity ratios between doxyl-cholestane and cholesterol bicelles. The error bars in panel D were propagated from S/N of peak pairs and calibrated with duplicate measurements of the bicelle sample without cholesterol (analog).

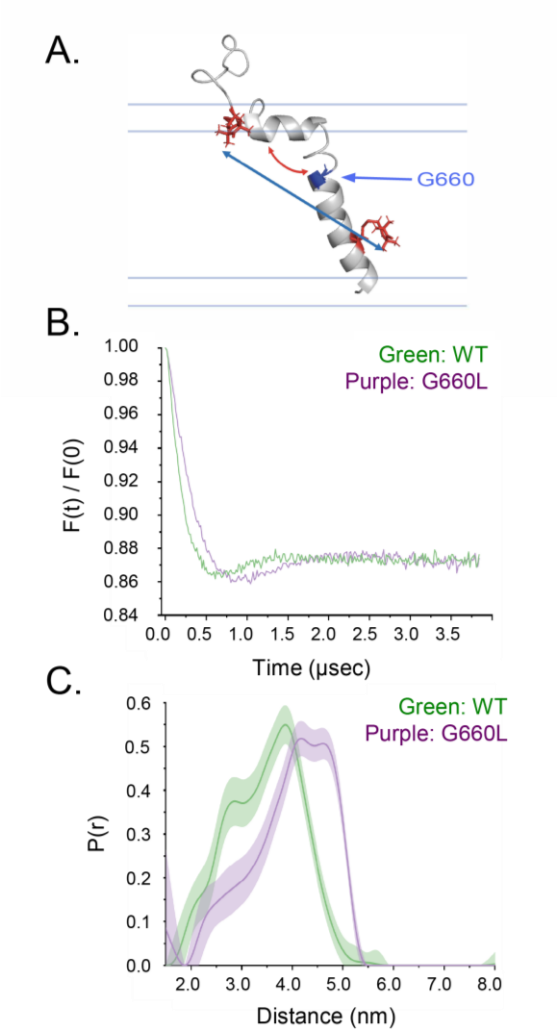


**Figure 3.3. Distance distribution obtained using DEER on double-MTSL-labeled WT and G660L EBOV MPER/TM in DMPC/DHPC bicelles. A.** Cartoon showing the position of the labels (N643C and A670C, red) in the EBOV MPER/TM structure (Lee et al., 2017). The position of G660 is also indicated (blue). Increasing the distance between the two label positions increases the indicated angle between the MPER and TM helices of MPER/TM. **B.** Background-corrected DEER data for WT and G660L EBOV MPER/TMs. **C.** Distance distributions obtained from DEER data of WT (green) and G660L (purple) EBOV MPER/TMs. The G660L mutation results in a shift towards longer distance components consistent with an opening of the MPER/TM angle.

**Viral membrane cholesterol enhances fusion and cell entry**

Imaging single fusion events allows the states of docking and fusion to be distinguished (Domanska et al., 2009; Domanska et al., 2010; Floyd et al., 2008; Kiessling

et al., 2010; A. J. B. Kreutzberger et al., 2017; Kreutzberger et al., 2015; Yang et al., 2015; Yang et al., 2017; S. T. Yang et al., 2016). Previously, influenza hemagglutinin incorporated into a planar supported lipid bilayer (SLB) was shown to fuse with labeled liposomes in a pH dependent manner (Hinterdorfer et al., 1994). Similarly, we incorporated EBOV GP2 into SLBs and monitored its interaction with individual liposomes dually-labeled with a membrane (DiD) and a self-quenched content (sulforhodamine B) dye using TIRF microscopy. Three distinct types of events were recorded: (A) *docking:* liposomes bind to the GP2-SLB but do not fuse (Figure 3.4A). (B) *fusion:* liposomes bind and then, after some time, fuse with the GP2-SLB (Figure 3.4B). (C) *stalled hemifusion:* liposomes bind and undergo lipid mixing, but no content mixing (Figure 3.4C). Stalled hemifusion events have previously been characterized in the context of SNARE-mediated fusion as off pathway events that infrequently proceed to full fusion (Kreutzberger et al., 2015). Similarly, during GP2-mediated fusion further changes in membrane or content dye distribution were seldom observed for the hemifusion events. The characteristic fluorescence traces originating from membrane dyes that distinguish stalled hemifusion from full fusion allow imaging to be done using only a membrane dye, as shown in Figure 3.4D.

The pH dependence of GP2-mediated fusion was explored utilizing this single particle assay. Injecting liposomes at different pH values and recording the total fluorescence within the evanescence field revealed a requirement for low pH for liposomes to efficiently bind to the GP2-SLB (Figure 3.4E and Supplemental Figure 3.S5). This lipid binding activity is likely due to pH dependent conformational changes in GP2 including changes in the structure of the fusion loop (Gregory et al., 2011), that lead to a quite deep insertion of the GP2 fusion loop into the liposome membrane (Gregory et al., 2011). In order to test that the fusion loop of GP2 is responsible for the pH dependent docking, we utilized a mutant (LIAA) with two substitutions in the fusion loop (L529A and I544A; boxed in blue in Figure 3.1B). Indeed, replacing WT GP2 with the LIAA mutant of GP2, in the single liposome fusion assay, abolished liposome binding at pH 5.5, which correlates with the previously shown inability of the LIAA EBOV GP fusion

loop to bind tightly to target membranes and to mediate fusion and cell entry (Gregory et al., 2014).

Single liposome assays allow the quantification of fusion kinetics by measuring the delay time between docking and the onset of fusion. Cumulative distribution functions of these delay times showed that ~40% of the liposomes that bind, fuse within ~0.2 seconds of docking (Figure 3.4F). Changing the pH to 6.5 greatly lowered the number of docking events (Figure 3.4E), but for the liposomes that did bind, the fusion kinetics did not change significantly.

Examining the cholesterol dependence of fusion of liposomes (50 nm diameter) with GP2-containing SLBs revealed that in the absence of cholesterol there were few full fusion events, but many stalled hemifusion events (Figure 3.5A, B). Increasing cholesterol increased the number of full fusion events and decreased the number of stalled hemifusion events (Figure 3.5A, B). The distribution of the delay times between docking and fusion revealed biphasic kinetics with initial fast and later slow components. The fast component appeared most sensitive to the presence of cholesterol (Figure 3.5B). A similar enhancing effect of cholesterol was seen for GP2 proteoliposomes (100 nm diameter) interacting with protein-free SLBs (Figure 3.5C, D). Cross-linking of GP2 in proteoliposomes showed that GP2 formed trimers in POPC:POPG (85:15) bilayers (Supplemental Figure 3.S6).

The mutant G660L, which showed decreased cholesterol binding to the TM domain (Figure 3.2B, C) and a wider angle between the MPER and TM domains (Figure 3.3) behaved differently than WT GP2 when incorporated (as G660L GP2) into an SLB and assayed for fusion with liposomes. With 30% cholesterol in the SLB, G660L GP2 displayed less full fusion and more stalled hemifusion (Figure 3.5E, F). The fusion kinetics were also strongly reduced for G660L compared to WT GP2 (Figure 3.5F). Trimerization of GP2 in proteoliposomes was not impaired by the G660L mutation (Supplemental Figure S.36).

We found that the G660L mutation also affects virus entry into HEK293T cells. Filamentous EBOV VLPs were prepared with WT or G660L EBOV GP (trimers of GP1/GP2) and then tested in a VLP entry assay. VLPs with G660L GP were significantly compromised for target cell entry (Figure 3.6A), despite equivalent incorporation of G660L GP into VLPs (GP/VP40 ratio = 1.36 +/- 0.47 relative to the GP/VP40 ratio for WT GP; based on 3 samples of each prep run on a single SDS gel and blotted for GP and VP40). Over a 5-fold range of VLP inputs, the cell entry efficiency of G660L VLPs was less than 20% that of WT VLPs (Figure 3.6A). The cholesterol content of G660L VLPs was measured to be 76 % that of WT VLPs. Overall, the results in Figure 3.5E, F and Figure 3.6A verify that residue G660 in the GP2 TM domain is critical for full fusion to occur efficiently.

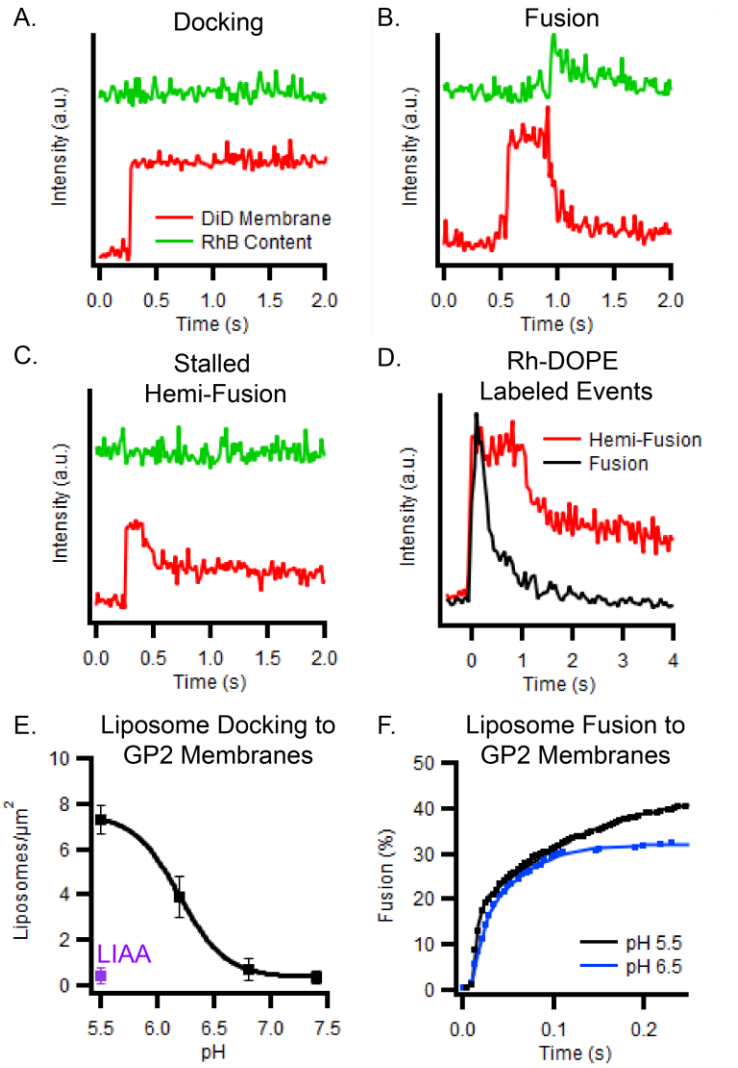


**Figure 3.4. Intensity traces of peak pixel intensity of DiD membrane label (red) and sulforhodamine B content label (green) of single vesicle events. A.** Binding (docking) of a liposome to a supported lipid bilayer containing EBOV GP2 is marked by the increase in DiD intensity seen when the vesicle enters the TIRF field. The sulforhodamine B label is self-quenched and no intensity change is observed. **B.** A fusion event followed by binding of a liposome to the GP2-containing supported bilayer. After ~0.5 s the membrane dye diffuses into the supported bilayer at the onset of fusion. The sulforhodamine B label dequenches at the moment of fusion and diffuses away into the cleft under the supported bilayer. **C.** A stalled hemifusion event where the membrane dye in the outer leaflet of the liposome diffused into the supported bilayer (loss of ~55% of the intensity) while no change in the content dye is observed. **D.** Full and hemifusion events can be observed using particles labeled with only a membrane dye (as shown for Rh-DOPE) by observing if all or half of the membrane dye diffuses into the supported bilayer. **E.** Effects of pH and a double-point mutation in the fusion loop, LIAA (purple); see Figure 3.1A) on liposome binding to GP2-containing supported lipid bilayers.

Experiments were conducted as shown in Supplemental Figure 3.S5 and saturation values were determined by single exponential fits. Data points show mean and s.e.m. of saturation values for triplicate experiments performed on 3 different supported bilayers. **F.** Cumulative fusion delay times for liposomes bound to GP2-containing supported bilayers at pH 5.5 or 6.5. Data were collected from 4 different supported bilayers. Data for panels E and F are available as Source Data.

**EBOV VLPs from statin-treated cells show reduced entry**

Based on the previous results, we hypothesized that VLPs budded from cholesterol-depleted cells would have less cholesterol in their membrane and therefore be impaired in membrane fusion and hence entry capacity. To test this hypothesis, we used a cholesterol-lowering statin to reduce the cholesterol content of the HEK293T cell plasma membrane from which VLPs are produced by budding. Two sets of VLPs were prepared in parallel: one set from mock (DMSO) treated and the second from statin-treated HEK293T cells. VLPs produced from statin treated cells exhibited markedly lower entry efficiency than VLPs produced from mock treated cells (Figure 3.6B). VLPs prepared from statin-treated cells contained 22% the level of cholesterol and approximately equivalent levels of GP (Supplemental Figure 3.S7) compared to VLPs produced from mock-treated cells.

The findings in Figure 3.6 are consistent with the demonstration that treatment of VLPs (from non-statin-treated producer cells) with MBCD decreases both their cholesterol content and entry efficiency (Figure 3.1D). We propose that, because of their lowered cholesterol content, VLPs with WT GP produced from statin treated cells enter target cells less efficiently than VLPs produced from mock treated cells (Figure 3.6C) because less cholesterol is available to bind to the GP2 TM, and therefore influence the structure of GP for optimal fusion. An inference is that VLPs with G660L GP should show the same (low) entry capacity whether or not depleted of cholesterol or when produced in untreated or statin-treated cells; we have not performed these experiments here because G660L VLP entry is already significantly suppressed compared to WT and a further reduction of entry capacity after cholesterol extraction would be

difficult to detect in a conclusive manner. However, such experiments may be interesting to explore in the future.

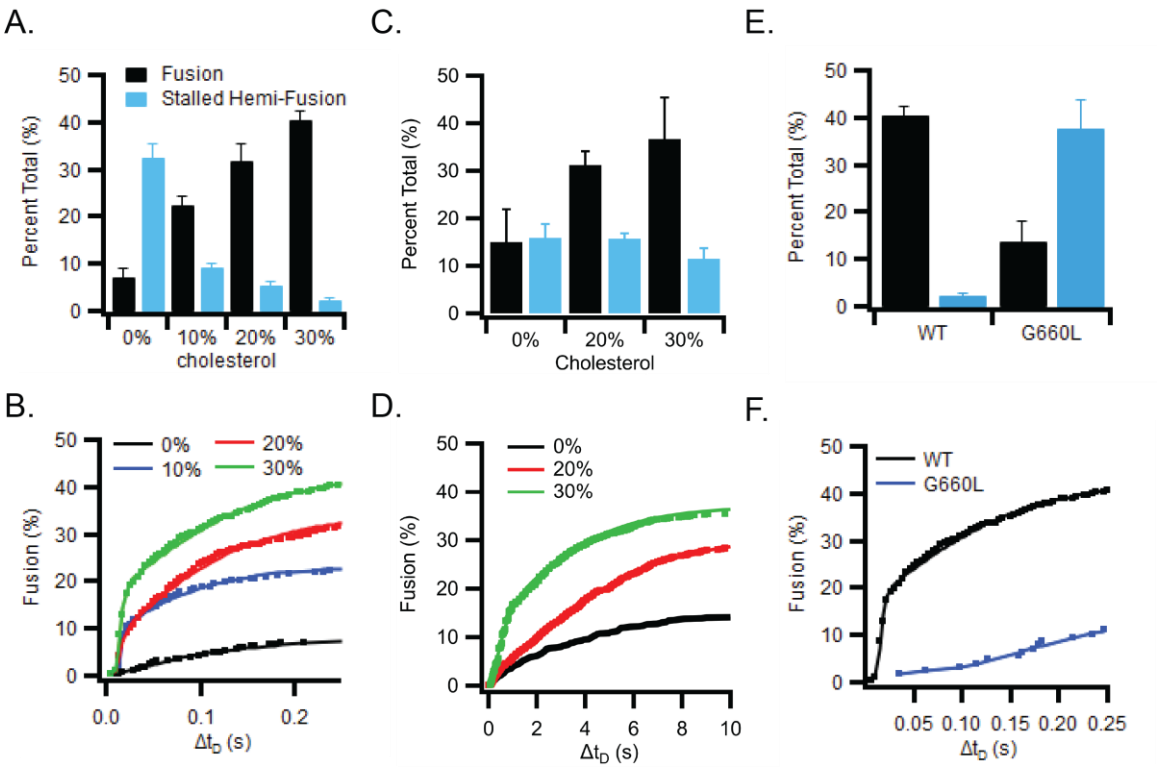


**Figure 3.5. The cholesterol dependence of fusion. A.** Fusion of liposomes (50 nm diameter) with supported bilayers containing GP2 (lipid:protein ratio of 1000) and increasing amounts of cholesterol. **B.** Cumulative distribution of the delay times from the time of binding until the time of fusion of liposomes to GP2-containing supported bilayers with increasing amounts of cholesterol. **C.** Fusion of GP2-proteolipsomes (100 nm diameter, POPC plus 1 mol% Rh-DOPE) plus 0, 20, or 30 mol% cholesterol with protein-free supported bilayers (77:20:3 POPC:Chol:DPS). **D.** Cumulative distribution of fusion delay times for GP2 proteoliposomes with 0, 20, or 30 mol% cholesterol. **E.** Fusion of liposomes to supported bilayers containing wt (black) or G660L (blue) GP2. **F.** Cumulative distribution of the delay times from the time of binding until the time of fusion for liposomes to supported bilayers containing wt (black) or G660L (blue) GP2. Bar graphs in panels A, C and E show mean and s.e.m. from 3–6 independent experiments under each condition. Typically, 1000-2000 particles were collectively counted in these experiments. The kinetic fusion data in panels B, D, and F were collected from the same experiments pooling all approximately 1000-2000 events from the 3-6 independent bilayers under each condition. Data including number of repeats and particles measured under each condition are available as Source Data.

## 3.4 Discussion

The lipid compositions of the membranes that partner in viral fusion events are important (S.-T. Yang et al., 2016), but this aspect has not been explored in detail for EBOV. In this study, we probed the role of cholesterol in EBOV GP-mediated fusion and cell entry. We found that cholesterol, in the membrane of three different viral membrane surrogates, promotes EBOV fusion and entry. NMR experiments revealed that the initiating glycine (G) in a $G_{660}$XXXA motif in the EBOV GP transmembrane domain promotes an interaction with cholesterol, and DEER experiments indicated that changing G660 to leucine (L) alters the tertiary structure of the membrane proximal external region-transmembrane (MPER/TM) domain of EBOV GP, which correlates with the diminished fusion and entry activity of GP constructs with the G660L mutation. Single particle fusion studies employing supported lipid bilayers (SLBs) and TIRF microscopy further showed that cholesterol in viral membrane surrogates promotes EBOV GP-mediated membrane fusion, and that a mutation (G660L) in the cholesterol binding site greatly reduces membrane fusion. These latter findings correlated with a reduced capacity of EBOV-GP VLPs with either reduced cholesterol content or the G660L mutation to enter cells.

Cholesterol is required in host cell membranes at both the entry and assembly stages of viral lifecycles (Schroeder, 2010). A cholesterol requirement for virus entry has been demonstrated for HIV (Lai et al., 2012; Yang et al., 2015; Yang et al., 2017; S. T. Yang et al., 2016), influenza (Biswas et al., 2008; Chlanda et al., 2016; Domanska et al., 2013; Goronzy et al., 2018; Zawada et al., 2016), herpes simplex (Wudiri et al., 2017), and human parainfluenza 3 (Tang et al., 2020) viruses. A cholesterol recognition amino acid consensus (CRAC) motif in the MPER of the gp41 subunit has been implicated in HIV's cholesterol dependence(Chen et al., 2009; Vincent et al., 2002), but the mechanism by which this motif promotes fusion has not been elucidated. Influenza also has been identified as having a cholesterol consensus motif (CCM) at the N-terminal end of the TMD of its hemagglutinin protein (de Vries et al., 2015). Hemolysis, lipid mixing, and cell-cell fusion were impaired by disrupting this motif in hemagglutinin (Hu et al.,

2019). While cholesterol has been identified as necessary for entry of other viruses (Tang et al., 2019; Wudiri et al., 2017), their sites for cholesterol binding and mechanism(s) by which cholesterol enhances their fusion activity remain unknown.

Here, after demonstrating a fusion-promoting role for cholesterol in the membrane of EBOV, we identified a cholesterol binding motif in EBOV GP2, employing NMR chemical shift analysis, with residues I652, G655, G657, T659 and G660, located in the region connecting the MPER and TM domains of MPER/TM, interacting with cholesterol (Figure 3.2C), with confirmation by PRE data (Figure 3.2D and Supplemental Figure 3.2). G660 is part of a GXXXA motif at the beginning of the TM domain of GP2 that was previously mutated to investigate the cell detachment effect caused by ectopic expression of EBOV GP (Hacke et al., 2015); that effect was found to be cholesterol-dependent, and the authors reported greater photoactivatable cholesterol binding to WT (GXXXA) than LXXXL GP. A second study asked whether the GXXXA motif is involved in the ability of EBOV to counter the effect of tetherin, a cellular interferon induced anti-viral protein; that response was found to be cholesterol independent (Brinkmann et al., 2016), and the authors reported an ~50% reduction in cell entry of pseudoviruses bearing LXXXL GP as well as a delay of infection, and an ~1 log decrease in titer of recombinant VSV bearing LXXXL GP. Our study provides direct biophysical evidence that GXXXA in the TM domain of EBOV GP indeed contributes to cholesterol binding. We also showed that cholesterol in the viral membrane and G660, are critical for optimal EBOV fusion and entry. The GXXXA sequence (G[V/I]IIA) is present in all annotated Ebolavirus GP2 sequences, whereas Marburgvirus GPs have the sequence LSIAV at the equivalent position.

How does cholesterol in the viral membrane enhance Ebola fusion? Cholesterol can affect the function of membrane proteins in cholesterol-containing bilayers by imparting general effects on membrane structure (e.g., curvature, phase behavior, and thickness) and also by binding to specific protein motifs, which include CRACs, CARCs, and CCMs (S.-T. Yang et al., 2016). We propose that cholesterol has a direct effect on EBOV GP. Specifically, we suggest that by binding to the GXXXA motif in the EBOV TMD

(Figure 3.2), cholesterol affects the environmental structure of the MPER/TM domain (the angle between the two helical segments is altered; Figure 3.3), which in turn affects the ability of GP to mediate fusion (Figures 3.5 and 3.6). This could be by preferentially positioning the MPER/TM for binding to the fusion loop (Lee et al., 2017) at the 'fold-back' stage of fusion, by altering the structure of the EBOV ectodomain and its consequent fusion ability, and/or by changing the structure or properties of the bilayer surrounding GP. The latter possibilities clearly require future experimentation.

In addition to its role in the viral membrane, cholesterol in the *target* membrane may also promote fusion. In the case of influenza, cholesterol in the target membrane was shown to promote full fusion and minimize stalled hemifusion reactions (Chlanda et al., 2016). For HIV (Graham, 2003) cholesterol is important in the target membrane (Liao et al., 2001), with fusion occurring preferentially at boundaries between cholesterol-rich ordered (Lo) and cholesterol-poor disordered (Ld) domains within target membranes (Yang et al., 2015; Yang et al., 2017). For EBOV, an early study showed that depletion of cholesterol from target membranes inhibits infection by EBOV GP pseudoviruses (Yonezawa et al., 2005). And, a 16-residue peptide from within the EBOV fusion loop was found to bind preferentially to cholesterol-rich domains in target membranes (Freitas et al., 2011). However, we observed only a mild enhancing effect of cholesterol in the target membrane (Figure 3.1C).

Our results also shed new light on how cholesterol lowering statins may reduce the burden of EBOV infections. For example, the statin simvastatin emerged in a screen of FDA-approved drugs for activity against EBOV in cell-based assays (Johansen et al., 2015). We found that VLPs produced from cells treated with 4 μM lovastatin had a reduced cholesterol content and consequently were impaired in their ability to enter cells by membrane fusion. Thus, our findings, using a lower dose (4 μM) of lovastatin, concur with the previous conclusion (Shrivastava-Ranjan et al., 2018) that treatment of producer cells with lovastatin (albeit higher doses; 20 and 50 μM) generates EBOV particles with reduced entry and infection capacity (Figure 3.6). Shrivastava-Ranjan et al. (Shrivastava-Ranjan et al., 2018) attributed the lowered infectivity of EBOV particles

produced in the presence of 20-50 μM lovastatin to reduced incorporation of EBOV GP, whereas we posit that a major cause of reduced infectivity in particles produced in the presence of (4 μM) lovastatin is reduced cholesterol binding to the GXXXA motif in the TMD of GP and its consequently reduced fusion activity. The collective results ((Fedson et al., 2015; Shrivastava-Ranjan et al., 2018), and this study) suggest that statins warrant consideration as part of a multi-component treatment for patients infected with EBOV.

In conclusion, this study provides direct biophysical evidence for a cholesterol binding (GXXXA) motif in the TM domain of the EBOV GP as well as molecular insight into how cholesterol, via this motif, alters the structure of the MPER/TMD region of GP. This change may affect the structural transformation of the EBOV GP ectodomain (and/or the membrane surrounding GP) that is required to facilitate membrane fusion. Our findings also bear on the mechanism by which statins may result in the production of fusion-inefficient EBOV particles and hence on considerations of whether and how (e.g., as part of a drug cocktail (Dyall et al., 2018)) to use statin drugs to treat EBOV-infected patients.

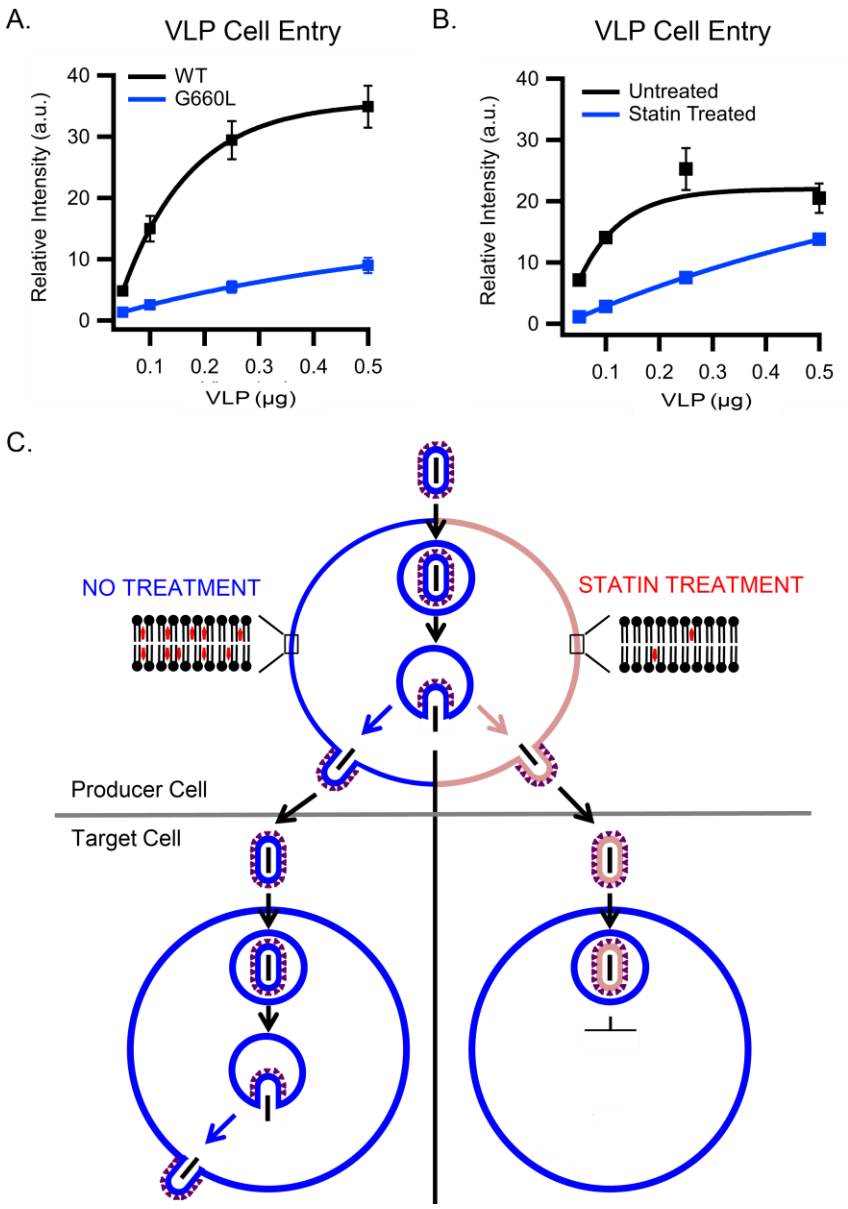


**Figure 3.6. A mutation (G660L) in the cholesterol binding domain in EBOV GP2 or preparation of EBOV VLPs from statin-treated cells inhibits the entry capacity of EBOV GP VLPs. A.** VLPs were prepared with WT or G660L EBOV GP and assayed for VLP cell entry as in the legend to Figure 3.1D. Data are mean and s.d. of cell entry values from triplicate samples of the indicated input of the indicated VLP preparation. **B.** Increasing amounts of VLPs produced from untreated (black) or statin-treated (blue) cells were added to HEK293T cells and assayed (in triplicate) and analyzed for cytoplasmic entry as in (A). The experiment displayed is representative of 2 independent experiments. **C.** Schematic depicting (top) VLP production from untreated (left) or statin-treated (right) producer cells and (bottom) their subsequent entry into fresh

(untreated) HEK293T cells. Blue denotes VLPs and plasma membranes with normal content of cholesterol; pink depicts VLPs and plasma membranes depleted for cholesterol (by virtue of statin treatment). Data for panels A and B are available as Source Data.

## 3.5 Materials and Methods

**Expression and purification of MPER/TM domain and GP2 constructs**

Expression and purification of EBOV MPER/TM was carried out as described previously with slight modification (Lee et al., 2017). Briefly, cells were grown to OD600? 0.8 at 37°C and incubated 4 hrs after induction with the final concentration of 1 mM IPTG. MPER/TM was then purified as follows. Cells were harvested and resuspended in 20 mM Tris, 300 mM NaCl, and 10% sucrose, pH 8, sonicated and then centrifuged for 1 hr at 40,000xg at 15°C. The resulting pellets containing inclusion bodies were solubilized with 20 mM Tris, 300 mM NaCl, 8 M urea and 1% Triton X-100, pH 8. Following the same sonication and centrifugation steps, the supernatant was incubated with 5 mL of Ni-NTA beads for 1 hr. The beads were washed with an 8 M to 0 M urea gradient to remove urea and Trition X-100. Thrombin (in 20 mM Tris, 300 mM NaCl, 1% n-octyl-β-D-glucopyranoside [β-OG]) was then added to the Ni-NTA beads and incubated overnight to elute the EBOV MPER/TM.

Preparation of full-length GP2 was carried out as described previously (Lee et al., 2017) using the previously described pET-24a vector (kanamycin resistant) encoding (N- to C-) a Trp leader protein, a thrombin cleavage site, and Ebola GP2 followed by an N-terminal His-tag; C670 and C672 were mutated to alanine to avoid formation of non-native disulfides (Lee et al., 2017). One liter of BL21(DE3) cells transformed with the GP2 expression vector was grown to $O.D._{600}$ of 0.6-0.8, induced with 1 mM IPTG, and harvested 4 hrs later. The cells were resuspended in 100 mL 20 mM Tris buffer pH 8.0 containing 100 mM NaCl and 10% sucrose, lysed by sonication until homogeneous, and centrifuged for 30 min at 40,000 x g at 10 °C. The pellets, which contained inclusion bodies, were solubilized in 100 mL 20 mM Tris buffer pH 8.0 containing 100 mM NaCl, 8 M urea, and 1% Triton X-100 by sonication and the solution centrifuged as above. The

supernatant was collected and incubated with 5 mL of Ni affinity beads for $\geq$ 1 hr at 4°C. Finally, a urea gradient (total 500 mL of 8 to 0 M urea in Tris buffer) was applied to the Ni column to remove urea and Triton X-100. The Trp leader protein was then removed by treating resuspended Ni beads with 100 □L of 5 mg/ml thrombin (in 25 mL of DPC buffer: 20 mM Tris buffer pH 8.0 containing 100 mM NaCl and 0.2 % DPC). After 2 hrs (with rotation at RT), the beads were transferred to a column, the GP2 containing eluate was collected, and the beads were washed with another 20 mL of 0.2% DPC buffer thereby collecting all of the GP2 protein. Collected fractions were pooled, concentrated, and run over a Superdex 200 size exclusion column in the final required buffer with 0.2% DPC. For NMR studies, the final buffer was 20 mM Na phosphate pH 7 or pH 5.5 containing 100 mM NaCl and 0.2% DPC. For NMR samples, cells were grown in minimal media containing $^{15}NH_4SO_4$ and $^{13}C$-glucose and induction was performed at 25 °C overnight. The mutants of the respective constructs were prepared using the same protocols.

**Native gel of MPER/TM**

To check the oligomeric state of MPER/TM in DPC micelles and DMPC/DHPC (1:2) bicelles (prepared as for NMR experiments), samples of both were run on a pre-cast 4-16% Bis-Tris native gel (Invitrogen) following the manufacturer's protocol. Briefly, the gel samples were prepared by adding 0.5 µL of 5% G-250 sample additive (Thermo Fisher), 5 mM DDM and 5 µL of 4X NativePage sample buffer (Invitrogen) to 15 µL of micelle or bicelle samples each containing 15 µg MPER/TM. The samples were then loaded onto the gel and electrophoresis was performed on ice at constant voltage (150 V) for 100 minutes with cold 1X Anode Buffer and 1X Dark Blue Cathode Buffer (Invitrogen).

**Cross-linking of GP2 proteoliposomes**

POPC:POPG (85:15) proteoliposomes with WT and G660L GP2, with an estimated protein:lipid ratio 1:100, were incubated with 10 mM 3,3'-

dithiobis(sulfosuccinimidylpropionate) (DTSSP, Sigma Aldrich) for 0, 15 or 30 mins at room temperature. The reaction was quenched by adding 50 mM Tris pH 7.5. The samples were then boiled in the presence of SDS sample buffer for 5 minutes, and separated by non-reducing 4-20% SDS-PAGE. The gels were stained with silver stain (Merril et al., 1981).

**Incorporation of EBOV MPER/TM into bicelles**

The incorporation of EBOV MPER/TM into DMPC/DHPC bicelles was performed as described previously (Lee et al., 2017). In brief, the EBOV MPER/TM in β-OG buffer (20 mM Tris, 300 mM NaCl, 1% β-OG) was mixed with the appropriate amount of DMPC (16 mg for final 250uL) and dialyzed to remove β-OG. Dialysis was performed 3 days against NMR buffer (25 mM sodium phosphate, 100 mM NaCl) starting at pH 7.5 on the first day, 6.5 on the second day, and 5.5 on the third day at 4°C. Then, EBOV MPER/TM containing liposomes were concentrated and DHPC was added to form bicelles. The q value for all bicelles was 0.5. To prepare bicelles with varying mol% cholesterol or nitroxide cholesterol analog, 3β-doxyl-5α-cholestane (Sigma-Aldrich), preformed bicelles were added to tubes to which specific amounts of cholesterol (or analog) had previously been dried down from their respective stocks in chloroform (under a stream of nitrogen followed by vacuum desiccation). The tubes were then subjected to cycles of freeze-thawing (~5 cycles or until a clear solution was obtained) using liquid $N_2$ and hot (initially ~100 °C) water.

**NMR experiments**

After obtaining EBOV MPER/TM incorporated bicelles, all NMR spectra of the MPER/TM domain were acquired at 45°C on a Bruker Avance III 800 MHz spectrometer. $^{1}H$-$^{15}N$ TROSY based HSQC, $^{15}N$-heteronuclear NOEs, $^{15}N$ T1 and T2 experiments were performed as described (Lee et al., 2017) and all NMR data were processed using NMRPipe and SPARKY (Delaglio et al., 1995; Goddard & Kneller, 2008). Chemical shift perturbations, defined as $\Delta\delta comp = [\Delta\delta HN^2 + (\Delta\delta N/6.5)^2]^{1/2}$ were plotted as a function of residues. The error bars in the intensity ratio plots were propagated from S/N of peak

pairs and calibrated with duplicate measurements of the bicelle sample without cholesterol (analog).

**EBOV MPER/TM in bicelles and DEER experiments**

The EBOV MPER/TM construct was labeled with an MTSL nitroxide probe at both 643 and 670 positions using the method described previously (Lee et al., 2017). Double MTSL labeled EBOV MPER/TM was incorporated into DMPC/DHPC bicelles following the method described above. Approximately 15 µL of an EBOV MPER/TM bicelle sample with 15% deuterated glycerol was loaded into quartz capillary tubes with an inner diameter of 1.1 mm and outer diameter of 1.6 mm (Vitrocom). Samples were frozen in liquid nitrogen and loaded into a Bruker E580 spectrometer with an EN5107D2 resonator. DEER data were collected at Q-band and 80 K using a dead-time free four-pulse sequence with 16 step phase cycling. Pump and observe pulses were separated by 75 MHz. The program LongDistances by Christian Altenbach (UCLA) was used for the removal of background functions from initial V(t)/V(0) data and the model-free fitting regime was used to extract distance distributions from the resulting F(t)/F(0) (Jeschke & Polyhach, 2007). The value of the smoothing factor for the fits was 30.

**Bulk lipid mixing assay**

The fusion assay of full-length GP2 proteoliposomes was carried out as described previously (Lee et al., 2017). Briefly, POPC/POPG (85/15) liposomes were prepared in HMA buffer (10 mM HEPES/MES/Tris, 100 mM NaCl, pH 7.4) (HEPES: 4-(2-hydroxyethyl)piperazine-1-ethanesulfonic acid, N-(2-hydroxyethyl)piperazine-N'-(2-ethanesulfonic acid); MES: 2-(N-morpholino)ethanesulfonic acid hydrate, 4-morpholineethanesulfonic acid) by extrusion through 100-nm polycarbonate filters. Then, 20 mM Tris, 100 mM NaCl, pH 8, buffer containing 1% β-OG was added to the extruded liposomes to a final concentration of 0.125% β-OG and then incubated at room temperature for at least 1 hr. Then, EBOV GP2 in DPC was added to give an estimated protein:lipid ratio of 1:100 and incubated for at least 1 hr before dialysis.

Extensive dialysis against HMA buffer was performed to remove all detergent and to incorporate EBOV GP2 into the liposomes. Cholesterol concentration was changed from 0 to 30 mol% relative to total lipid concentration while keeping the POPG concentration constant. Labeled liposomes containing 1.5 mol % of both Rh-DOPE and NBD-DOPE were prepared by extrusion as described above.

To measure fusion, fluorescent liposomes and unlabeled proteoliposomes were mixed at a ratio of 1:9 in HMA buffer. Relief of NBD-Rh FRET was recorded at 37°C as a function of time with mixing between each reading. Excitation and emission wavelengths were set at 460 nm and 538 nm, respectively. Percent lipid mixing (fusion) was determined as the fraction of the maximal FRET relief observed after addition of 2% Triton X-100 at the end of each reaction. All mutant lipid mixing data were normalized to the extent of lipid mixing observed with the WT protein.

**Preparation of protein-free liposomes**

POPC lipids and the desired membrane dye (1 mol% of either rhodamine-DOPE or DiD) were pipetted into a glass tube at the desired concentration from chloroform solutions and then dried down using $N_2$ gas. Lipids were further dried in a vacuum desiccator for >1 hr. Lipids were then suspended in the desired volume of buffer (for content dye experiments, 50 mM sulforhodamine B was included in the buffer that the POPC/DiD liposomes were suspended in). The lipid suspension was freeze-thawed in liquid nitrogen and a water bath 5 times, followed by extrusion through a 100 nm pore polycarbonate filter (Avestin). After extrusion, the membrane labeled (Rhodamine-DOPE) liposomes were used within 36 hrs. The content/membrane labeled liposomes were run over a G-50 superfine Sephadex size exclusion column (GE Healthcare, Piscataway, NJ) to remove the free sulforhodamine B label and the collected liposomes were used within 36 hr.

**Preparation of planar supported bilayers containing EBOV GP2**

Planar supported bilayers containing EBOV GP2 were prepared by the Langmuir-Blodgett/vesicle fusion technique as described in previous studies (Hinterdorfer et al., 1994; Kalb et al., 1992). Quartz slides were cleaned by dipping in sulfuric acid/hydrogen peroxide (3:1) for 15 mins using a Teflon holder. Slides were then rinsed thoroughly in water. The first leaflet of the bilayer was prepared by Langmuir-Blodgett transfer directly onto the quartz slide using a Nima 611 Langmuir-Blodgett trough by applying POPC and the indicated amount of cholesterol from a chloroform solution to the air-water interface of the trough. Where indicated 3 mol% of 1,2-dimyristoyl-*sn*-gycero-3-phosphatidylethanolamine-PEG3400-triethoxysilane (DPS) was included in the Langmuir film to produce a polymer-cushioned supported bilayer. After allowing the solvent to evaporate for 10 min, the monolayer was compressed at a rate of 10 $cm^2$/min to reach a surface pressure of 32 mN/m. After equilibration for 5 to 10 min, a clean quartz slide was rapidly (68 mm/min) dipped into the trough and slowly (5 mm/min) withdrawn while a computer maintained a constant surface pressure and monitored the transfer of lipids with head groups down onto the hydrophilic substrate. POPC liposomes with the indicated amount of cholesterol reconstituted with GP2 at a lipid/protein ratio of 1000:1 was incubated with the Langmuir-Blodgett monolayer in a perfusable holding cell to form the outer leaflet of the planar supported bilayer. After incubation of the proteoliposomes for 2 hrs, the excess proteoliposomes were removed by washing with 10 ml of HMA buffer (10 mM Hepes, 10 mM MES, 10 mM NaOAc and 100 mM, NaCl, pH 7.4).

**Single particle binding and fusion assay**

For planar supported bilayer binding assays and single particle fusion assays, holding cells with the planar supported bilayers were mounted on a Zeiss Axiovert 25 fluorescence microscope (Carl Zeiss, Thornwood, NY) equipped with a 63x water immersion objective (Zeiss; N.A. 0.95) and prism-based TIRF illumination. The light source was an OBIS 532 LS laser from Coherent Inc. (Santa Clara, Ca.). Fluorescence was

observed through a 610 nm bandpass filter (D610/60; Chroma, Brattleboro, VT) by an electron multiplying CCD (DU-860E; Andor Technologies). The EMCCD was cooled to -70°C. The prism-quartz interface was lubricated with glycerol to allow easy translocation of the holding cell on the microscope stage. The beam was totally internally reflected at an angle of 72° from the surface normal, resulting in an evanescent wave that decays exponentially with a characteristic penetration depth of ~100 nm. An elliptical area of 250 x 65 µm was illuminated. The laser intensity, shutter, and camera were controlled by a homemade program written in LabVIEW (National Instruments, Austin, TX).

The binding assay was performed by injecting POPC liposomes (10 µM lipid with 1 mol% rhodamine-DOPE). One image was taken before injecting liposomes, and images were taken every 30 sec thereafter for 5 mins. This was done at the pH values indicated in the text and the total intensity of the field of view was recorded.

Single particle fusion data were obtained by injecting 500 nM lipid of POPC:Chol:Rh-DOPE (79:20:1) containing liposomes. This was first done at pH 7.4 to confirm that no docking or fusion occurred at neutral pH. The planar supported bilayers were then washed and the solution replaced with one containing pH 5.5 (or pH 6.5 as indicated in the text) buffer and a second replacement with 500 nM lipid of liposomes in the same buffer. Five movies were recorded for 1 min for each bilayer at a rate of 4 frames/ms. Single-particle fusion data were analyzed using a program written in LabVIEW (National Instruments). Stacks of images were filtered by a moving average filter. The maximum intensity for each pixel over the whole stack was projected on a single image. Liposomes were located in this image by a single-particle detection algorithm described in Kiessling et al. (Kiessling et al., 2006). The peak (central pixel) and mean fluorescence intensities of a 5-pixel x 5-pixel area around each identified center of mass were plotted as a function of time for all particles in the image series. The exact time points of docking and fusion were determined from the central pixel similar to previous work (Domanska et al., 2009; Kiessling et al., 2010). Fusion times of individual events were determined from the time of binding to the time of fusion and cumulative distribution fusion vs.

time plots were constructed from typically 200-300 events depending on the condition. Fusion efficiencies were determined from the number of liposomes that underwent fusion compared with the total number of liposomes that bound.

For content and membrane labeled single liposome fusion experiments, planar supported bilayers were mounted on a Zeiss Axiovert 200 fluorescence microscope (Carl Zeiss, Thornwood, NY) equipped with a 63x water immersion objective (Zeiss; N.A. 0.95) and a prism-based TIRF illumination system. The beams of a 514 nm line of an argon ion laser (Innova 90C, Coherent, Palo Alto, CA), controlled through an acousto-optic modulator (Isomet, Springfield, VA), and a diode laser (Cube 640, Coherent) emitting light at 640 nm were directed (72° from the normal) into a prism above the quartz slide to illuminate the sample by total internal reflection with a characteristic penetration depth of ~102 and ~130 nm for the 514 and the 640 nm lasers, respectively. The prism-quartz interface was lubricated with glycerol to allow easy translocation of the sample cell on the microscope stage. An OptoSplit (Andor-Technologies, South Windsor, CT) was used to separate the fluorescence from the lipid and soluble dyes. Fluorescence signals were recorded by an electron-multiplying charge-coupled device camera (iXon DV887ESC-BV, Andor, Belfast, UK). The EMCCD camera was cooled to -70°C. The laser intensities, light-blocking shutters, and cameras were controlled by a program written in LabVIEW (National Instruments, Austin, TX). POPC liposomes with a sulforhodamine B content label and a DiD membrane label were injected at a concentration of 0.5 µM lipid. Images were recorded at a frame rate of 20 ms (the slower acquisition rate was in order to observe the content dye). Single fusion events were analyzed as described above. Behavior of the content dye verified that full fusion only occurred when all of the membrane dye diffused away from the fusion site, as seen previously for SNARE-mediated fusion (Kreutzberger et al., 2015). All experimental conditions were repeated at least 4 times with at least 4 independent samples and errors are standard errors of the mean. For each individual experiment, data from on the order of 100 individual particles were collected.

**VLP production and cell entry assays**

The production of EBOV VLPs and the assay to measure their entry into cells were performed as described previously (Lee et al., 2017). In brief, HEK293T/17 cells were co-transfected with plasmids encoding VP40, β-lactamase-VP40, mCherry-VP40, and WT or G660L EBOV GP with a C-terminal V5 tag using polyethylenimine. The ratio of respective plasmids was 1:2.25:2.25:1.5. After 48 hr at 37°C, the cell medium was collected, cleared of debris by centrifugation, and the cleared media (containing VLPs) was subjected to ultracentrifugation through a 20% sucrose cushion. VLP pellets were resuspended in HM buffer (20 mM HEPES, 20 mM MES, 130 mM NaCl, pH 7.4) overnight and subsequently repelleted. Final VLP pellets were resuspended in 10% sucrose-HM buffer, aliquoted, and stored at -80 °C.

Methyl-β-cyclodextrin (MβCD) was used to deplete/replenish cholesterol in VLPs after production. For depletion, purified VLPs were incubated with 20 mM MβCD at 37°C for 30 min. After incubation, VLPs were centrifuged at 13,000 rpm (15,700 xg) at 4°C for 2-3 hr. The supernatant was then removed, and the pellet was washed with HM buffer and centrifuged again. After the wash step, VLPs were resuspended in 10% sucrose-HM buffer overnight at 4°C. For replenishment, cholesterol-depleted VLPs were incubated at 37°C for 30 mins with cholesterol saturated MβCD (5 mM final concentration). After incubation, VLPs were subjected to the purification protocol described above.

Production of EBOV VLPs from statin-treated cells was performed as follows. HEK 293T/17 cells were pretreated with DMEM containing 0.01% FBS and 4 μM of lovastatin or DMSO (control) 24 hrs prior to transfection, and the cells were maintained in this media (DMEM with 0.01% FBS and 4 μM of lovastatin or DMSO) throughout VLP production. VLPs were then harvested (after 48 hrs) and purified as described above.

All VLPs were analyzed for total protein concentrations (by BCA assay) and for their content of EBOV GP and VP40 (by Western blotting). Where indicated, the cholesterol content of VLPs was determined using the Amplex cholesterol kit following the manufacturer's instructions.

To measure cell entry, VLPs were bound to HEK293T/17 cells by centrifugation (250 x g) for 1 hr at 4°C and then allowed to enter for 3 hrs at 37°C in a 5% $CO_2$ incubator. The fluorescent CCF2-AM β-lactamase substrate was then incubated with the cells for 1 hr at RT in the dark. Cells were washed and incubated overnight in the dark at room temperature. Cells were lifted, fixed, and analyzed by flow cytometry on a FACSCalibur flow cytometer. The degree of the shift in fluorescence from green to blue was used to measure entry (Yonezawa et al., 2005). All data were analyzed using FlowJo software.

Further information on experimental design is available in the Nature Research Reporting Summary linked to this article.

**Data Availability**

NMR chemical shift data for EBOV MPER/TM WT and G660L have been deposited in the Biomolecular Magnetic Resonance Data Bank under accession number 50584 and 50591, respectively.

## 3.6 Supplemental Figures

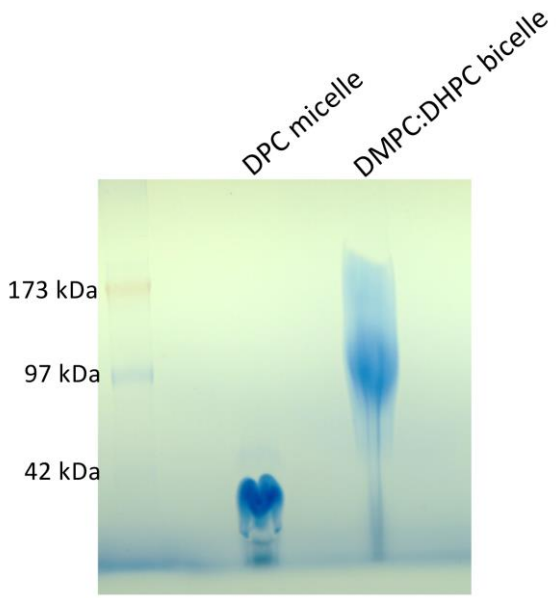


**Figure 3.S1:** Native gel of EBOV MPER/TM in DPC micelle and q=0.5 DMPC/DHPC bicelle

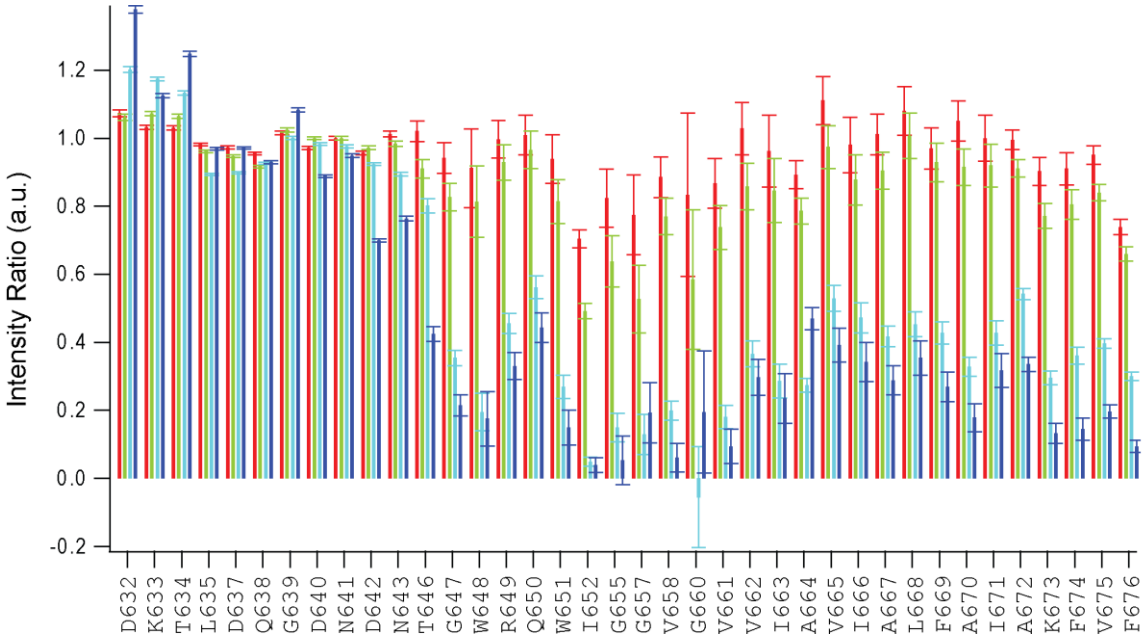


**Figure 3.S2**: NMR titration of the nitroxide free-radical cholesterol analog 3b-doxyl-5a-cholestane into a EBOV MPER/TM q=0.5 DMPC/DHPC bicelle sample. Amide proton intensity ratios between bicelles with 1 (red), 3 (green), 5 (cyan), 10 (blue) mol% 3b-doxyl-5a-cholestane (relative to DMPC) and cholesterol analog free bicelles are plotted.

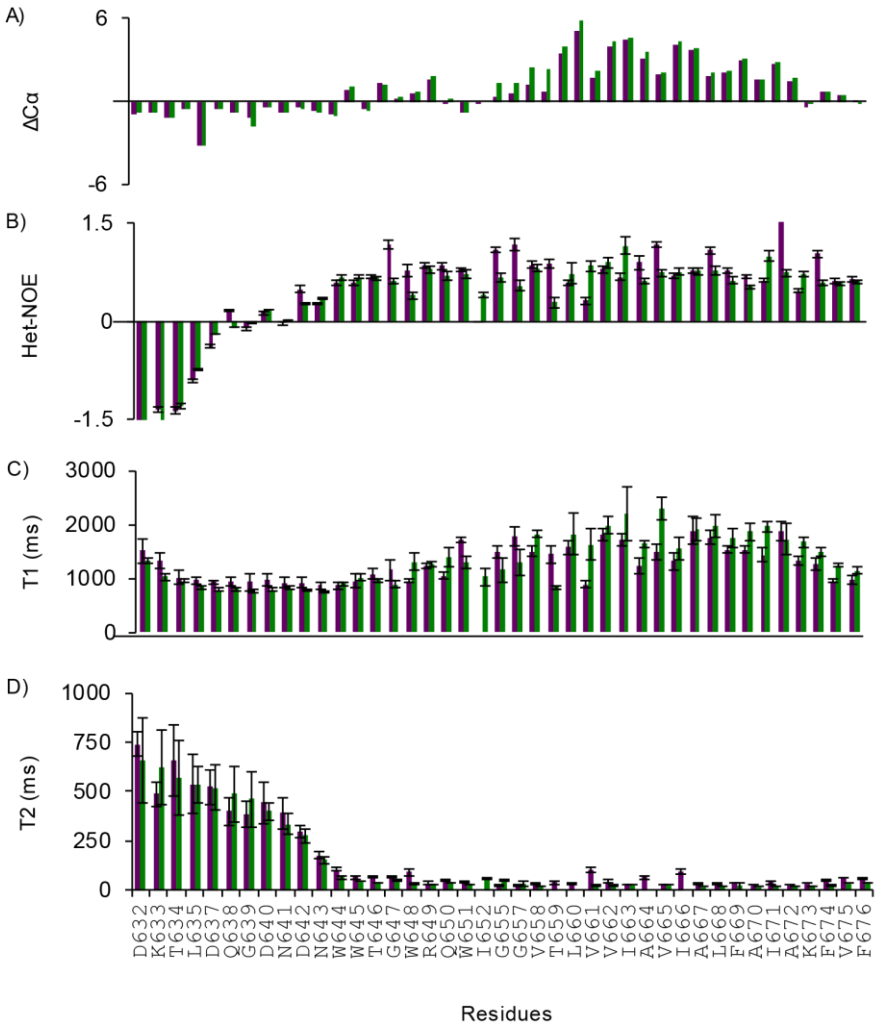


**Figure 3.S3:** Secondary structure and polypeptide backbone dynamics measurements of EBOV WT and G660L MPER/TM in DMPC/DHPC bicelles at pH 5.5, 45°C. **A.** Cα chemical shift index of WT (green) and G660L mutant (purple). Both show a helix-turn-helix motif (see also Figure 3.3). **B-D.** Backbone dynamics measurements of WT (green) and G660L mutant (purple) showing that the N-terminus is flexible and the TM domain is rigid in both constructs (Arora & Tamm, 2001). B) Heteronuclear $^{15}$N-NOEs. C) $^{15}$N $T_1$ spin-lattice and D) $^{15}$N $T_2$ spin-spin relaxation times.

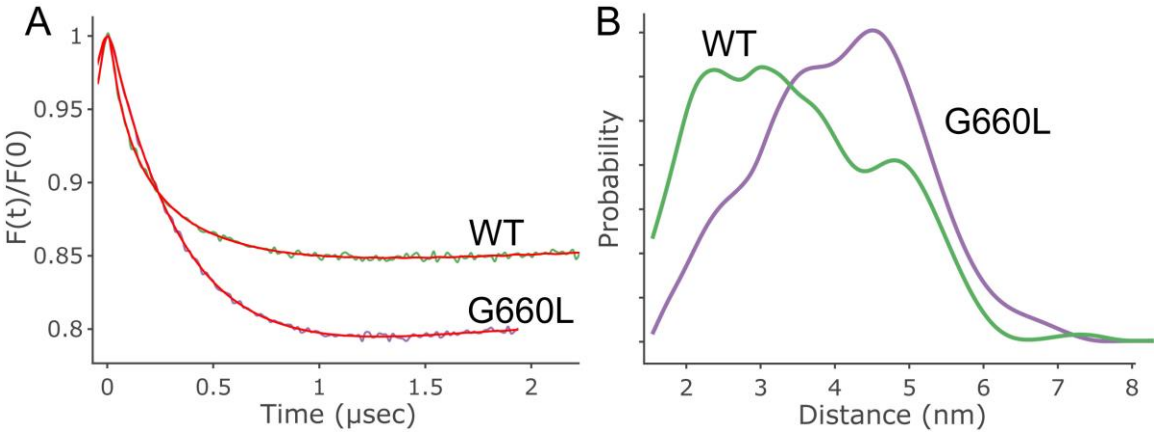


**Figure 3.S4:** Distance distribution obtained using DEER on double-MTSL-labeled EBOV MPER/TM and G660L in POPC liposomes at pH 5.5. **A.** Background-corrected DEER data for WT (green) and G660L (purple) EBOV MPER/TM in POPC liposomes. **B.** Distance distributions obtained by a best fit to the data in (A). As seen with the bicelle data, the addition of the G660L mutation causes a shift towards longer distance elements consistent with an opening of the MPER/TM angle.

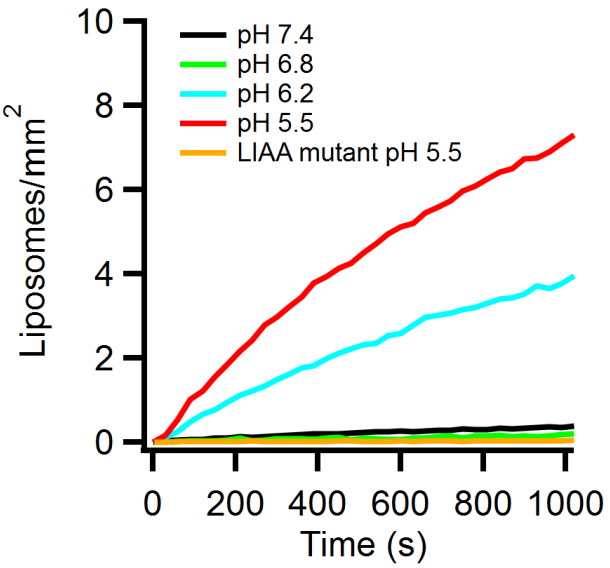


**Figure 3.S5:** Docking of liposomes (79:20:1 POPC:Chol:Rh-DOPE) to SLBs (80:20 POPC:Chol) containing GP2 (lipid:protein 1000). Liposomes (5μM, 50 nm diameter) were injected at time 0 and the fluorescence within in the TIRF field was recorded. The average fluorescence intensities were determined from initial frames and used to determine the density of liposomes on the SLB. Docking was determined as a function of pH and also assessed for the fusion-deficient LIAA mutant at pH 5.5.

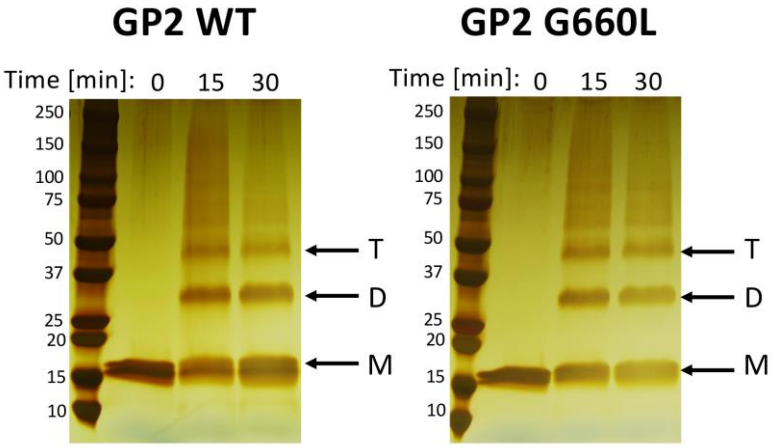


**Figure 3.S6:** SDS-PAGE gels of crosslinked WT and G660L GP2 in POPC:POPG (85:15) proteoliposomes. Samples of WT and G660L GP2 proteoliposomes (each with ~10 μg GP2) were incubated with 10 mM DTSSP for the indicated times at room temperature. After quenching, the samples were run, at the same time, on parallel SDS-PAGE gels, after which proteins were visualized by silver staining. The positions of the monomeric (M), dimeric (D) and trimeric (T) forms of GP2 are indicated with black arrows.

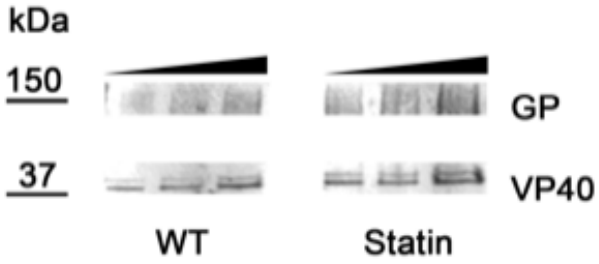


**Figure 3.S7:** Western Blot of VLPs produced from untreated HEK293T cells (WT) or HEK293T cells treated with 4 μM lovastatin (Statin). 1, 2, and 5 μg of each type of VLP was applied to the gel. After probing for EBOV GP and VP40 (see Methods), the relative amounts of GP to VP40 were calculated for each lane. When normalized to WT VLPs, the ratio of GP:VP40 in Statin VLPs was 1.1 +/- 0.07 that in WT VLPs based on analysis of all lanes. The ratio was 0.86 +/- 0.07 based on analysis of the lanes with the last 2 lanes of each gel. VLPs produced in cells treated with 20 or 50 μM lovastatin showed reduced GP incorporation (Shrivastava-Ranjan et al., 2018).

# Chapter 4. Purification and Structure of Human NPC1 Luminal Domain C

Laura Odongo, Kaneil K. Zadrozny, William E. Diehl, Jeremy Luban, Judith M. White, Barbie K. Ganser-Pornillos, Lukas K. Tamm, Owen Pornillos

Acta Crystallographica Section F. 2023. 79, 45-50.
doi: 10.1107/S2053230X23000705

For this project, I expressed non-glycosylated NPC1-C in *E. coli*, purified the expression product, set up crystal trays of the described combinations of proteins with Kaneil Zadrozny, and refined the crystal structure with Owen Pornillos.

## 4.1 Abstract

Niemann-Pick C1 (NPC1) is a membrane protein that primarily resides in late endosomes and lysosomes and plays an important role in cholesterol homeostasis in the cell. The second luminal domain of NPC1 (NPC1-C) serves as the intracellular receptor for Ebola and Marburg viruses. Here, we report the recombinant production of non-glycosylated and glycosylated NPC1-C and a new crystal form of the non-glycosylated protein. The $P2_1$ crystals diffracted to 2.3 Å resolution. The structure is similar to other reported structures of NPC1-C, with differences observed in the protruding loops when compared to NPC1-C in complex with Ebola virus glycoprotein or NPC2.

## 4.2 Introduction

Cholesterol is delivered to cells by low-density lipoprotein (LDL) particles, which contain the esterified form of cholesterol. LDL is transported to lysosomes where it encounters acid hydrolases that convert cholesteryl ester to cholesterol (Goldstein et al., 1975). The cholesterol is then trafficked to the plasma membrane and ER (Storch & Xu, 2009). Two endosomal proteins involved in cholesterol transport are Niemann-Pick type C1 (NPC1) and C2 (NPC2) (Storch & Xu, 2009). NPC1 is a 13-pass transmembrane glycoprotein that resides primarily in late endosomes and lysosomes. NPC1, along with other membrane proteins in lysosomes, are highly glycosylated, forming the glycocalyx, which is thought to protect the limiting membrane from hydrolytic degradation (Rudnik & Damme, 2020). NPC1 is proposed to regulate cholesterol egress by facilitating cholesterol transit through the glycocalyx (Kwon et al., 2009; Li et al., 2015) as well as regulating endoplasmic reticulum contact sites with late endosomes (Höglinger et al., 2019). Loss-of-function mutations in NPC1 or NPC2 result in Niemann-Pick type C disease (Evans & Hendriksz, 2017). This disease is characterized by the accumulation of sphingosine, which causes dysregulation of calcium homeostasis and this in turn results in the secondary storage of cholesterol and sphingolipids (Lloyd-Evans et al., 2008).

NPC1 is also a critical host factor for filovirus entry and infection, serving as an obligate endosomal receptor (Carette et al., 2011; Côté et al., 2011). Filoviruses, including Ebola and Marburg viruses, cause hemorrhagic fever associated with fatality rates of up to 90%. The viral glycoprotein (GP) interacts with domain C of NPC1 (termed here as NPC1-C), which is one of three large luminal loops of the protein. NPC1-C is minimally sufficient for the interaction with GP but all three NPC1 luminal domains are required for efficient viral entry (E. H. Miller et al., 2012). Viral entry is not dependent on the cholesterol transport activity (Carette et al., 2011; Côté et al., 2011).

In this study, we report detailed methods for purifying NPC1-C and its X-ray crystal structure at 2.3 Å resolution.

## 4.3 Results and Discussion

### Production of non-glycosylated NPC1-C

The goal was to co-crystallize NPC1-C in complex with primed A82V Ebola virus glycoprotein (GP), as part of an effort to explore the basis of enhanced infectivity of the A82V variant in the 2013-2016 Ebola Outbreak in West Africa (Diehl et al., 2016; Urbanowicz et al., 2016; Wang et al., 2017). Human NPC1-C (residues 371-621) (Figure 4.1A) was expressed as a C-terminally polyhistidine-tagged fusion protein in *E. coli* as insoluble inclusion bodies. After denaturation with urea and a nickel-affinity chromatography step, the protein was refolded at pH 8 using the glutathione redox system to facilitate correct disulfide bond formation (De Bernardez Clark et al., 1999; Mayer & Buchner, 2004). Since NPC1 is an endolysosomal protein where the pH range is 4.5-5.5, buffer exchange was performed to lower the pH to 5.5. Additionally, more protein aggregation was observed at pH 8 than low pH 5.5. The precipitate that formed upon pH change from 8 to 5.5 was removed by centrifugation. The supernatant was then concentrated and applied to a size exclusion column. The protein eluted as a single major species, with SDS-PAGE revealing a pure protein with the expected apparent molecular mass of approximately 30 kDa (Figure 4.1B). Additional smaller peaks observed in the chromatogram are likely aggregates of NPC1-C or low levels of impurities.

### Crystal structure of NPC1-C

We set up screens with non-glycosylated NPC1-C as well as glycosylated NPC1-C (from 293F cells) with primed and glycosylated A82V EBOV GP (Chandran et al., 2005; Schornberg et al., 2006). To aid the crystallization efforts, we also prepared glycosylated NPC1-C from kifunensine-treated cells. Kifunensine is a mannosidase inhibitor that results in the formation of a glycoprotein with short mannose-rich sugar chains (Chang et al., 2007; Elbein et al., 1990; Nettleship et al., 2009). We obtained crystals from initial screens with all three forms of NPC1-C but only obtained high-resolution diffraction data from samples containing non-glycosylated NPC1-C.

Although the objective was to obtain a crystal of a protein complex of NPC1-C with the primed and glycosylated form of A82V EBOV GP, the proteins did not co-crystallize, regardless of the glycosylation state of NPC1-C, with non-glycosylated NPC1-C crystallizing alone. After molecular replacement, modeled coordinates were refined against data extending to 2.3 Å (Table 1). NPC1-C crystallized in space group $P2_1$ (Figure 4.1C), with two molecules in the asymmetric unit (Figure 4.1D). Electron densities were well-defined for residues 400-606 in chain A and residues 401-607 in chain C. The two polypeptide chains packed as an antiparallel fashion in the asymmetric unit; however, the protein purified as a monomer, as determined by size exclusion chromatography (Figure 4.1B). Non-crystallographic dimer packing resulted in unfolding of an N-terminal $\alpha$-helix (residues 384-399) observed in a published crystal structure of NPC1-C (PDB 5F18 (Wang et al., 2016)). Two disulfide bonds expected in the structure, i.e., Cys468-Cys479 and Cys516-Cys533, are seen clearly resolved in electron density, indicating that the refolding protocol was effective.

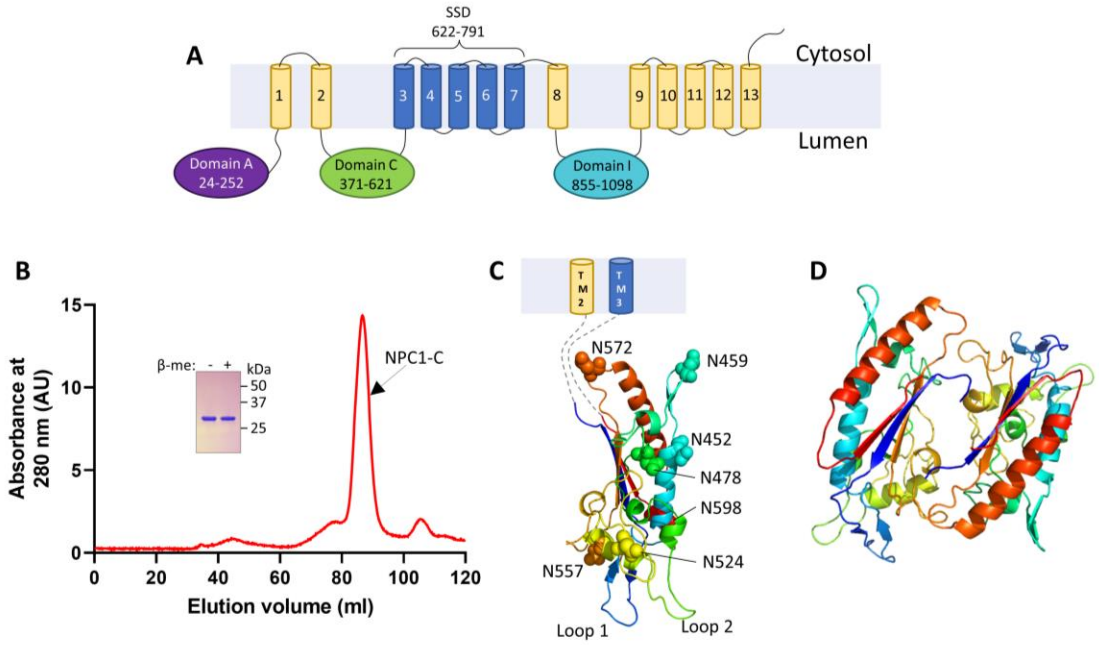


**Figure 4.1**. **A.** A schematic of NPC1 showing 13 transmembrane domains (1-13), luminal domains A, C, I, and the sterol-sensing domain (SSD). **B.** Ni-NTA affinity purified $His_8$-tagged NPC1-C was refolded and purified to homogeneity by using size-exclusion chromatography. Shown is a representative Superdex 200 16/60 gel filtration profile of the refolded protein. The expected molecular weight of NPC1-C is 30 kDa. The inset shows the SDS-PAGE profiles of the final purified protein taken from the labeled peak and prepared under non-reducing (β-me -) and reducing (β-me +) buffer conditions. **B.** Ribbons representation of NPC1-C in the crystallographic asymmetric unit. **C.** Cartoon representation of an NPC1-C monomer, rainbow-colored from N- (blue) to C-terminus (red), with the seven predicted N-linked glycosylation sites (N452, N459, N478, N524, N557, N572 and N598) indicated as spheres. The dashed lines indicate linker segments between NPC1-C and transmembrane domains 2 and 3 (TM2 and TM3). **D.** Antiparallel dimer in the asymmetric unit.

**Table 1.** Structure determination statistics

| | |
|---|---|
| **Data Collection** | |
| Beamline | APS 22ID |
| Wavelength, Å | 1.000 |
| Processing program | HKL2000 |
| Space group | P21 |
| Cell dimensions | a = 53.145 Å, b = 65.207 Å, c = 68.534 Å |
| | $\alpha = \gamma = 90°$, $\beta = 91.686°$ |
| Resolution range, Å | 50-2.30 (2.37-2.30) |
| Rmeas, Rpim | 0.133 (0.677), 0.053 (0.302) |
| CC1/2 | 0.998 (0.772) |
| Mean I/σI | 13.1 (3.1) |
| Completeness, % | 98.2 (97.4) |
| Average redundancy | 5.5 (4.8) |
| Wilson B-factor, Å$^2$ | 26.7 |
| **Phasing** | |
| Phasing program | MOLREP |
| Method | Molecular replacement |
| Search model | PDB 5F18 |
| **Refinement** | |
| Refinement program | PHENIX v1.20.1-4487 (phenix.refine) |
| Resolution range | 41.2-2.30 (2.40-2.30) |
| No. of unique reflections, free | 20,421 (2,292), 1,088 (136) |
| $R_{work}$, $R_{free}$ | 0.19 (0.25), 0.23 (0.31) |
| No. of non-hydrogen atoms | 3,343 protein, 160 water |
| Average B-factor, Å$^2$ | 32.8 protein, 33.8 water |
| Bond length deviations, Å | 0.003 |
| Bond angle deviations, ° | 0.646 |
| **Validation and Deposition** | |
| Ramachandran favored, outliers, % | 96.82, 0 |
| Ramachandran z-score | -0.09 |
| Rotamer outliers, % | 1.08 |
| MolProbity clashscore | 1.38 |
| PDB ID | 8EUS |

Values in parenthesis indicate highest resolution shell

**Comparison with other published structures of NPC1-C**

We compared our structure of non-glycosylated NPC1-C with published structures of apo non-glycosylated NPC1-C (PDB 5F18 (Wang et al., 2016)), apo glycosylated NPC1-C (PDB 5HNS (Zhao et al., 2016)), NPC1-C in complex with NPC2 (PDB

5KWY (Li et al., 2016)), NPC1-C in complex with primed EBOV GP (PDB 5F1B (Wang et al., 2016)) and the full-length structure of NPC1 (PDB 6W5R (Qian et al., 2020)). The overall structure of NPC1-C is similar to other published structures of NPC1, as expected, with root-mean-square deviations on all common Cα atoms for each aligned pair ranging from 0.36 to 0.78 Å. In full-length NPC1, domain C and I fold into similar structures, intertwine with each other through an extensive interface, and form a tunnel that may function as a path for cholesterol transfer (Qian et al., 2020). It is likely that the absence of domain I allowed NPC1-C to crystallize as dimers using the same domain I packing interface. Of note, the crystal structure of apo glycosylated NPC1-C (PDB 5HNS) also crystallized as an apparent dimer (Zhao et al., 2016). While another structure of apo non-glycosylated NPC1-C (PDB 5F18) did not crystallize as a dimer, some of the crystal packing contacts also formed along the domain I-interacting interface (Wang et al., 2016). The main differences between our structure and NPC1-C in complex with primed EBOV GP (Wang et al., 2016) or NPC2 (Li et al., 2016) is in the configurations of protruding loops (loop 1: Y420-D428 and loop 2: D501-Y506) (indicated in Figure 4.2A-B). NPC1-C uses these loops to engage with its binding partners, explaining the different configurations. In another apo NPC1-C structure (PDB 5F18), both loops are engaged in crystal contacts (Wang et al., 2016). Our structure provides further support for the conclusion that the luminal C domain is a stably folded interaction module of NPC1.

NPC1-C has seven predicted N-glycosylation sites: N452, N459, N478, N524, N557, N572 and N598 (Figure 4.1C) (Gong et al., 2016; Zhao et al., 2016). N-glycosylation does not affect binding to primed EBOV GP (Ndungo et al., 2016; Wang et al., 2016); consistent with this, comparison of our non-glycosylated structure to that of glycosylated NPC1-C (PDB 5HNS) does not indicate large conformational changes. Currently, the known role of glycosylation of NPC1 is to contribute to the glycocalyx, which protects the membrane proteins and lipids from hydrolytic enzymes (Rudnik & Damme, 2020).

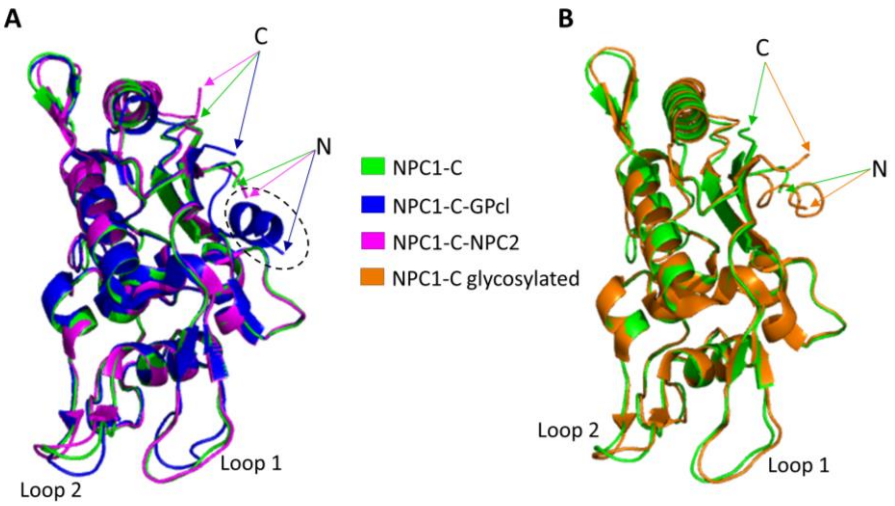


**Figure 4.2. A.** Overlay of NPC1-C with NPC1-C-$GP_{cl}$ (PDB ID code 5F1B) and NPC1-C-NPC2 (PDB ID code 5KWY). Dashed oval indicates the location of the N-terminal helix, which is unfolded in our structure **B.** Overlay of NPC1-C with crystal structure of glycosylated form of NPC1-C (PDB ID code 5HNS). The N- and C-termini are indicated by N and C, respectively.

Interestingly, non-crystallographic packing of the two NPC1-C copies in our crystal resulted in unfolding of an N-terminal $\alpha$-helix (residues 384-399) that is observed in the apo non-glycosylated form of NPC1-C (PDB 5F18) and is partially folded in the structure of the NPC1-C:EBOV GP complex (PFB 5F1B) (Wang et al., 2016) (dashed oval in Figure 4.1C). This helix is also not resolved in other published structures of NPC1-C (Li et al., 2016). This result may indicate the dynamic nature of this portion of NPC1-C, which is connected to one of the transmembrane segments that undergo conformational rearrangements during cholesterol transport ((Qian et al., 2020).

## 4.4 Conclusion

The results of our structural study add to the existing body of work on NPC1 as well as a detailed protocol for how to efficiently produce recombinant NPC1-C expressed in *E. coli*. Domain C of NPC1 is an independently folding module with flexible protruding loops that interact with different binding partners, including EBOV GP and NPC2 (Li et al., 2016; Wang et al., 2016).

**Acknowledgements:** We thank Lucie Fénéant and Katarzyna Szymańska-de Wijs for assistance with preparation of glycosylated NPC1-C. We also thank Jonathan Wagner for assistance with X-ray data collection and Justin Acheson for help with structure refinement. This work was supported by NIH grant R01 AI30557 to LKT and 5R01AI148784 to JL.

## 4.5 Methods

### Protein expression and purification

**Production of non-glycosylated NPC1-C:** Human NPC1-C (residues 371-621) was expressed using pET41a vector in *E. coli* BL21(DE3) cells with a C-terminal $His_8$-tag. Cells were grown to $OD_{600}$ of 0.6-0.8 and protein production was induced with 0.5 mM IPTG for 4 h at 30°C. Cells were harvested by centrifugation (3,700xg at 4°C for 15 min) and stored at -80°C. To purify the protein, a 0.5-L bacterial cell pellet was thawed and resuspended in 50 mL lysis buffer (20 mM Tris pH 8.0, 300 mM NaCl, 5 mM β-mercaptoethanol) supplemented with protease inhibitor cocktail (Thermo Scientific). Cells were lysed by sonication and the cell lysate centrifuged at 18,000xg at 4°C for 30 min. The pellet was resuspended in 50 mL solubilization buffer (8 M urea, 20 mM Tris pH 8.0, 300 mM NaCl, 5 mM β-mercaptoethanol) and incubated at room temperature for 30 min. The suspension was then centrifuged at 18,000xg at 10°C for 30 min. The supernatant was incubated with 4 mL Ni-NTA beads (Thermo Scientific) pre-equilibrated with solubilization buffer and incubated overnight on a rotator at room temperature. Beads were then washed with 100 mL solubilization buffer. The protein was eluted using elution buffer (8 M urea, 20 mM Tris pH 8.0, 300 mM NaCl, 200 mM imidazole, 5 mM β-mercaptoethanol). To refold the protein, sequential dialysis was performed at 4°C: 2 L of buffer A (4 M urea, 50 mM Tris pH 8.0, 200 mM NaCl) for 10-12 h, 2 L of buffer B (2 M urea, 50 mM Tris pH 8.0, 100 mM NaCl) overnight, 500 mL refolding buffer (100 mM Tris pH 8.0, 400 mM L-Arg, 5 mM reduced glutathione, 0.5 mM oxidized glutathione) for 2 h, and finally 2 L dialysis buffer C (20 mM Tris pH 8.0) for 2x24 h. The sample was then concentrated using a filter cell (10,000 MWCO filter) and mixed with equal volume of

size-exclusion chromatography (SEC) buffer (20 mM MES pH 5.5, 100 mM NaCl). Precipitate was removed by centrifugation (4,000xg at 4°C for 20 min). The supernatant was then concentrated in a 10,000 MWCO Amicon filter (MilliporeSigma) to 2-3 mL and further purified by size-exclusion chromatography on a Superdex 200 16/60 column (GE Healthcare) equilibrated with SEC buffer. Fractions containing the target protein were pooled and concentrated. The concentrated protein was stored at -80°C. Our purification protocol reproducibly yielded around 2 mg of pure, folded NPC1-C per liter of *E. coli* culture.

**Production of glycosylated NPC1-C:** A pDisplay plasmid encoding human NPC1-C (V372-V621) with an N-terminal $His_6$-tag, with the NPC1 residues flanked by sequences that form a coiled coil (Deffieu & Pfeffer, 2011) was used. 293F cells were seeded in 125-mL shaker flasks ($1x10^6$ cells/mL) and transfected with the plasmid using 293fection reagent with or without 5 μM kifunensine. 24 h post-transfection, 10 mM sodium butyrate was added to induce protein expression. 72 h post-transfection, the cell suspension was collected and cleared by centrifugation (2,400xg, 4°C, 5 min). The cleared media was filtered (0.2 μm), supplemented with protease inhibitor cocktail, and concentrated using Amicon Ultra-15, 30,000 MWCO. The concentrated protein solution was then added to 5 mL Ni-Sepharose beads that were pre-equilibrated with binding buffer (50 mM MES, pH 6.5, 150 mM NaCl, 20 mM imidazole) and incubated overnight at 4°C with gentle agitation. After washing, the protein was eluted using elution buffer (50 mM MES pH 6.5, 150 mM NaCl, 300 mM imidazole), dialyzed 3x against 1 L of dialysis buffer (50 mM MES pH 5.5, 150 mM NaCl), concentrated using an Amicon filter (30,000 MWCO) and stored at -80°C.

**Production of glycosylated A82V Ebola virus (EBOV) glycoprotein (GP):** The A82V EBOV GP construct had the mucin-like and transmembrane domains (residues 312-462) and 633-676) removed and two N-linked glycosylation sites (T42V) mutated (Lee et al., 2008). Recombinant baculoviruses expressing A82V EBOV GP with C-terminal One-STrEP-FLAG (OSF) tag was generated using the Bac-to-Bac baculovirus expression system (Thermo Scientific). Suspension Sf9 insect cells grown in ESF-921 medium (Expression

Systems) were infected with recombinant baculoviruses at an MOI of 10 (Hanson et al., 2007). 72 hours after infection, the cell supernatant was collected, filtered, and concentrated using Sartorius a tangential flow filtration system with a 10,000 MWCO filter (Sartorius). The pH of the concentrate was adjusted to pH 7.5 with 1 M Tris pH 9 and clarified by centrifugation (38,400xg, 30 min). The concentrate was further filter using PES 0.22 µm filtration unit. The filtered concentrate was then loaded onto StrepTactin beads (IBA Lifesciences) that were pre-equilibrated in PBS and incubated overnight with gentle agitation. The StrepTactin-supernatant slurry was loaded into a 1.5 x 20 cm glass chromatography column (BioRad). Following column loading, the flow-through was passed a second time through the column and subsequently washed extensively (x3 column volumes) with PBS, and the protein eluted with 10 mM desthiobiotin in PBS. The eluate was first concentrated using Amicon filter (50 kDa MWCO) then the buffer exchanged to HMSS (thermolysin) buffer (20 mM HEPES, 20 mM MES, 150 mM NaCl, 10% w/v sucrose, pH 7.9). The protein was cleaved with 1 mg/ml thermolysin (MilliporeSigma) (1:50 by mass, enzyme:substrate) in the presence of 50 mM $CaCl_2$ to generate primed (~19 kDa) A82V EBOV GP. Proteolysis was allowed to proceed for 18-24 h at 4°C and the reaction terminated by adding 10 mM phosphoramidon (MilliporeSigma). The cleaved protein was immediately applied onto a Superdex 200 (Santa Cruz) column preequilibrated in HMS buffer (20 mM HEPES, 20 mM MES, 130 mM NaCl, pH 7.5). Fractions corresponding to primed A82V EBOV GP were pooled and concentrated using an Amicon filter (30,000 MWCO), and stored at -80°C. Following collection, all steps were performed at 4°C.

## Crystallization and structure determination

Crystallization trials were performed by mixing 5 mg/mL of NPC1-C with 5 mg/mL of primed A82V EBOV GP, in an attempt to co-crystallize the complex. Crystals were grown at 20°C in sitting drops in equal volumes of protein solution and precipitant (0.1 M sodium malonate pH 6, 20% w/v PEG 3350) for at least 3 days. Crystals were cryoprotected with 20% v/v glycerol and flash-frozen in liquid nitrogen. Diffraction data

were collected at the Advanced Photon Source beamline 22ID. Indexing, integration and scaling were performed with HKL2000 (Otwinowski & Minor, 1997). Although diffraction spots were observed beyond 2.3 Å, data was truncated at this resolution to ensure high completeness and keep CC1/2 at the last resolution shell above 0.2. The structure was solved by molecular replacement with MOLREP (Vagin & Teplyakov, 2010), using PDB entry 5F18 as search model. Iterative refinement, model building and validation were performed using Phenix (Adams et al., 2011) and Coot (Emsley et al., 2010). Structure validation was performed throughout the refinement process using Molprobity (Chen et al., 2010), as implemented in Phenix. Figures were prepared using PyMOL (Schrödinger, 2020).

# Chapter 5. Summary and Future Directions

The goal of this thesis work was to gain further insight into the later stages of EBOV entry, particularly the events immediately preceding membrane fusion. To do so, we developed supported planar endosomal membranes (SPEMs), which are prepared from endosomes derived from HEK 293T cells, as described in Chapter 2. We validated the use of SPEMs as target membranes for viral fusion by recapitulating the known fusion pH dependences of influenza and Lassa viruses (Figures 2.2 and 2.3). Consistent with previous findings, we showed that fusion mediated by primed 19-kDa EBOV GP is dependent on low pH and enhanced by $Ca^{2+}$ (Figure 2.4). We also provided evidence that the final trigger for EBOV GP-mediated fusion is further cathepsin action. Additionally, immunofluorescence analysis of SPEMs indicated the presence of membrane-associated cathepsin B (Figure 2.S9).

We also investigated the role of cholesterol in EBOV entry. We found that EBOV GP interacts with cholesterol via several glycines (G655, G657, and G660) in the membrane-proximal external region and transmembrane (MPER/TM) domains. Mutating G660 to L, showed that G660, the initiating glycine in a GXXXA cholesterol binding motif, is critical. EBOV G660L MPER/TM showed decreased cholesterol binding to the TM domain (Figure 3.2), a wider angle between MPER and TM domains (Figure 3.3), and decreased fusion and entry activity (Figures 3.5 and 3.6).

Finally, we obtained the structure of non-glycosylated luminal domain C of NPC1 (NPC1-C). The goal was to obtain the structure of NPC1-C in complex with primed A82V EBOV $GP_{cl}$, as part of an effort to explore the basis of enhanced infectivity of the A82V variant in the 2013-2016 Ebola Outbreak in West Africa (Diehl et al., 2016; Urbanowicz et al., 2016; Wang et al., 2017). Although A82V $GP_{cl}$ did not crystallize, NPC1-C crystallized in the space group $P2_1$, which is different from other published structures of

NPC1-C (Figures 4.1 and 4.2). Additionally, we also showed that non-glycosylated NPC1-C is less thermally stable than the glycosylated from (Appendix B).

## 5.1 Further Exploration of EBOV GP cleavage

It is generally accepted that filovirus GP undergoes proteolytic processing by cathepsins in the endosome to yield $GP_{cl}$ (Chandran et al., 2005; Schornberg et al., 2006), which interacts with the EBOV receptor, NPC1 (Carette et al., 2011; Côté et al., 2011). However, data thus far suggest that cathepsin B and cathepsin L (CatB and L) are differentially involved in priming different filoviral GPs in different cells. EBOV entry into human dendritic cells and Vero cells has been shown to be dependent on CatB, but not CatL (Chandran et al., 2005; Martinez et al., 2010; Schornberg et al., 2006). Taï Forest virus (TAFV) entry is also CatB-dependent, while Sudan virus (SUDV), Reston virus (RESTV), Lloviu virus (LLOV), and Marburg virus (MARV) GP-mediated entry have reduced requirements for CatB activity (Marzi et al., 2007; Misasi et al., 2012; Ng et al., 2014; Wong et al., 2010). Misasi et al. postulated that variations at the C-terminus of GP1 as well as the presence of several endosomal cysteine proteases with overlapping substrate preferences may explain the virus-specific differences of CatB/L-dependence (Misasi et al., 2012).

Of note, work by Chandran and coworkers presented in a PhD thesis revealed that *in vitro* CatL removes five amino acids from the mature N-terminus of EBOV GP2 (Bortz, 2021). This removal by CatL does not affect infectivity or conformational stability but it does inhibit recognition and neutralization by several monoclonal antibodies. They also found that CatL cleaves TAFV GP2, albeit less efficiently, but does not cleave SUDV GP2. We speculate that removal of the five N-terminal residues of GP2 would make it easier for the fusion loop to insert into target membranes. Previous studies examining the sequences of primed EBOV $GP_{cl}$ obtained by thermolysin treatment showed that GP2 remained intact (Dube et al., 2009). It is likely that thermolysin does not produce the same cleavage products as CatL (or CatB) since they are members of different

protease families, metalloprotease and cysteine protease families, respectively. The discrepancy in GP2 cleavage between these two proteases warrants further investigation. Taken together, these findings may point to a revised model of EBOV entry where GP1 and GP2 both undergo (perhaps simultaneous) processing by cathepsins, which allows GP1 to interact with NPC1 and the fusion loop of GP2 to better insert into target membranes and thereby drive membrane fusion more efficiently.

Another question that may be worth exploring is whether all the GP2 subunits of all filoviruses undergo similar removal of amino-terminal residues. EBOV and TAFV GP2 are sensitive to CatL cleavage, while SUDV GP2 is insensitive to CatL cleavage (Bortz, 2021). It remains to be seen if this additional cleavage occurs in other filoviral GP2s. Perhaps different cysteine cathepsins process other filoviral GPs. Indeed, entry of the majority of filoviruses has been shown to be sensitive to E-64d but amongst them they display species-specific dependence on different cathepsins (Misasi et al., 2012; Ng et al., 2014). In this context, it is interesting that E-64d did not fully inhibit fusion in our EBOV $GP_{cl}$-to-SPEM system (Figure 2.4). Other cathepsins have been found to play a role in entry of other viruses. For example, cathepsin W, another cysteine protease, was recently identified as a host factor required for successful influenza A virus entry (Günther et al., 2022).

## 5.2 Future studies employing SPEMs as target membranes for studying viral entry

During viral entry of enveloped viruses, the viral core separates from the viral membrane to allow the internal viral content to enter cells upon fusion of the viral and host membranes. This process is generally referred to as membrane uncoating (Haywood, 2010), and typically also involves disassembly of the viral matrix that links the membrane envelopes to the genome containing cores of viruses. Several matrices/cores of endosome-entering viruses have been shown to undergo pH-mediated disassembly, including those of EBOV (Winter et al., 2022), influenza A virus

(Stauffer et al., 2014), and vesicular stomatitis virus (Mire et al., 2009). SPEMs may be well suited to investigate the role of matrix disassembly on full fusion of endosome-entering enveloped viruses.

Non-enveloped viruses use various strategies to facilitate membrane penetration while maintaining similar basic steps of entry as enveloped viruses. Engagement with the host cell induces conformational changes in the surface proteins of viral particles that expose hydrophobic moieties or release of lytic factors. This in turn compromises the integrity of host cell membranes allowing the viral particle, or just the viral genome, to cross those membranes (Tsai, 2007). It is interesting that several endosome-entering non-enveloped viruses have been found to require endosomal factors for efficient entry. For example, rotaviruses require the activity of cathepsins B, L, and S for entry (Díaz-Salinas et al., 2014). Bluetongue virus utilizes the late endosomal lipid, bis(monoacylglycerol)phosphate (BMP), for productive membrane penetration (Patel et al., 2016). Thus, SPEMs could provide a useful platform to explore how host cell factors including pH, ion concentration ($K^+$, $Ca^{2+}$), and endosomal proteins, affect endosomal cell entry of non-enveloped viruses.

## 5.3 Summary

In this work, we developed SPEMs, as a model membrane system for studying virus entry through endosomes, provided further evidence that cathepsin activity is required for EBOV entry, showed that cholesterol enhances EBOV membrane fusion and cell entry by interacting with and affecting the structure of its MPER/TM domains, and provided a new structure of NPC1-C at 2.3 Å resolution. Overall, the work provides further insight into the complex processes of EBOV entry and fusion. Moreover, the SPEM model system should be generally useful for probing entry requirements for both additional enveloped as well as non-enveloped endosome-entering viruses.

# Appendix A: Phospholipid bis(monoacylglycerol)phosphate (BMP) enhances lipid mixing, but not docking, of pseudoviruses bearing Lassa GP with supported planar endosomal membranes (SPEMs)

## A.1 Introduction

Lassa virus (LASV), an Old World arenavirus, is the causative agent of Lassa fever, which is a hemorrhagic fever that affects 100,000-300,000 individuals annually, resulting in an estimated 5,000 deaths (Bell-Kareem & Smither, 2021). Lassa fever is endemic to parts of West Africa and is primarily transmitted through contact with excrement from infected multimammate rats (*Mastomys natalensis*), and nosocomial transmission through contact with bodily fluids (CDC, 2022c). Due to the possibility of aerosol transmission of Lassa, as well as its high lethality, LASV has been deemed a category A agent by the Centers for Disease Control and Prevention (CDC, 2018). Currently, there are no FDA-approved vaccines, and the only treatment options include supportive care and off-label usage of the antiviral ribavirin. However, recent studies suggest that ribavarin may be ineffective (and may even be harmful) in the treatment of Lassa fever (Eberhardt et al., 2019; Salam et al., 2022).

All arenaviruses have a bi-segmented, negative sense RNA genome comprising a large (L) and a small (S) segment. The L segment encodes the RNA-dependent RNA polymerase complex and the multifunctional matrix protein, while the S segment encodes the glycoprotein precursor complex (GPC) and the nucleoprotein (Hallam et al., 2018). The GPC is proteolytically processed by cellular signal peptidase and subtilisin kexin isozyme-1/site-1 protease (SKI-1/S1P), generating three functional units: stable signal peptide (SSP), GP1 and GP2 (Eichler et al., 2003; Lenz et al., 2001). These three subunits stay associated via noncovalent interactions to ultimately form a tripartite

glycoprotein spike in the viral membrane. GP1 mediates interaction with the host cell, GP2 is responsible for driving membrane fusion, and SSP has several roles including, intracellular trafficking of GPC, and sensing pH changes to induce fusion (Hallam et al., 2018; Pennington & Lee, 2022).

During LASV entry, GP1 engages with at least two different cellular receptors: the alpha subunit of dystroglycan (α-DG) at the cell surface (Cao et al., 1998) and lysosomal-associated membrane protein 1 (Lamp1) in endosomes (Cohen-Dvashi et al., 2015; Jae et al., 2014; Katz et al., 2022). Once in an appropriate endosome, low pH triggers a fusion cascade mediated by GP2 that results in fusion of the host and viral membranes followed by the delivery of the viral genome into the cytoplasm (Pennington & Lee, 2022). Lamp1 is not strictly necessary for GP-mediated entry but it raises the pH threshold for fusion thereby increasing the efficiency of infection (Hulseberg et al., 2018).

The endosomal lipid composition also influences fusion (Mazzon & Mercer, 2014), with anionic lipid, bis(monoacylglycerol)phosphate (BMP; also known as lysobisphosphatidic acid (LBPA)), having been shown to be a critical factor for entry of several viruses. BMP promotes fusion of Lassa virus (Markosyan et al., 2021), as well as dengue virus (Nour et al., 2013; Zaitseva et al., 2010), vesicular stomatitis virus (VSV) (Roth & Whittaker, 2011), and influenza virus (Mannsverk et al., 2022). The non-enveloped bluetongue virus also utilizes BMP for productive membrane penetration and viral entry (Patel et al., 2016). BMP is a structural isomer of phosphatidylglycerol (PG) with an unusual chemical configuration, *sn*-1-glycerophosphate-*sn*-1’-glycerol (compared to the standard *sn*-3 of other mammalian phospholipids) (Figure A.1). This atypical stereoconfiguration renders BMP resistant to hydrolysis by most phospholipases (Gruenberg, 2020). BMP is restricted to late endosomes, amounting to 15-20 mol% of the phospholipids of late endosomes (Kobayashi et al., 2002; Kobayashi et al., 1998).

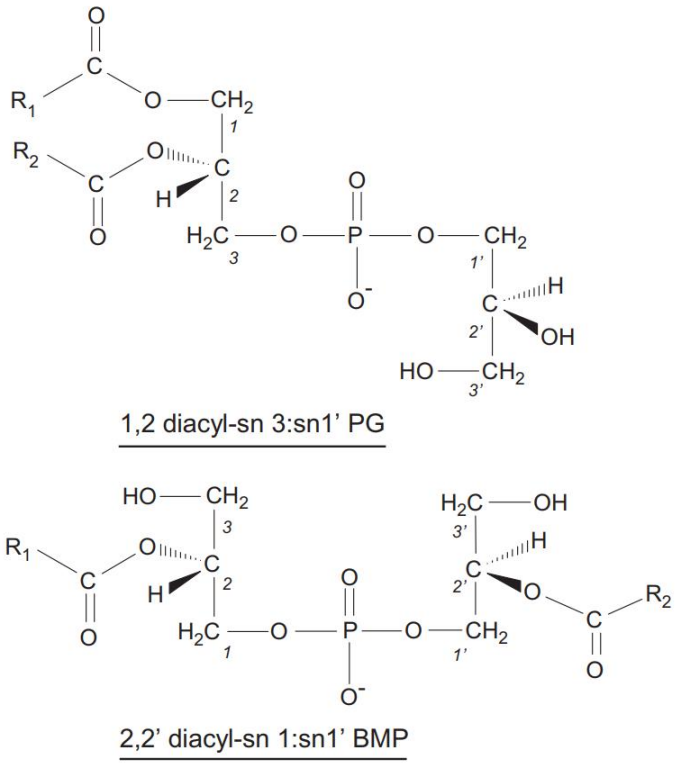


**Figure A1. Structure of PG and BMP.** BMP possesses unusual *sn*-1:*sn*-1' stereoconfiguration different from other mammalian phospholipids that exhibit *sn*-3:*sn*-1' configuration. Adapted from (Hullin-Matsuda et al., 2009).

As discussed in Chapter 2, using the *in vitro* SPEM fusion assay that we developed, we demonstrated the Lamp1 and pH dependences of LASV GP-mediated fusion. We also observed a modest increase in docking of HIV particles pseudotyped with LASV GP to supported planar endosomal membranes (SPEMs) with and without Lamp1 at low pH. We therefore explored the possibility of BMP being a binding partner for LASV GP. In agreement with previous findings (Markosyan et al., 2021), we show that BMP enhances lipid mixing, but not docking of the virus to the SPEMs.

## A.2 Results and Discussion

We tested the ability of LASV pseudoviruses to fuse with SPEMs. As described in Chapter 2, fusion efficiency increased when the pH was lowered from 7.4 to below 6.0 and then sharply increased at pH 5.5 with SPEMs derived from wild-type cells. The

fusion probability decreased when the pH was further lowered. In Lamp1-negative SPEMs, we observed a similar increase in fusion probability with lowering of the pH, without a peak at pH 5.5. We next assessed the docking of LASV pseudoviruses to Lamp1- positive and negative SPEMs. Docking of LASV pseudoviruses to SPEMs with and without Lamp1 was slightly increased at lower pHs (Figure A.2.1 A; see Chapter 2). However, there was little difference in docking between SPEMs with and without Lamp1. To investigate this observation, we examined if there would be increased docking of LASV pseudoviruses to supported lipid bilayers (SLBs) prepared from liposomes with or without BMP. Docking events were monitored for 2.5 minutes. There was no difference observed in docking to SLBs with or without BMP at neutral and low pH (Figure A.2.1 B). We also examined lipid mixing of LASV pseudoviruses with SPEMs and SLBs. As expected, there was increased lipid mixing with SPEMs with or without Lamp1 at pH 5.75 (Figure A.2.2 A). Lipid mixing of LASV pseudovirus with SLBs at low pH was enhanced (~3-fold) by the presence of BMP in the target membrane (Figure A.2.2 B). This is in agreement with other recent findings showing that BMP promotes LASV GP-mediated fusion (Markosyan et al., 2021).

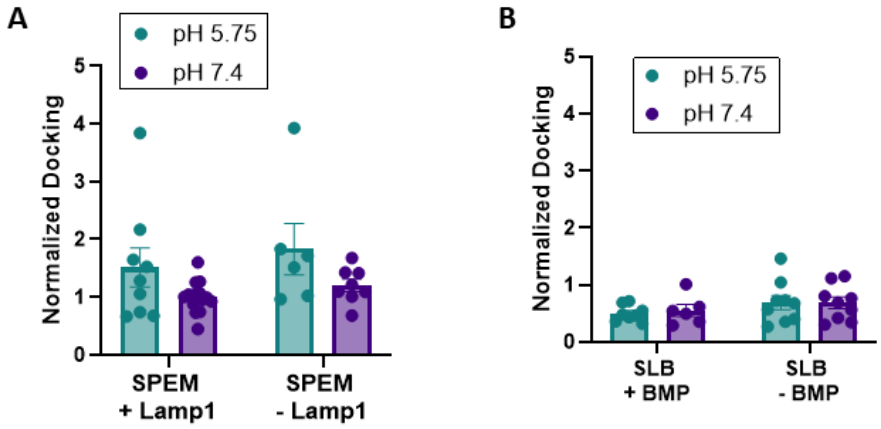


**Figure A.2.1.** Docking of LASV pseudovirus particles to SPEMs with or without Lamp1 (A) or supported lipid bilayer (SLB) composed of lipids only with or without BMP (B).

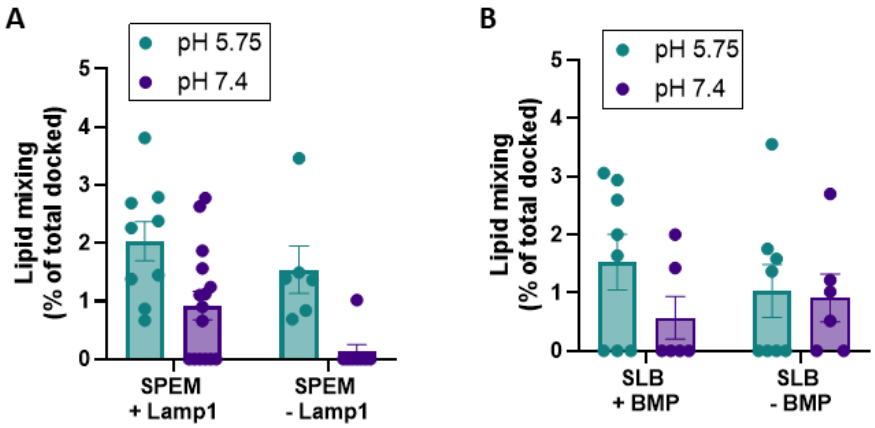


**Figure A.2.2.** Lipid mixing of LASV pseudovirus particles with SPEMs with or without Lamp1 (A) or supported lipid bilayer (SLB) composed of lipids only with or without BMP (B).

Lassa virus has been shown to utilize Lamp1 for efficient entry (Jae et al., 2014); however, Lamp1 is not explicitly necessary for entry (Hulseberg et al., 2018). Since Lamp1 is an extensively glycosylated protein (Carlsson & Fukuda, 1990), LASV GP may be interacting non-specifically with other glycosylated proteins present in the endosomal membrane. Additionally, LASV GP may also be interacting non-specifically with lipids allowing for interaction with both SPEMs and SLBs.

## A.3 Methods

Endosome enrichment protocol and preparation of supported planar endosomal membranes (SPEMs) is described in Chapter 2.

**Preparation of protein-free liposomes:** brain PC and cholesterol (80:20) were pipetted into a glass tube from chloroform solutions and dried down using $N_2$ gas. For BMP-containing liposomes, 15 mol% BMP was also included. 5 Lipids were further dried in a vacuum desiccator overnight. Lipids were then suspended in the desired volume of buffer. The lipid suspension was put through 7-10 freeze -thaw cycles in liquid nitrogen

and a water bath, followed by extrusion through a 100-nm pore polycarbonate filter (Avestin). After extrusion, the liposomes were used within 48 hours.

**Preparation of supported lipid-only bilayers (SLBs):** Supported lipid-only bilayers were prepared in the same way as SPEMs with one difference: protein-free liposomes composed of brain PC, cholesterol and/or BMP, were used instead of the endosomes in the vesicle fusion step on the preformed supported monolayers.

# Appendix B: Effect of Glycosylation on the Stability of the Human NPC1 Luminal Domain C

## B.1 Introduction

Glycosylation is a very common and essential form of post-translational modification that occurs during or after protein synthesis. Glycosylation generates diversity in proteins with glycoforms sharing an identical backbone but having different oligosaccharide units (Lis & Sharon, 1993). There are six glycosylation types: N-, O- and S-linked glycosylation, C-linked mannosylation, glypiation (addition of a glycosylphosphatidylinositol (GPI) anchor), and phosphoglycation (Mikolajczyk et al., 2020). N-linked glycosylation is the best-studied form of protein glycosylation. N-glycans are biosynthesized in the endoplasmic reticulum and attached to asparagine within a consensus sequence, usually Asn-X-Ser/Thr tripeptide, where X can be any amino acid except Pro (Moremen et al., 2012). N-glycosylation plays an important role in protein stability by protecting proteins from proteolytic degradation, extreme pH, aggregation and thermal denaturation (Zhou & Qiu, 2019).

Niemann-Pick C1 (NPC1) is a 1278-residue, 13-pass transmembrane glycoprotein that is a resident of late endosomes and lysosomes. NPC1 has three large luminal domains: A, C and I (Davies & Ioannou, 2000). N-glycosylated proteins in the limiting membrane of lysosomes form the glycocalyx, which is thought to offer protection from hydrolytic enzymes (Rudnik & Damme, 2020). NPC1 plays a role in cholesterol homeostasis by facilitating cholesterol export from late endosomes (Kwon et al., 2011; Li et al., 2015) and regulating endoplasmic reticulum (ER)-late endosome contact sites to mediate cholesterol egress to the ER (Höglinger et al., 2019). Mutations in NPC1 can lead to a rare but severe neurodegenerative lysosomal storage disorder named Niemann-Pick type C disease (Evans & Hendriksz, 2017). NPC1 has also been implicated in filoviral entry and infection (Carette et al., 2011; Côté et al., 2011), with the NPC1

domain C (NPC1-C) being minimally sufficient for interaction with Ebola virus glycoprotein (E. H. Miller et al., 2012).

In this study, we demonstrate that the glycosylated form of NPC1-C is more thermostable than the non-glycosylated form.

## B.2 Methods, Results and Discussion

Non-glycosylated NPC1-C (non-glyNPC1-C) was expressed in *E. coli* and glycosylated NPC1-C (glyNPC1-C) was obtained by expressing it in 293F cells as described in Chapter 4 (Figure B2.1 A). The stability of non-glyNPC1-C and glyNPC1-C was determined by measuring the melting temperature using a thermal shift assay (TSA). Protein samples at 0.1 mg/mL were mixed with 1x SYPRO Orange dye (Thermo Fisher) at the desired pH, in a final volume of 50 µl. Samples were placed in a semi-skirted 96-well PCR plate, sealed and heated in an RT-PCR machine with a temperature gradient from 25°C to 90°C. Experiments were carried out in triplicate.

GlyNPC1-C had a higher melting temperature ($T_m$) than non-glyNPC1-C across the pH range 5.5-7.5, suggesting that protein stability increases with glycosylation (Figure B2.1 B). This observation is in agreement with other studies done on glycosylated proteins (Dekoster & Robertson, 1997; Shental-Bechor & Levy, 2008; Wang et al., 1996). When cells were grown in the presence of the mannosisidase inhibitor kifunensin, the melting temperatures were the same as in its absence, demonstrating that potential cleavage of terminal mannose units did not contribute any decreased stability of GlyNPC1-C. Additionally, the pH dependence of the thermal stability of NPC1-C was studied in the same pH range. The $T_m$ increases with decreasing pH, with the difference in $T_m$ between pH 7.5 and 5.5 for non-glycosylated NPC1-C being 9.4°C and for glycosylated NPC1-C, 11.1°C. The melting temperatures of non-glycosylated and glycosylated NPC1-C are listed in Table B2.1.

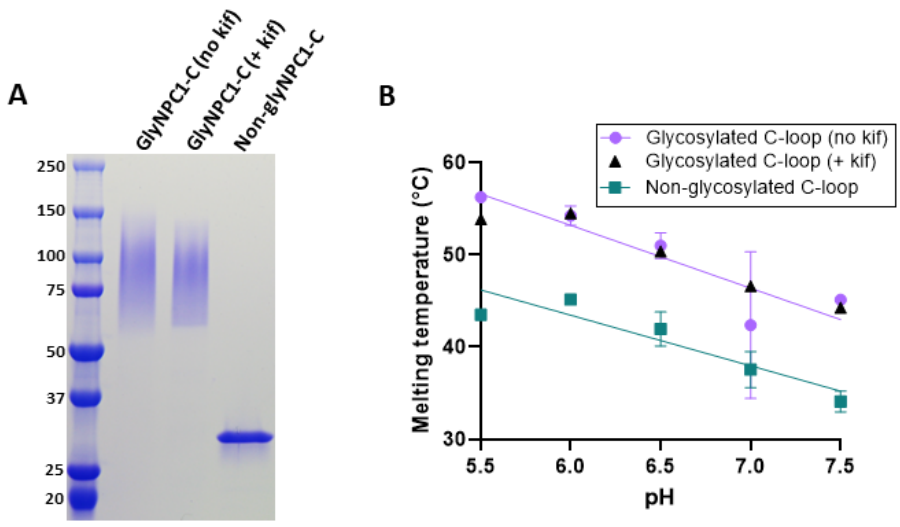


**Figure B2.1**. **Thermal shift assay of glycosylated and non-glycosylated NPC1-C. A.** SDS-PAGE of glyNPC1-C and non-glyNPC1-C. The glycosylated NPC1-C was expressed in 293F cells in the presence or absence of kifunensine (kif), a mannosidase inhibitor. **B.** The effect of glycosylation on the melting temperature of NPC1-C at different pHs. The error bars indicate standard error. The lines are linear regressions of the data.

**Table B.1 Melting temperature of NPC1-C at different pHs**

| | **pH** | | | | |
|---|---|---|---|---|---|
| | **5.5** | **6** | **6.5** | **7** | **7.5** |
| **Non-glyNPC1-C** | 43.5 ± 0 | 45.2 ± 0.4 | 42.0 ± 1.9 | 37.6 ± 2.0 | 34.1 ± 1.1 |
| **GlyNPC1-C** | 56.3 ± 0.4 | 54.3 ± 1.1 | 51.0 ± 1.4 | 42.4 ± 8.0 | 45.2 ± 0.2 |

Non-gly: non-glycosylated, Gly: glycosylated

NPC1 is a highly glycosylated protein with 14 N-glycosylation sites: 5 on domain A, 7 on domain C and 2 on domain I (Gong et al., 2016). The glycosylation sites on NPC1-C are N452, N459, N478, N524, N557, N572 and N598. Of note, glycosylation of NPC1-C is not required for interaction with Ebola virus glycoprotein (Ndungo et al., 2016; Wang et al., 2016).

In summary, our data show that the non-glycosylated form of NPC1-C is less thermally stable than the glycosylated form. Shental-Bechor and Levy propose that the

stabilization effect of glycans is due to destabilization of the unfolded state and an increase in the unfolding energy barrier (Shental-Bechor & Levy, 2008). Hence, glycosylation of NPC1 not only contributes to the lysosomal glycocalyx, but also increases the stability of NPC1.

# References


Adams, P. D., Afonine, P. V., Bunkóczi, G., Chen, V. B., Echols, N., Headd, J. J., Hung, L. W., Jain, S., Kapral, G. J., Grosse Kunstleve, R. W., McCoy, A. J., Moriarty, N. W., Oeffner, R. D., Read, R. J., Richardson, D. C., Richardson, J. S., Terwilliger, T. C., & Zwart, P. H. (2011). The Phenix software for automated determination of macromolecular structures. *Methods*, *55*(1), 94-106. https://doi.org/10.1016/j.ymeth.2011.07.005

Adu-Gyamfi, E., Johnson, K. A., Fraser, M. E., Scott, J. L., Soni, S. P., Jones, K. R., Digman, M. A., Gratton, E., Tessier, C. R., & Stahelin, R. V. (2015). Host Cell Plasma Membrane Phosphatidylserine Regulates the Assembly and Budding of Ebola Virus. *Journal of Virology*, *89*(18), 9440-9453. https://doi.org/doi:10.1128/JVI.01087-15

Agnello, V., Abel, G., Elfahal, M., Knight, G. B., & Zhang, Q. X. (1999). Hepatitis C virus and other flaviviridae viruses enter cells via low density lipoprotein receptor. *Proc Natl Acad Sci U S A*, *96*(22), 12766-12771. https://doi.org/10.1073/pnas.96.22.12766

Aleksandrowicz, P., Marzi, A., Biedenkopf, N., Beimforde, N., Becker, S., Hoenen, T., Feldmann, H., & Schnittler, H. J. (2011). Ebola virus enters host cells by macropinocytosis and clathrin-mediated endocytosis. *J Infect Dis*, *204 Suppl 3*(Suppl 3), S957-967. https://doi.org/10.1093/infdis/jir326

Alvarez, C. P., Lasala, F., Carrillo, J., Muñiz, O., Corbí, A. L., & Delgado, R. (2002). C-type lectins DC-SIGN and L-SIGN mediate cellular entry by Ebola virus in cis and in trans. *J Virol*, *76*(13), 6841-6844. https://doi.org/10.1128/jvi.76.13.6841-6844.2002

Amara, A., & Mercer, J. (2015). Viral apoptotic mimicry. *Nat Rev Micro*, *13*(8), 461-469. http://dx.doi.org/10.1038/nrmicro3469

Amman, B. R., Carroll, S. A., Reed, Z. D., Sealy, T. K., Balinandi, S., Swanepoel, R., Kemp, A., Erickson, B. R., Comer, J. A., Campbell, S., Cannon, D. L., Khristova, M. L., Atimnedi, P., Paddock, C. D., Crockett, R. J. K., Flietstra, T. D., Warfield, K. L., Unfer, R., Katongole-Mbidde, E., . . . Towner, J. S. (2012). Seasonal pulses of Marburg virus circulation in juvenile Rousettus aegyptiacus bats coincide with periods of increased risk of human infection. *PLOS Pathogens*, *8*(10), e1002877-e1002877. https://doi.org/10.1371/journal.ppat.1002877

Amman, B. R., Swanepoel, R., Nichol, S. T., & Towner, J. S. (2017). Ecology of Filoviruses. *Curr Top Microbiol Immunol*, *411*, 23-61. https://doi.org/10.1007/82_2017_10

Arora, A., & Tamm, L. K. (2001). Biophysical approaches to membrane protein structure determination. *Current Opinion in Structural Biology*, *11*(5), 540-547. https://doi.org/https://doi.org/10.1016/S0959-440X(00)00246-3

Authier, F., Mort, J. S., Bell, A. W., Posner, B. I., & Bergeron, J. J. (1995). Proteolysis of glucagon within hepatic endosomes by membrane-associated cathepsins B and D. *J Biol Chem*, *270*(26), 15798-15807. https://doi.org/10.1074/jbc.270.26.15798

Bach, S., Demper, J. C., Grünweller, A., Becker, S., Biedenkopf, N., & Hartmann, R. K. (2020). Regulation of VP30-Dependent Transcription by RNA Sequence and Structure in the Genomic Ebola Virus Promoter. *J Virol*, *95*(5). https://doi.org/10.1128/jvi.02215-20

Baize, S., Pannetier, D., Oestereich, L., Rieger, T., Koivogui, L., Magassouba, N. F., Soropogui, B., Sow, M. S., Keïta, S., De Clerck, H., Tiffany, A., Dominguez, G., Loua, M., Traoré, A., Kolié, M., Malano, E. R., Heleze, E., Bocquin, A., Mély, S., . . . Günther, S. (2014). Emergence of Zaire Ebola Virus Disease in Guinea. *New England Journal of Medicine*, *371*(15), 1418-1425. https://doi.org/10.1056/NEJMoa1404505

Bakkers, M. J. G., Moon-Walker, A., Herlo, R., Brusic, V., Stubbs, S. H., Hastie, K. M., Saphire, E. O., Kirchhausen, T. L., & Whelan, S. P. J. (2022). CD164 is a host factor for lymphocytic

choriomeningitis virus entry. *Proceedings of the National Academy of Sciences*, *119*(10), e2119676119. https://doi.org/doi:10.1073/pnas.2119676119

Bale, S., Dias, J. M., Fusco, M. L., Hashiguchi, T., Wong, A. C., Liu, T., Keuhne, A. I., Li, S., Woods, V. L., Jr., Chandran, K., Dye, J. M., & Saphire, E. O. (2012). Structural basis for differential neutralization of ebolaviruses. *Viruses*, *4*(4), 447-470. https://doi.org/10.3390/v4040447

Bale, S., Liu, T., Li, S., Wang, Y., Abelson, D., Fusco, M., Woods, V. L., & Ollmann Saphire, E. (2011). Ebola Virus Glycoprotein Needs an Additional Trigger, beyond Proteolytic Priming for Membrane Fusion. *PLoS Neglected Tropical Diseases*, *5*(11), e1395-e1395. https://doi.org/10.1371/journal.pntd.0001395

Banadyga, L., Hoenen, T., Ambroggio, X., Dunham, E., Groseth, A., & Ebihara, H. (2017). Ebola virus VP24 interacts with NP to facilitate nucleocapsid assembly and genome packaging. *Scientific Reports*, *7*(1), 7698. https://doi.org/10.1038/s41598-017-08167-8

Baribaud, F., Pöhlmann, S., Leslie, G., Mortari, F., & Doms, R. W. (2002). Quantitative expression and virus transmission analysis of DC-SIGN on monocyte-derived dendritic cells. *J Virol*, *76*(18), 9135-9142. https://doi.org/10.1128/jvi.76.18.9135-9142.2002

Basler, C. F., Wang, X., Mühlberger, E., Volchkov, V., Paragas, J., Klenk, H. D., García-Sastre, A., & Palese, P. (2000). The Ebola virus VP35 protein functions as a type I IFN antagonist. *Proc Natl Acad Sci U S A*, *97*(22), 12289-12294. https://doi.org/10.1073/pnas.220398297

Bavari , S., Bosio , C. M., Wiegand , E., Ruthel , G., Will , A. B., Geisbert , T. W., Hevey , M., Schmaljohn , C., Schmaljohn , A., & Aman , M. J. (2002). Lipid Raft Microdomains : A Gateway for Compartmentalized Trafficking of Ebola and Marburg Viruses✪✪The online version of this article contains supplemental material. *Journal of Experimental Medicine*, *195*(5), 593-602. https://doi.org/10.1084/jem.20011500

Bell-Kareem, A. R., & Smither, A. R. (2021). Epidemiology of Lassa Fever. *Curr Top Microbiol Immunol*. https://doi.org/10.1007/82_2021_234

Belouzard, S., Chu, V. C., & Whittaker, G. R. (2009). Activation of the SARS coronavirus spike protein via sequential proteolytic cleavage at two distinct sites. *Proceedings of the National Academy of Sciences*, *106*(14), 5871-5876. https://doi.org/doi:10.1073/pnas.0809524106

Bestle, D., Heindl, M. R., Limburg, H., Van Lam van, T., Pilgram, O., Moulton, H., Stein, D. A., Hardes, K., Eickmann, M., Dolnik, O., Rohde, C., Klenk, H. D., Garten, W., Steinmetzer, T., & Böttcher-Friebertshäuser, E. (2020). TMPRSS2 and furin are both essential for proteolytic activation of SARS-CoV-2 in human airway cells. *Life Sci Alliance*, *3*(9). https://doi.org/10.26508/lsa.202000786

Bhattacharyya, S., Warfield, K. L., Ruthel, G., Bavari, S., Aman, M. J., & Hope, T. J. (2010). Ebola virus uses clathrin-mediated endocytosis as an entry pathway. *Virology*, *401*(1), 18-28. https://doi.org/10.1016/j.virol.2010.02.015

Biedenkopf, N., Hartlieb, B., Hoenen, T., & Becker, S. (2013). Phosphorylation of Ebola Virus VP30 Influences the Composition of the Viral Nucleocapsid Complex: IMPACT ON VIRAL TRANSCRIPTION AND REPLICATION*. *Journal of Biological Chemistry*, *288*(16), 11165-11174. https://doi.org/https://doi.org/10.1074/jbc.M113.461285

Biedenkopf, N., Lier, C., & Becker, S. (2016). Dynamic Phosphorylation of VP30 Is Essential for Ebola Virus Life Cycle. *Journal of Virology*, *90*(10), 4914-4925. https://doi.org/10.1128/JVI.03257-15

Biswas, S., Yin, S. R., Blank, P. S., & Zimmerberg, J. (2008). Cholesterol promotes hemifusion and pore widening in membrane fusion induced by influenza hemagglutinin. *J Gen Physiol*, *131*(5), 503-513. https://doi.org/10.1085/jgp.200709932

Bo, Y., Qiu, S., Mulloy, R. P., & Côté, M. (2020). Filoviruses Use the HOPS Complex and UVRAG To Traffic to Niemann-Pick C1 Compartments during Viral Entry. *Journal of Virology*, *94*(16), e01002-01020. https://doi.org/doi:10.1128/JVI.01002-20

Bornholdt, Z. A., Ndungo, E., Fusco, M. L., Bale, S., Flyak, A. I., Crowe, J. E., Jr., Chandran, K., & Saphire, E. O. (2016). Host-Primed Ebola Virus GP Exposes a Hydrophobic NPC1 Receptor-Binding Pocket, Revealing a Target for Broadly Neutralizing Antibodies. *mBio*, *7*(1), e02154-02115. https://doi.org/10.1128/mBio.02154-15

Bornholdt, Z. A., Noda, T., Abelson, D. M., Halfmann, P., Wood, M. R., Kawaoka, Y., & Saphire, E. O. (2013). Structural rearrangement of ebola virus VP40 begets multiple functions in the virus life cycle. *Cell*, *154*(4), 763-774. https://doi.org/10.1016/j.cell.2013.07.015

Bortz, R. H., 3rd. (2021). *Antiviral therapeutics exploit entry-related structural changes in the Ebola virus glycoprotein.* Albert Einstein College of Medicine].

Bortz, R. H., 3rd, Florez, C., Laudermilch, E., Wirchnianski, A. S., Lasso, G., Malonis, R. J., Georgiev, G. I., Vergnolle, O., Herrera, N. G., Morano, N. C., Campbell, S. T., Orner, E. P., Mengotto, A., Dieterle, M. E., Fels, J. M., Haslwanter, D., Jangra, R. K., Celikgil, A., Kimmel, D., . . . Chandran, K. (2020). Development, clinical translation, and utility of a COVID-19 antibody test with qualitative and quantitative readouts. *medRxiv*. https://doi.org/10.1101/2020.09.10.20192187

Boulant, S., Stanifer, M., & Lozach, P.-Y. (2015). Dynamics of Virus-Receptor Interactions in Virus Binding, Signaling, and Endocytosis. *Viruses*, *7*(6), 2794-2815. https://www.mdpi.com/1999-4915/7/6/2747

Brecher, M., Schornberg, K. L., Delos, S. E., Fusco, M. L., Saphire, E. O., & White, J. M. (2012). Cathepsin cleavage potentiates the Ebola virus glycoprotein to undergo a subsequent fusion-relevant conformational change. *Journal of Virology*, *86*(1), 364-372. https://doi.org/10.1128/JVI.05708-11

Brinkmann, C., Nehlmeier, I., Walendy-Gnirß, K., Nehls, J., González Hernández, M., Hoffmann, M., Qiu, X., Takada, A., Schindler, M., & Pöhlmann, S. (2016). The Tetherin Antagonism of the Ebola Virus Glycoprotein Requires an Intact Receptor-Binding Domain and Can Be Blocked by GP1-Specific Antibodies. *J Virol*, *90*(24), 11075-11086. https://doi.org/10.1128/jvi.01563-16

Bullough, P. A., Hughson, F. M., Skehel, J. J., & Wiley, D. C. (1994). Structure of influenza haemagglutinin at the pH of membrane fusion. *Nature*, *371*(6492), 37-43. http://dx.doi.org/10.1038/371037a0

Bulow, U., Govindan, R., & Munro, J. B. (2020). Acidic pH Triggers Lipid Mixing Mediated by Lassa Virus GP. *Viruses*, *12*(7). https://doi.org/10.3390/v12070716

Burki, T. K. (2016). Post-Ebola syndrome. *Lancet Infect Dis*, *16*(7), 780-781. https://doi.org/10.1016/s1473-3099(15)00259-5

Büttiker, P., Stefano, G. B., Weissenberger, S., Ptacek, R., Anders, M., Raboch, J., & Kream, R. M. (2022). HIV, HSV, SARS-CoV-2 and Ebola Share Long-Term Neuropsychiatric Sequelae. *Neuropsychiatr Dis Treat*, *18*, 2229-2237. https://doi.org/10.2147/ndt.S382308

Cagno, V., Tseligka, E. D., Jones, S. T., & Tapparel, C. (2019). Heparan Sulfate Proteoglycans and Viral Attachment: True Receptors or Adaptation Bias? *Viruses*, *11*(7). https://doi.org/10.3390/v11070596

Cantoni, D., Hamlet, A., Michaelis, M., Wass, M. N., & Rossman, J. S. (2016). Risks Posed by Reston, the Forgotten Ebolavirus. *mSphere*, *1*(6). https://doi.org/10.1128/mSphere.00322-16

Cao, W., Henry, M. D., Borrow, P., Yamada, H., Elder, J. H., Ravkov, E. V., Nichol, S. T., Compans, R. W., Campbell, K. P., & Oldstone, M. B. A. (1998). Identification of α-Dystroglycan as a

Receptor for Lymphocytic Choriomeningitis Virus and Lassa Fever Virus. *Science*, *282*(5396), 2079-2081. https://doi.org/doi:10.1126/science.282.5396.2079

Carette, J. E., Raaben, M., Wong, A. C., Herbert, A. S., Obernosterer, G., Mulherkar, N., Kuehne, A. I., Kranzusch, P. J., Griffin, A. M., Ruthel, G., Cin, P. D., Dye, J. M., Whelan, S. P., Chandran, K., & Brummelkamp, T. R. (2011). Ebola virus entry requires the cholesterol transporter Niemann-Pick C1. *Nature*, *477*(7364), 340-343. http://dx.doi.org/10.1038/nature10348

Carlsson, S. R., & Fukuda, M. (1990). The polylactosaminoglycans of human lysosomal membrane glycoproteins lamp-1 and lamp-2. Localization on the peptide backbones. *J Biol Chem*, *265*(33), 20488-20495.

Carod-Artal, F. J. (2015a). Illness due the Ebola virus: epidemiology and clinical manifestations within the context of an international public health emergency. *Rev Neurol*, *60*(6), 267-277. (Enfermedad por el virus del Ébola: epidemiología y manifestaciones clínicas en un contexto de emergencia de salud pública internacional.)

Carod-Artal, F. J. (2015b). Post-Ebolavirus disease syndrome: what do we know? *Expert Rev Anti Infect Ther*, *13*(10), 1185-1187. https://doi.org/10.1586/14787210.2015.1079128

Carr, C. M., Chaudhry, C., & Kim, P. S. (1997). Influenza hemagglutinin is spring-loaded by a metastable native conformation. *Proceedings of the National Academy of Sciences of the United States of America*, *94*(26), 14306-14313.

Carroll, D., Daszak, P., Wolfe, N. D., Gao, G. F., Morel, C. M., Morzaria, S., Pablos-Méndez, A., Tomori, O., & Mazet, J. A. K. (2018). The Global Virome Project. *Science*, *359*(6378), 872-874. https://doi.org/doi:10.1126/science.aap7463

Casillas, A. M., Nyamathi, A. M., Sosa, A., Wilder, C. L., & Sands, H. (2003). A current review of Ebola virus: pathogenesis, clinical presentation, and diagnostic assessment. *Biol Res Nurs*, *4*(4), 268-275. https://doi.org/10.1177/1099800403252603

CDC. (2018). *Bioterrorism Agents/Diseases*. Retrieved 21 Dec 2022 from https://emergency.cdc.gov/agent/agentlist-category.asp

CDC. (2022a). *History of Ebola Outbreaks*. Retrieved 20 Nov 2022 from https://www.cdc.gov/vhf/ebola/history/chronology.html#anchor_1526565058132

CDC. (2022b). *History of Marburg Virus Disease (MVD) Outbreaks*. Retrieved 20 Nov 2022 from https://www.cdc.gov/vhf/marburg/outbreaks/chronology.html

CDC. (2022c). *Lassa Fever*. Retrieved 21 Dec 2022 from https://www.cdc.gov/vhf/lassa/index.html

Chandran, K., Sullivan, N. J., Felbor, U., Whelan, S. P., & Cunningham, J. M. (2005). Endosomal Proteolysis of the Ebola Virus Glycoprotein Is Necessary for Infection. *Science*, *308*(5728), 1643-1645. http://science.sciencemag.org/content/308/5728/1643.abstract

Chang, V. T., Crispin, M., Aricescu, A. R., Harvey, D. J., Nettleship, J. E., Fennelly, J. A., Yu, C., Boles, K. S., Evans, E. J., Stuart, D. I., Dwek, R. A., Jones, E. Y., Owens, R. J., & Davis, S. J. (2007). Glycoprotein structural genomics: solving the glycosylation problem. *Structure*, *15*(3), 267-273. https://doi.org/10.1016/j.str.2007.01.011

Changula, K., Kajihara, M., Mori-Kajihara, A., Eto, Y., Miyamoto, H., Yoshida, R., Shigeno, A., Hang'ombe, B., Qiu, Y., Mwizabi, D., Squarre, D., Ndebe, J., Ogawa, H., Harima, H., Simulundu, E., Moonga, L., Kapila, P., Furuyama, W., Kondoh, T., . . . Takada, A. (2018). Seroprevalence of Filovirus Infection of Rousettus aegyptiacus Bats in Zambia. *J Infect Dis*, *218*(suppl_5), S312-s317. https://doi.org/10.1093/infdis/jiy266

Chao, L. H., Klein, D. E., Schmidt, A. G., Peña, J. M., & Harrison, S. C. (2014). Sequential conformational rearrangements in flavivirus membrane fusion. *eLife*, *3*, e04389. https://doi.org/10.7554/eLife.04389

Chen, S. S., Yang, P., Ke, P. Y., Li, H. F., Chan, W. E., Chang, D. K., Chuang, C. K., Tsai, Y., & Huang, S. C. (2009). Identification of the LWYIK motif located in the human immunodeficiency virus type 1 transmembrane gp41 protein as a distinct determinant for viral infection. *J Virol*, *83*(2), 870-883. https://doi.org/10.1128/jvi.01088-08

Chen, V. B., Arendall, W. B., 3rd, Headd, J. J., Keedy, D. A., Immormino, R. M., Kapral, G. J., Murray, L. W., Richardson, J. S., & Richardson, D. C. (2010). MolProbity: all-atom structure validation for macromolecular crystallography. *Acta Crystallogr D Biol Crystallogr*, *66*(Pt 1), 12-21. https://doi.org/10.1107/s0907444909042073

Chernomordik, L. V., & Kozlov, M. M. (2003). Protein-lipid interplay in fusion and fission of biological membranes. *Annual Review of Biochemistry*, *72*, 175-207. https://doi.org/10.1146/annurev.biochem.72.121801.161504

Chlanda, P., Mekhedov, E., Waters, H., Schwartz, C. L., Fischer, E. R., Ryham, R. J., Cohen, F. S., Blank, P. S., & Zimmerberg, J. (2016). The hemifusion structure induced by influenza virus haemagglutinin is determined by physical properties of the target membranes. *Nat Microbiol*, *1*(6), 16050. https://doi.org/10.1038/nmicrobiol.2016.50

Churchward, M. A., Rogasevskaia, T., Höfgen, J., Bau, J., & Coorssen, J. R. (2005). Cholesterol facilitates the native mechanism of Ca2+-triggered membrane fusion. *J Cell Sci*, *118*(Pt 20), 4833-4848. https://doi.org/10.1242/jcs.02601

Cobián Güemes, A. G., Youle, M., Cantú, V. A., Felts, B., Nulton, J., & Rohwer, F. (2016). Viruses as Winners in the Game of Life. *Annu Rev Virol*, *3*(1), 197-214. https://doi.org/10.1146/annurev-virology-100114-054952

Cohen-Dvashi, H., Cohen, N., Israeli, H., & Diskin, R. (2015). Molecular Mechanism for LAMP1 Recognition by Lassa Virus. *Journal of Virology*, *89*(15), 7584-7592. https://doi.org/10.1128/jvi.00651-15

Côté, M., Misasi, J., Ren, T., Bruchez, A., Lee, K., Filone, C. M., Hensley, L., Li, Q., Ory, D., Chandran, K., & Cunningham, J. (2011). Small molecule inhibitors reveal Niemann-Pick C1 is essential for Ebola virus infection. *Nature*, *477*(7364), 344-348. https://doi.org/10.1038/nature10380

Coyne, C. B., Shen, L., Turner, J. R., & Bergelson, J. M. (2007). Coxsackievirus entry across epithelial tight junctions requires occludin and the small GTPases Rab34 and Rab5. *Cell Host Microbe*, *2*(3), 181-192. https://doi.org/10.1016/j.chom.2007.07.003

Cureton, D. K., Massol, R. H., Saffarian, S., Kirchhausen, T. L., & Whelan, S. P. J. (2009). Vesicular Stomatitis Virus Enters Cells through Vesicles Incompletely Coated with Clathrin That Depend upon Actin for Internalization. *PLOS Pathogens*, *5*(4), e1000394-e1000394. https://doi.org/10.1371/journal.ppat.1000394

Dahlmann, F., Biedenkopf, N., Babler, A., Jahnen-Dechent, W., Karsten, C. B., Gnirß, K., Schneider, H., Wrensch, F., O'Callaghan, C. A., Bertram, S., Herrler, G., Becker, S., Pöhlmann, S., & Hofmann-Winkler, H. (2015). Analysis of Ebola Virus Entry Into Macrophages. *The Journal of Infectious Diseases*, *212*(suppl_2), S247-S257. https://doi.org/10.1093/infdis/jiv140

Dai, X., Zhang, X., Ostrikov, K., & Abrahamyan, L. (2020). Host receptors: the key to establishing cells with broad viral tropism for vaccine production. *Critical Reviews in Microbiology*, *46*(2), 147-168. https://doi.org/10.1080/1040841X.2020.1735992

Damm, E. M., Pelkmans, L., Kartenbeck, J., Mezzacasa, A., Kurzchalia, T., & Helenius, A. (2005). Clathrin- and caveolin-1-independent endocytosis: entry of simian virus 40 into cells devoid of caveolae. *J Cell Biol*, *168*(3), 477-488. https://doi.org/10.1083/jcb.200407113

Das, D. K., Bulow, U., Diehl, W. E., Durham, N. D., Senjobe, F., Chandran, K., Luban, J., & Munro, J. B. (2020). Conformational changes in the Ebola virus membrane fusion machine

induced by pH, Ca2+, and receptor binding. *PLoS Biology*, *18*(2), e3000626-e3000626. https://doi.org/10.1371/journal.pbio.3000626

Davey, R. A., Shtanko, O., Anantpadma, M., Sakurai, Y., Chandran, K., & Maury, W. (2017). Mechanisms of Filovirus Entry. *Curr Top Microbiol Immunol*, *411*, 323-352. https://doi.org/10.1007/82_2017_14

Davies, J. P., & Ioannou, Y. A. (2000). Topological Analysis of Niemann-Pick C1 Protein Reveals That the Membrane Orientation of the Putative Sterol-sensing Domain Is Identical to Those of 3-Hydroxy-3-methylglutaryl-CoA Reductase and Sterol Regulatory Element Binding Protein Cleavage-activating Protein *. *Journal of Biological Chemistry*, *275*(32), 24367-24374. https://doi.org/10.1074/jbc.M002184200

de Araùjo, M. E. G., Hube, L. A., & Stasyk, T. (2008). Isolation of endocitic organelles by density gradient centrifugation. In *Methods in molecular biology (Clifton, N.J.)* (Vol. 424, pp. 317-331): Humana Press.

De Bernardez Clark, E., Schwarz, E., & Rudolph, R. (1999). Inhibition of aggregation side reactions during in vitro protein folding. *Methods in Enzymology*, *309*, 217-236. https://doi.org/10.1016/S0076-6879(99)09017-5

de Greslan, T., Billhot, M., Rousseau, C., Mac Nab, C., Karkowski, L., Cournac, J.-M., Bordes, J., Gagnon, N., Dubrous, P., Duron, S., Moroge, S., Quentin, B., Koulibaly, F., Bompaire, F., Renard, J.-L., & Cellarier, G. (2016). Ebola Virus–Related Encephalitis. *Clinical Infectious Diseases*, *63*(8), 1076-1078. https://doi.org/10.1093/cid/ciw469

de La Vega, M.-A., Stein, D., & Kobinger, G. P. (2015). Ebolavirus Evolution: Past and Present. *PLOS Pathogens*, *11*(11), e1005221-e1005221. https://doi.org/10.1371/journal.ppat.1005221

de Vries, M., Herrmann, A., & Veit, M. (2015). A cholesterol consensus motif is required for efficient intracellular transport and raft association of a group 2 HA from influenza virus. *Biochem J*, *465*(2), 305-314. https://doi.org/10.1042/bj20141114

Deffieu, M. S., & Pfeffer, S. R. (2011). Niemann-Pick type C 1 function requires lumenal domain residues that mediate cholesterol-dependent NPC2 binding. *Proceedings of the National Academy of Sciences of the United States of America*, *108*(47), 18932-18936. https://doi.org/10.1073/pnas.1110439108

Dekoster, G. T., & Robertson, A. D. (1997). Thermodynamics of Unfolding for Kazal-Type Serine Protease Inhibitors: Entropic Stabilization of Ovomucoid First Domain by Glycosylation †. https://pubs.acs.org/sharingguidelines

Delaglio, F., Grzesiek, S., Vuister, G. W., Zhu, G., Pfeifer, J., & Bax, A. (1995). NMRPipe: a multidimensional spectral processing system based on UNIX pipes. *J Biomol NMR*, *6*(3), 277-293. https://doi.org/10.1007/bf00197809

Delpeut, S., Noyce, R. S., & Richardson, C. D. (2014). The tumor-associated marker, PVRL4 (nectin-4), is the epithelial receptor for morbilliviruses. *Viruses*, *6*(6), 2268-2286. https://doi.org/10.3390/v6062268

Díaz-Salinas, M. A., Silva-Ayala, D., López, S., & Arias, C. F. (2014). Rotaviruses reach late endosomes and require the cation-dependent mannose-6-phosphate receptor and the activity of cathepsin proteases to enter the cell. *J Virol*, *88*(8), 4389-4402. https://doi.org/10.1128/jvi.03457-13

Diehl, W. E., Lin, A. E., Grubaugh, N. D., Carvalho, L. M., Kim, K., Kyawe, P. P., McCauley, S. M., Donnard, E., Kucukural, A., McDonel, P., Schaffner, S. F., Garber, M., Rambaut, A., Andersen, K. G., Sabeti, P. C., & Luban, J. (2016). Ebola Virus Glycoprotein with Increased Infectivity Dominated the 2013-2016 Epidemic. *Cell*, *167*(4), 1088-1098.e1086. https://doi.org/10.1016/j.cell.2016.10.014

Diment, S., Leech, M. S., & Stahl, P. D. (1988). Cathepsin D is membrane-associated in macrophage endosomes. *Journal of Biological Chemistry*, *263*(14), 6901-6907. https://doi.org/https://doi.org/10.1016/S0021-9258(18)68729-0

Dimitrov, D. S. (2004). Virus entry: molecular mechanisms and biomedical applications. *Nature Reviews Microbiology*, *2*(2), 109-122. https://doi.org/10.1038/nrmicro817

Dolnik, O., Volchkova, V., Garten, W., Carbonnelle, C., Becker, S., Kahnt, J., Ströher, U., Klenk, H.-D., & Volchkov, V. (2004). Ectodomain shedding of the glycoprotein GP of Ebola virus. *The EMBO Journal*, *23*(10), 2175-2184. https://doi.org/10.1038/sj.emboj.7600219

Domanska, M. K., Dunning, R. A., Dryden, K. A., Zawada, K. E., Yeager, M., & Kasson, P. M. (2015). Hemagglutinin Spatial Distribution Shifts in Response to Cholesterol in the Influenza Viral Envelope. *Biophys J*, *109*(9), 1917-1924. https://doi.org/10.1016/j.bpj.2015.09.014

Domanska, M. K., Kiessling, V., Stein, A., Fasshauer, D., & Tamm, L. K. (2009). Single vesicle millisecond fusion kinetics reveals number of SNARE complexes optimal for fast SNARE mediated membrane fusion. *Journal of Biological Chemistry*. https://doi.org/10.1074/jbc.M109.047381

Domanska, M. K., Kiessling, V., & Tamm, L. K. (2010). Docking and fast fusion of synaptobrevin vesicles depends on the lipid compositions of the vesicle and the acceptor SNARE complex-containing target membrane. *Biophysical Journal*. https://doi.org/10.1016/j.bpj.2010.09.011

Domanska, M. K., Wrona, D., & Kasson, P. M. (2013). Multiphasic effects of cholesterol on influenza fusion kinetics reflect multiple mechanistic roles. *Biophys J*, *105*(6), 1383-1387. https://doi.org/10.1016/j.bpj.2013.08.003

Dong, X.-p., Shen, D., Wang, X., Dawson, T., Li, X., Zhang, Q., Cheng, X., Zhang, Y., Weisman, L. S., Delling, M., & Xu, H. (2010). PI(3,5)P2 controls membrane trafficking by direct activation of mucolipin Ca2+ release channels in the endolysosome. *Nature Communications*, *1*(1), 38. https://doi.org/10.1038/ncomms1037

Du, C., Guan, X., & Yan, J. (2022). Two-pore channel blockade by phosphoinositide kinase inhibitors YM201636 and PI-103 determined by a histidine residue near pore-entrance. *Communications Biology*, *5*(1), 738. https://doi.org/10.1038/s42003-022-03701-5

Dube, D., Brecher, M. B., Delos, S. E., Rose, S. C., Park, E. W., Schornberg, K. L., Kuhn, J. H., & White, J. M. (2009). The Primed Ebolavirus Glycoprotein (19-Kilodalton GP1,2): Sequence and Residues Critical for Host Cell Binding. *Journal of Virology*, *83*(7), 2883-2891. https://doi.org/10.1128/jvi.01956-08

Durham, N. D., Howard, A. R., Govindan, R., Senjobe, F., Fels, J. M., Diehl, W. E., Luban, J., Chandran, K., & Munro, J. B. (2020). Real-Time Analysis of Individual Ebola Virus Glycoproteins Reveals Pre-Fusion, Entry-Relevant Conformational Dynamics. *Viruses*, *12*(1), 103-103. https://doi.org/10.3390/v12010103

Dyall, J., Nelson, E. A., DeWald, L. E., Guha, R., Hart, B. J., Zhou, H., Postnikova, E., Logue, J., Vargas, W. M., Gross, R., Michelotti, J., Deiuliis, N., Bennett, R. S., Crozier, I., Holbrook, M. R., Morris, P. J., Klumpp-Thomas, C., McKnight, C., Mierzwa, T., . . . White, J. M. (2018). Identification of Combinations of Approved Drugs With Synergistic Activity Against Ebola Virus in Cell Cultures. *J Infect Dis*, *218*(suppl_5), S672-s678. https://doi.org/10.1093/infdis/jiy304

Eberhardt, K. A., Mischlinger, J., Jordan, S., Groger, M., Günther, S., & Ramharter, M. (2019). Ribavirin for the treatment of Lassa fever: A systematic review and meta-analysis. *International Journal of Infectious Diseases*, *87*, 15-20. https://doi.org/10.1016/j.ijid.2019.07.015

Ebola haemorrhagic fever in Sudan, 1976. Report of a WHO/International Study Team. (1978). *Bull World Health Organ*, *56*(2), 247-270.

Ebola haemorrhagic fever in Zaire, 1976. (1978). *Bull World Health Organ*, *56*(2), 271-293.

Eichler, R., Lenz, O., Strecker, T., Eickmann, M., Klenk, H. D., & Garten, W. (2003). Identification of Lassa virus glycoprotein signal peptide as a trans-acting maturation factor. *EMBO Rep*, *4*(11), 1084-1088. https://doi.org/10.1038/sj.embor.embor7400002

Elbein, A. D., Tropea, J. E., Mitchell, M., & Kaushal, G. P. (1990). Kifunensine, a potent inhibitor of the glycoprotein processing mannosidase I. *J Biol Chem*, *265*(26), 15599-15605.

EMA. (2020a). *Mvabea*. Retrieved 9 June 2022 from https://www.ema.europa.eu/en/medicines/human/EPAR/mvabea

EMA. (2020b). *Zabdeno*. Retrieved 9 June 2022 from https://www.ema.europa.eu/en/medicines/human/EPAR/zabdeno

Empig, C. J., & Goldsmith, M. A. (2002). Association of the caveola vesicular system with cellular entry by filoviruses. *J Virol*, *76*(10), 5266-5270. https://doi.org/10.1128/jvi.76.10.5266-5270.2002

Emsley, P., Lohkamp, B., Scott, W. G., & Cowtan, K. (2010). Features and development of Coot. *Acta Crystallogr D Biol Crystallogr*, *66*(Pt 4), 486-501. https://doi.org/10.1107/s0907444910007493

Escudero-Pérez, B., Volchkova, V. A., Dolnik, O., Lawrence, P., & Volchkov, V. E. (2014). Shed GP of Ebola virus triggers immune activation and increased vascular permeability. *PLoS Pathog*, *10*(11), e1004509. https://doi.org/10.1371/journal.ppat.1004509

Evans, W. R. H., & Hendriksz, C. J. (2017). Niemann-Pick type C disease – the tip of the iceberg? A review of neuropsychiatric presentation, diagnosis and treatment. *BJPsych Bulletin*, *41*(2), 109-114. https://doi.org/10.1192/pb.bp.116.054072

FDA. (2019). *ERVEBO*. Retrieved 9 June 2022 from https://www.fda.gov/vaccines-blood-biologics/ervebo

FDA. (2020a). *FDA Approves First Treatment for Ebola Virus*. Retrieved 9 June 2022 from https://www.fda.gov/news-events/press-announcements/fda-approves-first-treatment-ebola-virus

FDA. (2020b). *FDA approves treatment for ebola virus*. Retrieved 9 June 2022 from https://www.fda.gov/drugs/news-events-human-drugs/fda-approves-treatment-ebola-virus

Fedson, D. S., Jacobson, J. R., Rordam, O. M., & Opal, S. M. (2015). Treating the Host Response to Ebola Virus Disease with Generic Statins and Angiotensin Receptor Blockers. *mBio*, *6*(3), e00716. https://doi.org/10.1128/mBio.00716-15

Feldmann, H., & Geisbert, T. W. (2011a). Ebola haemorrhagic fever. *Lancet*, *377*(9768), 849-862. https://doi.org/10.1016/S0140-6736(10)60667-8

Feldmann, H., & Geisbert, T. W. (2011b). Ebola haemorrhagic fever. *Lancet (London, England)*, *377*(9768), 849-862. https://doi.org/10.1016/S0140-6736(10)60667-8

Feldmann, H., Volchkov, V. E., Volchkova, V. A., Stroher, U., & Klenk, H. D. (2001). Biosynthesis and role of filoviral glycoproteins. *The Journal of general virology*, *82*(Pt 12), 2839-2848. https://doi.org/10.1099/0022-1317-82-12-2839

Fénéant, L., Szymańska-de Wijs, K. M., Nelson, E. A., & White, J. M. (2019). An exploration of conditions proposed to trigger the Ebola virus glycoprotein for fusion. *PLOS ONE*, *14*(7), e0219312-e0219312. https://doi.org/10.1371/journal.pone.0219312

Floyd, D. L., Ragains, J. R., Skehel, J. J., Harrison, S. C., & van Oijen, A. M. (2008). Single-particle kinetics of influenza virus membrane fusion. *Proceedings of the National Academy of*

*Sciences of the United States of America*, *105*(40), 15382-15387. https://doi.org/10.1073/pnas.0807771105

Forbes, K. M., Webala, P. W., Jääskeläinen, A. J., Abdurahman, S., Ogola, J., Masika, M. M., Kivistö, I., Alburkat, H., Plyusnin, I., Levanov, L., Korhonen, E. M., Huhtamo, E., Mwaengo, D., Smura, T., Mirazimi, A., Anzala, O., Vapalahti, O., & Sironen, T. (2019). Bombali Virus in Mops condylurus Bat, Kenya. *Emerg Infect Dis*, *25*(5), 955-957. https://doi.org/10.3201/eid2505.181666

Forzan, M., Marsh, M., & Roy, P. (2007). Bluetongue virus entry into cells. *J Virol*, *81*(9), 4819-4827. https://doi.org/10.1128/jvi.02284-06

Francica, J. R., Matukonis, M. K., & Bates, P. (2009). Requirements for cell rounding and surface protein down-regulation by Ebola virus glycoprotein. *Virology*, *383*(2), 237-247. https://doi.org/10.1016/j.virol.2008.10.029

Freeman, G. J., Casasnovas, J. M., Umetsu, D. T., & DeKruyff, R. H. (2010). TIM genes: a family of cell surface phosphatidylserine receptors that regulate innate and adaptive immunity. *Immunological Reviews*, *235*(1), 172-189. https://doi.org/https://doi.org/10.1111/j.0105-2896.2010.00903.x

Freitas, M. S., Follmer, C., Costa, L. T., Vilani, C., Bianconi, M. L., Achete, C. A., & Silva, J. L. (2011). Measuring the strength of interaction between the Ebola fusion peptide and lipid rafts: implications for membrane fusion and virus infection. *PLOS ONE*, *6*(1), e15756. https://doi.org/10.1371/journal.pone.0015756

Fujita, K., Miura, R., Yoneda, M., Shimizu, F., Sato, H., Muto, Y., Endo, Y., Tsukiyama-Kohara, K., & Kai, C. (2007). Host range and receptor utilization of canine distemper virus analyzed by recombinant viruses: Involvement of heparin-like molecule in CDV infection. *Virology*, *359*(2), 324-335. https://doi.org/10.1016/j.virol.2006.09.018

Furuyama, W., & Marzi, A. (2019). Ebola Virus: Pathogenesis and Countermeasure Development. *Annu Rev Virol*, *6*(1), 435-458. https://doi.org/10.1146/annurev-virology-092818-015708

Geisbert, T. W., Young, H. A., Jahrling, P. B., Davis, K. J., Larsen, T., Kagan, E., & Hensley, L. E. (2003). Pathogenesis of Ebola hemorrhagic fever in primate models: evidence that hemorrhage is not a direct effect of virus-induced cytolysis of endothelial cells. *The American journal of pathology*, *163*(6), 2371-2382. https://doi.org/10.1016/S0002-9440(10)63592-4

Gelderblom, H. R. (1996). Structure and Classification of Viruses. In S. Baron (Ed.), *Medical Microbiology*. University of Texas Medical Branch at Galveston



Germi, R., Crance, J. M., Garin, D., Guimet, J., Lortat-Jacob, H., Ruigrok, R. W., Zarski, J. P., & Drouet, E. (2002). Heparan sulfate-mediated binding of infectious dengue virus type 2 and yellow fever virus. *Virology*, *292*(1), 162-168. https://doi.org/10.1006/viro.2001.1232

Ghez, D., Lepelletier, Y., Lambert, S., Fourneau, J. M., Blot, V., Janvier, S., Arnulf, B., van Endert, P. M., Heveker, N., Pique, C., & Hermine, O. (2006). Neuropilin-1 is involved in human T-cell lymphotropic virus type 1 entry. *J Virol*, *80*(14), 6844-6854. https://doi.org/10.1128/jvi.02719-05

Ghigo, E., Kartenbeck, J., Lien, P., Pelkmans, L., Capo, C., Mege, J. L., & Raoult, D. (2008). Ameobal pathogen mimivirus infects macrophages through phagocytosis. *PLoS Pathog*, *4*(6), e1000087. https://doi.org/10.1371/journal.ppat.1000087

Ghosh, D. K., & Ranjan, A. (2020). The metastable states of proteins. *Protein Science*, *29*(7), 1559-1568. https://doi.org/https://doi.org/10.1002/pro.3859

Gianni, T., Salvioli, S., Chesnokova, L. S., Hutt-Fletcher, L. M., & Campadelli-Fiume, G. (2013). αvβ6- and αvβ8-integrins serve as interchangeable receptors for HSV gH/gL to promote endocytosis and activation of membrane fusion. *PLoS Pathog*, *9*(12), e1003806. https://doi.org/10.1371/journal.ppat.1003806

Gire, S. K., Goba, A., Andersen, K. G., Sealfon, R. S. G., Park, D. J., Kanneh, L., Jalloh, S., Momoh, M., Fullah, M., Dudas, G., Wohl, S., Moses, L. M., Yozwiak, N. L., Winnicki, S., Matranga, C. B., Malboeuf, C. M., Qu, J., Gladden, A. D., Schaffner, S. F., . . . Sabeti, P. C. (2014). Genomic surveillance elucidates Ebola virus origin and transmission during the 2014 outbreak. *Science (New York, N.Y.)*, *345*(6202), 1369-1372. https://doi.org/10.1126/science.1259657

Glebe, D., & Bremer, C. M. (2013). The molecular virology of hepatitis B virus. *Semin Liver Dis*, *33*(2), 103-112. https://doi.org/10.1055/s-0033-1345717

Goddard, T. D., & Kneller, D. G. (2008). *SPARKY v.3.114*. In University of California, San Francisco.

Goldstein, J. L., Dana, S. E., Faust, J. R., Beaudet, A. L., & Brown, M. S. (1975). Role of lysosomal acid lipase in the metabolism of plasma low density lipoprotein. Observations in cultured fibroblasts from a patient with cholesteryl ester storage disease. *Journal of Biological Chemistry*.

Goldstein, T., Anthony, S. J., Gbakima, A., Bird, B. H., Bangura, J., Tremeau-Bravard, A., Belaganahalli, M. N., Wells, H. L., Dhanota, J. K., Liang, E., Grodus, M., Jangra, R. K., DeJesus, V. A., Lasso, G., Smith, B. R., Jambai, A., Kamara, B. O., Kamara, S., Bangura, W., . . . Mazet, J. A. K. (2018). The discovery of Bombali virus adds further support for bats as hosts of ebolaviruses. *Nature Microbiology*, *3*(10), 1084-1089. https://doi.org/10.1038/s41564-018-0227-2

Gong, X., Qian, H., Zhou, X., Wu, J., Wan, T., Cao, P., Huang, W., Zhao, X., Wang, X., Wang, P., Shi, Y., Gao, George F., Zhou, Q., & Yan, N. (2016). Structural Insights into the Niemann-Pick C1 (NPC1)-Mediated Cholesterol Transfer and Ebola Infection. *Cell*, *165*(6), 1467-1478. https://doi.org/10.1016/j.cell.2016.05.022

Goodfellow, I. G., Sioofy, A. B., Powell, R. M., & Evans, D. J. (2001). Echoviruses bind heparan sulfate at the cell surface. *J Virol*, *75*(10), 4918-4921. https://doi.org/10.1128/jvi.75.10.4918-4921.2001

Gordon, T. B., Hayward, J. A., Marsh, G. A., Baker, M. L., & Tachedjian, G. (2019). Host and Viral Proteins Modulating Ebola and Marburg Virus Egress. *Viruses*, *11*(1).

Goronzy, I. N., Rawle, R. J., Boxer, S. G., & Kasson, P. M. (2018). Cholesterol enhances influenza binding avidity by controlling nanoscale receptor clustering. *Chem Sci*, *9*(8), 2340-2347. https://doi.org/10.1039/c7sc03236f

Graham, S. M. (2003). Impact of HIV on childhood respiratory illness: differences between developing and developed countries. *Pediatr Pulmonol*, *36*(6), 462-468. https://doi.org/10.1002/ppul.10343

Gramberg, T., Hofmann, H., Möller, P., Lalor, P. F., Marzi, A., Geier, M., Krumbiegel, M., Winkler, T., Kirchhoff, F., Adams, D. H., Becker, S., Münch, J., & Pöhlmann, S. (2005). LSECtin interacts with filovirus glycoproteins and the spike protein of SARS coronavirus. *Virology*, *340*(2), 224-236. https://doi.org/10.1016/j.virol.2005.06.026

Gregory, S. M., Harada, E., Liang, B., Delos, S. E., White, J. M., & Tamm, L. K. (2011). Structure and function of the complete internal fusion loop from Ebolavirus glycoprotein 2. *Proceedings of the National Academy of Sciences of the United States of America*, *108*(27), 11211-11216. https://doi.org/10.1073/pnas.1104760108

Gregory, S. M., Larsson, P., Nelson, E. A., Kasson, P. M., White, J. M., & Tamm, L. K. (2014). Ebolavirus entry requires a compact hydrophobic fist at the tip of the fusion loop. *Journal of Virology*, *88*(12), 6636-6649. https://doi.org/10.1128/JVI.00396-14

Grove, J., & Marsh, M. (2011). The cell biology of receptor-mediated virus entry. *The Journal of Cell Biology*, *195*(7), 1071 LP-1082. http://jcb.rupress.org/content/195/7/1071.abstract

Gruenberg, J. (2020). Life in the lumen: The multivesicular endosome. *Traffic*, *21*(1), 76-93. https://doi.org/10.1111/TRA.12715

Günther, S. C., Martínez-Romero, C., Sempere Borau, M., Pham, C. T. N., García-Sastre, A., & Stertz, S. (2022). Proteomic Identification of Potential Target Proteins of Cathepsin W for Its Development as a Drug Target for Influenza. *Microbiol Spectr*, *10*(4), e0092122. https://doi.org/10.1128/spectrum.00921-22

Haasnoot, J., de Vries, W., Geutjes, E. J., Prins, M., de Haan, P., & Berkhout, B. (2007). The Ebola virus VP35 protein is a suppressor of RNA silencing. *PLoS Pathog*, *3*(6), e86. https://doi.org/10.1371/journal.ppat.0030086

Hacke, M., Bjorkholm, P., Hellwig, A., Himmels, P., de Almodovar, C. R., Brugger, B., Wieland, F., & Ernst, A. M. (2015). Inhibition of Ebola virus glycoprotein-mediated cytotoxicity by targeting its transmembrane domain and cholesterol. *Nat Commun*, *6*. http://dx.doi.org/10.1038/ncomms8688

http://10.0.4.14/ncomms8688

Haldar, S., Okamoto, K., Dunning, R. A., & Kasson, P. M. (2020). Precise Triggering and Chemical Control of Single-Virus Fusion within Endosomes. *J Virol*, *95*(1). https://doi.org/10.1128/jvi.01982-20

Hallam, S. J., Koma, T., Maruyama, J., & Paessler, S. (2018). Review of Mammarenavirus Biology and Replication. *Front Microbiol*, *9*, 1751. https://doi.org/10.3389/fmicb.2018.01751

Hanson, M. A., Brooun, A., Baker, K. A., Jaakola, V. P., Roth, C., Chien, E. Y., Alexandrov, A., Velasquez, J., Davis, L., Griffith, M., Moy, K., Ganser-Pornillos, B. K., Hua, Y., Kuhn, P., Ellis, S., Yeager, M., & Stevens, R. C. (2007). Profiling of membrane protein variants in a baculovirus system by coupling cell-surface detection with small-scale parallel expression. *Protein Expr Purif*, *56*(1), 85-92. https://doi.org/10.1016/j.pep.2007.06.003

Harrison, A. R., David, C. T., Rawlinson, S. M., & Moseley, G. W. (2021). The Ebola Virus Interferon Antagonist VP24 Undergoes Active Nucleocytoplasmic Trafficking. *Viruses*, *13*(8). https://doi.org/10.3390/v13081650

Harrison, J. S., Higgins, C. D., Chandran, K., & Lai, J. R. (2011). Designed protein mimics of the Ebola virus glycoprotein GP2 α-helical bundle: stability and pH effects. *Protein Sci*, *20*(9), 1587-1596. https://doi.org/10.1002/pro.688

Harrison, Joseph S., Higgins, Chelsea D., O'Meara, Matthew J., Koellhoffer, Jayne F., Kuhlman, Brian A., & Lai, Jonathan R. (2013). Role of Electrostatic Repulsion in Controlling pH-Dependent Conformational Changes of Viral Fusion Proteins. *Structure*, *21*(7), 1085-1096. https://doi.org/https://doi.org/10.1016/j.str.2013.05.009

Harrison, S. C. (2008). Viral membrane fusion. *Nat Struct Mol Biol*, *15*(7), 690-698. https://doi.org/10.1038/nsmb.1456

Hartlieb, B., Muziol, T., Weissenhorn, W., & Becker, S. (2007). Crystal structure of the C-terminal domain of Ebola virus VP30 reveals a role in transcription and nucleocapsid association. *Proceedings of the National Academy of Sciences*, *104*(2), 624-629. https://doi.org/doi:10.1073/pnas.0606730104

Haywood, A. M. (2010). Membrane uncoating of intact enveloped viruses. *J Virol*, *84*(21), 10946-10955. https://doi.org/10.1128/jvi.00229-10

He, J., Melnik, L. I., Komin, A., Wiedman, G., Fuselier, T., Morris, C. F., Starr, C. G., Searson, P. C., Gallaher, W. R., Hristova, K., Garry, R. F., & Wimley, W. C. (2017). Ebola Virus Delta Peptide Is a Viroporin. *J Virol*, *91*(16). https://doi.org/10.1128/jvi.00438-17

Hinterdorfer, P., Baber, G., & Tamm, L. K. (1994). Reconstitution of membrane fusion sites. A total internal reflection fluorescence microscopy study of influenza hemagglutinin-mediated membrane fusion. *Journal of Biological Chemistry*, *269*(32), 20360-20368. http://www.jbc.org/content/269/32/20360.abstract

Hoenen, T., Biedenkopf, N., Zielecki, F., Jung, S., Groseth, A., Feldmann, H., & Becker, S. (2010). Oligomerization of Ebola Virus VP40 Is Essential for Particle Morphogenesis and Regulation of Viral Transcription. *Journal of Virology*, *84*(14), 7053-7063. https://doi.org/doi:10.1128/JVI.00737-10

Hoenen, T., Groseth, A., Falzarano, D., & Feldmann, H. (2006). Ebola virus: unravelling pathogenesis to combat a deadly disease. *Trends Mol Med*, *12*(5), 206-215. https://doi.org/10.1016/j.molmed.2006.03.006

Hoenen, T., Groseth, A., & Feldmann, H. (2019). Therapeutic strategies to target the Ebola virus life cycle. *Nature Reviews Microbiology*, *17*(10), 593-606. https://doi.org/10.1038/s41579-019-0233-2

Hoffmann, M., Kleine-Weber, H., & Pöhlmann, S. (2020). A Multibasic Cleavage Site in the Spike Protein of SARS-CoV-2 Is Essential for Infection of Human Lung Cells. *Molecular Cell*, *78*(4), 779-784.e775. https://doi.org/10.1016/j.molcel.2020.04.022

Hoffmann, M., Kleine-Weber, H., Schroeder, S., Krüger, N., Herrler, T., Erichsen, S., Schiergens, T. S., Herrler, G., Wu, N. H., Nitsche, A., Müller, M. A., Drosten, C., & Pöhlmann, S. (2020). SARS-CoV-2 Cell Entry Depends on ACE2 and TMPRSS2 and Is Blocked by a Clinically Proven Protease Inhibitor. *Cell*, *181*(2), 271-280.e278. https://doi.org/10.1016/j.cell.2020.02.052

Höglinger, D., Burgoyne, T., Sanchez-Heras, E., Hartwig, P., Colaco, A., Newton, J., Futter, C. E., Spiegel, S., Platt, F. M., & Eden, E. R. (2019). NPC1 regulates ER contacts with endocytic organelles to mediate cholesterol egress. *Nature Communications*, *10*(1), 1-14. https://doi.org/10.1038/s41467-019-12152-2

Hood, C. L., Abraham, J., Boyington, J. C., Leung, K., Kwong, P. D., & Nabel, G. J. (2010). Biochemical and structural characterization of cathepsin L-processed Ebola virus glycoprotein: implications for viral entry and immunogenicity. *Journal of Virology*, *84*(6), 2972-2982. https://doi.org/10.1128/JVI.02151-09

Hu, B., Höfer, C. T., Thiele, C., & Veit, M. (2019). Cholesterol Binding to the Transmembrane Region of a Group 2 Hemagglutinin (HA) of Influenza Virus Is Essential for Virus Replication, Affecting both Virus Assembly and HA Fusion Activity. *Journal of Virology*, *93*(15). https://doi.org/10.1128/jvi.00555-19

Hu, L., Crawford, S. E., Czako, R., Cortes-Penfield, N. W., Smith, D. F., Le Pendu, J., Estes, M. K., & Prasad, B. V. (2012). Cell attachment protein VP8* of a human rotavirus specifically interacts with A-type histo-blood group antigen. *Nature*, *485*(7397), 256-259. https://doi.org/10.1038/nature10996

Huang, Y., Xu, L., Sun, Y., & Nabel, G. J. (2002). The assembly of Ebola virus nucleocapsid requires virion-associated proteins 35 and 24 and posttranslational modification of nucleoprotein. *Mol Cell*, *10*(2), 307-316. https://doi.org/10.1016/s1097-2765(02)00588-9

Hullin-Matsuda, F., Luquain-Costaz, C., Bouvier, J., & Delton-Vandenbroucke, I. (2009). Bis(monoacylglycero)phosphate, a peculiar phospholipid to control the fate of

cholesterol: Implications in pathology. *Prostaglandins Leukot Essent Fatty Acids*, *81*(5-6), 313-324. https://doi.org/10.1016/j.plefa.2009.09.006

Hulseberg, C. E., Fénéant, L., Szymańska, K. M., & White, J. M. (2018). Lamp1 increases the efficiency of lassa virus infection by promoting fusion in less acidic endosomal compartments. *mBio*, *9*(1). https://doi.org/10.1128/mBio.01818-17

Hume, A. J., & Mühlberger, E. (2019). Distinct Genome Replication and Transcription Strategies within the Growing Filovirus Family. *J Mol Biol*, *431*(21), 4290-4320. https://doi.org/10.1016/j.jmb.2019.06.029

Hunt, C. L., Kolokoltsov, A. A., Davey, R. A., & Maury, W. (2011). The Tyro3 Receptor Kinase Axl Enhances Macropinocytosis of Zaire Ebolavirus. *Journal of Virology*, *85*(1), 334-347. https://doi.org/doi:10.1128/JVI.01278-09

Husby, M. L., Amiar, S., Prugar, L. I., David, E. A., Plescia, C. B., Huie, K. E., Brannan, J. M., Dye, J. M., Pienaar, E., & Stahelin, R. V. (2022). Phosphatidylserine clustering by the Ebola virus matrix protein is a critical step in viral budding. *EMBO Rep*, *23*(11), e51709. https://doi.org/10.15252/embr.202051709

Israelsson, S., Gullberg, M., Jonsson, N., Roivainen, M., Edman, K., & Lindberg, A. M. (2010). Studies of Echovirus 5 interactions with the cell surface: Heparan sulfate mediates attachment to the host cell. *Virus Research*, *151*(2), 170-176. https://doi.org/https://doi.org/10.1016/j.virusres.2010.05.001

Ito, H., Watanabe, S., Takada, A., & Kawaoka, Y. (2001). Ebola virus glycoprotein: proteolytic processing, acylation, cell tropism, and detection of neutralizing antibodies. *J Virol*, *75*(3), 1576-1580. https://doi.org/10.1128/jvi.75.3.1576-1580.2001

Jacob, S. T., Crozier, I., Fischer, W. A., Hewlett, A., Kraft, C. S., Vega, M.-A. d. L., Soka, M. J., Wahl, V., Griffiths, A., Bollinger, L., & Kuhn, J. H. (2020). Ebola virus disease. *Nature Reviews Disease Primers*, *6*(1), 13. https://doi.org/10.1038/s41572-020-0147-3

Jae, L. T., Raaben, M., Herbert, A. S., Kuehne, A. I., Wirchnianski, A. S., Soh, T. K., Stubbs, S. H., Janssen, H., Damme, M., Saftig, P., Whelan, S. P., Dye, J. M., & Brummelkamp, T. R. (2014). Lassa virus entry requires a trigger-induced receptor switch. *Science*, *344*(6191), 1506-1510. https://doi.org/10.1126/science.1252480

Jayme, S. I., Field, H. E., de Jong, C., Olival, K. J., Marsh, G., Tagtag, A. M., Hughes, T., Bucad, A. C., Barr, J., Azul, R. R., Retes, L. M., Foord, A., Yu, M., Cruz, M. S., Santos, I. J., Lim, T. M. S., Benigno, C. C., Epstein, J. H., Wang, L.-F., . . . Newman, S. H. (2015). Molecular evidence of Ebola Reston virus infection in Philippine bats. *Virology Journal*, *12*(1), 107. https://doi.org/10.1186/s12985-015-0331-3

Jeffers, S. A., Sanders, D. A., & Sanchez, A. (2002). Covalent Modifications of the Ebola Virus Glycoprotein. *Journal of Virology*, *76*(24), 12463-12472. https://doi.org/doi:10.1128/JVI.76.24.12463-12472.2002

Jemielity, S., Wang, J. J., Chan, Y. K., Ahmed, A. A., Li, W., Monahan, S., Bu, X., Farzan, M., Freeman, G. J., Umetsu, D. T., DeKruyff, R. H., & Choe, H. (2013). TIM-family Proteins Promote Infection of Multiple Enveloped Viruses through Virion-associated Phosphatidylserine. *PLOS Pathogens*, *9*(3), e1003232. https://doi.org/10.1371/journal.ppat.1003232

Jeschke, G., & Polyhach, Y. (2007). Distance measurements on spin-labelled biomacromolecules by pulsed electron paramagnetic resonance. *Phys Chem Chem Phys*, *9*(16), 1895-1910. https://doi.org/10.1039/b614920k

Jin, C., Che, B., Guo, Z., Li, C., Liu, Y., Wu, W., Wang, S., Li, D., Cui, Z., & Liang, M. (2020). Single virus tracking of Ebola virus entry through lipid rafts in living host cells. *Biosaf Health*, *2*(1), 25-31. https://doi.org/10.1016/j.bsheal.2019.12.009

Johansen, L. M., DeWald, L. E., Shoemaker, C. J., Hoffstrom, B. G., Lear-Rooney, C. M., Stossel, A., Nelson, E., Delos, S. E., Simmons, J. A., Grenier, J. M., Pierce, L. T., Pajouhesh, H., Lehár, J., Hensley, L. E., Glass, P. J., White, J. M., & Olinger, G. G. (2015). A screen of approved drugs and molecular probes identifies therapeutics with anti–Ebola virus activity. *Science Translational Medicine*, *7*(290), 290ra289-290ra289. https://doi.org/doi:10.1126/scitranslmed.aaa5597

John, S. P., Wang, T., Steffen, S., Longhi, S., Schmaljohn, C. S., & Jonsson, C. B. (2007). Ebola virus VP30 is an RNA binding protein. *J Virol*, *81*(17), 8967-8976. https://doi.org/10.1128/jvi.02523-06

Johnson, K. A., Taghon, G. J. F., Scott, J. L., & Stahelin, R. V. (2016). The Ebola Virus matrix protein, VP40, requires phosphatidylinositol 4,5-bisphosphate (PI(4,5)P2) for extensive oligomerization at the plasma membrane and viral egress. *Scientific Reports*, *6*(1), 19125. https://doi.org/10.1038/srep19125

Jolly, C. L., & Sattentau, Q. J. (2013). Attachment factors. *Adv Exp Med Biol*, *790*, 1-23. https://doi.org/10.1007/978-1-4614-7651-1_1

Kalb, E., Frey, S., & Tamm, L. K. (1992). Formation of supported planar bilayers by fusion of vesicles to supported phospholipid monolayers. *Biochimica et Biophysica Acta (BBA) - Biomembranes*, *1103*(2), 307-316. https://doi.org/https://doi.org/10.1016/0005-2736(92)90101-Q

Kaletsky, R. L., Simmons, G., & Bates, P. (2007). Proteolysis of the Ebola virus glycoproteins enhances virus binding and infectivity. *Journal of Virology*, *81*(24), 13378-13384. https://doi.org/10.1128/JVI.01170-07

Kamhi, E., Joo, E. J., Dordick, J. S., & Linhardt, R. J. (2013). Glycosaminoglycans in infectious disease. *Biological Reviews*, *88*(4), 928-943. https://doi.org/https://doi.org/10.1111/brv.12034

Kang, Y.-L., Chou, Y.-y., Rothlauf, P. W., Liu, Z., Soh, T. K., Cureton, D., Case, J. B., Chen, R. E., Diamond, M. S., Whelan, S. P. J., & Kirchhausen, T. (2020). Inhibition of PIKfyve kinase prevents infection by Zaire ebolavirus and SARS-CoV-2. *Proceedings of the National Academy of Sciences*, 202007837-202007837. https://doi.org/10.1073/pnas.2007837117

Karan, L. S., Makenov, M. T., Korneev, M. G., Sacko, N., Boumbaly, S., Yakovlev, S. A., Kourouma, K., Bayandin, R. B., Gladysheva, A. V., Shipovalov, A. V., Yurganova, I. A., Grigorieva, Y. E., Fedorova, M. V., Scherbakova, S. A., Kutyrev, V. V., Agafonov, A. P., Maksyutov, R. A., Shipulin, G. A., Maleev, V. V., . . . Popova, A. Y. (2019). Bombali Virus in Mops condylurus Bats, Guinea. *Emerg Infect Dis*, *25*(9), 1774-1775. https://doi.org/10.3201/eid2509.190581

Karasneh, G. A., & Shukla, D. (2011). Herpes simplex virus infects most cell types in vitro: clues to its success. *Virol J*, *8*, 481. https://doi.org/10.1186/1743-422x-8-481

Katz, M., Weinstein, J., Eilon-Ashkenazy, M., Gehring, K., Cohen-Dvashi, H., Elad, N., Fleishman, S. J., & Diskin, R. (2022). Structure and receptor recognition by the Lassa virus spike complex. *Nature 2022 603:7899*, *603*(7899), 174-179. https://doi.org/10.1038/s41586-022-04429-2

Kemble, G. W., Henis, Y. I., & White, J. M. (1993). GPI- and transmembrane-anchored influenza hemagglutinin differ in structure and receptor binding activity. *J Cell Biol*, *122*(6), 1253-1265. https://doi.org/10.1083/jcb.122.6.1253

Kemenesi, G., Kurucz, K., Dallos, B., Zana, B., Földes, F., Boldogh, S., Görföl, T., Carroll, M. W., & Jakab, F. (2018). Re-emergence of Lloviu virus in Miniopterus schreibersii bats, Hungary,

2016. *Emerging Microbes & Infections*, *7*(1), 1-4. https://doi.org/10.1038/s41426-018-0067-4

Kielian, M. (2014). Mechanisms of Virus Membrane Fusion Proteins. *Annual Review of Virology*, *1*(1), 171-189. https://doi.org/10.1146/annurev-virology-031413-085521

Kiessling, V., Crane, J. M., & Tamm, L. K. (2006). Transbilayer effects of raft-like lipid domains in asymmetric planar bilayers measured by single molecule tracking. *Biophys J*, *91*(9), 3313-3326. https://doi.org/10.1529/biophysj.106.091421

Kiessling, V., Domanska, M. K., & Tamm, L. K. (2010). Single SNARE-Mediated Vesicle Fusion Observed In Vitro by Polarized TIRFM. *Biophysical Journal*, *99*(12), 4047-4055. https://doi.org/10.1016/j.bpj.2010.10.022

Kiessling, V., Kreutzberger, A. J. B., Liang, B., Nyenhuis, S. B., Seelheim, P., Castle, J. D., Cafiso, D. S., & Tamm, L. K. (2018). A molecular mechanism for calcium-mediated synaptotagmin-triggered exocytosis. *Nature Structural and Molecular Biology*, *25*(10), 911-917. https://doi.org/10.1038/s41594-018-0130-9

Kim, I. S., Jenni, S., Stanifer, M. L., Roth, E., Whelan, S. P. J., van Oijen, A. M., & Harrison, S. C. (2017). Mechanism of membrane fusion induced by vesicular stomatitis virus G protein. *Proceedings of the National Academy of Sciences*, *114*(1), E28-E36. https://doi.org/doi:10.1073/pnas.1618883114

Kirchdoerfer, R. N., Wasserman, H., Amarasinghe, G. K., & Saphire, E. O. (2017). Filovirus Structural Biology: The Molecules in the Machine. *Curr Top Microbiol Immunol*, *411*, 381-417. https://doi.org/10.1007/82_2017_16

Kobayashi, T., Beuchat, M.-H., Chevallier, J., Makino, A., Mayran, N., Escola, J.-M., Lebrand, C., Cosson, P., Kobayashi, T., & Gruenberg, J. (2002). Separation and characterization of late endosomal membrane domains. *The Journal of biological chemistry*, *277*(35), 32157-32164. https://doi.org/10.1074/jbc.M202838200

Kobayashi, T., Stang, E., Fang, K. S., de Moerloose, P., Parton, R. G., & Gruenberg, J. (1998). A lipid associated with the antiphospholipid syndrome regulates endosome structure and function. *Nature*, *392*(6672), 193-197. https://doi.org/10.1038/32440

Kolatkar, P. R., Bella, J., Olson, N. H., Bator, C. M., Baker, T. S., & Rossmann, M. G. (1999). Structural studies of two rhinovirus serotypes complexed with fragments of their cellular receptor. *Embo j*, *18*(22), 6249-6259. https://doi.org/10.1093/emboj/18.22.6249

Kondratowicz, A. S., Lennemann, N. J., Sinn, P. L., Davey, R. A., Hunt, C. L., Moller-Tank, S., Meyerholz, D. K., Rennert, P., Mullins, R. F., Brindley, M., Sandersfeld, L. M., Quinn, K., Weller, M., McCray, P. B., Chiorini, J., & Maury, W. (2011). T-cell immunoglobulin and mucin domain 1 (TIM-1) is a receptor for Z*aire Ebolavirus* and *Lake Victoria Marburgvirus*>. *Proceedings of the National Academy of Sciences*, *108*(20), 8426-8431. https://doi.org/doi:10.1073/pnas.1019030108

Kreutzberger, A. J. B., Kiessling, V., Liang, B., Seelheim, P., Jakhanwal, S., Jahn, R., Castle, J. D., & Tamm, L. K. (2017). Reconstitution of calcium-mediated exocytosis of dense-core vesicles. *Science Advances*, *3*(7). http://advances.sciencemag.org/content/3/7/e1603208.abstract

Kreutzberger, A. J. B., Kiessling, V., Liang, B., Yang, S.-T., Castle, J. D., & Tamm, L. K. (2017). Asymmetric Phosphatidylethanolamine Distribution Controls Fusion Pore Lifetime and Probability. *Biophysical Journal*, *113*(9), 1912-1915. https://doi.org/10.1016/j.bpj.2017.09.014

Kreutzberger, Alex J. B., Kiessling, V., & Tamm, Lukas K. (2015). High Cholesterol Obviates a Prolonged Hemifusion Intermediate in Fast SNARE-Mediated Membrane Fusion. *Biophysical Journal*, *109*(2), 319-329. https://doi.org/10.1016/j.bpj.2015.06.022

Kreutzberger, A. J. B., Sanyal, A., Saminathan, A., Bloyet, L.-M., Stumpf, S., Liu, Z., Ojha, R., Patjas, M. T., Geneid, A., Scanavachi, G., Doyle, C. A., Somerville, E., Correia, R. B. D. C., Di Caprio, G., Toppila-Salmi, S., Mäkitie, A., Kiessling, V., Vapalahti, O., Whelan, S. P. J., . . . Kirchhausen, T. (2022). SARS-CoV-2 requires acidic pH to infect cells. *Proceedings of the National Academy of Sciences*, *119*(38), e2209514119. https://doi.org/doi:10.1073/pnas.2209514119

Kühl, A., & Pöhlmann, S. (2012). How Ebola virus counters the interferon system. *Zoonoses and public health*, *59 Suppl 2*(Suppl 2), 116-131. https://doi.org/10.1111/j.1863-2378.2012.01454.x

Kuhn, J. H. (2021). Virus Taxonomy. *Encyclopedia of Virology*, 28-37. https://doi.org/10.1016/b978-0-12-809633-8.21231-4

Kuhn, J. H., Amarasinghe, G. K., Basler, C. F., Bavari, S., Bukreyev, A., Chandran, K., Crozier, I., Dolnik, O., Dye, J. M., Formenty, P. B. H., Griffiths, A., Hewson, R., Kobinger, G. P., Leroy, E. M., Mühlberger, E., Netesov Нетёсов Сергей Викторович, S. V., Palacios, G., Pályi, B., Pawęska, J. T., . . . Ictv Report, C. (2019). ICTV Virus Taxonomy Profile: Filoviridae. *J Gen Virol*, *100*(6), 911-912. https://doi.org/10.1099/jgv.0.001252

Kuroda, M., Halfmann, P., & Kawaoka, Y. (2020). HER2-mediated enhancement of Ebola virus entry. *PLOS Pathogens*, *16*(10), e1008900. https://doi.org/10.1371/journal.ppat.1008900

Kwon, H. J., Abi-Mosleh, L., Wang, M. L., Deisenhofer, J., Goldstein, J. L., Brown, M. S., & Infante, R. E. (2009). Structure of N-terminal domain of NPC1 reveals distinct subdomains for binding and transfer of cholesterol. *Cell*, *137*(7), 1213-1224. https://doi.org/10.1016/j.cell.2009.03.049

Kwon, H. J., Palnitkar, M., & Deisenhofer, J. (2011). The Structure of the NPC1L1 N-Terminal Domain in a Closed Conformation. *PLOS ONE*, *6*(4), e18722-e18722. http://dx.doi.org/10.1371%2Fjournal.pone.0018722

Lai, Alex L., & Freed, Jack H. (2015). The Interaction between Influenza HA Fusion Peptide and Transmembrane Domain Affects Membrane Structure. *Biophysical Journal*, *109*(12), 2523-2536. https://doi.org/10.1016/j.bpj.2015.10.044

Lai, A. L., Moorthy, A. E., Li, Y., & Tamm, L. K. (2012). Fusion activity of HIV gp41 fusion domain is related to its secondary structure and depth of membrane insertion in a cholesterol-dependent fashion. *J Mol Biol*, *418*(1-2), 3-15. https://doi.org/10.1016/j.jmb.2012.02.010

Lamas Longarela, O., Schmidt, T. T., Schöneweis, K., Romeo, R., Wedemeyer, H., Urban, S., & Schulze, A. (2013). Proteoglycans act as cellular hepatitis delta virus attachment receptors. *PLOS ONE*, *8*(3), e58340. https://doi.org/10.1371/journal.pone.0058340

Lambert, S., Bouttier, M., Vassy, R., Seigneuret, M., Petrow-Sadowski, C., Janvier, S., Heveker, N., Ruscetti, F. W., Perret, G., Jones, K. S., & Pique, C. (2009). HTLV-1 uses HSPG and neuropilin-1 for entry by molecular mimicry of VEGF165. *Blood*, *113*(21), 5176-5185. https://doi.org/10.1182/blood-2008-04-150342

Languon, S., & Quaye, O. (2019). Filovirus Disease Outbreaks: A Chronological Overview. *Virology : research and treatment*, *10*, 1178122X19849927-11178122X19849927. https://doi.org/10.1177/1178122X19849927

Lasala, F., Arce, E., Otero, J. R., Rojo, J., & Delgado, R. (2003). Mannosyl glycodendritic structure inhibits DC-SIGN-mediated Ebola virus infection in cis and in trans. *Antimicrob Agents Chemother*, *47*(12), 3970-3972. https://doi.org/10.1128/aac.47.12.3970-3972.2003

Le Guenno, B., Formenty, P., Wyers, M., Gounon, P., Walker, F., & Boesch, C. (1995). Isolation and partial characterisation of a new strain of Ebola virus. *The Lancet*, *345*(8960), 1271-1274. https://doi.org/https://doi.org/10.1016/S0140-6736(95)90925-7

Lebarbenchon, C., Goodman, S. M., Hoarau, A. O. G., Le Minter, G., Dos Santos, A., Schoeman, M. C., Léculier, C., Raoul, H., Gudo, E. S., & Mavingui, P. (2022). Bombali Ebolavirus in Mops condylurus Bats (Molossidae), Mozambique. *Emerg Infect Dis*, *28*(12), 2583-2585. https://doi.org/10.3201/eid2812.220853

Lee, D. E., Lew, M. G., & Woodbury, D. J. (2013). Vesicle fusion to planar membranes is enhanced by cholesterol and low temperature. *Chem Phys Lipids*, *166*, 45-54. https://doi.org/10.1016/j.chemphyslip.2012.11.004

Lee, H., Callaway, H. M., Cifuente, J. O., Bator, C. M., Parrish, C. R., & Hafenstein, S. L. (2019). Transferrin receptor binds virus capsid with dynamic motion. *Proceedings of the National Academy of Sciences*, *116*(41), 20462-20471. https://doi.org/doi:10.1073/pnas.1904918116

Lee, J., Gregory, S. M., Nelson, E. A., White, J. M., & Tamm, L. K. (2016). The roles of histidines and charged residues as potential triggers of a conformational change in the fusion loop of ebola virus glycoprotein. *PLOS ONE*, *11*(3). https://doi.org/10.1371/journal.pone.0152527

Lee, J., Nyenhuis, D. A., Nelson, E. A., Cafiso, D. S., White, J. M., & Tamm, L. K. (2017). Structure of the Ebola virus envelope protein MPER/TM domain and its interaction with the fusion loop explains their fusion activity. *Proceedings of the National Academy of Sciences of the United States of America*. https://doi.org/10.1073/pnas.1708052114

Lee, J. E., Fusco, M. L., Hessell, A. J., Oswald, W. B., Burton, D. R., & Saphire, E. O. (2008). Structure of the Ebola virus glycoprotein bound to an antibody from a human survivor. *Nature*, *454*(7201), 177-182. https://doi.org/10.1038/nature07082

Lee, J. E., & Saphire, E. O. (2009). Ebolavirus glycoprotein structure and mechanism of entry. *Future Virology*, *4*(6), 621-635. https://doi.org/10.2217/fvl.09.56

Leistner, C. M., Gruen-Bernhard, S., & Glebe, D. (2008). Role of glycosaminoglycans for binding and infection of hepatitis B virus. *Cell Microbiol*, *10*(1), 122-133. https://doi.org/10.1111/j.1462-5822.2007.01023.x

Lenz, O., ter Meulen, J., Klenk, H.-D., Seidah, N. G., & Garten, W. (2001). The Lassa virus glycoprotein precursor GP-C is proteolytically processed by subtilase SKI-1/S1P. *Proceedings of the National Academy of Sciences*, *98*(22), 12701-12705. https://doi.org/doi:10.1073/pnas.221447598

Leroy, E. M., Epelboin, A., Mondonge, V., Pourrut, X., Gonzalez, J. P., Muyembe-Tamfum, J. J., & Formenty, P. (2009). Human Ebola outbreak resulting from direct exposure to fruit bats in Luebo, Democratic Republic of Congo, 2007. *Vector Borne Zoonotic Dis*, *9*(6), 723-728. https://doi.org/10.1089/vbz.2008.0167

Li, J., Deffieu, M. S., Lee, P. L., Saha, P., & Pfeffer, S. R. (2015). Glycosylation inhibition reduces cholesterol accumulation in NPC1 protein-deficient cells. *Proceedings of the National Academy of Sciences of the United States of America*, *112*(48), 14876-14881. https://doi.org/10.1073/pnas.1520490112

Li, Q., Liu, Q., Huang, W., Li, X., & Wang, Y. (2018). Current status on the development of pseudoviruses for enveloped viruses. *Rev Med Virol*, *28*(1). https://doi.org/10.1002/rmv.1963

Li, X., Saha, P., Li, J., Blobel, G., & Pfeffer, S. R. (2016). Clues to the mechanism of cholesterol transfer from the structure of NPC1 middle lumenal domain bound to NPC2.

*Proceedings of the National Academy of Sciences of the United States of America*. https://doi.org/10.1073/pnas.1611956113

Li, Y., Wang, L., Zhu, T., Wu, S., Feng, L., Cheng, P., Liu, J., & Wang, J. (2018). Establishing China's National Standard for the Recombinant Adenovirus Type 5 Vector-Based Ebola Vaccine (Ad5-EBOV) Virus Titer. *Hum Gene Ther Clin Dev*, *29*(4), 226-232. https://doi.org/10.1089/humc.2018.129

Liao, Z., Cimakasky, L. M., Hampton, R., Nguyen, D. H., & Hildreth, J. E. (2001). Lipid rafts and HIV pathogenesis: host membrane cholesterol is required for infection by HIV type 1. *AIDS Res Hum Retroviruses*, *17*(11), 1009-1019. https://doi.org/10.1089/088922201300343690

Lin, G., Simmons, G., Pöhlmann, S., Baribaud, F., Ni, H., Leslie, G. J., Haggarty, B. S., Bates, P., Weissman, D., Hoxie, J. A., & Doms, R. W. (2003). Differential N-Linked Glycosylation of Human Immunodeficiency Virus and Ebola Virus Envelope Glycoproteins Modulates Interactions with DC-SIGN and DC-SIGNR. *Journal of Virology*, *77*(2), 1337-1346. https://doi.org/doi:10.1128/JVI.77.2.1337-1346.2003

Lis, H., & Sharon, N. (1993). Protein glycosylation. *European Journal of Biochemistry*, *218*(1), 1-27. https://doi.org/https://doi.org/10.1111/j.1432-1033.1993.tb18347.x

Liu, K. N., & Boxer, S. G. (2020). Target Membrane Cholesterol Modulates Single Influenza Virus Membrane Fusion Efficiency but Not Rate. *Biophys J*, *118*(10), 2426-2433. https://doi.org/10.1016/j.bpj.2020.03.021

Liu, S.-L., Wang, Z.-G., Xie, H.-Y., Liu, A.-A., Lamb, D. C., & Pang, D.-W. (2020). Single-Virus Tracking: From Imaging Methodologies to Virological Applications. https://doi.org/10.1021/acs.chemrev.9b00692

Liu, T., Luo, S., Libby, P., & Shi, G. P. (2020). Cathepsin L-selective inhibitors: A potentially promising treatment for COVID-19 patients. *Pharmacol Ther*, *213*, 107587. https://doi.org/10.1016/j.pharmthera.2020.107587

Lloyd-Evans, E., Morgan, A. J., He, X., Smith, D. A., Elliot-Smith, E., Sillence, D. J., Churchill, G. C., Schuchman, E. H., Galione, A., & Platt, F. M. (2008). Niemann-Pick disease type C1 is a sphingosine storage disease that causes deregulation of lysosomal calcium. *Nature medicine*, *14*(11), 1247-1255. https://doi.org/10.1038/nm.1876

Löfling, J., Lyi, S. M., Parrish, C. R., & Varki, A. (2013). Canine and feline parvoviruses preferentially recognize the non-human cell surface sialic acid N-glycolylneuraminic acid. *Virology*, *440*(1), 89-96. https://doi.org/10.1016/j.virol.2013.02.009

Lubaki, N. M., Ilinykh, P., Pietzsch, C., Tigabu, B., Freiberg, A. N., Koup, R. A., & Bukreyev, A. (2013). The lack of maturation of Ebola virus-infected dendritic cells results from the cooperative effect of at least two viral domains. *Journal of Virology*, *87*(13), 7471-7485. https://doi.org/10.1128/JVI.03316-12

Luczkowiak, J., Arribas, J. R., Gómez, S., Jiménez-Yuste, V., de la Calle, F., Viejo, A., & Delgado, R. (2016). Specific neutralizing response in plasma from convalescent patients of Ebola Virus Disease against the West Africa Makona variant of Ebola virus. *Virus Res*, *213*, 224-229. https://doi.org/10.1016/j.virusres.2015.12.019

Macovei, A., Radulescu, C., Lazar, C., Petrescu, S., Durantel, D., Dwek, R. A., Zitzmann, N., & Nichita, N. B. (2010). Hepatitis B Virus Requires Intact Caveolin-1 Function for Productive Infection in HepaRG Cells. *Journal of Virology*, *84*(1), 243-253. https://doi.org/doi:10.1128/JVI.01207-09

Malashkevich, V. N., Schneider, B. J., McNally, M. L., Milhollen, M. A., Pang, J. X., & Kim, P. S. (1999). Core structure of the envelope glycoprotein GP2 from Ebola virus at 1.9-A

resolution. *Proceedings of the National Academy of Sciences of the United States of America*, *96*(6), 2662-2667.

Mannsverk, S., Villamil Giraldo, A. M., & Kasson, P. M. (2022). Influenza Virus Membrane Fusion Is Promoted by the Endosome-Resident Phospholipid Bis(monoacylglycero)phosphate. *J Phys Chem B*. https://doi.org/10.1021/acs.jpcb.2c06642

Marí Saéz, A., Weiss, S., Nowak, K., Lapeyre, V., Zimmermann, F., Düx, A., Kühl, H. S., Kaba, M., Regnaut, S., Merkel, K., Sachse, A., Thiesen, U., Villányi, L., Boesch, C., Dabrowski, P. W., Radonić, A., Nitsche, A., Leendertz, S. A. J., Petterson, S., . . . Leendertz, F. H. (2015). Investigating the zoonotic origin of the West African Ebola epidemic. *EMBO molecular medicine*, *7*(1), 17-23. https://doi.org/10.15252/emmm.201404792

Markmann, S., Thelen, M., Cornils, K., Schweizer, M., Brocke-Ahmadinejad, N., Willnow, T., Heeren, J., Gieselmann, V., Braulke, T., & Kollmann, K. (2015). Lrp1/LDL Receptor Play Critical Roles in Mannose 6-Phosphate-Independent Lysosomal Enzyme Targeting. *Traffic*, *16*(7), 743-759. https://doi.org/https://doi.org/10.1111/tra.12284

Markosyan, R. M., Marin, M., Zhang, Y., Cohen, F. S., & Melikyan, G. B. (2021). The late endosome-resident lipid bis(monoacylglycero)phosphate is a cofactor for Lassa virus fusion. *PLOS Pathogens*, *17*(9), e1009488-e1009488. https://doi.org/10.1371/JOURNAL.PPAT.1009488

Marsh, M., & Helenius, A. (2006). Virus entry: open sesame. *Cell*, *124*(4), 729-740. https://doi.org/10.1016/j.cell.2006.02.007

Martinez, O., Johnson, J., Manicassamy, B., Rong, L., Olinger, G. G., Hensley, L. E., & Basler, C. F. (2010). Zaire Ebola virus entry into human dendritic cells is insensitive to cathepsin L inhibition. *Cellular Microbiology*, *12*(2), 148-157. https://doi.org/https://doi.org/10.1111/j.1462-5822.2009.01385.x

Maruyama, T., Rodriguez, L. L., Jahrling, P. B., Sanchez, A., Khan, A. S., Nichol, S. T., Peters, C. J., Parren, P. W., & Burton, D. R. (1999). Ebola virus can be effectively neutralized by antibody produced in natural human infection. *J Virol*, *73*(7), 6024-6030. https://doi.org/10.1128/jvi.73.7.6024-6030.1999

Marzi, A., Möller, P., Hanna, S. L., Harrer, T., Eisemann, J., Steinkasserer, A., Becker, S., Baribaud, F., & Pöhlmann, S. (2007). Analysis of the interaction of Ebola virus glycoprotein with DC-SIGN (dendritic cell-specific intercellular adhesion molecule 3-grabbing nonintegrin) and its homologue DC-SIGNR. *J Infect Dis*, *196 Suppl 2*(Suppl 2), S237-246. https://doi.org/10.1086/520607

Marzi, A., Reinheckel, T., & Feldmann, H. (2012). Cathepsin B & L are not required for ebola virus replication. *PLoS Negl Trop Dis*, *6*(12), e1923. https://doi.org/10.1371/journal.pntd.0001923

Más, V., & Melero, J. A. (2013). Entry of enveloped viruses into host cells: membrane fusion. *Subcell Biochem*, *68*, 467-487. https://doi.org/10.1007/978-94-007-6552-8_16

Maurer, K., Krey, T., Moennig, V., Thiel, H. J., & Rümenapf, T. (2004). CD46 is a cellular receptor for bovine viral diarrhea virus. *J Virol*, *78*(4), 1792-1799. https://doi.org/10.1128/jvi.78.4.1792-1799.2004

Maxmen, A. (2019). Science under fire: Ebola researchers fight to test drugs and vaccines in a war zone. *Nature*, *572*(7767), 16-17. https://doi.org/10.1038/d41586-019-02258-4

Mayer, M., & Buchner, J. (2004). Refolding of inclusion body proteins. *Methods Mol Med*, *94*, 239-254. https://doi.org/10.1385/1-59259-679-7:239

Mazzon, M., & Mercer, J. (2014). Lipid interactions during virus entry and infection. *Cellular Microbiology*, *16*(10), 1493-1502. https://doi.org/10.1111/cmi.12340

McElroy, A. K., Akondy, R. S., Davis, C. W., Ellebedy, A. H., Mehta, A. K., Kraft, C. S., Lyon, G. M., Ribner, B. S., Varkey, J., Sidney, J., Sette, A., Campbell, S., Ströher, U., Damon, I., Nichol, S. T., Spiropoulou, C. F., & Ahmed, R. (2015). Human Ebola virus infection results in substantial immune activation. *Proceedings of the National Academy of Sciences*, *112*(15), 4719-4724. https://doi.org/doi:10.1073/pnas.1502619112

Mecham, J. O., & McHolland, L. E. (2010). Measurement of bluetongue virus binding to a mammalian cell surface receptor by an in situ immune fluorescent staining technique. *J Virol Methods*, *165*(1), 112-115. https://doi.org/10.1016/j.jviromet.2009.12.011

Mehedi, M., Falzarano, D., Seebach, J., Hu, X., Carpenter, M. S., Schnittler, H.-J., & Feldmann, H. (2011). A New Ebola Virus Nonstructural Glycoprotein Expressed through RNA Editing. *Journal of Virology*, *85*(11), 5406-5414. https://doi.org/doi:10.1128/JVI.02190-10

Melnik, L. I., Guha, S., Ghimire, J., Smither, A. R., Beddingfield, B. J., Hoffmann, A. R., Sun, L., Ungerleider, N. A., Baddoo, M. C., Flemington, E. K., Gallaher, W. R., Wimley, W. C., & Garry, R. F. (2022). Ebola virus delta peptide is an enterotoxin. *Cell Rep*, *38*(1), 110172. https://doi.org/10.1016/j.celrep.2021.110172

Mercer, J., & Helenius, A. (2008). Vaccinia Virus Uses Macropinocytosis and Apoptotic Mimicry to Enter Host Cells. *Science*, *320*(5875), 531-535. https://doi.org/doi:10.1126/science.1155164

Mercer, J., & Helenius, A. (2009). Virus entry by macropinocytosis. *Nature cell biology*, *11*(5), 510-520. https://doi.org/10.1038/ncb0509-510

Merril, C. R., Dunau, M. L., & Goldman, D. (1981). A rapid sensitive silver stain for polypeptides in polyacrylamide gels. *Anal Biochem*, *110*(1), 201-207. https://doi.org/10.1016/0003-2697(81)90136-6

Mikolajczyk, K., Kaczmarek, R., & Czerwinski, M. (2020). How glycosylation affects glycosylation: the role of N-glycans in glycosyltransferase activity. *Glycobiology*, *30*(12), 941-969. https://doi.org/10.1093/glycob/cwaa041

Miller, E. H., Obernosterer, G., Raaben, M., Herbert, A. S., Deffieu, M. S., Krishnan, A., Ndungo, E., Sandesara, R. G., Carette, J. E., Kuehne, A. I., Ruthel, G., Pfeffer, S. R., Dye, J. M., Whelan, S. P., Brummelkamp, T. R., & Chandran, K. (2012). Ebola virus entry requires the host-programmed recognition of an intracellular receptor. *The EMBO Journal*, *31*(8), 1947-1960. https://doi.org/10.1038/emboj.2012.53

Miller, M. E., Adhikary, S., Kolokoltsov, A. A., & Davey, R. A. (2012). Ebolavirus Requires Acid Sphingomyelinase Activity and Plasma Membrane Sphingomyelin for Infection. *Journal of Virology*, *86*(14), 7473-7483. https://doi.org/doi:10.1128/JVI.00136-12

Millet, J. K., & Whittaker, G. R. (2014). Host cell entry of Middle East respiratory syndrome coronavirus after two-step, furin-mediated activation of the spike protein. *Proceedings of the National Academy of Sciences*, *111*(42), 15214-15219. https://doi.org/doi:10.1073/pnas.1407087111

Mingo, R. M., Simmons, J. A., Shoemaker, C. J., Nelson, E. A., Schornberg, K. L., D'Souza, R. S., Casanova, J. E., & White, J. M. (2015). Ebola virus and severe acute respiratory syndrome coronavirus display late cell entry kinetics: evidence that transport to NPC1+ endolysosomes is a rate-defining step. *Journal of Virology*, *89*(5), 2931-2943. https://doi.org/10.1128/JVI.03398-14

Mire, C. E., Dube, D., Delos, S. E., White, J. M., & Whitt, M. A. (2009). Glycoprotein-Dependent Acidification of Vesicular Stomatitis Virus Enhances Release of Matrix Protein. *Journal of Virology*, *83*(23), 12139-12150. https://doi.org/doi:10.1128/JVI.00955-09

Misasi, J., Chandran, K., Yang, J. Y., Considine, B., Filone, C. M., Côté, M., Sullivan, N., Fabozzi, G., Hensley, L., & Cunningham, J. (2012). Filoviruses require endosomal cysteine proteases

for entry but exhibit distinct protease preferences. *J Virol*, *86*(6), 3284-3292. https://doi.org/10.1128/jvi.06346-11

Misinzo, G., Delputte, P. L., Meerts, P., Lefebvre, D. J., & Nauwynck, H. J. (2006). Porcine circovirus 2 uses heparan sulfate and chondroitin sulfate B glycosaminoglycans as receptors for its attachment to host cells. *J Virol*, *80*(7), 3487-3494. https://doi.org/10.1128/jvi.80.7.3487-3494.2006

Mohan, G. S., Li, W., Ye, L., Compans, R. W., & Yang, C. (2012). Antigenic subversion: a novel mechanism of host immune evasion by Ebola virus. *PLoS Pathog*, *8*(12), e1003065. https://doi.org/10.1371/journal.ppat.1003065

Mohan, G. S., Ye, L., Li, W., Monteiro, A., Lin, X., Sapkota, B., Pollack, B. P., Compans, R. W., & Yang, C. (2015). Less is more: Ebola virus surface glycoprotein expression levels regulate virus production and infectivity. *Journal of Virology*, *89*(2), 1205-1217. https://doi.org/10.1128/JVI.01810-14

Moller-Tank, S., Kondratowicz, A. S., Davey, R. A., Rennert, P. D., & Maury, W. (2013). Role of the Phosphatidylserine Receptor TIM-1 in Enveloped-Virus Entry. *Journal of Virology*, *87*(15), 8327-8341. https://doi.org/doi:10.1128/JVI.01025-13

Monini, P., Cafaro, A., Srivastava, I. K., Moretti, S., Sharma, V. A., Andreini, C., Chiozzini, C., Ferrantelli, F., Cossut, M. R., Tripiciano, A., Nappi, F., Longo, O., Bellino, S., Picconi, O., Fanales-Belasio, E., Borsetti, A., Toschi, E., Schiavoni, I., Bacigalupo, I., . . . Ensoli, B. (2012). HIV-1 tat promotes integrin-mediated HIV transmission to dendritic cells by binding Env spikes and competes neutralization by anti-HIV antibodies. *PLOS ONE*, *7*(11), e48781. https://doi.org/10.1371/journal.pone.0048781

Moremen, K. W., Tiemeyer, M., & Nairn, A. V. (2012). Vertebrate protein glycosylation: diversity, synthesis and function. *Nature Reviews Molecular Cell Biology*, *13*(7), 448-462. https://doi.org/10.1038/nrm3383

Morizono, K., Xie, Y., Olafsen, T., Lee, B., Dasgupta, A., Wu, Anna M., & Chen, Irvin S. Y. (2011). The Soluble Serum Protein Gas6 Bridges Virion Envelope Phosphatidylserine to the TAM Receptor Tyrosine Kinase Axl to Mediate Viral Entry. *Cell Host & Microbe*, *9*(4), 286-298. https://doi.org/https://doi.org/10.1016/j.chom.2011.03.012

Mulangu, S., Dodd, L. E., Davey, R. T., Tshiani Mbaya, O., Proschan, M., Mukadi, D., Lusakibanza Manzo, M., Nzolo, D., Tshomba Oloma, A., Ibanda, A., Ali, R., Coulibaly, S., Levine, A. C., Grais, R., Diaz, J., Lane, H. C., Muyembe-Tamfum, J.-J., & the PALM Writing Group. (2019). A Randomized, Controlled Trial of Ebola Virus Disease Therapeutics. *New England Journal of Medicine*, *381*(24), 2293-2303. https://doi.org/10.1056/NEJMoa1910993

Mulherkar, N., Raaben, M., de la Torre, J. C., Whelan, S. P., & Chandran, K. (2011). The Ebola virus glycoprotein mediates entry via a non-classical dynamin-dependent macropinocytic pathway. *Virology*, *419*(2), 72-83. https://doi.org/10.1016/j.virol.2011.08.009

Muñoz-Fontela, C., & McElroy, A. K. (2017). Ebola Virus Disease in Humans: Pathophysiology and Immunity. *Curr Top Microbiol Immunol*, *411*, 141-169. https://doi.org/10.1007/82_2017_11

Nanbo, A., Imai, M., Watanabe, S., Noda, T., Takahashi, K., Neumann, G., Halfmann, P., & Kawaoka, Y. (2010). Ebolavirus Is Internalized into Host Cells via Macropinocytosis in a Viral Glycoprotein-Dependent Manner. *PLOS Pathogens*, *6*(9), e1001121. https://doi.org/10.1371/journal.ppat.1001121

Nanbo, A., Maruyama, J., Imai, M., Ujie, M., Fujioka, Y., Nishide, S., Takada, A., Ohba, Y., & Kawaoka, Y. (2018). Ebola virus requires a host scramblase for externalization of

phosphatidylserine on the surface of viral particles. *PLOS Pathogens*, *14*(1), e1006848. https://doi.org/10.1371/journal.ppat.1006848

Nathan, L., & Daniel, S. (2019). Single Virion Tracking Microscopy for the Study of Virus Entry Processes in Live Cells and Biomimetic Platforms. *Adv Exp Med Biol*, *1215*, 13-43. https://doi.org/10.1007/978-3-030-14741-9_2

Nathan, L., Lai, A. L., Millet, J. K., Straus, M. R., Freed, J. H., Whittaker, G. R., & Daniel, S. (2020). Calcium Ions Directly Interact with the Ebola Virus Fusion Peptide to Promote Structure-Function Changes That Enhance Infection. *ACS Infectious Diseases*, *6*(2), 250-260. https://doi.org/10.1021/ACSINFECDIS.9B00296/ASSET/IMAGES/LARGE/ID9B00296_0005.JPEG

Nauwynck, H. J., Sanchez, R., Meerts, P., Lefebvre, D. J., Saha, D., Huang, L., & Misinzo, G. (2012). Cell tropism and entry of porcine circovirus 2. *Virus Res*, *164*(1-2), 43-45. https://doi.org/10.1016/j.virusres.2011.11.003

Ndungo, E., Herbert, A. S., Raaben, M., Obernosterer, G., Biswas, R., Miller, E. H., Wirchnianski, A. S., Carette, J. E., Brummelkamp, T. R., Whelan, S. P., Dye, J. M., & Chandran, K. (2016). A Single Residue in Ebola Virus Receptor NPC1 Influences Cellular Host Range in Reptiles. *mSphere*, *1*(2). http://msphere.asm.org/content/1/2/e00007-16.abstract

Negredo, A., Palacios, G., Vázquez-Morón, S., González, F., Dopazo, H., Molero, F., Juste, J., Quetglas, J., Savji, N., de la Cruz Martínez, M., Herrera, J. E., Pizarro, M., Hutchison, S. K., Echevarría, J. E., Lipkin, W. I., & Tenorio, A. (2011). Discovery of an Ebolavirus-Like Filovirus in Europe. *PLOS Pathogens*, *7*(10), e1002304. https://doi.org/10.1371/journal.ppat.1002304

Nelson, E. A., Dyall, J., Hoenen, T., Barnes, A. B., Zhou, H., Liang, J. Y., Michelotti, J., Dewey, W. H., DeWald, L. E., Bennett, R. S., Morris, P. J., Guha, R., Klumpp-Thomas, C., McKnight, C., Chen, Y.-C., Xu, X., Wang, A., Hughes, E., Martin, S., . . . White, J. M. (2017). The phosphatidylinositol-3-phosphate 5-kinase inhibitor apilimod blocks filoviral entry and infection. *PLoS Neglected Tropical Diseases*, *11*(4), e0005540. https://doi.org/10.1371/journal.pntd.0005540

Nettleship, J. E., Rahman-Huq, N., & Owens, R. J. (2009). The production of glycoproteins by transient expression in Mammalian cells. *Methods Mol Biol*, *498*, 245-263. https://doi.org/10.1007/978-1-59745-196-3_16

Neumann, G., Watanabe, T., Ito, H., Watanabe, S., Goto, H., Gao, P., Hughes, M., Perez, D. R., Donis, R., Hoffmann, E., Hobom, G., & Kawaoka, Y. (1999). Generation of influenza A viruses entirely from cloned cDNAs. *Proceedings of the National Academy of Sciences of the United States of America*, *96*(16), 9345-9350. https://doi.org/10.1073/pnas.96.16.9345

Ng, M., Ndungo, E., Jangra, R. K., Cai, Y., Postnikova, E., Radoshitzky, S. R., Dye, J. M., Ramirez de Arellano, E., Negredo, A., Palacios, G., Kuhn, J. H., & Chandran, K. (2014). Cell entry by a novel European filovirus requires host endosomal cysteine proteases and Niemann-Pick C1. *Virology*, *468-470*, 637-646. https://doi.org/10.1016/j.virol.2014.08.019

Nour, A. M., Li, Y., Wolenski, J., & Modis, Y. (2013). Viral Membrane Fusion and Nucleocapsid Delivery into the Cytoplasm are Distinct Events in Some Flaviviruses. *PLOS Pathogens*, *9*(9), e1003585. https://doi.org/10.1371/journal.ppat.1003585

O'Hearn, A., Wang, M., Cheng, H., Lear-Rooney, C. M., Koning, K., Rumschlag-Booms, E., Varhegyi, E., Olinger, G., & Rong, L. (2015). Role of EXT1 and Glycosaminoglycans in the Early Stage of Filovirus Entry. *Journal of Virology*, *89*(10), 5441-5449. https://doi.org/doi:10.1128/JVI.03689-14

Otwinowski, Z., & Minor, W. (1997). [20] Processing of X-ray diffraction data collected in oscillation mode. In *Methods in Enzymology* (Vol. 276, pp. 307-326). Academic Press. https://doi.org/https://doi.org/10.1016/S0076-6879(97)76066-X

Patel, A., Mohl, B. P., & Roy, P. (2016). Entry of Bluetongue Virus Capsid Requires the Late Endosome-specific Lipid Lysobisphosphatidic Acid. *J Biol Chem*, *291*(23), 12408-12419. https://doi.org/10.1074/jbc.M115.700856

Peng, W., Rayaprolu, V., Parvate, A. D., Pronker, M. F., Hui, S., Parekh, D., Shaffer, K., Yu, X., Saphire, E. O., & Snijder, J. (2022). Glycan shield of the ebolavirus envelope glycoprotein GP. *Communications Biology*, *5*(1), 785. https://doi.org/10.1038/s42003-022-03767-1

Pennington, Hallie N., & Lee, J. (2022). Lassa virus glycoprotein complex review: insights into its unique fusion machinery. *Bioscience Reports*, *42*(2). https://doi.org/10.1042/BSR20211930

Perez-Zsolt, D., Erkizia, I., Pino, M., García-Gallo, M., Martin, M. T., Benet, S., Chojnacki, J., Fernández-Figueras, M. T., Guerrero, D., Urrea, V., Muñiz-Trabudua, X., Kremer, L., Martinez-Picado, J., & Izquierdo-Useros, N. (2019). Anti-Siglec-1 antibodies block Ebola viral uptake and decrease cytoplasmic viral entry. *Nature Microbiology*, *4*(9), 1558-1570. https://doi.org/10.1038/s41564-019-0453-2

Plemper, R. K. (2011). Cell entry of enveloped viruses. *Current opinion in virology*, *1*(2), 92-100. https://doi.org/10.1016/j.coviro.2011.06.002

Poch, O., Blumberg, B. M., Bougueleret, L., & Tordo, N. (1990). Sequence Comparison of Five Polymerases (L proteins) of Unsegmented Negative-strand RNA Viruses: Theoretical Assignment of Functional Domains. *Journal of General Virology*, *71*(5), 1153-1162. https://doi.org/https://doi.org/10.1099/0022-1317-71-5-1153

Powlesland, A. S., Fisch, T., Taylor, M. E., Smith, D. F., Tissot, B., Dell, A., Pöhlmann, S., & Drickamer, K. (2008). A Novel Mechanism for LSECtin Binding to Ebola Virus Surface Glycoprotein through Truncated Glycans *<sup></sup>. *Journal of Biological Chemistry*, *283*(1), 593-602. https://doi.org/10.1074/jbc.M706292200

Pratakpiriya, W., Seki, F., Otsuki, N., Sakai, K., Fukuhara, H., Katamoto, H., Hirai, T., Maenaka, K., Techangamsuwan, S., Lan, N. T., Takeda, M., & Yamaguchi, R. (2012). Nectin4 is an epithelial cell receptor for canine distemper virus and involved in neurovirulence. *J Virol*, *86*(18), 10207-10210. https://doi.org/10.1128/jvi.00824-12

Qian, H., Wu, X., Du, X., Yao, X., Zhao, X., Lee, J., Yang, H., & Yan, N. (2020). Structural Basis of Low-pH-Dependent Lysosomal Cholesterol Egress by NPC1 and NPC2. *Cell*, *182*(1), 98-111.e118. https://doi.org/10.1016/j.cell.2020.05.020

Qiu, S., Leung, A., Bo, Y., Kozak, R. A., Anand, S. P., Warkentin, C., Salambanga, F. D. R., Cui, J., Kobinger, G., Kobasa, D., & Côté, M. (2018). Ebola virus requires phosphatidylinositol (3,5) bisphosphate production for efficient viral entry. *Virology*, *513*, 17-28. https://doi.org/https://doi.org/10.1016/j.virol.2017.09.028

Quinn, K., Brindley, M. A., Weller, M. L., Kaludov, N., Kondratowicz, A., Hunt, C. L., Sinn, P. L., McCray, P. B., Jr., Stein, C. S., Davidson, B. L., Flick, R., Mandell, R., Staplin, W., Maury, W., & Chiorini, J. A. (2009). Rho GTPases modulate entry of Ebola virus and vesicular stomatitis virus pseudotyped vectors. *Journal of Virology*, *83*(19), 10176-10186. https://doi.org/10.1128/JVI.00422-09

Raaben, M., Jae, L. T., Herbert, A. S., Kuehne, A. I., Stubbs, S. H., Chou, Y. Y., Blomen, V. A., Kirchhausen, T., Dye, J. M., Brummelkamp, T. R., & Whelan, S. P. (2017). NRP2 and CD63 Are Host Factors for Lujo Virus Cell Entry. *Cell Host Microbe*, *22*(5), 688-696.e685. https://doi.org/10.1016/j.chom.2017.10.002

Raff, A. B., Woodham, A. W., Raff, L. M., Skeate, J. G., Yan, L., Da Silva, D. M., Schelhaas, M., & Kast, W. M. (2013). The evolving field of human papillomavirus receptor research: a review of binding and entry. *J Virol*, *87*(11), 6062-6072. https://doi.org/10.1128/jvi.00330-13

Reynard, S., Journeaux, A., Gloaguen, E., Schaeffer, J., Varet, H., Pietrosemoli, N., Mateo, M., Baillet, N., Laouenan, C., Raoul, H., Mullaert, J., & Baize, S. (2019). Immune parameters and outcomes during Ebola virus disease. *JCI Insight*, *4*(1). https://doi.org/10.1172/jci.insight.125106

Rhein, B. A., Brouillette, R. B., Schaack, G. A., Chiorini, J. A., & Maury, W. (2016). Characterization of Human and Murine T-Cell Immunoglobulin Mucin Domain 4 (TIM-4) IgV Domain Residues Critical for Ebola Virus Entry. *Journal of Virology*, *90*(13), 6097-6111. https://doi.org/doi:10.1128/JVI.00100-16

Richard, A. S., Zhang, A., Park, S.-J., Farzan, M., Zong, M., & Choe, H. (2015). Virion-associated phosphatidylethanolamine promotes TIM1-mediated infection by Ebola, dengue, and West Nile viruses. *Proceedings of the National Academy of Sciences*, *112*(47), 14682-14687. https://doi.org/doi:10.1073/pnas.1508095112

Rimoin, A. W., Lu, K., Bramble, M. S., Steffen, I., Doshi, R. H., Hoff, N. A., Mukadi, P., Nicholson, B. P., Alfonso, V. H., Olinger, G., Sinai, C., Yamamoto, L. K., Ramirez, C. M., Okitolonda Wemakoy, E., Kebela Illunga, B., Pettitt, J., Logue, J., Bennett, R. S., Jahrling, P., . . . Simmons, G. (2018). Ebola Virus Neutralizing Antibodies Detectable in Survivors of theYambuku, Zaire Outbreak 40 Years after Infection. *The Journal of Infectious Diseases*, *217*(2), 223-231. https://doi.org/10.1093/INFDIS/JIX584

Rojek, J. M., Perez, M., & Kunz, S. (2008). Cellular Entry of Lymphocytic Choriomeningitis Virus. *Journal of Virology*, *82*(3), 1505-1517. https://doi.org/doi:10.1128/JVI.01331-07

Roth, S. L., & Whittaker, G. R. (2011). Promotion of vesicular stomatitis virus fusion by the endosome-specific phospholipid bis(monoacylglycero)phosphate (BMP). *FEBS Letters*, *585*(6), 865-869. https://doi.org/10.1016/J.FEBSLET.2011.02.015

Rubin, H. (1965). GENETIC CONTROL OF CELLULAR SUSCEPTIBILITY TO PSEUDOTYPES OF ROUS SARCOMA VIRUS. *Virology*, *26*, 270-276. https://doi.org/10.1016/0042-6822(65)90274-6

Rudnik, S., & Damme, M. (2020). The lysosomal membrane—export of metabolites and beyond. *The FEBS journal*, *288*.

Rugarabamu, S., Mboera, L., Rweyemamu, M., Mwanyika, G., Lutwama, J., Paweska, J., & Misinzo, G. (2020). Forty-two years of responding to Ebola virus outbreaks in Sub-Saharan Africa: a review. *BMJ global health*, *5*(3), e001955-e001955. https://doi.org/10.1136/bmjgh-2019-001955

Ruibal, P., Oestereich, L., Lüdtke, A., Becker-Ziaja, B., Wozniak, D. M., Kerber, R., Korva, M., Cabeza-Cabrerizo, M., Bore, J. A., Koundouno, F. R., Duraffour, S., Weller, R., Thorenz, A., Cimini, E., Viola, D., Agrati, C., Repits, J., Afrough, B., Cowley, L. A., . . . Muñoz-Fontela, C. (2016). Unique human immune signature of Ebola virus disease in Guinea. *Nature*, *533*(7601), 100-104. https://doi.org/10.1038/nature17949

Ruiz, M. C., Leon, T., Diaz, Y., & Michelangeli, F. (2009). Molecular biology of rotavirus entry and replication. *ScientificWorldJournal*, *9*, 1476-1497. https://doi.org/10.1100/tsw.2009.158

Rust, M. J., Lakadamyali, M., Zhang, F., & Zhuang, X. (2004). Assembly of endocytic machinery around individual influenza viruses during viral entry. *Nat Struct Mol Biol*, *11*(6), 567-573. https://doi.org/10.1038/nsmb769

Ryu, C. J., Cho, D. Y., Gripon, P., Kim, H. S., Guguen-Guillouzo, C., & Hong, H. J. (2000). An 80-kilodalton protein that binds to the pre-S1 domain of hepatitis B virus. *J Virol*, *74*(1), 110-116. https://doi.org/10.1128/jvi.74.1.110-116.2000

Ryu, W. S. (2017). Virus Life Cycle. *Molecular Virology of Human Pathogenic Viruses*, 31-45. https://doi.org/10.1016/b978-0-12-800838-6.00003-5

Saeed, M. F., Kolokoltsov, A. A., Albrecht, T., & Davey, R. A. (2010). Cellular entry of ebola virus involves uptake by a macropinocytosis-like mechanism and subsequent trafficking through early and late endosomes. *PLoS Pathog*, *6*(9), e1001110. https://doi.org/10.1371/journal.ppat.1001110

Saeed, M. F., Kolokoltsov, A. A., Freiberg, A. N., Holbrook, M. R., & Davey, R. A. (2008). Phosphoinositide-3 kinase-Akt pathway controls cellular entry of Ebola virus. *PLOS Pathogens*, *4*(8), e1000141-e1000141. https://doi.org/10.1371/journal.ppat.1000141

Sakurai, Y., Kolokoltsov, A. A., Chen, C.-C., Tidwell, M. W., Bauta, W. E., Klugbauer, N., Grimm, C., Wahl-Schott, C., Biel, M., & Davey, R. A. (2015). Two-pore channels control Ebola virus host cell entry and are drug targets for disease treatment. *Science*, *347*(6225), 995-998. http://science.sciencemag.org/content/347/6225/995.abstract

Salam, A. P., Duvignaud, A., Jaspard, M., Malvy, D., Carroll, M., Tarning, J., Olliaro, P. L., & Horby, P. W. (2022). Ribavirin for treating Lassa fever: A systematic review of pre-clinical studies and implications for human dosing. *PLoS Negl Trop Dis*, *16*(3), e0010289. https://doi.org/10.1371/journal.pntd.0010289

Salvador, B., Sexton, N. R., Carrion, R., Jr., Nunneley, J., Patterson, J. L., Steffen, I., Lu, K., Muench, M. O., Lembo, D., & Simmons, G. (2013). Filoviruses utilize glycosaminoglycans for their attachment to target cells. *J Virol*, *87*(6), 3295-3304. https://doi.org/10.1128/jvi.01621-12

Sanchez, A. (2007). Analysis of Filovirus Entry into Vero E6 Cells, Using Inhibitors of Endocytosis, Endosomal Acidification, Structural Integrity, and Cathepsin (B and L) Activity. *The Journal of Infectious Diseases*, *196*(Supplement_2), S251-S258. https://doi.org/10.1086/520597

Sanchez, A., Kiley, M. P., Holloway, B. P., & Auperin, D. D. (1993). Sequence analysis of the Ebola virus genome: organization, genetic elements, and comparison with the genome of Marburg virus. *Virus Res*, *29*(3), 215-240. https://doi.org/10.1016/0168-1702(93)90063-s

Sanchez, A., Kiley, M. P., Holloway, B. P., McCormick, J. B., & Auperin, D. D. (1989). The nucleoprotein gene of Ebola virus: cloning, sequencing, and in vitro expression. *Virology*, *170*(1), 81-91. https://doi.org/10.1016/0042-6822(89)90354-1

Sanchez, A., Lukwiya, M., Bausch, D., Mahanty, S., Sanchez, A. J., Wagoner, K. D., & Rollin, P. E. (2004). Analysis of human peripheral blood samples from fatal and nonfatal cases of Ebola (Sudan) hemorrhagic fever: cellular responses, virus load, and nitric oxide levels. *J Virol*, *78*(19), 10370-10377. https://doi.org/10.1128/jvi.78.19.10370-10377.2004

Sanchez, A., Trappier, S. G., Mahy, B. W., Peters, C. J., & Nichol, S. T. (1996). The virion glycoproteins of Ebola viruses are encoded in two reading frames and are expressed through transcriptional editing. *Proc Natl Acad Sci U S A*, *93*(8), 3602-3607. https://doi.org/10.1073/pnas.93.8.3602

Saphire, A. C. S., Bobardt, M. D., Zhang, Z., David, G., & Gallay, P. A. (2001). Syndecans Serve as Attachment Receptors for Human Immunodeficiency Virus Type 1 on Macrophages. *Journal of Virology*, *75*(19), 9187-9200. https://doi.org/doi:10.1128/JVI.75.19.9187-9200.2001

Sarzotti-Kelsoe, M., Bailer, R. T., Turk, E., Lin, C. L., Bilska, M., Greene, K. M., Gao, H., Todd, C. A., Ozaki, D. A., Seaman, M. S., Mascola, J. R., & Montefiori, D. C. (2014). Optimization and validation of the TZM-bl assay for standardized assessments of neutralizing antibodies

against HIV-1. *J Immunol Methods*, *409*, 131-146. https://doi.org/10.1016/j.jim.2013.11.022

Scherm, M. J., Gangloff, M., & Gay, N. J. (2022). Activation of Toll-like receptor 4 by Ebola virus-shed glycoprotein is direct and requires the internal fusion loop but not glycosylation. *Cell Reports*, *41*(4), 111562. https://doi.org/https://doi.org/10.1016/j.celrep.2022.111562

Schindell, B. G., Webb, A. L., & Kindrachuk, J. (2018). Persistence and Sexual Transmission of Filoviruses. *Viruses*, *10*(12), 683. https://www.mdpi.com/1999-4915/10/12/683

Schneider-Schaulies, J., ter Meulen, V., & Schneider-Schaulies, S. (2001). Measles virus interactions with cellular receptors: consequences for viral pathogenesis. *J Neurovirol*, *7*(5), 391-399. https://doi.org/10.1080/135502801753170246

Schornberg, K., Matsuyama, S., Kabsch, K., Delos, S., Bouton, A., & White, J. (2006). Role of endosomal cathepsins in entry mediated by the Ebola virus glycoprotein. *Journal of Virology*, *80*(8), 4174-4178. https://doi.org/10.1128/JVI.80.8.4174-4178.2006

Schrödinger, L., & DeLano, W. . (2020). *The PyMOL Molecular Graphics System, Version 2.0 Schrödinger, LLC*. In http://www.pymol.org/pymol

Schroeder, C. (2010). Cholesterol-binding viral proteins in virus entry and morphogenesis. *Subcell Biochem*, *51*, 77-108. https://doi.org/10.1007/978-90-481-8622-8_3

Schudt, G., Dolnik, O., Kolesnikova, L., Biedenkopf, N., Herwig, A., & Becker, S. (2015). Transport of Ebolavirus Nucleocapsids Is Dependent on Actin Polymerization: Live-Cell Imaging Analysis of Ebolavirus-Infected Cells. *The Journal of Infectious Diseases*, *212*(suppl_2), S160-S166. https://doi.org/10.1093/infdis/jiv083

Schwarz, T. M., Edwards, M. R., Diederichs, A., Alinger, J. B., Leung, D. W., Amarasinghe, G. K., & Basler, C. F. (2017). VP24-Karyopherin Alpha Binding Affinities Differ between Ebolavirus Species, Influencing Interferon Inhibition and VP24 Stability. *Journal of Virology*, *91*(4), e01715-01716. https://doi.org/doi:10.1128/JVI.01715-16

Scott, J. T., Sesay, F. R., Massaquoi, T. A., Idriss, B. R., Sahr, F., & Semple, M. G. (2016). Post-Ebola Syndrome, Sierra Leone. *Emerg Infect Dis*, *22*(4), 641-646. https://doi.org/10.3201/eid2204.151302

Scott, J. T., Sharma, R., Meredith, L. W., Dunning, J., Moore, C. E., Sahr, F., Ward, S., Goodfellow, I., & Horby, P. (2020). Pharmacokinetics of TKM-130803 in Sierra Leonean patients with Ebola virus disease:  plasma concentrations exceed target levels, with drug accumulation in the most severe patients. *eBioMedicine*, *52*. https://doi.org/10.1016/j.ebiom.2019.102601

Shafti-Keramat, S., Handisurya, A., Kriehuber, E., Meneguzzi, G., Slupetzky, K., & Kirnbauer, R. (2003). Different heparan sulfate proteoglycans serve as cellular receptors for human papillomaviruses. *J Virol*, *77*(24), 13125-13135. https://doi.org/10.1128/jvi.77.24.13125-13135.2003

Shang, J., Wan, Y., Luo, C., Ye, G., Geng, Q., Auerbach, A., & Li, F. (2020). Cell entry mechanisms of SARS-CoV-2. *Proceedings of the National Academy of Sciences*, 202003138-202003138. https://doi.org/10.1073/pnas.2003138117

Shental-Bechor, D., & Levy, Y. (2008). Effect of glycosylation on protein folding: A close look at thermodynamic stabilization. *Proceedings of the National Academy of Sciences of the United States of America*, *105*(24), 8256-8261. https://doi.org/10.1073/PNAS.0801340105

Shi, M., Lin, X.-D., Chen, X., Tian, J.-H., Chen, L.-J., Li, K., Wang, W., Eden, J.-S., Shen, J.-J., Liu, L., Holmes, E. C., & Zhang, Y.-Z. (2018). The evolutionary history of vertebrate RNA viruses. *Nature*, *556*(7700), 197-202. https://doi.org/10.1038/s41586-018-0012-7

Shimojima, M., Takada, A., Ebihara, H., Neumann, G., Fujioka, K., Irimura, T., Jones, S., Feldmann, H., & Kawaoka, Y. (2006). Tyro3 Family-Mediated Cell Entry of Ebola and Marburg Viruses. *Journal of Virology*, *80*(20), 10109-10116. https://doi.org/doi:10.1128/JVI.01157-06

Shrivastava-Ranjan, P., Flint, M., Bergeron, É., McElroy, A. K., Chatterjee, P., Albariño, C. G., Nichol, S. T., & Spiropoulou, C. F. (2018). Statins Suppress Ebola Virus Infectivity by Interfering with Glycoprotein Processing. *mBio*, *9*(3). https://doi.org/10.1128/mBio.00660-18

Shukla, D., Liu, J., Blaiklock, P., Shworak, N. W., Bai, X., Esko, J. D., Cohen, G. H., Eisenberg, R. J., Rosenberg, R. D., & Spear, P. G. (1999). A Novel Role for 3-O-Sulfated Heparan Sulfate in Herpes Simplex Virus 1 Entry. *Cell*, *99*(1), 13-22. https://doi.org/10.1016/S0092-8674(00)80058-6

Siegel, D. P. (2008). The Gaussian curvature elastic energy of intermediates in membrane fusion. *Biophys J*, *95*(11), 5200-5215. https://doi.org/10.1529/biophysj.108.140152

Simmons, G., Wool-Lewis, R. J., Baribaud, F., Netter, R. C., & Bates, P. (2002). Ebola virus glycoproteins induce global surface protein down-modulation and loss of cell adherence. *J Virol*, *76*(5), 2518-2528. https://doi.org/10.1128/jvi.76.5.2518-2528.2002

Simmons, J. A., D'Souza, R. S., Ruas, M., Galione, A., Casanova, J. E., & White, J. M. (2016). Ebolavirus Glycoprotein Directs Fusion through NPC1+ Endolysosomes. *Journal of Virology*, *90*(1), 605-610. https://doi.org/10.1128/JVI.01828-15

Singh, P., Mukherji, S., Basak, S., Hoffmann, M., & Das, D. K. (2022). Dynamic Ca2+ sensitivity stimulates the evolved SARS-CoV-2 spike strain-mediated membrane fusion for enhanced entry. *Cell Reports*, *39*(3), 110694. https://doi.org/https://doi.org/10.1016/j.celrep.2022.110694

Sissoko, D., Laouenan, C., Folkesson, E., M'Lebing, A.-B., Beavogui, A.-H., Baize, S., Camara, A.-M., Maes, P., Shepherd, S., Danel, C., Carazo, S., Conde, M. N., Gala, J.-L., Colin, G., Savini, H., Bore, J. A., Le Marcis, F., Koundouno, F. R., Petitjean, F., . . . Group, J. S. (2016). Experimental Treatment with Favipiravir for Ebola Virus Disease (the JIKI Trial): A Historically Controlled, Single-Arm Proof-of-Concept Trial in Guinea. *PLoS Medicine*, *13*(3), e1001967. https://doi.org/10.1371/journal.pmed.1001967

Slenczka, W. (2017). Filovirus Research: How it Began. *Curr Top Microbiol Immunol*, *411*, 3-21. https://doi.org/10.1007/82_2017_8

Smith, B. A., & McConnell, H. M. (1978). Determination of molecular motion in membranes using periodic pattern photobleaching. *Proceedings of the National Academy of Sciences of the United States of America*, *75*(6), 2759-2763. https://doi.org/10.1073/pnas.75.6.2759

Spence, J. S., Krause, T. B., Mittler, E., Jangra, R. K., & Chandran, K. (2016). Direct Visualization of Ebola Virus Fusion Triggering in the Endocytic Pathway. *mBio*, *7*(1), e01857-01815. https://doi.org/10.1128/mBio.01857-15

Stauffer, S., Feng, Y., Nebioglu, F., Heilig, R., Picotti, P., & Helenius, A. (2014). Stepwise priming by acidic pH and a high K+ concentration is required for efficient uncoating of influenza A virus cores after penetration. *J Virol*, *88*(22), 13029-13046. https://doi.org/10.1128/jvi.01430-14

Stencel-Baerenwald, J. E., Reiss, K., Reiter, D. M., Stehle, T., & Dermody, T. S. (2014). The sweet spot: defining virus–sialic acid interactions. *Nature Reviews Microbiology*, *12*(11), 739-749. https://doi.org/10.1038/nrmicro3346

Stewart, C. M., Phan, A., Bo, Y., LeBlond, N. D., Smith, T. K. T., Laroche, G., Giguère, P. M., Fullerton, M. D., Pelchat, M., Kobasa, D., & Côté, M. (2021). Ebola virus triggers receptor

tyrosine kinase-dependent signaling to promote the delivery of viral particles to entry-conducive intracellular compartments. *PLOS Pathogens*, *17*(1), e1009275. https://doi.org/10.1371/journal.ppat.1009275

Storch, J., & Xu, Z. (2009). Niemann–Pick C2 (NPC2) and intracellular cholesterol trafficking. *Biochimica et Biophysica Acta (BBA) - Molecular and Cell Biology of Lipids*, *1791*(7), 671-678. https://doi.org/10.1016/j.bbalip.2009.02.001

Sun, X., & Whittaker, G. R. (2003). Role for influenza virus envelope cholesterol in virus entry and infection. *J Virol*, *77*(23), 12543-12551. https://doi.org/10.1128/jvi.77.23.12543-12551.2003

Takada, A., Fujioka, K., Tsuiji, M., Morikawa, A., Higashi, N., Ebihara, H., Kobasa, D., Feldmann, H., Irimura, T., & Kawaoka, Y. (2004). Human macrophage C-type lectin specific for galactose and N-acetylgalactosamine promotes filovirus entry. *J Virol*, *78*(6), 2943-2947. https://doi.org/10.1128/jvi.78.6.2943-2947.2004

Takamatsu, Y., Kolesnikova, L., & Becker, S. (2018). Ebola virus proteins NP, VP35, and VP24 are essential and sufficient to mediate nucleocapsid transport. *Proceedings of the National Academy of Sciences*, *115*(5), 1075-1080. https://doi.org/doi:10.1073/pnas.1712263115

Takamatsu, Y., Yoshikawa, T., Kurosu, T., Fukushi, S., Nagata, N., Shimojima, M., Ebihara, H., Saijo, M., & Noda, T. (2022). Role of VP30 Phosphorylation in Ebola Virus Nucleocapsid Assembly and Transport. *J Virol*, *96*(17), e0108322. https://doi.org/10.1128/jvi.01083-22

Talekar, A., Moscona, A., & Porotto, M. (2013). Measles virus fusion machinery activated by sialic acid binding globular domain. *J Virol*, *87*(24), 13619-13627. https://doi.org/10.1128/jvi.02256-13

Tamhankar, M., Gerhardt, D. M., Bennett, R. S., Murphy, N., Jahrling, P. B., & Patterson, J. L. (2018). Heparan sulfate is an important mediator of Ebola virus infection in polarized epithelial cells. *Virology Journal*, *15*(1), 135. https://doi.org/10.1186/s12985-018-1045-0

Tamm, L. K., Crane, J., & Kiessling, V. (2003). Membrane fusion: a structural perspective on the interplay of lipids and proteins. *Current Opinion in Structural Biology*, *13*(4), 453-466. https://doi.org/https://doi.org/10.1016/S0959-440X(03)00107-6

Tang, D., Wang, Y., Dong, X., Yuan, Y., Kang, F., Tian, W., Wang, K., Li, H., & Qi, S. (2022). Scramblases and virus infection. *Bioessays*, *44*(12), e2100261. https://doi.org/10.1002/bies.202100261

Tang, Q., Liu, P., Chen, M., & Qin, Y. (2019). Virion-Associated Cholesterol Regulates the Infection of Human Parainfluenza Virus Type 3. *Viruses*, *11*(5), 438. https://www.mdpi.com/1999-4915/11/5/438

Tang, T., Bidon, M., Jaimes, J. A., Whittaker, G. R., & Daniel, S. (2020). Coronavirus membrane fusion mechanism offers a potential target for antiviral development. *Antiviral Research*, *178*, 104792-104792. https://doi.org/10.1016/j.antiviral.2020.104792

Taylor, M. W. (2014). What Is a Virus? In M. W. Taylor (Ed.), *Viruses and Man: A History of Interactions* (pp. 23-40). Springer International Publishing. https://doi.org/10.1007/978-3-319-07758-1_2

Timothy, J. W. S., Hall, Y., Akoi-Boré, J., Diallo, B., Tipton, T. R. W., Bower, H., Strecker, T., Glynn, J. R., & Carroll, M. W. (2019). Early transmission and case fatality of Ebola virus at the index site of the 2013-16 west African Ebola outbreak: a cross-sectional seroprevalence survey. *Lancet Infect Dis*, *19*(4), 429-438. https://doi.org/10.1016/s1473-3099(18)30791-6

Towner, J. S., Pourrut, X., Albariño, C. G., Nkogue, C. N., Bird, B. H., Grard, G., Ksiazek, T. G., Gonzalez, J.-P., Nichol, S. T., & Leroy, E. M. (2007). Marburg Virus Infection Detected in a

Common African Bat. *PLOS ONE*, *2*(8), e764. https://doi.org/10.1371/journal.pone.0000764

Tsai, B. (2007). Penetration of Nonenveloped Viruses into the Cytoplasm. *Annual Review of Cell and Developmental Biology*, *23*(1), 23-43. https://doi.org/10.1146/annurev.cellbio.23.090506.123454

Tshiani Mbaya, O., Mukumbayi, P., & Mulangu, S. (2021). Review: Insights on Current FDA-Approved Monoclonal Antibodies Against Ebola Virus Infection [Review]. *Frontiers in Immunology*, *12*. https://doi.org/10.3389/fimmu.2021.721328

Turk, V., Stoka, V., Vasiljeva, O., Renko, M., Sun, T., Turk, B., & Turk, D. (2012). Cysteine cathepsins: From structure, function and regulation to new frontiers. *Biochimica et Biophysica Acta (BBA) - Proteins and Proteomics*, *1824*(1), 68-88. https://doi.org/10.1016/j.bbapap.2011.10.002

Urbanowicz, R. A., McClure, C. P., Sakuntabhai, A., Sall, A. A., Kobinger, G., Muller, M. A., Holmes, E. C., Rey, F. A., Simon-Loriere, E., & Ball, J. K. (2016). Human Adaptation of Ebola Virus during the West African Outbreak. *Cell*, *167*(4), 1079-1087.e1075. https://doi.org/10.1016/j.cell.2016.10.013

Uyeki, T. M., Mehta, A. K., Davey, R. T., Liddell, A. M., Wolf, T., Vetter, P., Schmiedel, S., Grünewald, T., Jacobs, M., Arribas, J. R., Evans, L., Hewlett, A. L., Brantsaeter, A. B., Ippolito, G., Rapp, C., Hoepelman, A. I. M., & Gutman, J. (2016). Clinical Management of Ebola Virus Disease in the United States and Europe. *New England Journal of Medicine*, *374*(7), 636-646. https://doi.org/10.1056/NEJMoa1504874

Vagin, A., & Teplyakov, A. (2010). Molecular replacement with MOLREP. *Acta Crystallogr D Biol Crystallogr*, *66*(Pt 1), 22-25. https://doi.org/10.1107/s0907444909042589

Velásquez, G. E., Aibana, O., Ling, E. J., Diakite, I., Mooring, E. Q., & Murray, M. B. (2015). Time From Infection to Disease and Infectiousness for Ebola Virus Disease, a Systematic Review. *Clin Infect Dis*, *61*(7), 1135-1140. https://doi.org/10.1093/cid/civ531

Vernet, M. A., Reynard, S., Fizet, A., Schaeffer, J., Pannetier, D., Guedj, J., Rives, M., Georges, N., Garcia-Bonnet, N., Sylla, A. I., Grovogui, P., Kerherve, J. Y., Savio, C., Savio-Coste, S., de Séverac, M. L., Zloczewski, P., Linares, S., Harouna, S., Abdoul, B. M., . . . Baize, S. (2017). Clinical, virological, and biological parameters associated with outcomes of Ebola virus infection in Macenta, Guinea. *JCI Insight*, *2*(6), e88864. https://doi.org/10.1172/jci.insight.88864

Vetter, P., Kaiser, L., Schibler, M., Ciglenecki, I., & Bausch, D. G. (2016). Sequelae of Ebola virus disease: the emergency within the emergency. *The Lancet Infectious Diseases*, *16*(6), e82-e91. https://doi.org/10.1016/S1473-3099(16)00077-3

Vincent, N., Genin, C., & Malvoisin, E. (2002). Identification of a conserved domain of the HIV-1 transmembrane protein gp41 which interacts with cholesteryl groups. *Biochimica et Biophysica Acta (BBA) - Biomembranes*, *1567*, 157-164. https://doi.org/https://doi.org/10.1016/S0005-2736(02)00611-9

Volchkov, V. E., Becker, S., Volchkova, V. A., Ternovoj, V. A., Kotov, A. N., Netesov, S. V., & Klenk, H.-D. (1995). GP mRNA of Ebola Virus Is Edited by the Ebola Virus Polymerase and by T7 and Vaccinia Virus Polymerases1. *Virology*, *214*(2), 421-430. https://doi.org/https://doi.org/10.1006/viro.1995.0052

Volchkov, V. E., Feldmann, H., Volchkova, V. A., & Klenk, H. D. (1998). Processing of the Ebola virus glycoprotein by the proprotein convertase furin. *Proceedings of the National Academy of Sciences of the United States of America*, *95*(10), 5762-5767. https://doi.org/10.1073/pnas.95.10.5762

Volchkova, V. A., Klenk, H.-D., & Volchkov, V. E. (1999). Delta-Peptide Is the Carboxy-Terminal Cleavage Fragment of the Nonstructural Small Glycoprotein sGP of Ebola Virus. *Virology*, *265*(1), 164-171. https://doi.org/https://doi.org/10.1006/viro.1999.0034

von Messling, V., Oezguen, N., Zheng, Q., Vongpunsawad, S., Braun, W., & Cattaneo, R. (2005). Nearby clusters of hemagglutinin residues sustain SLAM-dependent canine distemper virus entry in peripheral blood mononuclear cells. *J Virol*, *79*(9), 5857-5862. https://doi.org/10.1128/jvi.79.9.5857-5862.2005

Wagner, M. L., & Tamm, L. K. (2000). Tethered polymer-supported planar lipid bilayers for reconstitution of integral membrane proteins: silane-polyethyleneglycol-lipid as a cushion and covalent linker. *Biophysical Journal*, *79*(3), 1400-1414. https://doi.org/10.1016/S0006-3495(00)76392-2

Wan, W., Kolesnikova, L., Clarke, M., Koehler, A., Noda, T., Becker, S., & Briggs, J. A. G. (2017). Structure and assembly of the Ebola virus nucleocapsid. *Nature*, *551*(7680), 394-397. https://doi.org/10.1038/nature24490

Wang, C., Eufemi, M., Turano, C., & Giartosio, A. (1996). Influence of the Carbohydrate Moiety on the Stability of Glycoproteins†. *Biochemistry*, *35*(23). https://doi.org/10.1021/BI9517704

Wang, H., Shi, Y., Song, J., Qi, J., Lu, G., Yan, J., & Gao, G. F. (2016). Ebola Viral Glycoprotein Bound to Its Endosomal Receptor Niemann-Pick C1. *Cell*, *164*(1), 258-268. https://doi.org/10.1016/j.cell.2015.12.044

Wang, L.-F., & Anderson, D. E. (2019). Viruses in bats and potential spillover to animals and humans. *Current opinion in virology*, *34*, 79-89. https://doi.org/10.1016/j.coviro.2018.12.007

Wang, M. K., Lim, S.-Y., Lee, S. M., & Cunningham, J. M. (2017). Biochemical Basis for Increased Activity of Ebola Glycoprotein in the 2013–16 Epidemic. *Cell Host & Microbe*. https://doi.org/10.1016/j.chom.2017.02.002

Ward, A. E., Kiessling, V., Pornillos, O., White, J. M., Ganser-Pornillos, B. K., & Tamm, L. K. (2020). HIV-cell membrane fusion intermediates are restricted by Serincs as revealed by cryo-electron and TIRF microscopy. *J Biol Chem*, *295*(45), 15183-15195. https://doi.org/10.1074/jbc.RA120.014466

Warren, C. J., Yu, S., Peters, D. K., Barbachano-Guerrero, A., Yang, Q., Burris, B. L., Worwa, G., Huang, I. C., Wilkerson, G. K., Goldberg, T. L., Kuhn, J. H., & Sawyer, S. L. (2022). Primate hemorrhagic fever-causing arteriviruses are poised for spillover to humans. *Cell*, *185*(21), 3980-3991.e3918. https://doi.org/https://doi.org/10.1016/j.cell.2022.09.022

Watanabe, S., Noda, T., & Kawaoka, Y. (2006). Functional mapping of the nucleoprotein of Ebola virus. *J Virol*, *80*(8), 3743-3751. https://doi.org/10.1128/jvi.80.8.3743-3751.2006

Watt, A., Moukambi, F., Banadyga, L., Groseth, A., Callison, J., Herwig, A., Ebihara, H., Feldmann, H., & Hoenen, T. (2014). A Novel Life Cycle Modeling System for Ebola Virus Shows a Genome Length-Dependent Role of VP24 in Virus Infectivity. *Journal of Virology*, *88*(18), 10511-10524. https://doi.org/doi:10.1128/JVI.01272-14

Wehrly, K., & Chesebro, B. (1997). p24 antigen capture assay for quantification of human immunodeficiency virus using readily available inexpensive reagents. *Methods: A Companion to Methods in Enzymology*, *12*(4), 288-293. https://doi.org/10.1006/meth.1997.0481

Weissenhorn, W., Carf, A., Lee, K.-H., Skehel, J. J., & Wiley, D. C. (1998). Crystal Structure of the Ebola Virus Membrane Fusion Subunit, GP2, from the Envelope Glycoprotein Ectodomain. *Molecular Cell*, *2*(5), 605-616. https://doi.org/10.1016/S1097-2765(00)80159-8

White, J., Matlin, K., & Helenius, A. (1981). Cell fusion by Semliki Forest, influenza, and vesicular stomatitis viruses. *The Journal of Cell Biology*, *89*(3), 674-679.

White, J. M., Delos, S. E., Brecher, M., & Schornberg, K. (2008). Structures and mechanisms of viral membrane fusion proteins: multiple variations on a common theme. *Crit Rev Biochem Mol Biol*, *43*(3), 189-219. https://doi.org/10.1080/10409230802058320

White, J. M., & Schornberg, K. L. (2012). A new player in the puzzle of filovirus entry. *Nature reviews. Microbiology*, *10*(5), 317-322. https://doi.org/10.1038/nrmicro2764

White, J. M., & Whittaker, G. R. (2016). Fusion of Enveloped Viruses in Endosomes. *Traffic*, *17*(6), 593-614. https://doi.org/10.1111/tra.12389

WHO. *Ebola outbreak 2014-2016 - West Africa.* Retrieved 20 Nov 2022 from https://www.who.int/emergencies/situations/ebola-outbreak-2014-2016-West-Africa

WHO. (2021). *Ebola Virus Disease*. Retrieved 25 Nov 2022 from https://www.who.int/news-room/fact-sheets/detail/ebola-virus-disease

WHO. (2022a). *Disease Outbreak News; Ebola disease caused by Sudan ebolavirus – Uganda*. Retrieved 26 December 2022 from https://www.who.int/emergencies/disease-outbreak-news/item/2022-DON428

WHO. (2022b). *WHO steps up support to Uganda's evolving Ebola outbreak as hope for vaccines increases.* Retrieved 25 Nov 2022 from https://www.afro.who.int/countries/uganda/news/who-steps-support-ugandas-evolving-ebola-outbreak-hope-vaccines-increases

Wiedemann, A., Foucat, E., Hocini, H., Lefebvre, C., Hejblum, B. P., Durand, M., Krüger, M., Keita, A. K., Ayouba, A., Mély, S., Fernandez, J. C., Touré, A., Fourati, S., Lévy-Marchal, C., Raoul, H., Delaporte, E., Koivogui, L., Thiébaut, R., Lacabaratz, C., & Lévy, Y. (2020). Long-lasting severe immune dysfunction in Ebola virus disease survivors. *Nat Commun*, *11*(1), 3730. https://doi.org/10.1038/s41467-020-17489-7

Winter, S. L., Golani, G., Lolicato, F., Vallbracht, M., Thiyagarajah, K., Ahmed, S. S., Lüchtenborg, C., Fackler, O. T., Brügger, B., Hoenen, T., Nickel, W., Schwarz, U. S., & Chlanda, P. (2022). The Ebola virus VP40 matrix undergoes endosomal disassembly essential for membrane fusion. *bioRxiv*, 2022.2008.2024.505067. https://doi.org/10.1101/2022.08.24.505067

Wong, A. C., Sandesara, R. G., Mulherkar, N., Whelan, S. P., & Chandran, K. (2010). A forward genetic strategy reveals destabilizing mutations in the Ebolavirus glycoprotein that alter its protease dependence during cell entry. *Journal of Virology*, *84*(1), 163-175. https://doi.org/10.1128/JVI.01832-09

Wool-Lewis, R. J., & Bates, P. (1999). Endoproteolytic Processing of the Ebola Virus Envelope Glycoprotein: Cleavage Is Not Required for Function. *Journal of Virology*, *73*(2), 1419-1426. https://doi.org/doi:10.1128/JVI.73.2.1419-1426.1999

Woolhouse, M., Scott, F., Hudson, Z., Howey, R., & Chase-Topping, M. (2012). Human viruses: discovery and emergence. *Philos Trans R Soc Lond B Biol Sci*, *367*(1604), 2864-2871. https://doi.org/10.1098/rstb.2011.0354

Wudiri, G. A., Schneider, S. M., & Nicola, A. V. (2017). Herpes Simplex Virus 1 Envelope Cholesterol Facilitates Membrane Fusion. *Front Microbiol*, *8*, 2383. https://doi.org/10.3389/fmicb.2017.02383

Yadati, T., Houben, T., Bitorina, A., & Shiri-Sverdlov, R. (2020). The Ins and Outs of Cathepsins: Physiological Function and Role in Disease Management. *Cells*, *9*(7). https://doi.org/10.3390/cells9071679

Yang, S.-T., Kiessling, V., Simmons, J. A., White, J. M., & Tamm, L. K. (2015). HIV gp41–mediated membrane fusion occurs at edges of cholesterol-rich lipid domains. *Nature Chemical Biology*, *11*(6), 424-431. https://doi.org/10.1038/nchembio.1800

Yang, S.-T., Kreutzberger, A. J. B., Kiessling, V., Ganser-Pornillos, B. K., White, J. M., & Tamm, L. K. (2017). HIV virions sense plasma membrane heterogeneity for cell entry. *Science Advances*, *3*(6). http://advances.sciencemag.org/content/3/6/e1700338.abstract

Yang, S.-T., Kreutzberger, A. J. B., Lee, J., Kiessling, V., & Tamm, L. K. (2016). The role of cholesterol in membrane fusion. *Chemistry and Physics of Lipids*, *199*, 136-143. https://doi.org/10.1016/j.chemphyslip.2016.05.003

Yang, S. T., Kiessling, V., & Tamm, L. K. (2016). Line tension at lipid phase boundaries as driving force for HIV fusion peptide-mediated fusion. *Nature Communications*. https://doi.org/10.1038/ncomms11401

Yang, X.-L., Tan, C. W., Anderson, D. E., Jiang, R.-D., Li, B., Zhang, W., Zhu, Y., Lim, X. F., Zhou, P., Liu, X.-L., Guan, W., Zhang, L., Li, S.-Y., Zhang, Y.-Z., Wang, L.-F., & Shi, Z.-L. (2019). Characterization of a filovirus (Měnglà virus) from Rousettus bats in China. *Nature Microbiology*, *4*(3), 390-395. https://doi.org/10.1038/s41564-018-0328-y

Yang, Z.-y., Duckers, H. J., Sullivan, N. J., Sanchez, A., Nabel, E. G., & Nabel, G. J. (2000). Identification of the Ebola virus glycoprotein as the main viral determinant of vascular cell cytotoxicity and injury. *Nature medicine*, *6*(8), 886-889. https://doi.org/10.1038/78654

Yonezawa, A., Cavrois, M., & Greene, W. C. (2005). Studies of ebola virus glycoprotein-mediated entry and fusion by using pseudotyped human immunodeficiency virus type 1 virions: involvement of cytoskeletal proteins and enhancement by tumor necrosis factor alpha. *J Virol*, *79*(2), 918-926. https://doi.org/10.1128/jvi.79.2.918-926.2005

Yuan, B., Peng, Q., Cheng, J., Wang, M., Zhong, J., Qi, J., Gao, G. F., & Shi, Y. (2022). Structure of the Ebola virus polymerase complex. *Nature*, *610*(7931), 394-401. https://doi.org/10.1038/s41586-022-05271-2

Zaitseva, E., Yang, S. T., Melikov, K., Pourmal, S., & Chernomordik, L. V. (2010). Dengue virus ensures its fusion in late endosomes using compartment-specific lipids. *PLOS Pathogens*. https://doi.org/10.1371/journal.ppat.1001131

Zapatero-Belinchón, F. J., Dietzel, E., Dolnik, O., Döhner, K., Costa, R., Hertel, B., Veselkova, B., Kirui, J., Klintworth, A., Manns, M. P., Pöhlmann, S., Pietschmann, T., Krey, T., Ciesek, S., Gerold, G., Sodeik, B., Becker, S., & von Hahn, T. (2019). Characterization of the Filovirus-Resistant Cell Line SH-SY5Y Reveals Redundant Role of Cell Surface Entry Factors. *Viruses*, *11*(3), 275. https://www.mdpi.com/1999-4915/11/3/275

Zárate, S., Cuadras, M. A., Espinosa, R., Romero, P., Juárez, K. O., Camacho-Nuez, M., Arias, C. F., & López, S. (2003). Interaction of rotaviruses with Hsc70 during cell entry is mediated by VP5. *J Virol*, *77*(13), 7254-7260. https://doi.org/10.1128/jvi.77.13.7254-7260.2003

Zawada, K. E., Wrona, D., Rawle, R. J., & Kasson, P. M. (2016). Influenza viral membrane fusion is sensitive to sterol concentration but surprisingly robust to sterol chemical identity. *Sci Rep*, *6*, 29842. https://doi.org/10.1038/srep29842

Zhang, J., Wang, B., Gao, X., Peng, C., Shan, C., Johnson, S. F., Schwartz, R. C., & Zheng, Y.-H. (2022). RNF185 regulates proteostasis in Ebolavirus infection by crosstalk between the calnexin cycle, ERAD, and reticulophagy. *Nature Communications*, *13*(1), 6007. https://doi.org/10.1038/s41467-022-33805-9

Zhang, X., Lin, S. M., Chen, T. Y., Liu, M., Ye, F., Chen, Y. R., Shi, L., He, Y. L., Wu, L. X., Zheng, S. Q., Zhao, Y. R., & Zhang, S. L. (2011). Asialoglycoprotein receptor interacts with the

preS1 domain of hepatitis B virus in vivo and in vitro. *Arch Virol*, *156*(4), 637-645. https://doi.org/10.1007/s00705-010-0903-x

Zhang, Y., Carlos de la Torre, J., & Melikyan, G. B. (2022). Human LAMP1 accelerates Lassa virus fusion and potently promotes fusion pore dilation upon forcing viral fusion with non-endosomal membrane. *PLOS Pathogens*, *18*(8), e1010625. https://doi.org/10.1371/journal.ppat.1010625

Zhang, Y., Li, X., Becker, K. A., & Gulbins, E. (2009). Ceramide-enriched membrane domains—Structure and function. *Biochimica et Biophysica Acta (BBA) - Biomembranes*, *1788*(1), 178-183. https://doi.org/https://doi.org/10.1016/j.bbamem.2008.07.030

Zhao, Y., Ren, J., Harlos, K., & Stuart, D. I. (2016). Structure of glycosylated NPC1 luminal domain C reveals insights into NPC2 and Ebola virus interactions. *FEBS Letters*, *590*, 605-612. https://doi.org/10.1002/1873-3468.12089

Zhou, Q., & Qiu, H. (2019). The Mechanistic Impact of N-Glycosylation on Stability, Pharmacokinetics, and Immunogenicity of Therapeutic Proteins. *Journal of Pharmaceutical Sciences*, *108*(4), 1366-1377. https://doi.org/https://doi.org/10.1016/j.xphs.2018.11.029

Zhu, L., Gao, T., Yang, W., Liu, Y., Liu, X., Hu, Y., Jin, Y., Li, P., Xu, K., Zou, G., Zhao, L., Cao, R., Zhong, W., Xia, X., & Cao, C. (2020). Ebola virus replication is regulated by the phosphorylation of viral protein VP35. *Biochem Biophys Res Commun*, *521*(3), 687-692. https://doi.org/10.1016/j.bbrc.2019.10.147